Istituto Nazionale di Astrofisica
Osservatorio Astronomico di Torino

Proceedings of the

Second ENIGMA Meeting

Porto Venere, Italy – October 11-15, 2003

Edited by

Claudia M. Raiteri and Massimo Villata

Published by

Osservatorio Astronomico di Torino
Via Osservatorio 20, I-10025 Pino Torinese (TO), Italy

http://www.to.astro.it

Printed at Pino Torinese in November 2003

Meeting photographs by Luciano Lanteri

Souvenir photographs by Stefania Crapanzano and Luciano Lanteri

European
Network for the
Investigation of
Galactic nuclei through
Multifrequency
Analysis

ENIGMA is a Research Training Network funded within the FP5 program of the European Community

http://www.lsw.uni-heidelberg.de/enigma.html

Network Coordinator: **Stefan J. Wagner**

Contents

Preface

The second Meeting of the "European Network for the Investigation of Galactic nuclei through Multifrequency Analysis" (ENIGMA) took place from October 11 to 15, 2003, at the Royal Sporting Hotel located in the beautiful seaside village of Porto Venere, near La Spezia, in north-western Italy.

In total, 26 participants from the 8 European teams involved in the Network were present, and during the three working days we had 27 scientific talks, a "Young researchers session" in which the newly-appointed ENIGMA fellows discussed their research programmes, a "Team leaders session" dedicated to organization and financial aspects of the Network, and two sessions on past-ongoing as well as future observing campaigns, which are the tools through which we expect to achieve the ENIGMA scientific goals.

We took a bit of relax the last evening, when we went for a boat trip around the three little islands (Palmaria, Tino, and Tinetto) in front of Porto Venere, followed by a guided tour of the village in the magic framework of twilight.

The Meeting went on in a very friendly atmosphere, which is the best starting point towards a fruitful collaboration.

These Proceedings are a collection of the Meeting electronic presentations that were gathered directly on the spot. They are meant as a work record that can be useful to the Meeting participants to remind what was discussed, and especially to those ENIGMA members who could not participate, to let them know what was presented.

As a conclusion to this brief note, we want to thank once more all the ENIGMA participants for their contribution to the Meeting success.

Claudia M. Raiteri and Massimo Villata

List of participants

Heidelberg team:

Stefan J. Wagner - S.Wagner@lsw.uni-heidelberg.de
Dimitrios Emmanoulopoulos - d.emmanoulopoulos@lsw.uni-heidelberg.de
Konstantina Manolakou - k.manolakou@lsw.uni-heidelberg.de
Luisa Ostorero - l.ostorero@lsw.uni-heidelberg.de
Mirko Troeller - m.troeller@lsw.uni-heidelberg.de

Bonn team:

Thomas P. Krichbaum - tkrichbaum@mpifr-bonn.mpg.de
Emmanoulis Angelakis - angelaki@mpifr-bonn.mpg.de
Uwe Bach - ubach@mpifr-bonn.mpg.de
Jens Klare - jklare@mpifr-bonn.mpg.de

Tuorla team:

Leo O. Takalo - takalo@utu.fi

Metsähovi team:

Merja Tornikoski - mtt@cc.hut.fi

Torino team:

Claudia M. Raiteri - raiteri@to.astro.it
Massimo Villata - villata@to.astro.it
Luciano Lanteri - lanteri@to.astro.it
Stefania Crapanzano - crapanzano@to.astro.it
Nicola Marchili – marchili@fisica.unipg.it
Gino Tosti - Gino.Tosti@fisica.unipg.it
Stefano Ciprini - stefano.ciprini@fisica.unipg.it
Andrea Tramacere - andrea.tramacere@fisica.unipg.it

Milano team:

Gabriele Ghisellini - gabriele@merate.mi.astro.it
Fabrizio Tavecchio - fabrizio@merate.mi.astro.it
Anna Wolter - anna@brera.mi.astro.it
Boris Sbarufatti - boris.sbarufatti@uninsubria.it

Athens team:

Apostolos Mastichiadis - amastich@phys.uoa.gr

Cork team:

Niall Smith - nsmith@cit.ie
M. John Howard - mjhoward@cit.ie

Photo of participants

Introduction by the Network Coordinator

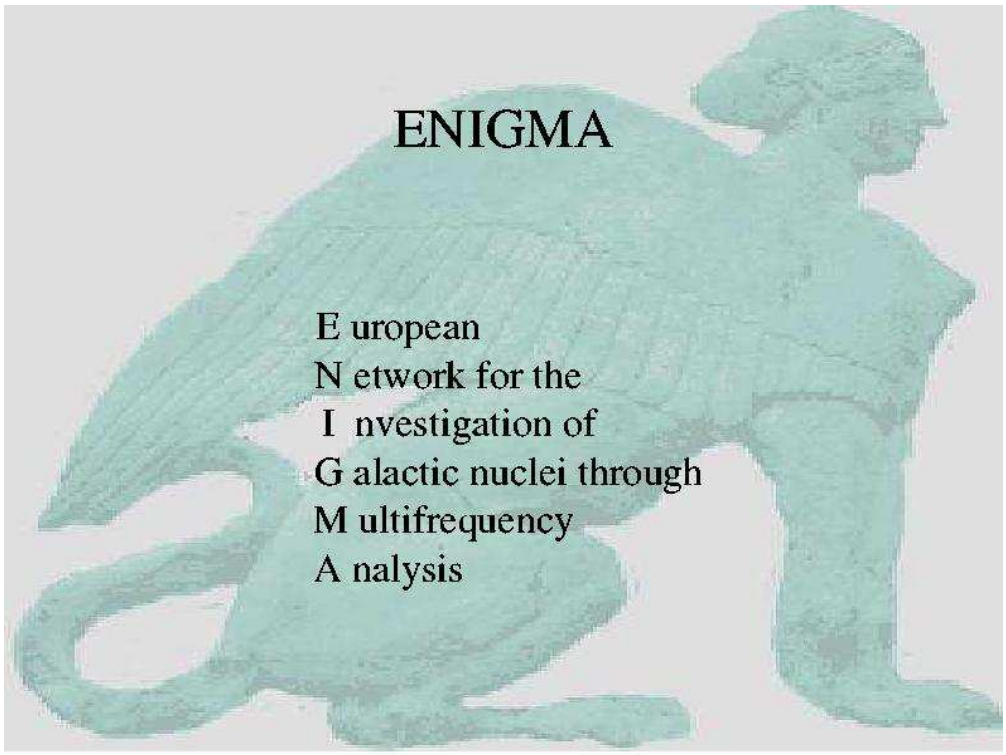
ENIGMA
E uropean
N etwork for the
I nvestigation of
G alactic nuclei through
M ultifrequency
A nalysis

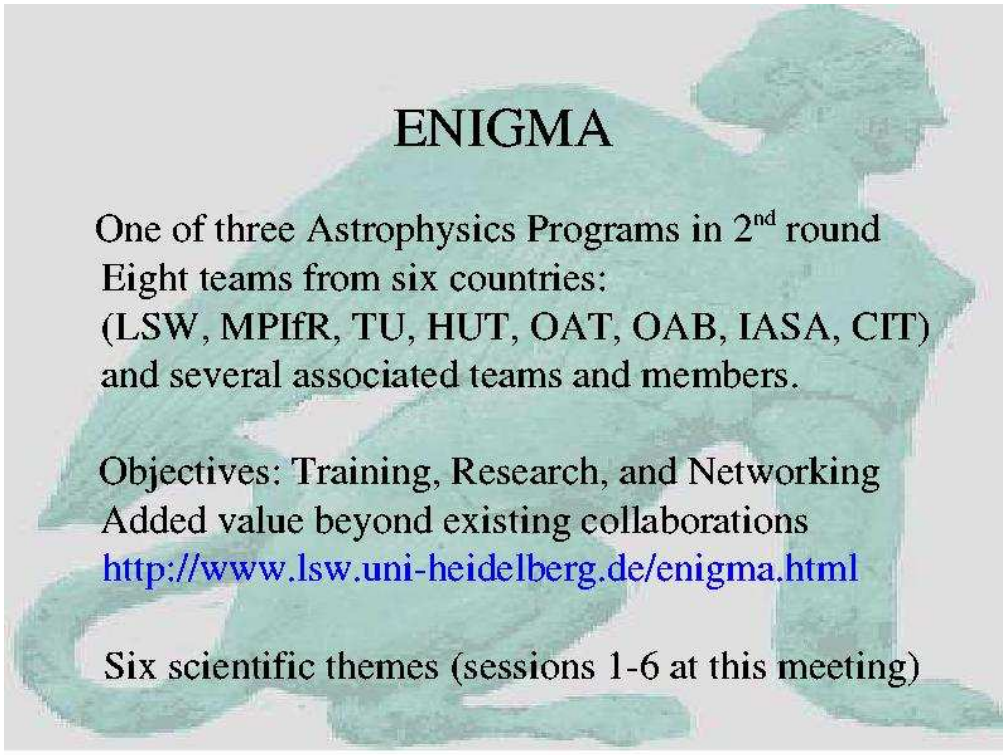
ENIGMA
One of three Astrophysics Programs in 2nd round
Eight teams from six countries:
(LSW, MPIfR, TU, HUT, OAT, OAB, IASA, CIT)
and several associated teams and members.
Objectives: Training, Research, and Networking
Added value beyond existing collaborations
http://www.lsw.uni-heidelberg.de/enigma.html
Six scientific themes (sessions 1-6 at this meeting)

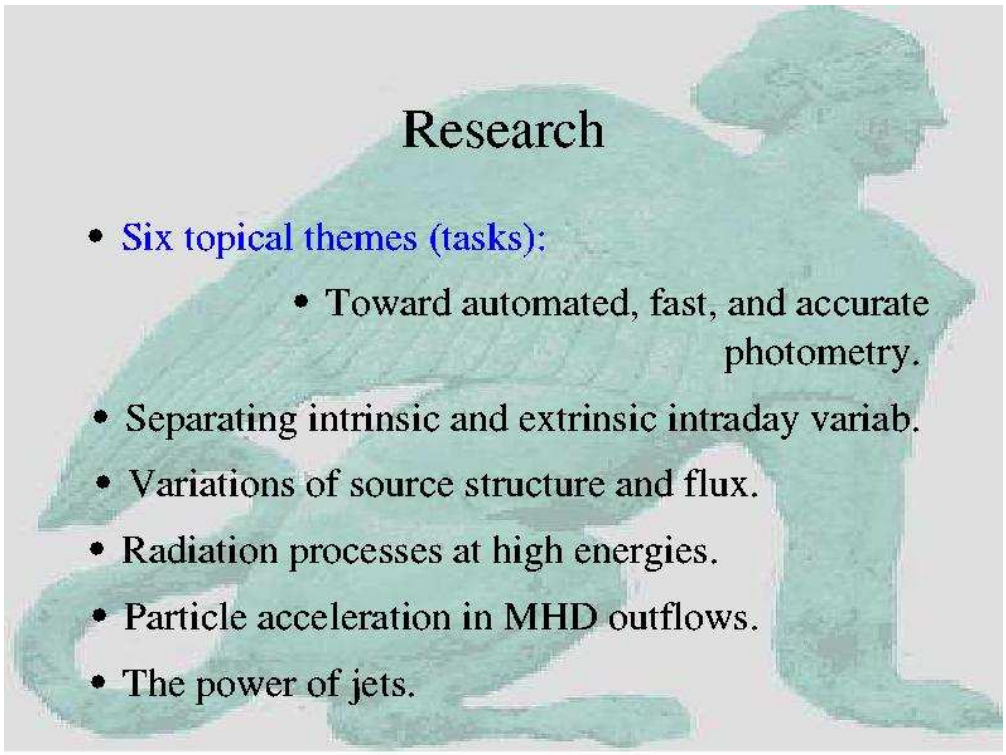
Research
• Six topical themes (tasks):
• Toward automated, fast, and accurate photometry.
• Separating intrinsic and extrinsic intraday variab.
• Variations of source structure and flux.
• Radiation processes at high energies.
• Particle acceleration in MHD outflows.
• The power of jets.

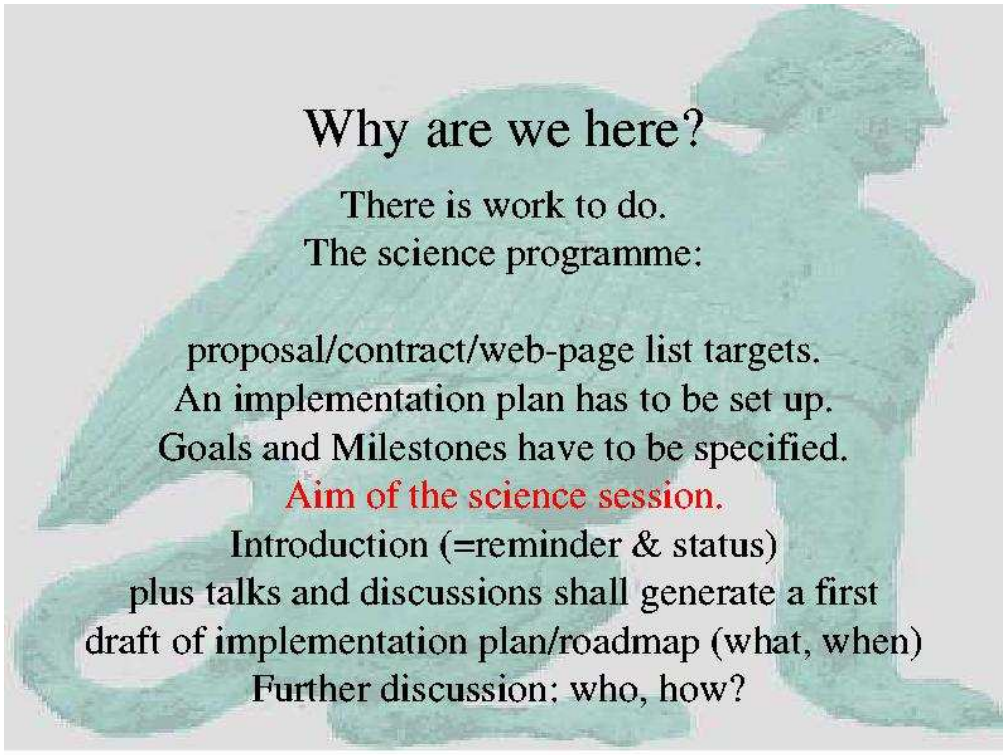
Why are we here?
There is work to do.
The science programme:
proposal/contract/web-page list targets.
An implementation plan has to be set up.
Goals and Milestones have to be specified.
Aim of the science session.
Introduction (=reminder & status)
plus talks and discussions shall generate a first
draft of implementation plan/roadmap (what, when)
Further discussion: who, how?

Additional action items:

- Young Researchers' session
- Monday morning (closed session).
- Team leaders session (closed session)
- Past, ongoing, and future campaigns (free format discussions of the first 3 completed projects, two ongoing campaigns, and several forthcoming activities. Other suggestions?)
- 3rd ENIGMA meeting, 1st ENIGMA school

General information

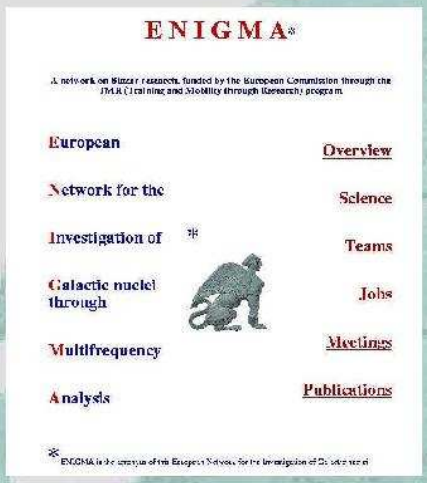

- WWW
  http://www.lsw.uni-heidelberg.de/enigma.html
- Linked pages:
  enigmavac.html
  enigmasci.html
- Comments, corrections, and additions welcome.
- On-line editing at this meeting

Session I: Towards automated, fast, and accurate photometry

Task 1. Towards automated, fast, and accurate photometry – N. Smith

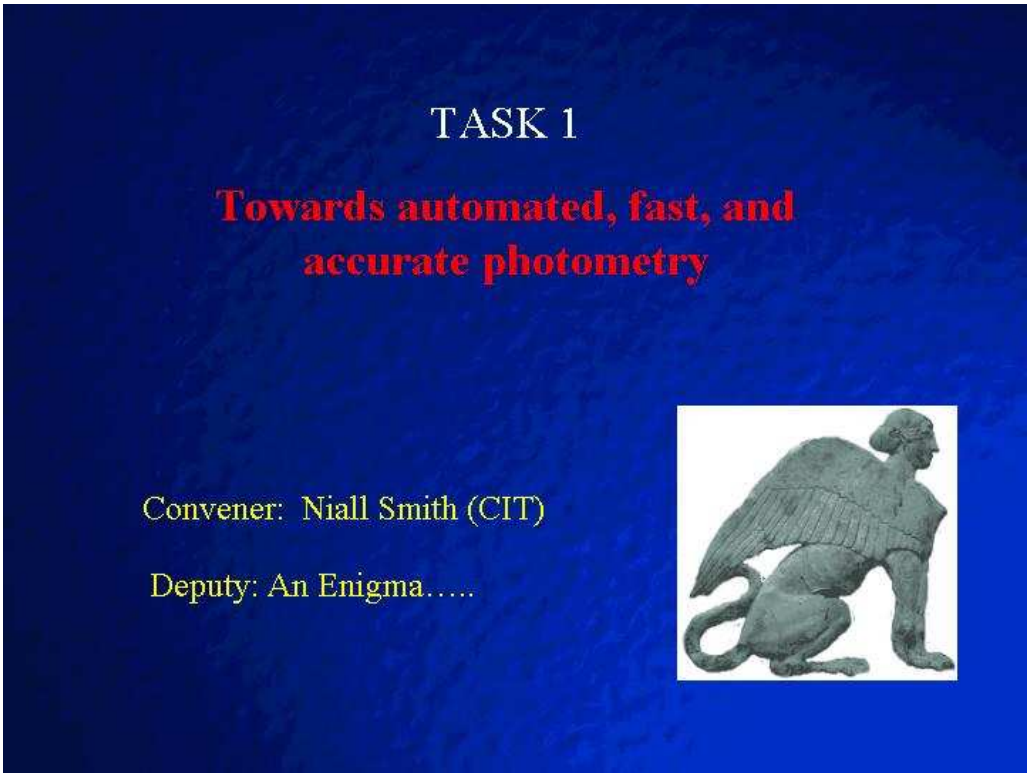

Original Proposal Statement

Currently most optical monitoring programs are run by observers specifying individual exposures, achieving accuracies of about 1% with sampling times of a few 100 to 10 000 sec.

In order to improve the quality and quantity of optical monitoring, the network aims at determining a better understanding of the parameters that affect the quality of the photometry of point sources in differential photometry and implementing programs that allow measurements with accuracies close to the photon flux limit.

In parallel it aims at an assessment of the technological requirements for robotic telescopes and practical implementation of a network of robotic telescopes that shall be operated by several teams of the network.

A Second "Big-Bang" Is Coming…

Do WE have a plan???

ENIGMA network has much expertise in photometry already

- WEBT
- Perugia Monitoring Programme
- Tuorla
- Abastumani Programme
- Heidelberg
- Cork

How do we distribute the knowledge?

How do network groups reduce their data currently?

Questions!

How do we reach the photon limit on photometric precision?

What are the factors that currently cause the limitations?

- flatfielding
- guiding
- undersampled psf's
- seeing (changes)
- CCD non-linearity
- focus shifts
- intra-pixel variations
- cosmic rays

Questions!

Simple example:

If stellar image covers 10 pixels on CCD with a well depth of 350,000 electrons

then

total electron count is 3,500,000

yielding

photometric error of 0.58mmag (~0.06%)

Systematics deriving Johnson magnitudes between observers

More questions!

How do we perform precision photometry on AGN with resolved hosts (e.g., the TeV emitters)?

How do we prepare for high-time resolution photometry and the Gbytes of data generated every night?

What should be the priority targets for monitoring campaigns

well-established sources ?
new sources (e.g., RASS-FIRST sources) ?

New approaches to pipelining – e.g., neural networks


Yet more questions
What is the best role for small, robotic telescopes
off-the-shelf commercial instruments up to 60cm ?
upgrades to existing instruments (e.g., KVA)
How do we coordinate a network of robotic telescopes?
Can it be achieved dynamically?
How might we fund instrument development within the ENIGMA network?

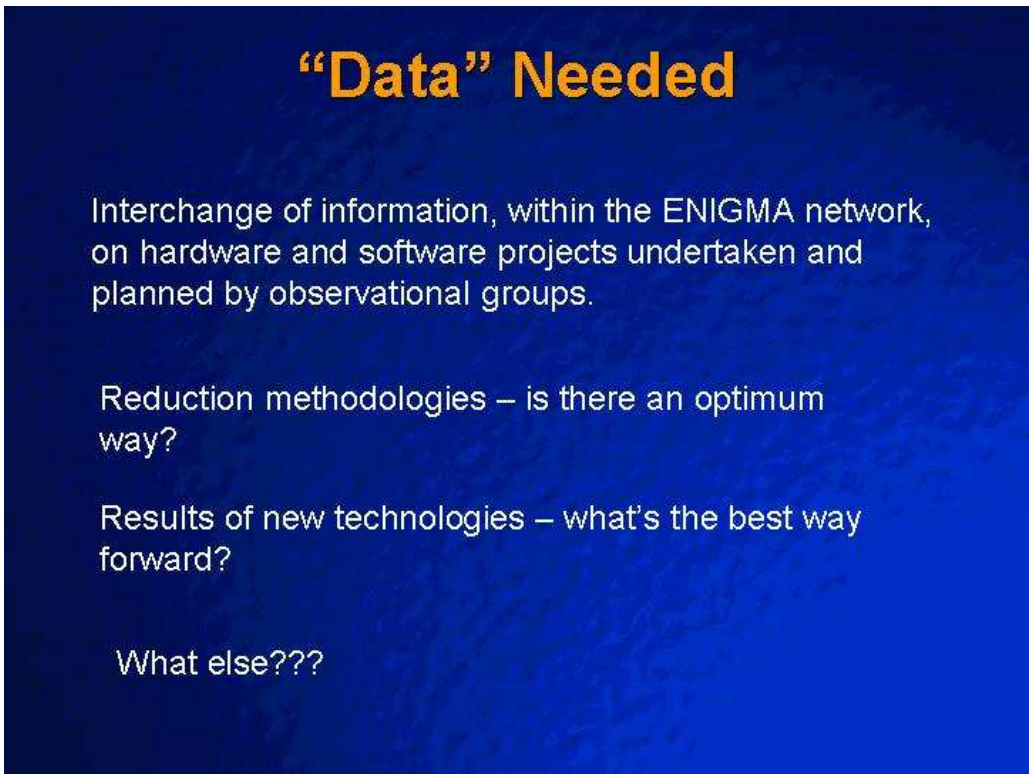
"Data" Needed
Interchange of information, within the ENIGMA network, on hardware and software projects undertaken and planned by observational groups.
Reduction methodologies – is there an optimum way?
Results of new technologies – what's the best way forward?
What else???

- Automatic management of data from robotic telescopes will become the norm.

Are WE Ready?

Milestones

1a: A better understanding of the parameters that affect the quality of differential photometry of point sources

1b: Implementation of programs that allow measurements close to the photon flux limit (or as close as modern CCD technology allows)

1c: Assessment of the technical requirements for robotic telescopes

1d: Practical implementation of a network of robotic telescopes operated by members of the network

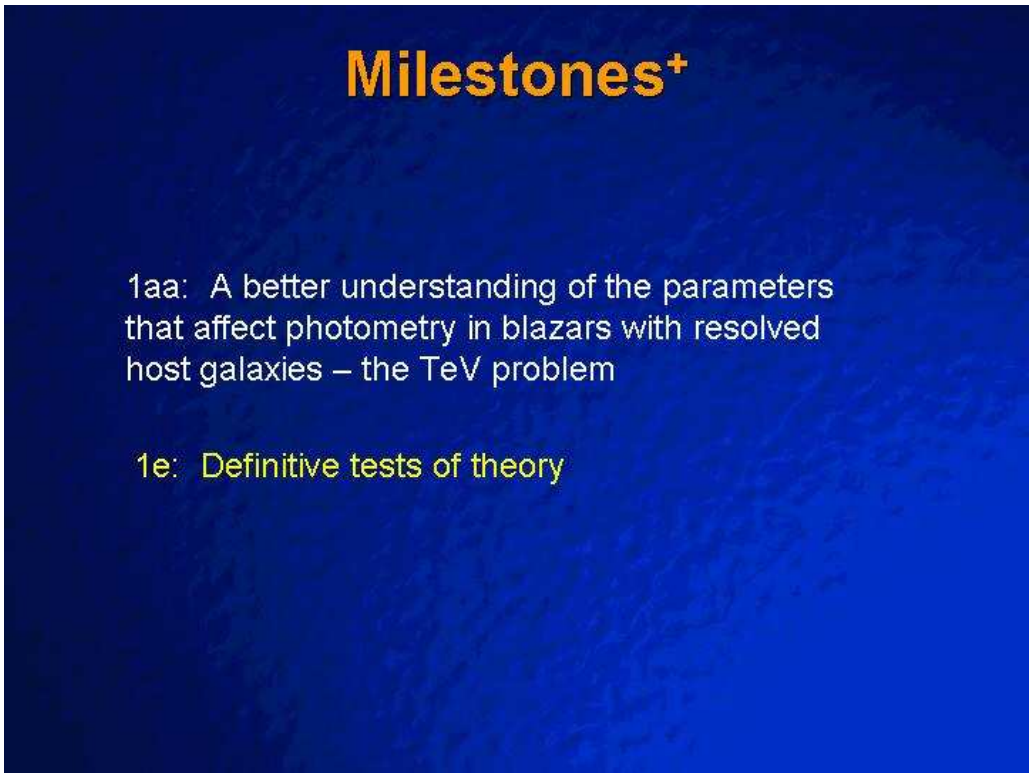
Milestones+
1aa: A better understanding of the parameters that affect photometry in blazars with resolved host galaxies – the TeV problem
1e: Definitive tests of theory

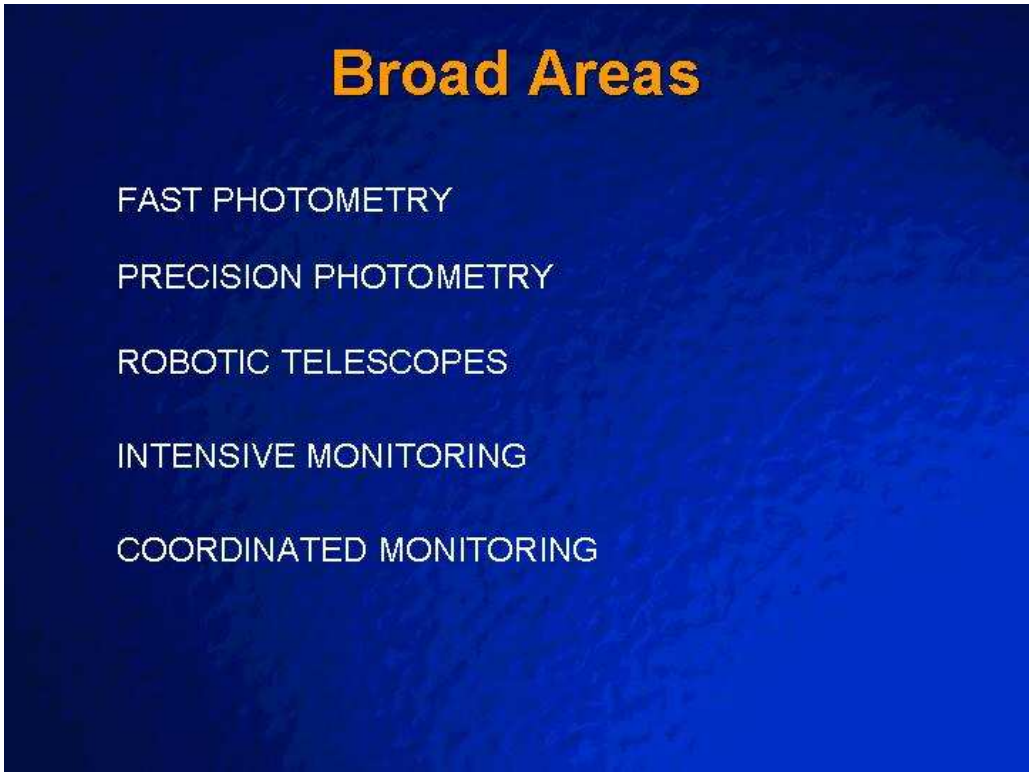
Broad Areas
FAST PHOTOMETRY
PRECISION PHOTOMETRY
ROBOTIC TELESCOPES
INTENSIVE MONITORING
COORDINATED MONITORING

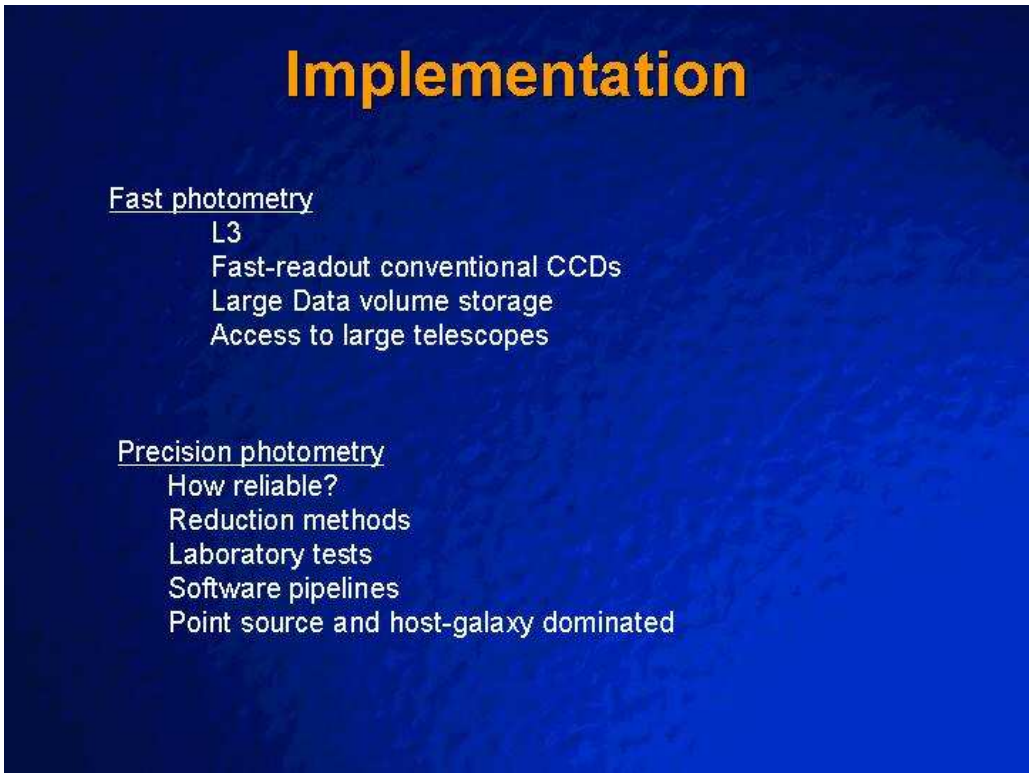
Implementation
Fast photometry
L3
Fast-readout conventional CCDs
Large Data volume storage
Access to large telescopes
Precision photometry
How reliable?
Reduction methods
Laboratory tests
Software pipelines
Point source and host-galaxy dominated

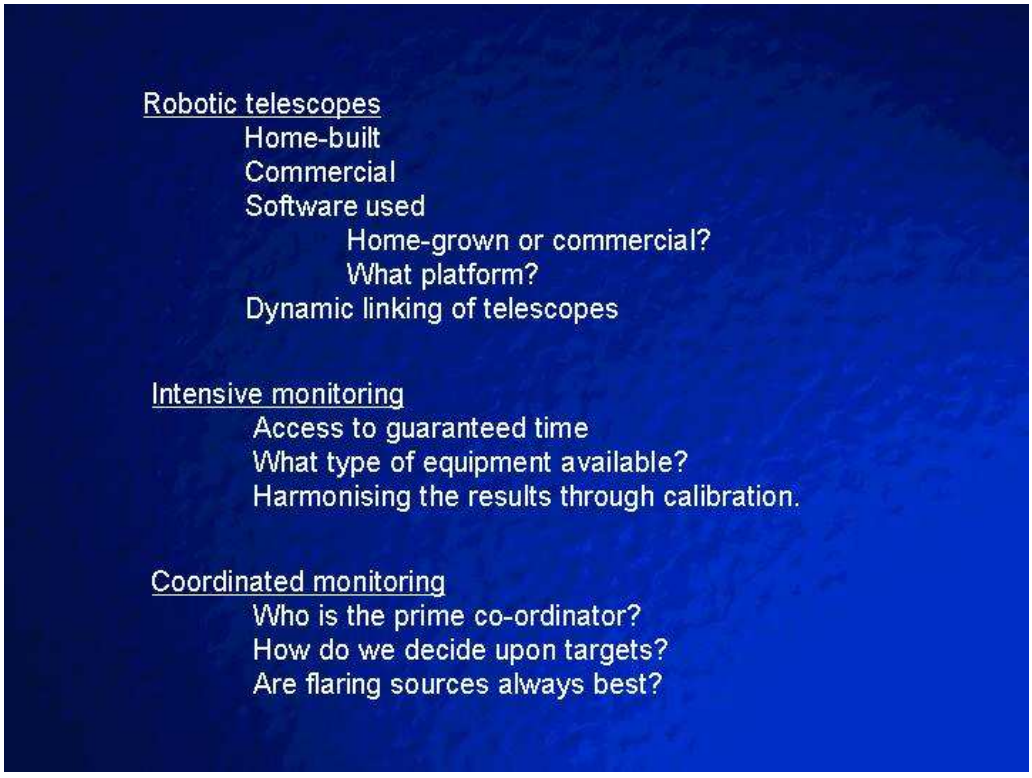
Robotic telescopes
Home-built
Commercial
Software used
Home-grown or commercial?
What platform?
Dynamic linking of telescopes
Intensive monitoring
Access to guaranteed time
What type of equipment available?
Harmonising the results through calibration.
Coordinated monitoring
Who is the prime co-ordinator?
How do we decide upon targets?
Are flaring sources always best?

Observations of blazars using EMCCD technology – N. Smith, A. O'Connor, J. Howard, A. Giltinan, S. O'Driscoll, S. Wagner, M. Hauser

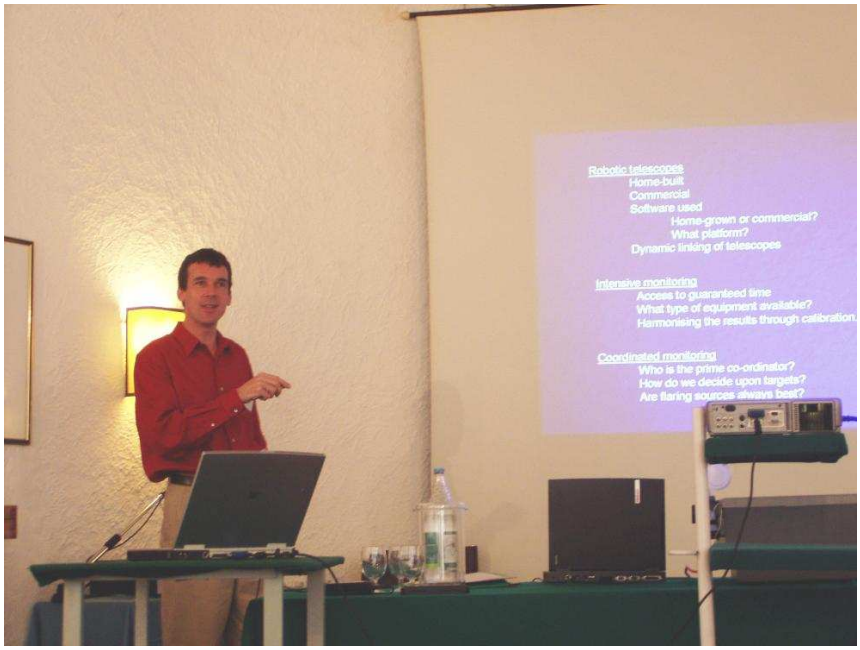

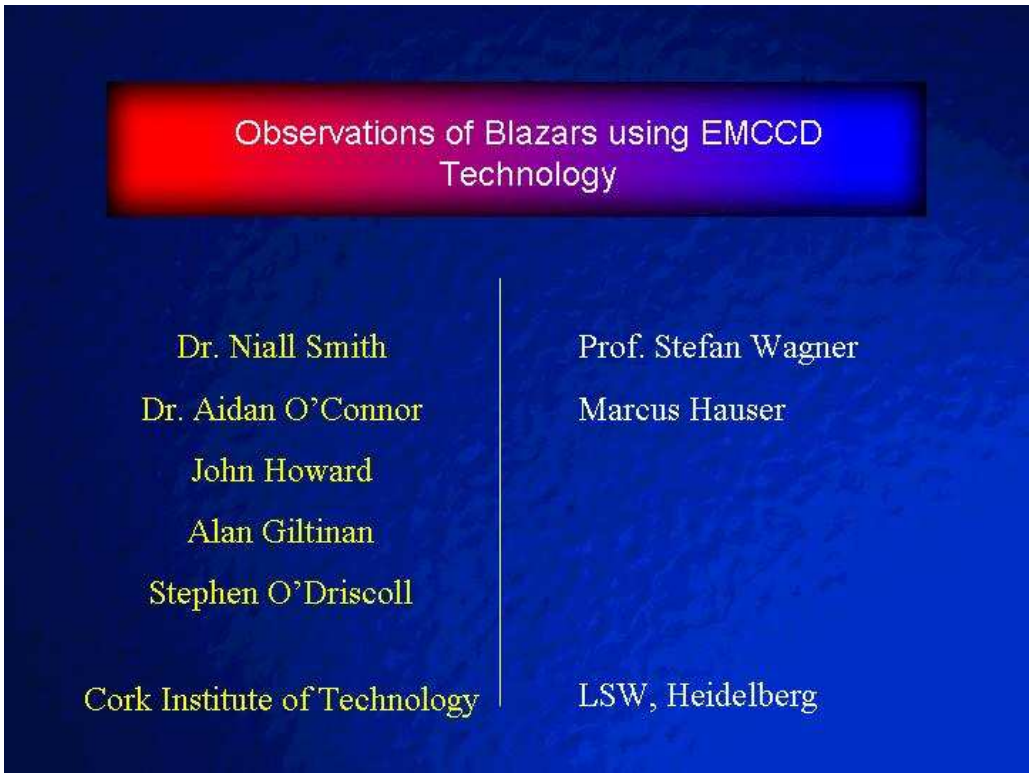

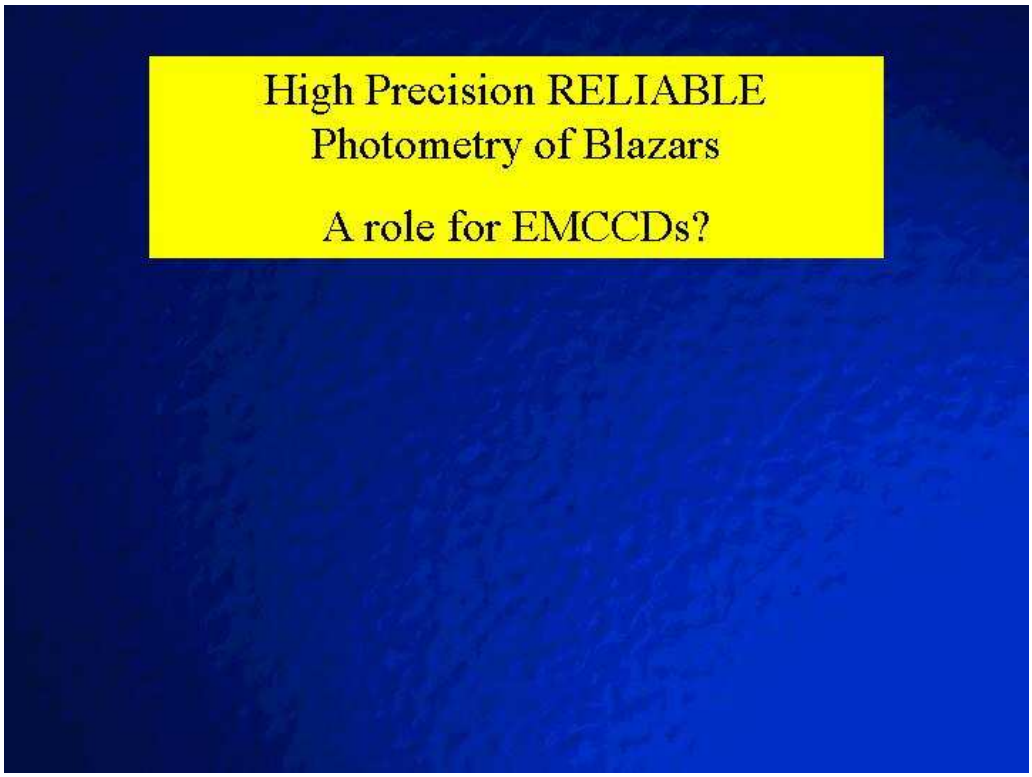
High Precision RELIABLE
Photometry of Blazars
A role for EMCCDs?

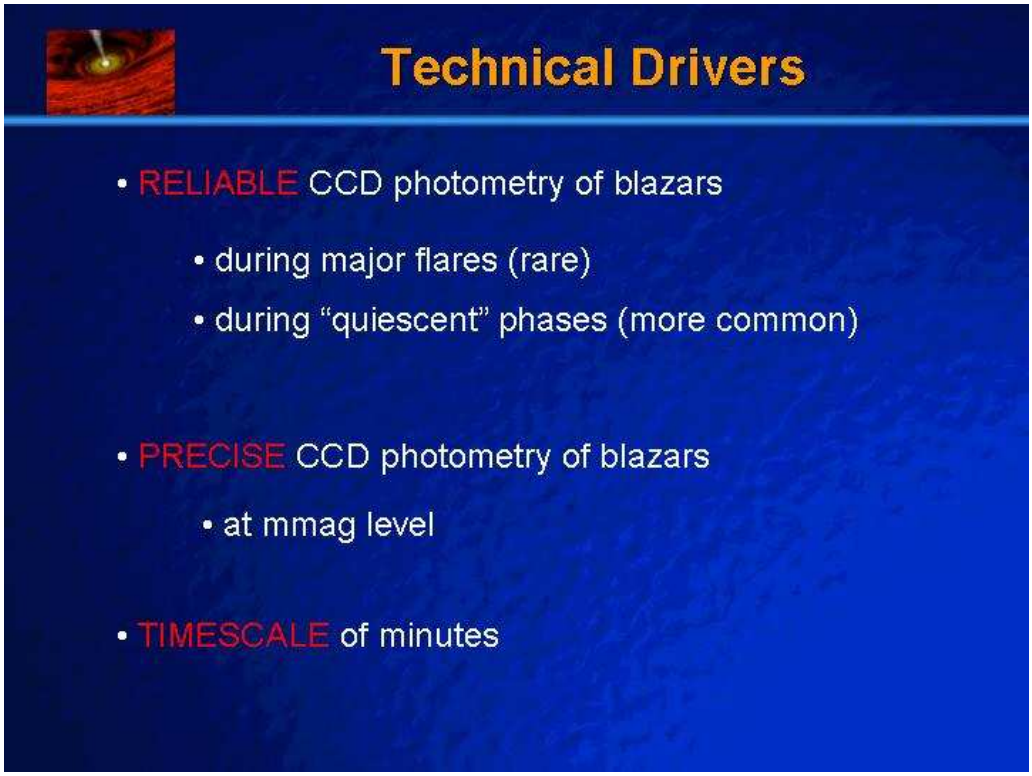
Technical Drivers
• RELIABLE CCD photometry of blazars
• during major flares (rare)
• during "quiescent" phases (more common)
• PRECISE CCD photometry of blazars
• at mmag level
• TIMESCALE of minutes

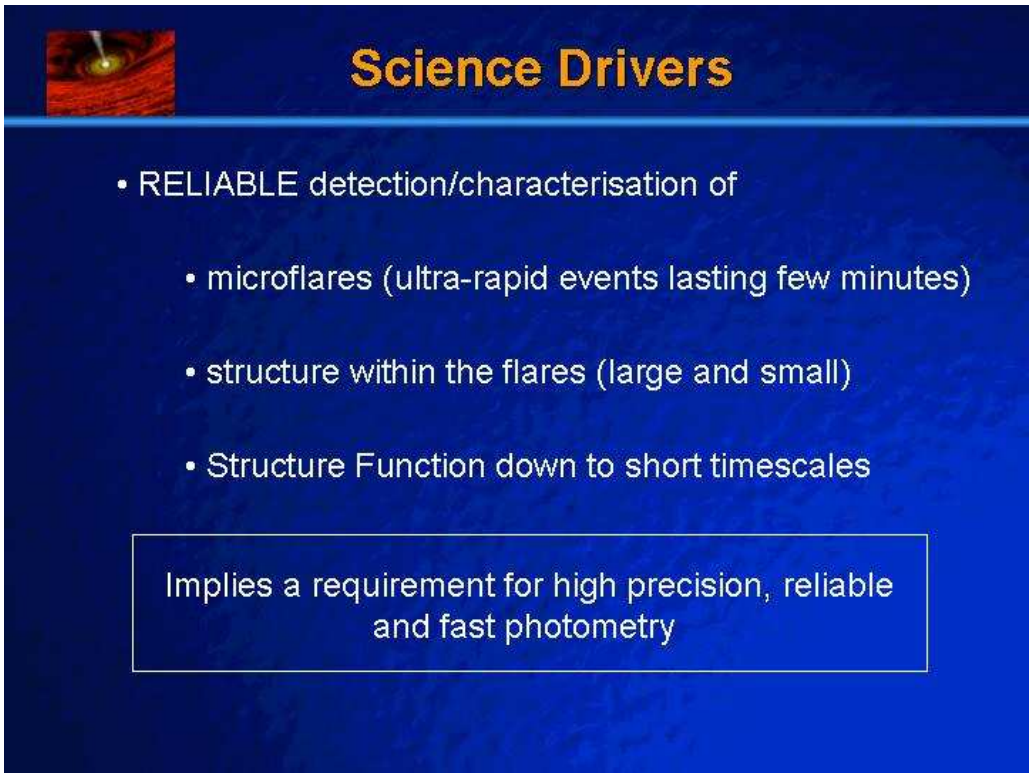
Science Drivers
• RELIABLE detection/characterisation of
• microflares (ultra-rapid events lasting few minutes)
• structure within the flares (large and small)
• Structure Function down to short timescales
Implies a requirement for high precision, reliable and fast photometry

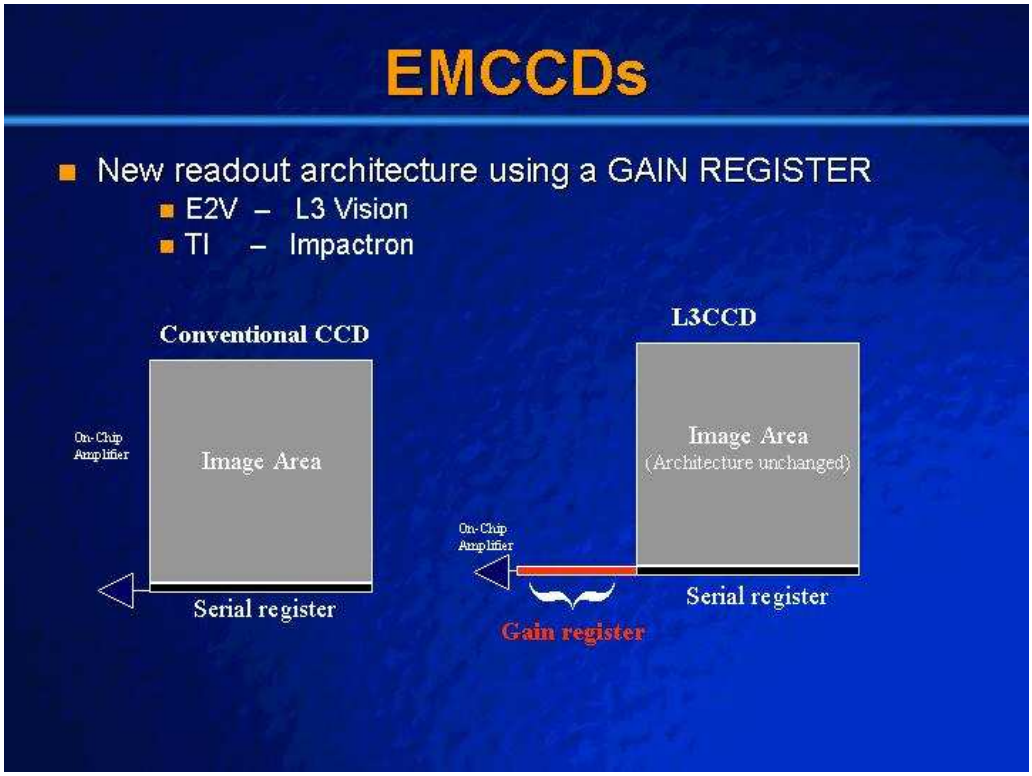
EMCCDs
New readout architecture using a GAIN REGISTER
E2V – L3 Vision
TI – Impactron
Conventional CCD
On-Chip Amplifier
Image Area
Serial register
L3CCD
Image Area
(Architecture unchanged)
On-Chip Amplifier
Serial register
Gain register

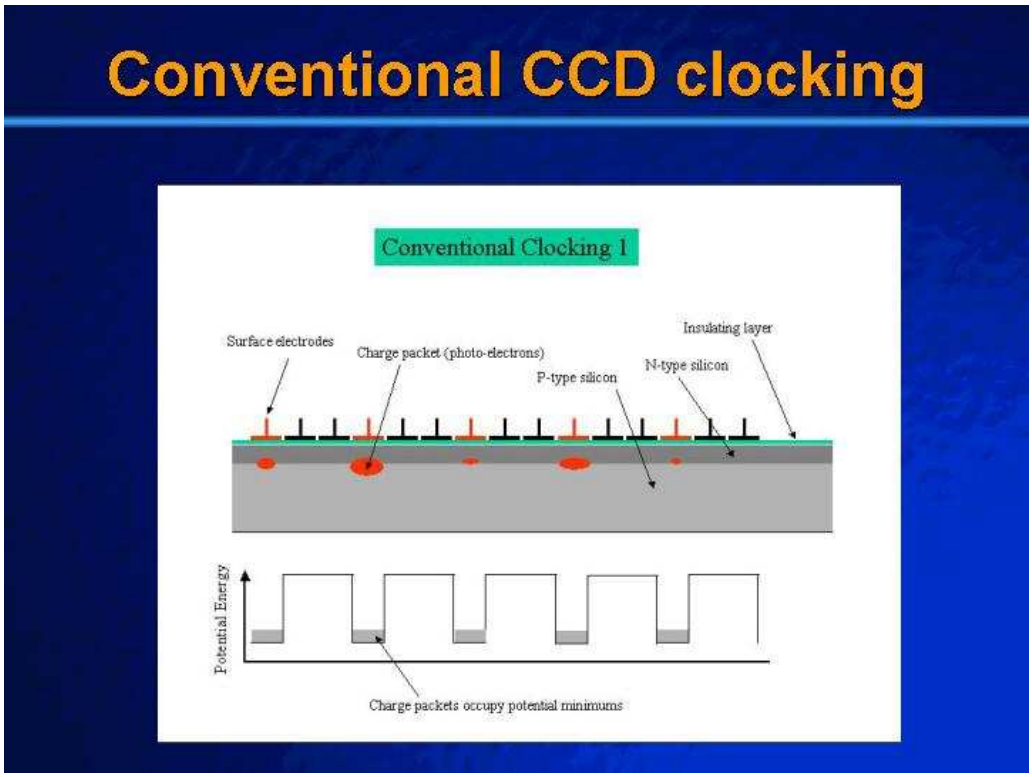
Conventional CCD clocking
Conventional Clocking 1
Surface electrodes
Charge packet (photo-electrons)
P-type silicon
N-type silicon
Insulating layer
Potential Energy
Charge packets occupy potential minimums

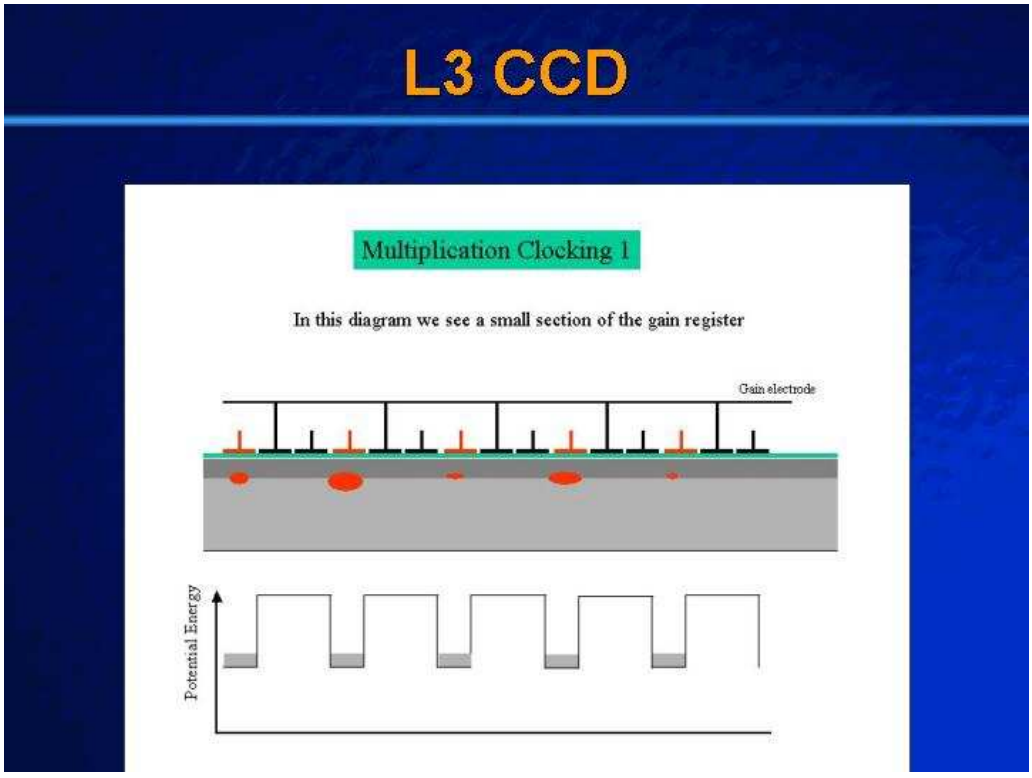
L3 CCD
Multiplication Clocking 1
In this diagram we see a small section of the gain register
Gain electrode
Potential Energy


SNR for Conventional CCD
Conventional CCD SNR Equation
SNR = Q.I.t.[Q.t.(I +B_SKY) +N_r^2]^-0.5
Q = Quantum Efficiency
I = Photons per pixel per second
t = Integration time in seconds
B_SKY = Sky background in photons per pixel per second
N_r = Amplifier (read-out) noise in electrons RMS
Trade-off between readout speed and readout noise

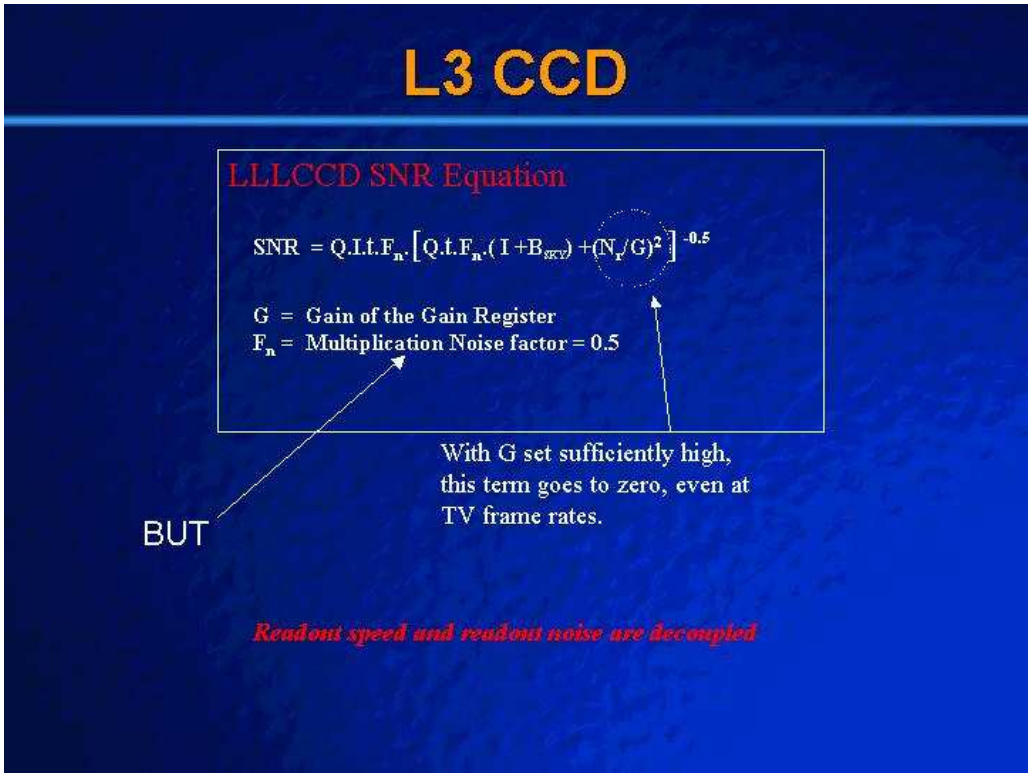
L3 CCD
LLLCCD SNR Equation
SNR = Q.I.t.F_n.[Q.t.F_n.(I +B_SKY) +(N_r/G)^2]^-0.5
G = Gain of the Gain Register
F_n = Multiplication Noise factor = 0.5
With G set sufficiently high,
this term goes to zero, even at
TV frame rates.
BUT
Readout speed and readout noise are decoupled

L3 CCD

- L3 CCDs are most effective when used under low-light levels
  - photon counting (small telescopes)
  - high time resolution (big telescopes)
- L3 CCDs are outperformed by conventional CCDs at "high" light levels

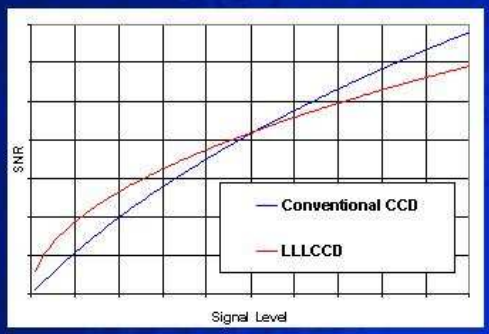

L3 ENIGMA Campaign

DV887A (Andor Technology)

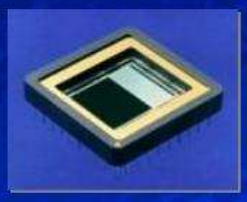

- 512x512 pixels, 16μm/pixel
- Well depth ~250,000 e^-
- Readout noise 30 at G=1
  ≤1 at G=200!
- 10MHz readout rate @ 14 bit resolution
- 1MHz readout rate @ 16 bit resolution
- Two-stage thermoelectric cooling to –75 ^{0}C

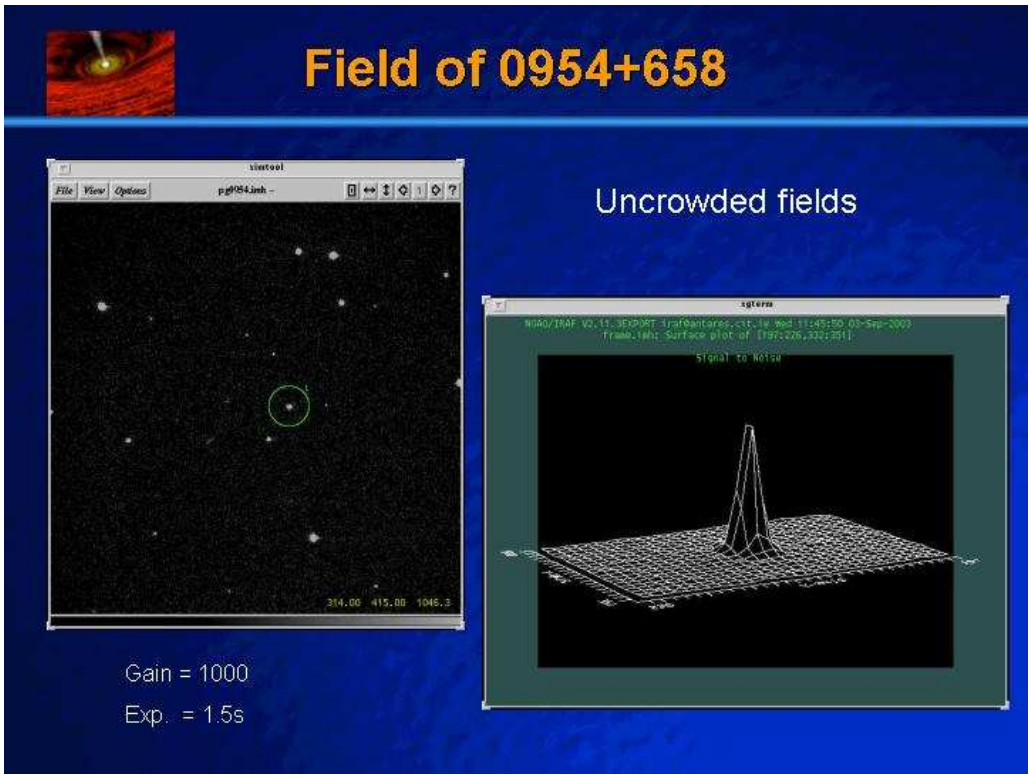
Field of 0954+658
Uncrowded fields
Gain = 1000
Exp. = 1.5s

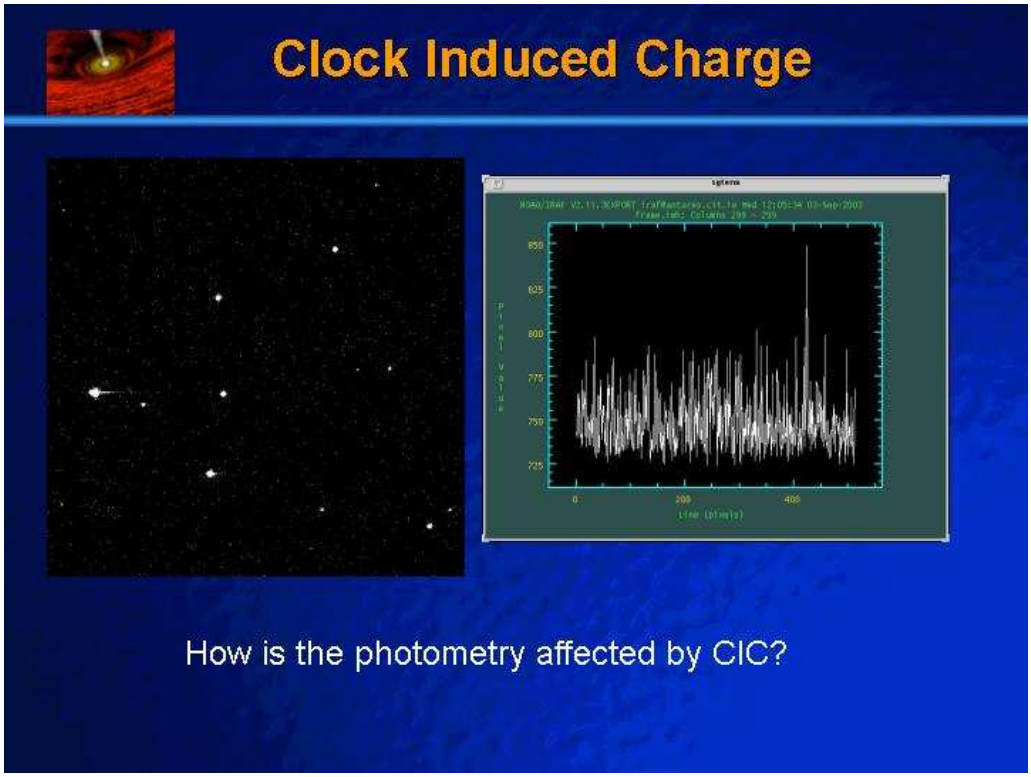
Clock Induced Charge
How is the photometry affected by CIC?

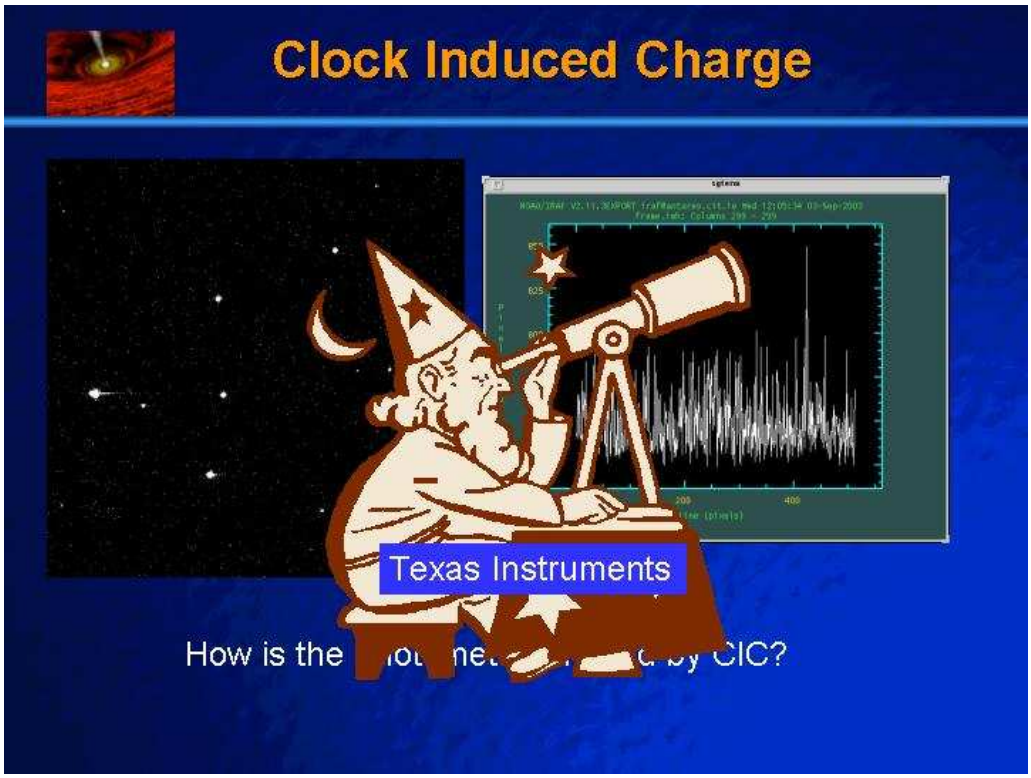
Clock Induced Charge
Texas Instruments
How is the

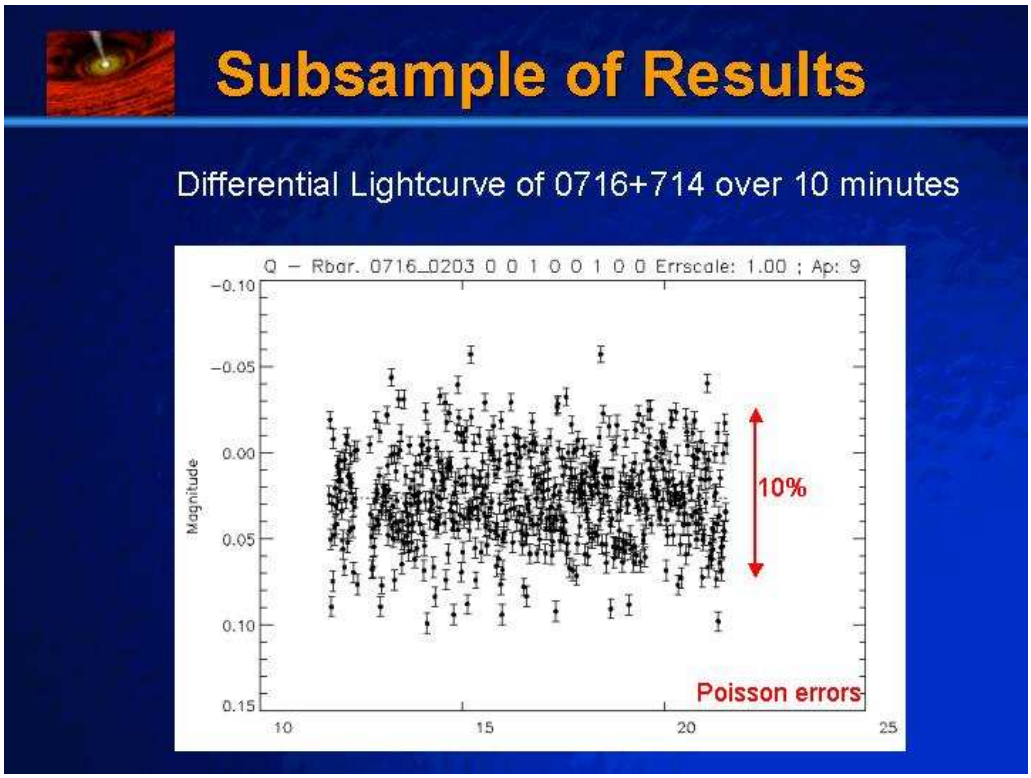
Subsample of Results
Differential Lightcurve of 0716+714 over 10 minutes
Q – Rbar. 0716_0203 0 0 1 0 0 1 0 0 Errscale: 1.00 ; Ap: 9
Magnitude
10%
Poisson errors

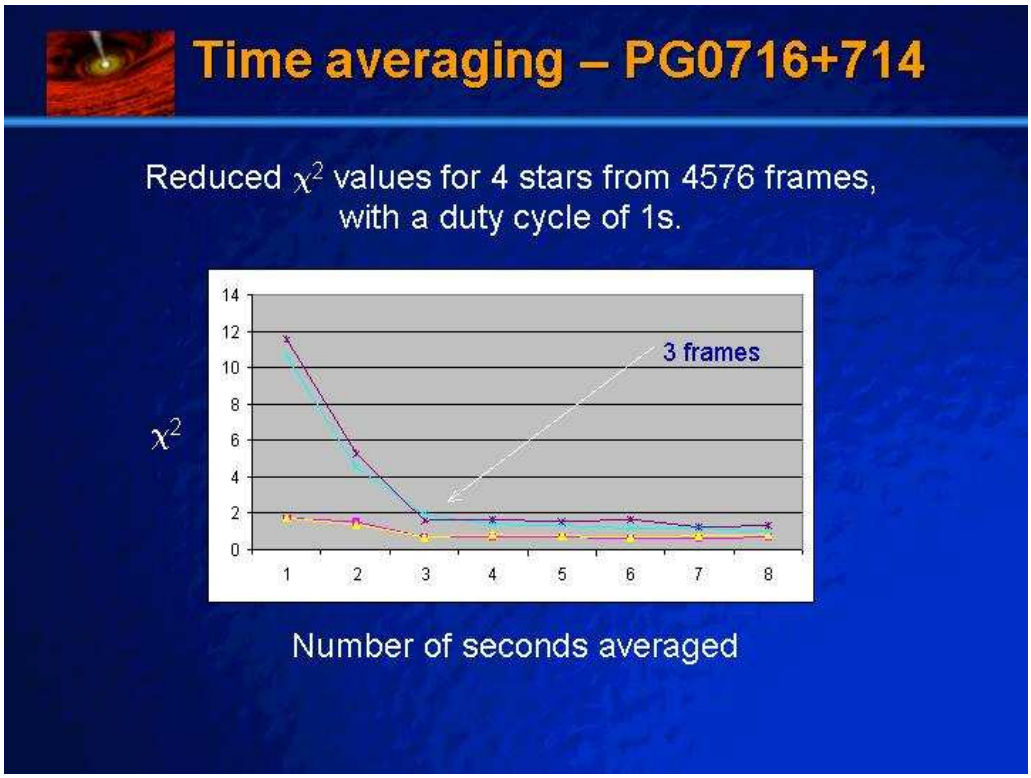
Time averaging – PG0716+714
Reduced χ^2 values for 4 stars from 4576 frames, with a duty cycle of 1s.
3 frames
χ^2
Number of seconds averaged

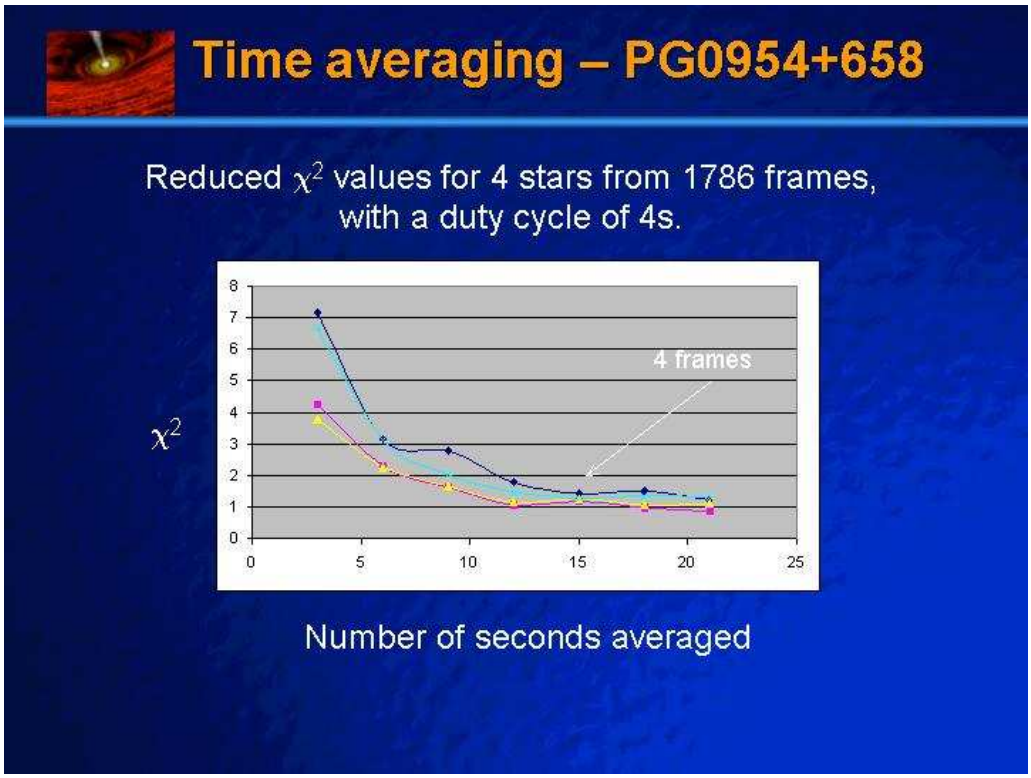
Time averaging – PG0954+658
Reduced χ^2 values for 4 stars from 1786 frames, with a duty cycle of 4s.
4 frames
χ^2
Number of seconds averaged

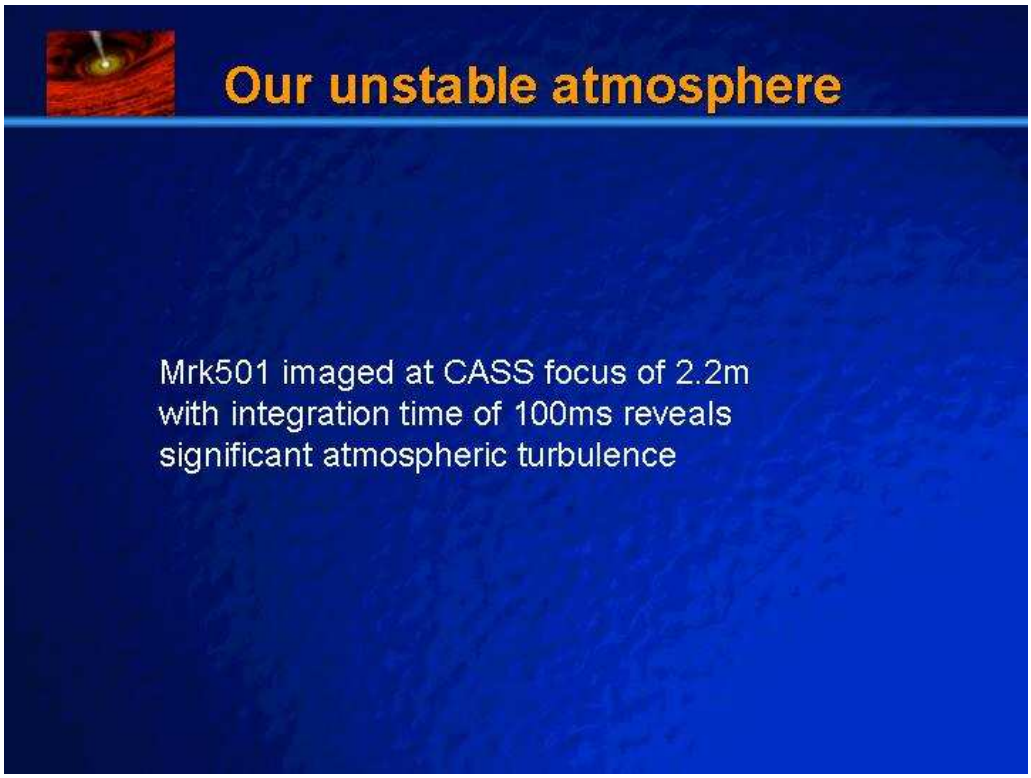
Our unstable atmosphere
Mrk501 imaged at CASS focus of 2.2m
with integration time of 100ms reveals
significant atmospheric turbulence

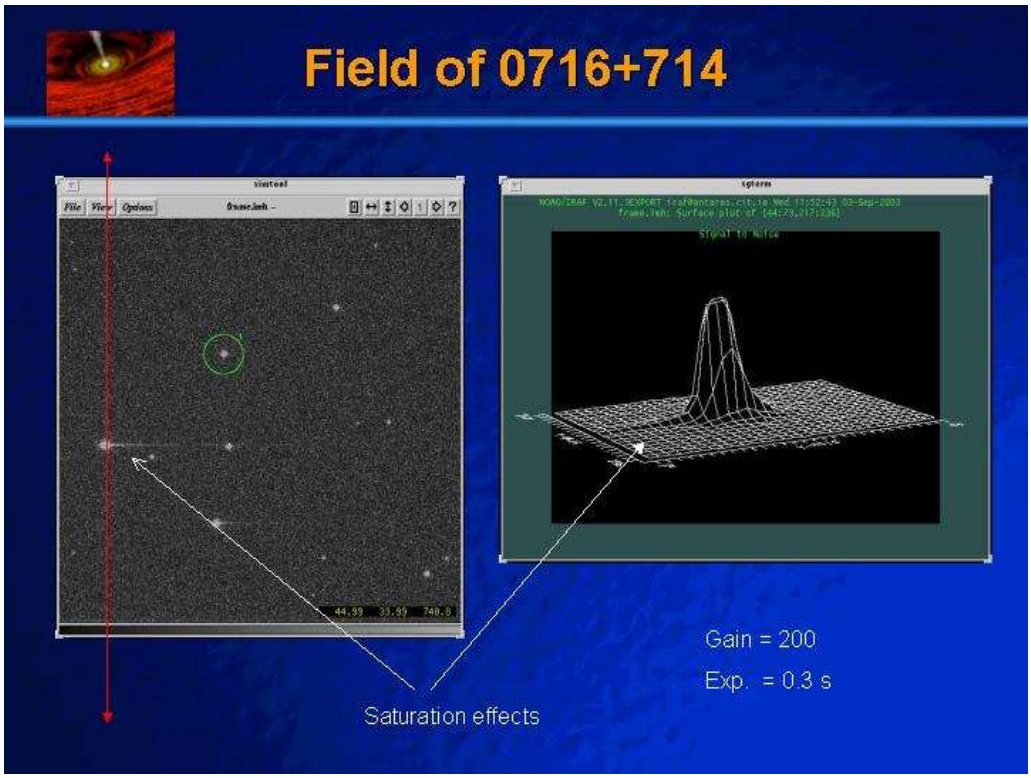
Field of 0716+714
Gain = 200
Exp. = 0.3 s
Saturation effects

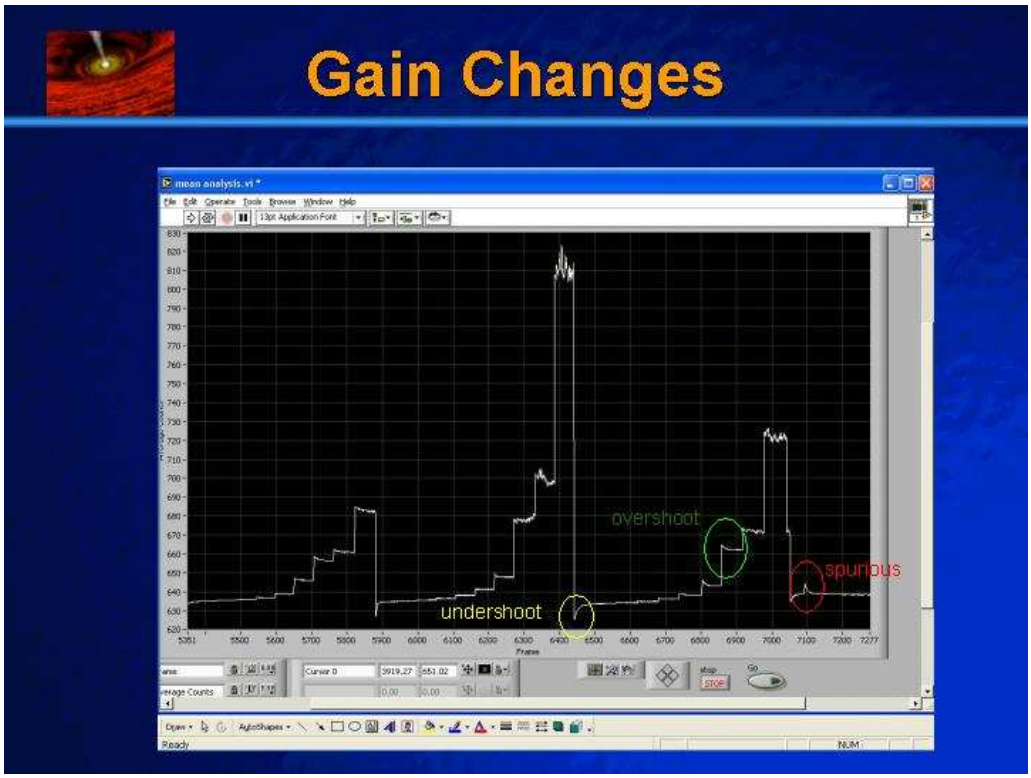
Gain Changes
overshoot
spurious
undershoot

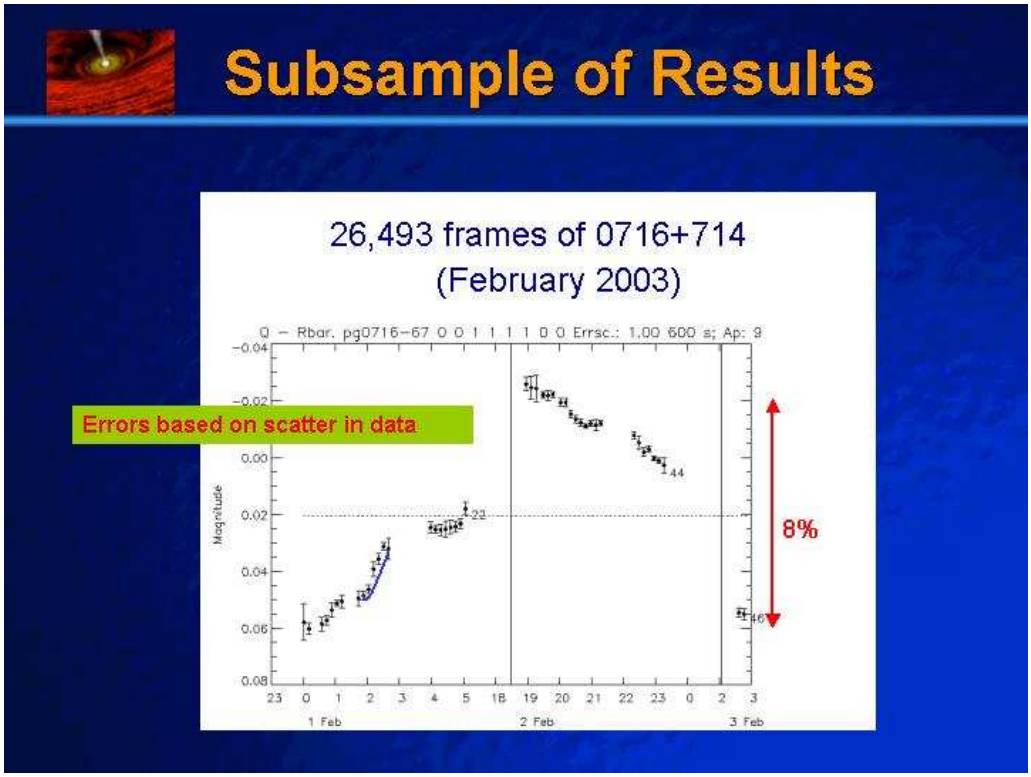
Subsample of Results
26,493 frames of 0716+714
(February 2003)
Errors based on scatter in data
8%
Magnitude
1 Feb
2 Feb
3 Feb

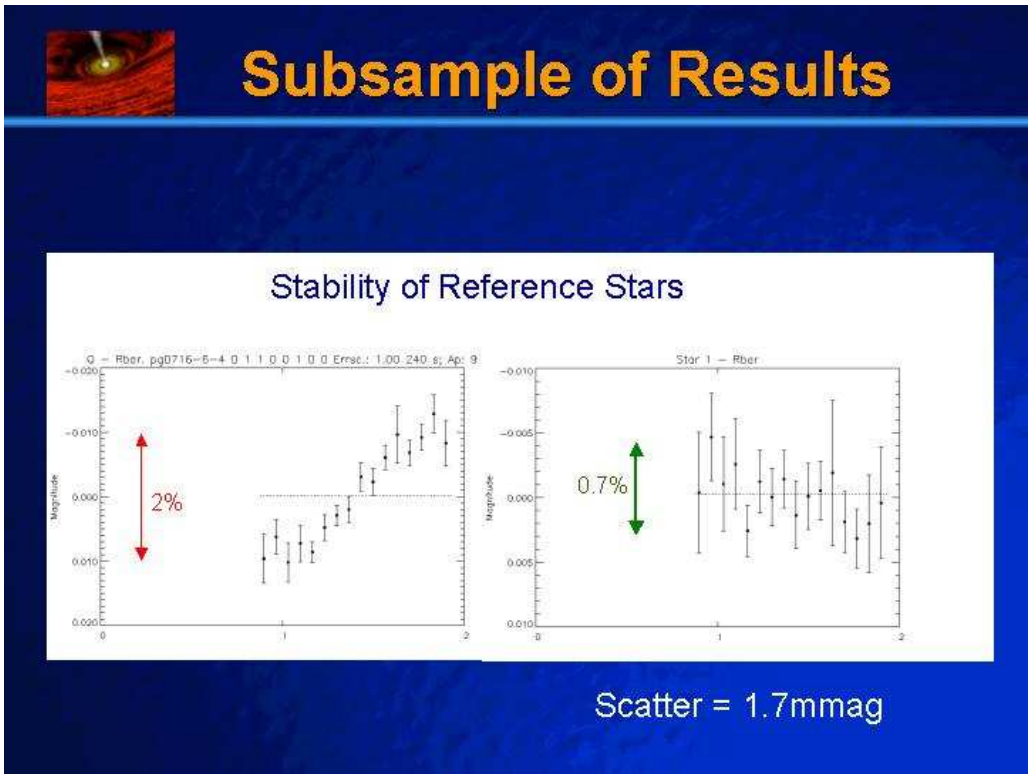
Subsample of Results
Stability of Reference Stars
2%
0.7%
Scatter = 1.7mmag

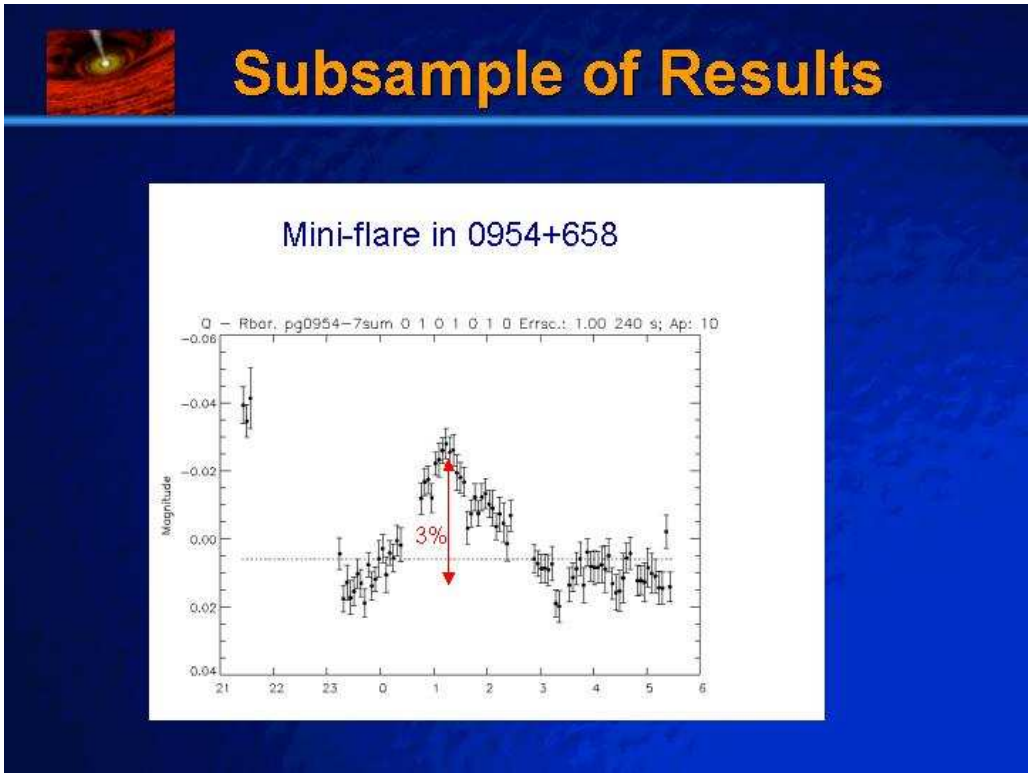
Subsample of Results
Mini-flare in 0954+658
3%

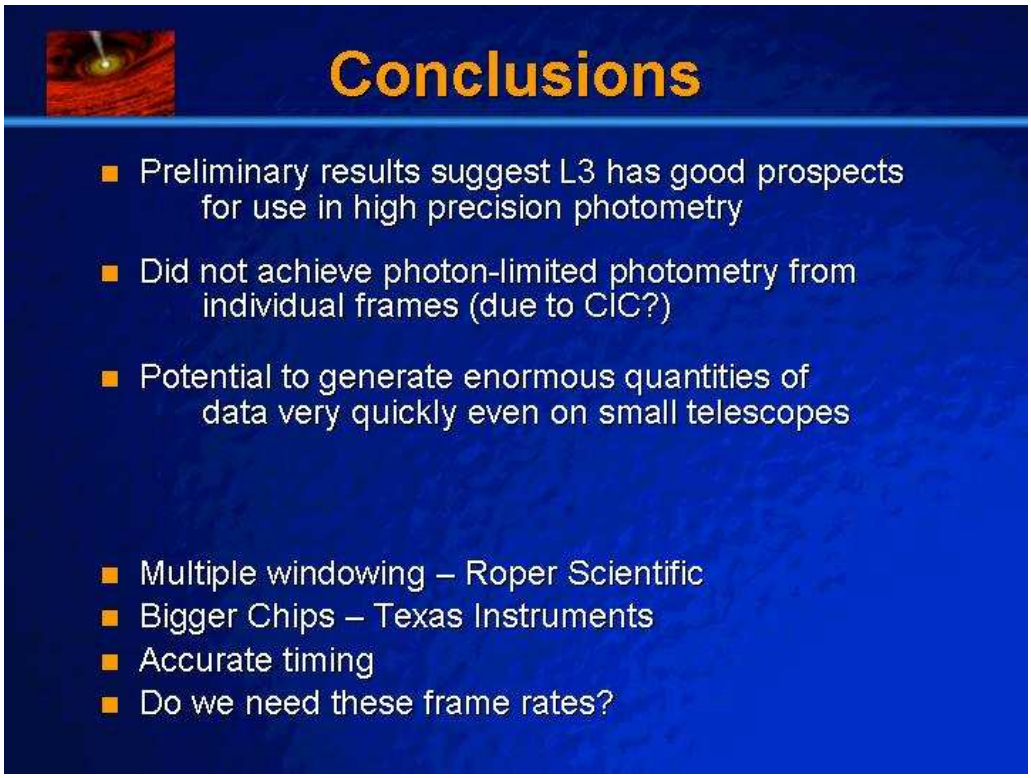
Conclusions
Preliminary results suggest L3 has good prospects for use in high precision photometry
Did not achieve photon-limited photometry from individual frames (due to CIC?)
Potential to generate enormous quantities of data very quickly even on small telescopes
Multiple windowing – Roper Scientific
Bigger Chips – Texas Instruments
Accurate timing
Do we need these frame rates?

Optical & radio analysis of radio intermediate quasar – PG 1718+481

– M. J. Howard

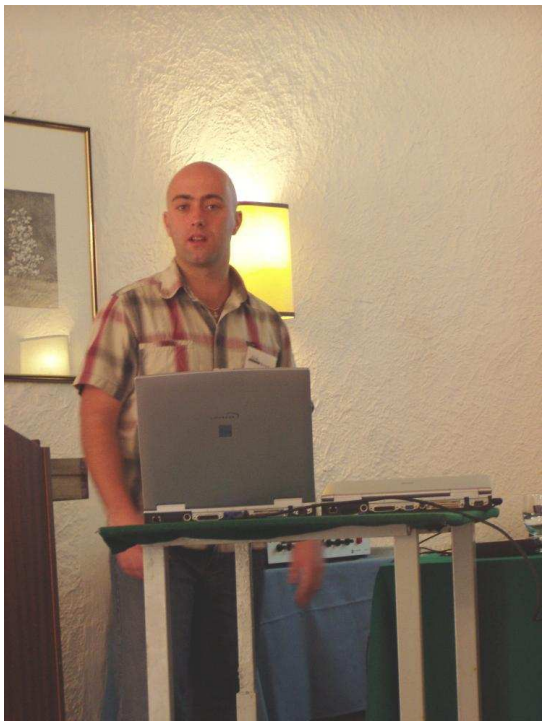

EMSSG
Environmental Monitoring & Space Science Group

Optical & Radio analysis of Radio Intermediate Quasar – PG1718+481

Enigma Meeting – Portovenere, Italy 2003

M. John Howard,
Environmental Monitoring & Space Science Group,
Cork Institute of Technology.
IRELAND

Research Partners:
Landessternwarte, Heidelberg, Germany
University College Cork
University College Dublin

EMSSG
Environmental Monitoring & Space Science Group

Overview

- Quasars (Intermediate) - what are they and why do we investigate them?
- Acquiring data and the reduction steps
- Optical Light Curves
- Radio Map of PG1718+481
- Conclusion

EMSSG
Environmental Monitoring & Space Science Group

1 - What is a Radio Intermediate Quasar (RIQ)?

- Loud Quasar - down throat of jet - highly energetic - high amplitude variability in optical
- Quiet Quasar - no jet
- Intermediate Quasar - At best low amplitude variability expected
- Hence, reason for high precision photometry
- Weak optical Jet or not???
- Possible answers to jet formation?

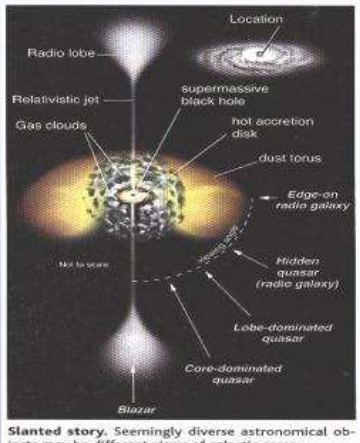

Slanted story. Seemingly diverse astronomical objects may be different views of galactic cores.

EMSSG
Environmental Monitoring & Space Science Group

- Radio luminosities of quasars form a bimodal distribution
  Radio Loud – highly energetic powerful jets –
  Radio Quiet – possible supernovae in a highly compact environment - (Terlevich et al., 1992)

- $10 < R < 250$

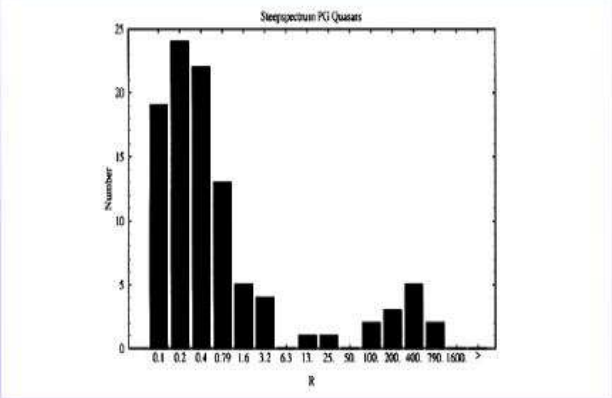

Falcke 1996

RQQ's with flat radio spectra – common for RLQ's with Jets

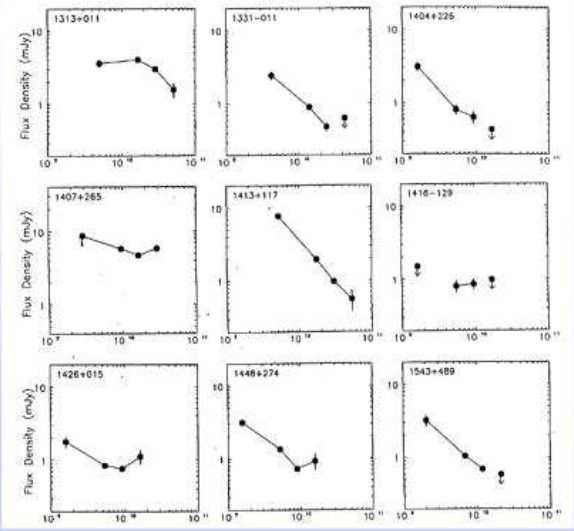

Barvainis 2000

EMSSG
Environmental Monitoring & Space Science Group

- Evidence for RIQ's
  - six RIQ's (Falcke et el., 1996 a,b)
  - relativistic boosting
  - Lorentz factors of 2-4
  - suggestive of low power jets
- IIIzw 2 (0007+106) – superluminal motion (Brunthaler et al., 2000)
- 3 objects – high brightness temp - ~10^{10} K & compact cores (EVN & Merlin)
- High brightness temp & compact cores appears to rule out starburst models…

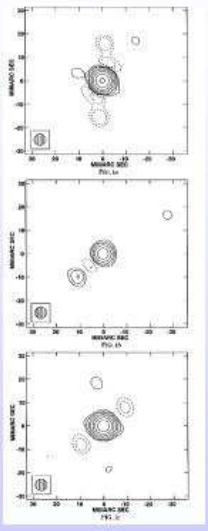

Falcke 2000

EMSSG
Environmental Monitoring & Space Science Group

Radio-Loud / Radio-Quiet dichotomy

Why do only 10% have jets?

- RIQ's could represent a link between radio-QUIET quasars and radio-LOUD quasars…

EMSSG
Environmental Monitoring & Space Science Group

2 – Optical Data Reduction

- Over the past decade astronomy has experienced a "data-explosion" – envelope for high end projects at TByte volumes
- Trend has affected more modest projects – data from a week long observing run on a medium sized telescope now approaches GB volumes. – Example, recent run to Calar Alto took 340 GB
- Recent emergence of L3 CCDs will exacerbate this problem
- Feasibility of visual interaction with the images in our data sets will diminish

EMSSG
Environmental Monitoring & Space Science Group

Ultra High Precision Photometry

- Differential Photometry compares brightness changes of quasar with master reference star

- From raw frames to light curves - two programs
  - Photmate (S. O Driscoll) – Generates an aperture magnitude file for entire data set
  - Qvar (A. O Connor) – Creates differential light curves from photmate text file

EMSSG
Environmental Monitoring & Space Science Group

3 – PG 1718+481 in the R-Band

- Two nights of data with L3 CCD camera at Calar Alto
- Night 1 – 19/20 – sep 2003
- 4530 frames in 15 minutes (5 frames per second)
- Night 2 – 20/21 – sep 2003
- 1715 frames in 15 minutes (2 frames per second)
- Total = 6245 frames in 30 mins
- Data was windowed – improved readout rate
- Kinetics mode on night 1 – 2.5 times faster then normal night 2 mode
- 7 reference stars for accurate photometry

EMSSG
Environmental Monitoring & Space Science Group

Q-Rbar nightly averages

- Q-Rbar nightly averages
- Very small error bars
- No variability within a few milli mag

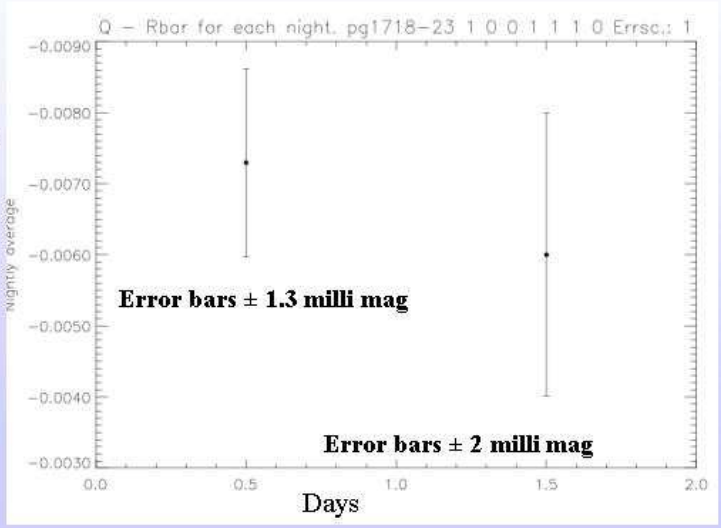

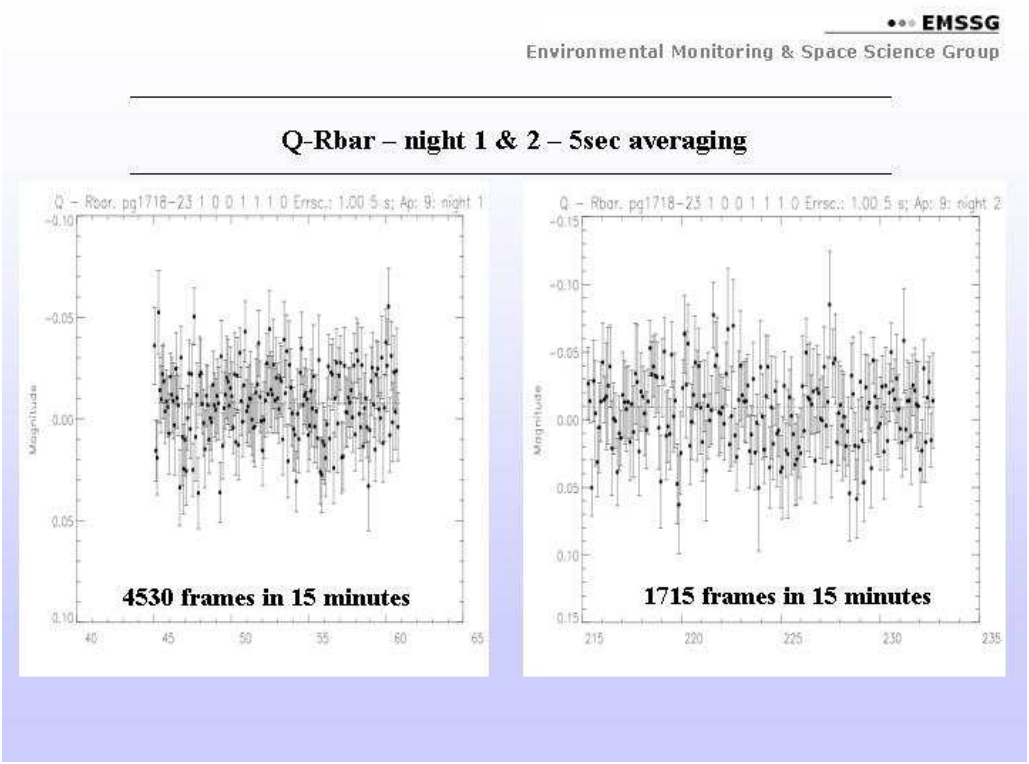
EMSSG
Environmental Monitoring & Space Science Group
Q-Rbar – night 1 & 2 – 5sec averaging
4530 frames in 15 minutes
1715 frames in 15 minutes

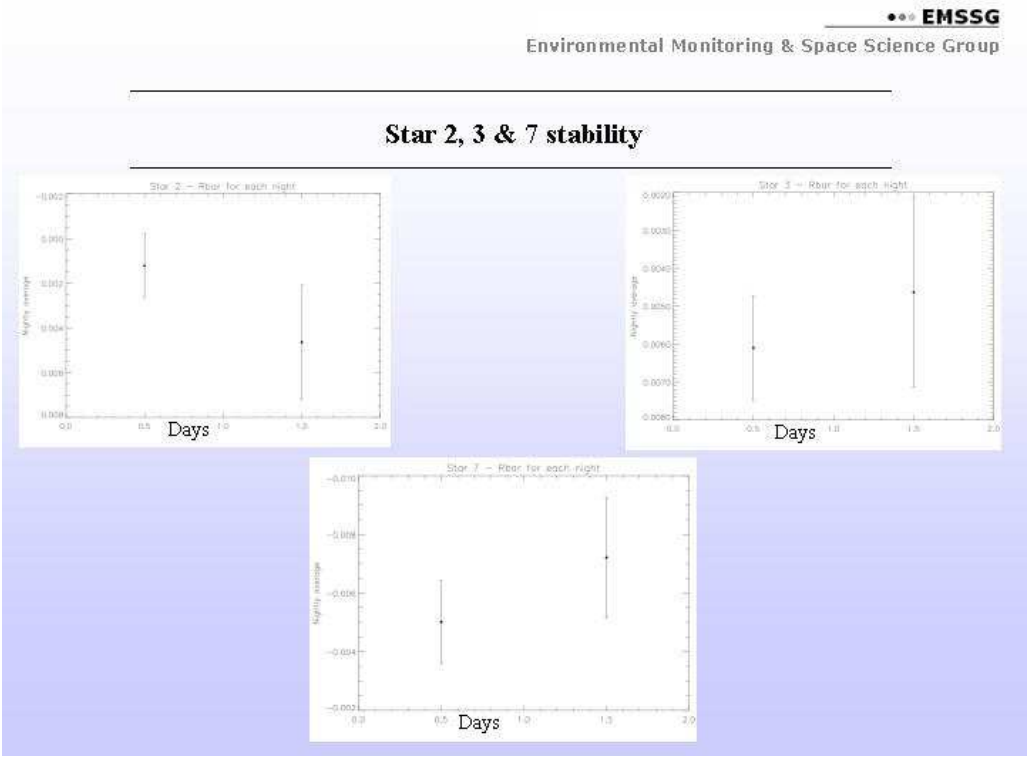
EMSSG
Environmental Monitoring & Space Science Group
Star 2, 3 & 7 stability
Days
Days
Days

EMSSG
Environmental Monitoring & Space Science Group

Reference star 5

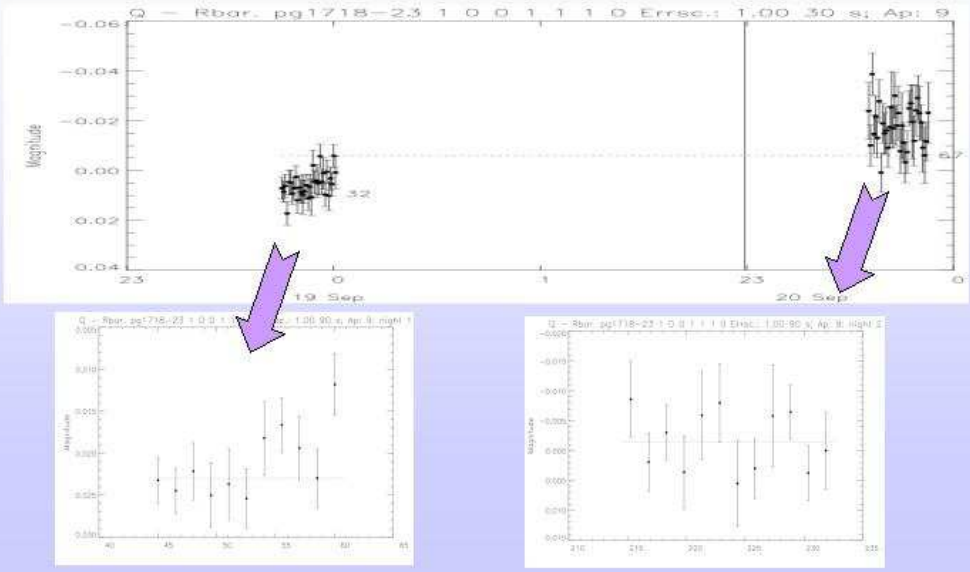

EMSSG
Environmental Monitoring & Space Science Group

4 - PG 1718+481 in the Radio

- EVN Data taken on Nov 9th 2002
- Project by Niall Smith, John Howard & Denise Gabuzda (UCC)
- Telescopes involved: Medicina, Efflesberg, Westerboork, Noto*, Onsala, Torun, Jodrell Bank, Urumqi* & Sheshan (*=failed)
- 5 GHz (6 cm)

RIQ - List

Name	RA (1950)	DEC (1950)	6 CM FLUX (mJ)	z
PG 0007+106	00:07:56.70	10:41:48.2	155	0.09
PG 1718+48	17:18:17.7	48:07:10.5	164	0.02
PG 2209+18	22:09:30.43	18:26:59.0	117	0.7

EMSSG
Environmental Monitoring & Space Science Group

Reasons for study

- Test hypothesis that radio emission of these sources is associated with Doppler boosted intrinsically low power jets
- Place better constraints on the brightness temperatures of individual compact components
- Determine the degree of ordering and orientation of the magnetic field in the core region and inner jet (Polarisation studies)

- IF the jets of RIQ's are relativistic but have modest bulk lorentz factors
  - VLBI polarisation properties similar to BL Lac objects
  - » BL Lac B field perpendicular to the jet axis
  - Evidence points towards these jets being of relatively low power compared to quasars

EMSSG
Environmental Monitoring & Space Science Group

Analysis by Puschell et al.

- 6 cm observations by Puschell et al. (1986)
- 70% flux – unresolved component
- 30% flux – curious structure – faint jet?
- Concluded that any extended emission – much weaker than normal radio galaxies

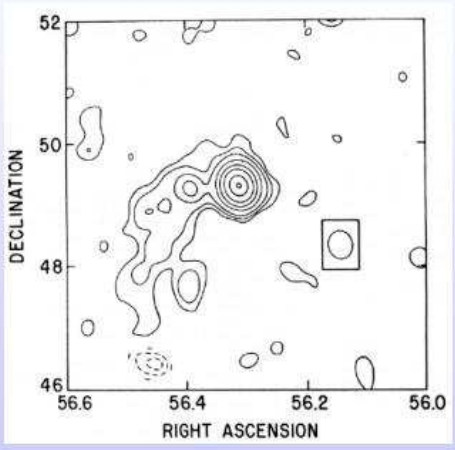

100 mas

EMSSG
Environmental Monitoring & Space Science Group

Analysis by Caccianiga et al.

- 6 cm EVN+MERLIN observations by Caccianiga et al. (2000) revealed a core component and a secondary component (jet?) separated by 21.9 mas

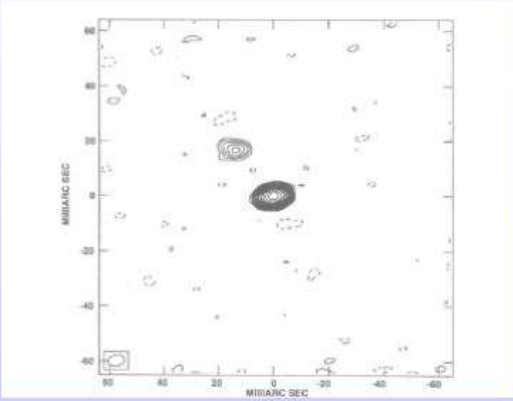

20 mas

EMSSG
Environmental Monitoring & Space Science Group

Final Map

- 5 GHz Map
- Core – 3 mas x 3 mas
- Extended feature 4 mas from core & ~ 60° ?
- Similar direction to Caccianiga and Puschell radio maps
- European telescopes alone – check for seconday component on Caccianiga map

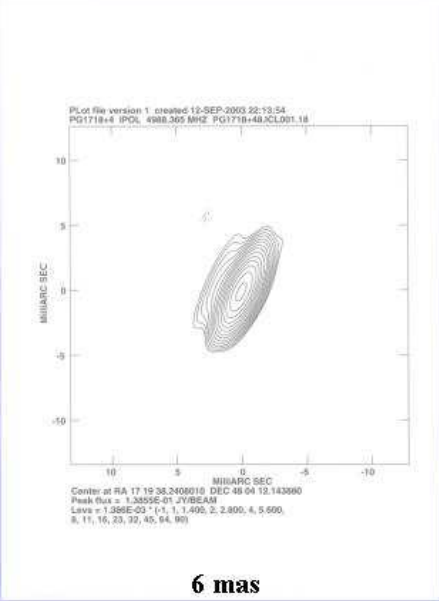

6 mas

EMSSG
Environmental Monitoring & Space Science Group

Conclusion

- No variability within 1 milli mag from night to night or within a night for PG 1718+481
- Some structure from inner component (6 mas) at 5 GHz
- Make a map with European telescope to look for secondary component
- Produce maps of IIIZw2 and PG 2209+18

Optical monitoring in Torino and near-IR observations at TIRGO –

S. Crapanzano, M. Villata, C. M. Raiteri, L. Lanteri, N. Marchili

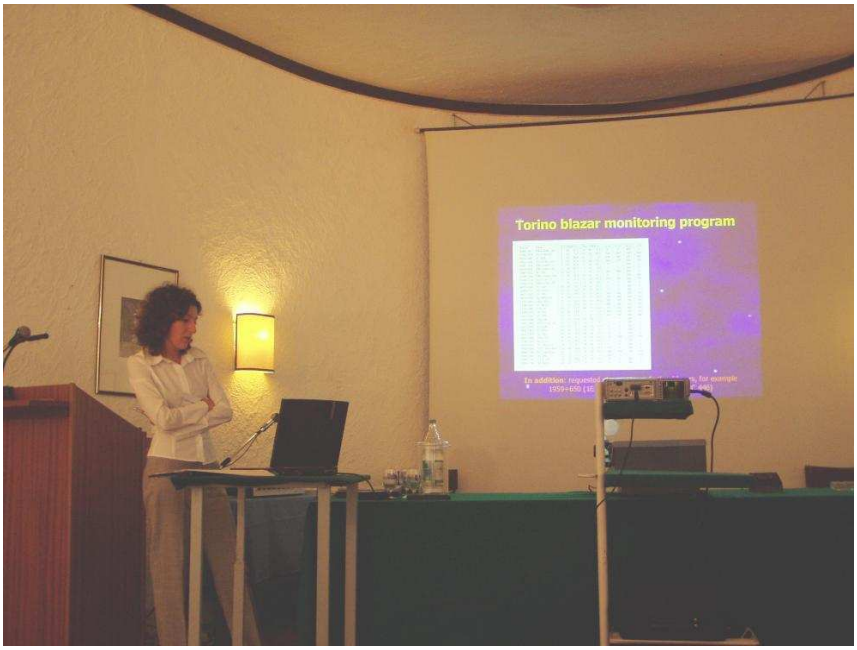

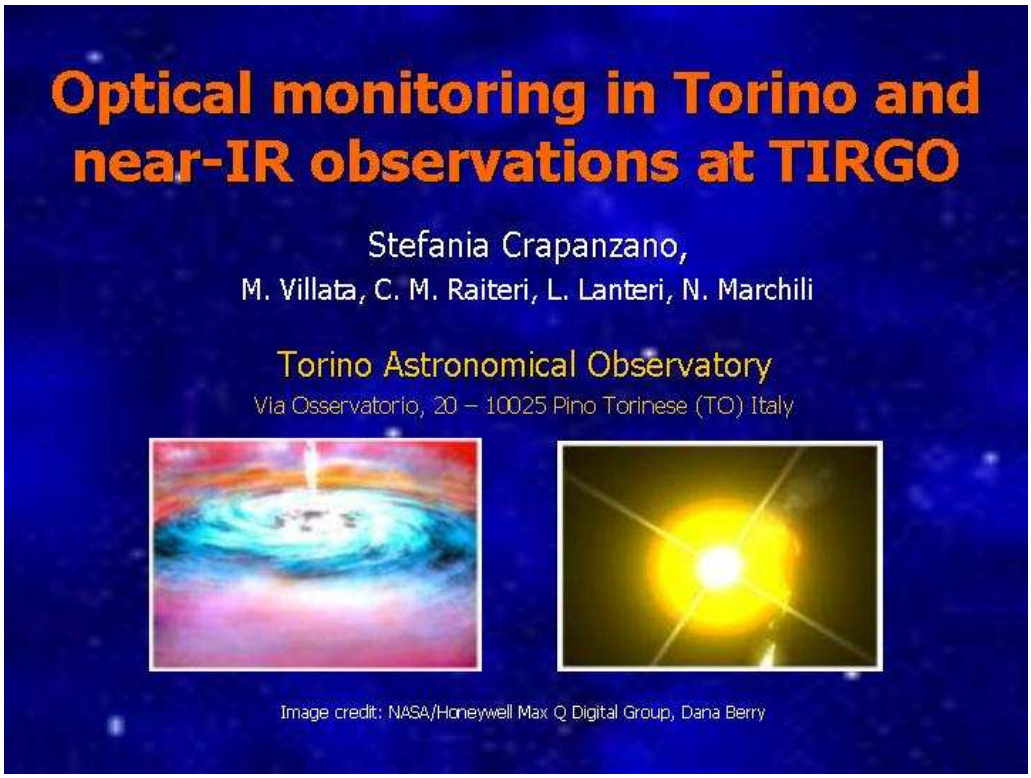

Optical monitoring in Torino

Systematic multiband optical photometric monitoring of blazars from November 1994

Torino blazar monitoring program

Source	Name	RA (2000.0)			Dec (2000.0)			t_B(s)	t_V(s)	t_R(s)	t_I(s)
0048−097	PKS 0048−09	0	50	41.3	-9	29	5.0	0	0	420	0
0109+224	S2 0109+22	1	12	5.7	22	44	39.2	420	300	240	240
0219+428	3C 66A	2	22	39.6	43	2	8.0	420	300	240	240
0235+164	AO 0235+16	2	38	38.9	16	36	59.1	600	540	480	420
0420−014	PKS 0420−01	4	23	15.8	-1	20	33.1	0	0	300	0
0422+004	PKS 0422+00	4	24	46.8	0	36	6.6	0	0	240	0
0430+052	3C 120	4	33	11.1	5	21	15.7	300	360	480	0
0528+134	PKS 0528+134	5	30	56.4	13	31	55.1	0	0	600	600
0716+714	S5 0716+71	7	21	53.4	71	20	36.3	420	300	240	240
0735+178	PKS 0735+17	7	38	13.7	17	42	19.0	0	0	300	0
0827+243	OJ 248	8	30	52.0	24	10	59.9	0	0	480	0
0836+710	4C 71.07	8	41	24.3	70	53	42.2	0	0	480	0
0851+202	OJ 287	8	54	48.9	20	6	30.7	420	300	240	240
0954+658	S4 0954+65	9	58	47.3	65	33	54.7	480	360	300	240
1101+384	Mkn 421	11	4	34.2	38	14	26.0	360	240	180	180
1156+295	4C 29.45	11	59	45.4	29	14	41.7	600	480	420	360
1219+285	ON 231	12	21	31.7	28	13	58.5	420	300	240	240
1226+023	3C 273	12	28	55.6	2	3	6.6	300	240	180	180
1253−055	3C 279	12	56	11.1	-5	47	21.5	600	480	420	360
1418+546	OQ 530	14	19	46.6	54	23	14.8	0	0	360	0
1510−089	PKS 1510−08	15	12	50.5	-9	6	0.1	0	0	420	0
1611+343	DA 406	16	13	41.1	34	12	47.9	0	0	420	0
1633+382	4C 38.41	16	35	15.4	38	8	4.5	0	0	420	0
1641+399	3C 345	16	42	58.8	39	48	37.0	0	0	420	0
1652+398	Mkn 501	16	53	44.0	39	45	35.9	420	300	240	240
1739+522	4C 51.37	17	40	36.9	52	11	43.3	0	0	420	0
1803+784	S5 1803+78	18	0	45.7	78	28	4.0	0	0	480	0
1959+650	1ES 1959+650	19	59	59.9	65	8	55.0	420	0	300	0
2200+420	BL Lacertae	22	2	43.2	42	16	40.0	360	300	240	240
2223−052	3C 446	22	25	47.2	-4	57	1.7	600	0	0	600
2230+114	CTA 102	22	32	30.8	11	43	50.7	0	0	360	0
2251+158	3C 454.3	22	53	57.7	16	8	53.4	0	0	360	0

3C 66A
AO 0235+16
S5 0716+71

OJ 287
S4 0954+65
Mkn 421, Mkn 501
ON 231
3C 273, 3C 279
PKS 1510-08
BL Lac, CTA 102

In addition: requested observations of other blazars, for example 1959+650 (1ES 1959+650) and 2223-457 (3C 446)

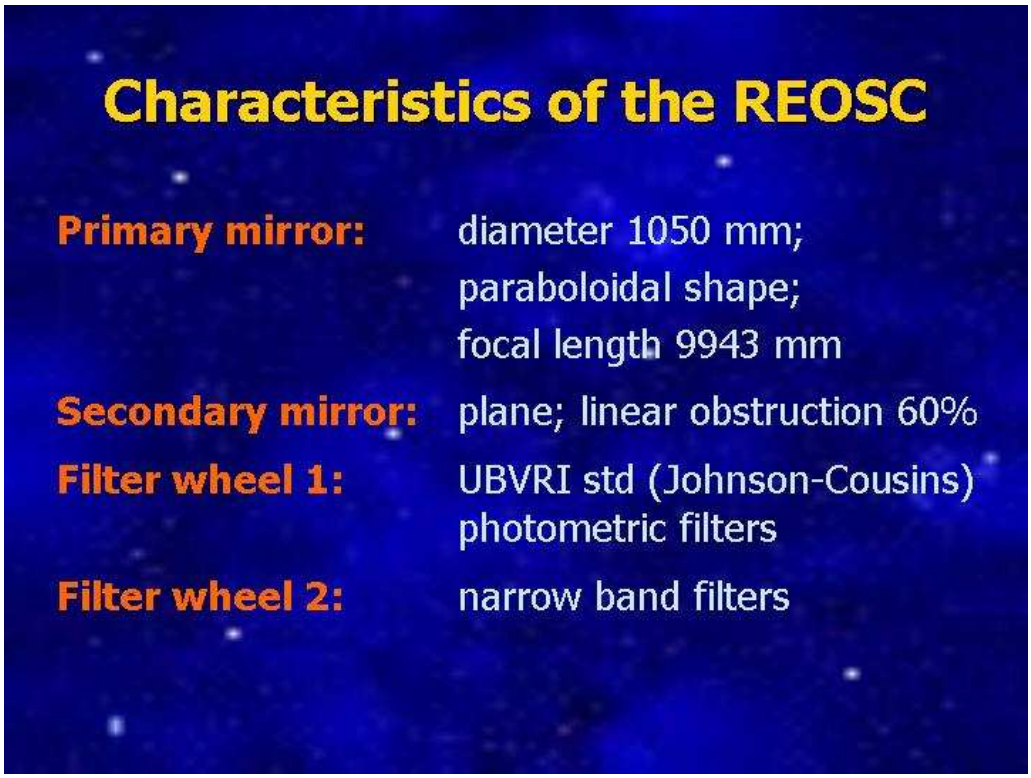
Characteristics of the REOSC
Primary mirror:
diameter 1050 mm;
paraboloidal shape;
focal length 9943 mm
Secondary mirror:
plane; linear obstruction 60%
Filter wheel 1:
UBVRI std (Johnson-Cousins) photometric filters
Filter wheel 2:
narrow band filters

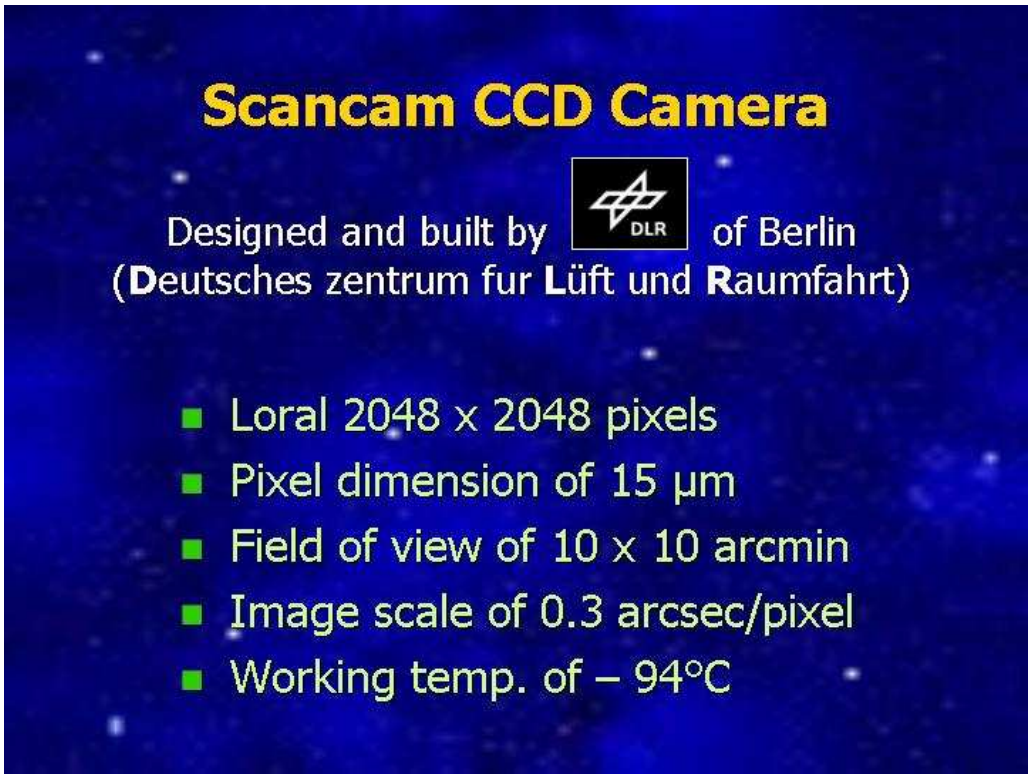
Scancam CCD Camera
Designed and built by DLR of Berlin
(Deutsches zentrum fur Lüft und Raumfahrt)
Loral 2048 x 2048 pixels
Pixel dimension of 15 µm
Field of view of 10 x 10 arcmin
Image scale of 0.3 arcsec/pixel
Working temp. of – 94°C

REOSC automation project

Was performed by ATEC Robotics
(**A**dvanced **TEC**hnologies for Research and Industry)

- Changes in telescope and dome
- Addition of meteorological station
- Hardware and software layout

Local meteo data

- Rain
- Wind direction
- Wind speed
- Temperature
- Humidity
- Pressure


Telescope, auxiliary and CCD control system
CLIENT/SERVER ARCHITECTURE
THREE CONTROL SYSTEMS:
Observatory Control System,
Telescope Control System,
Imager Control System


IR observations at TIRGO
Two observing runs:
December 2002 and March 2003

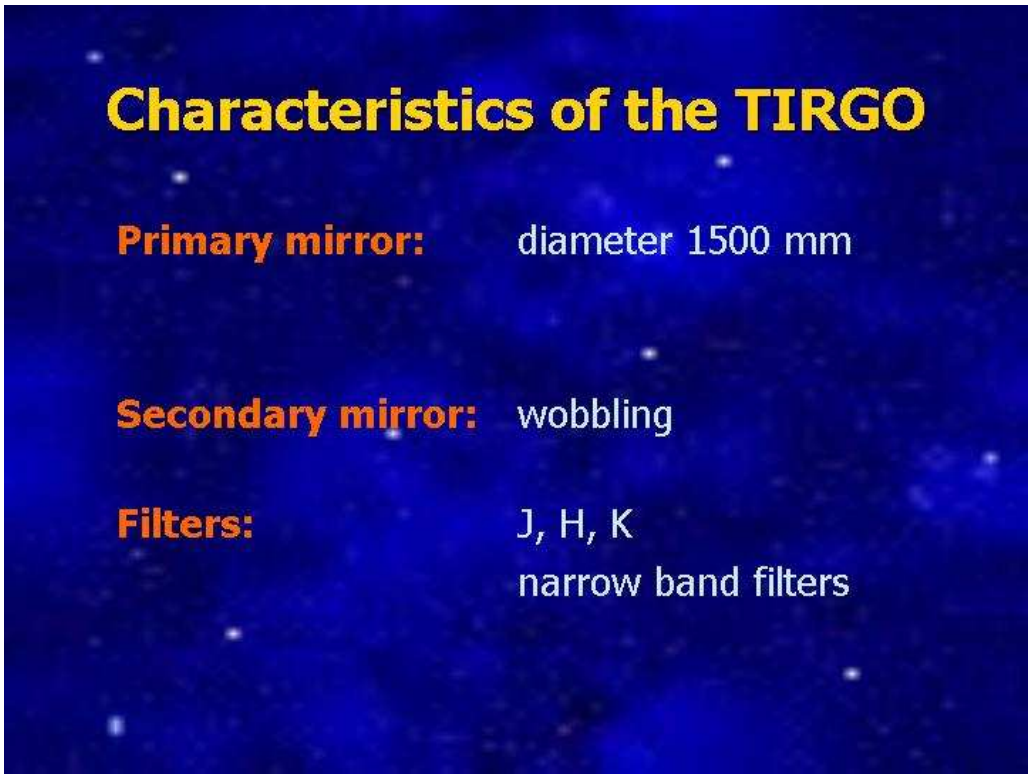
Characteristics of the TIRGO
Primary mirror:
diameter 1500 mm
Secondary mirror:
wobbling
Filters:
J, H, K
narrow band filters

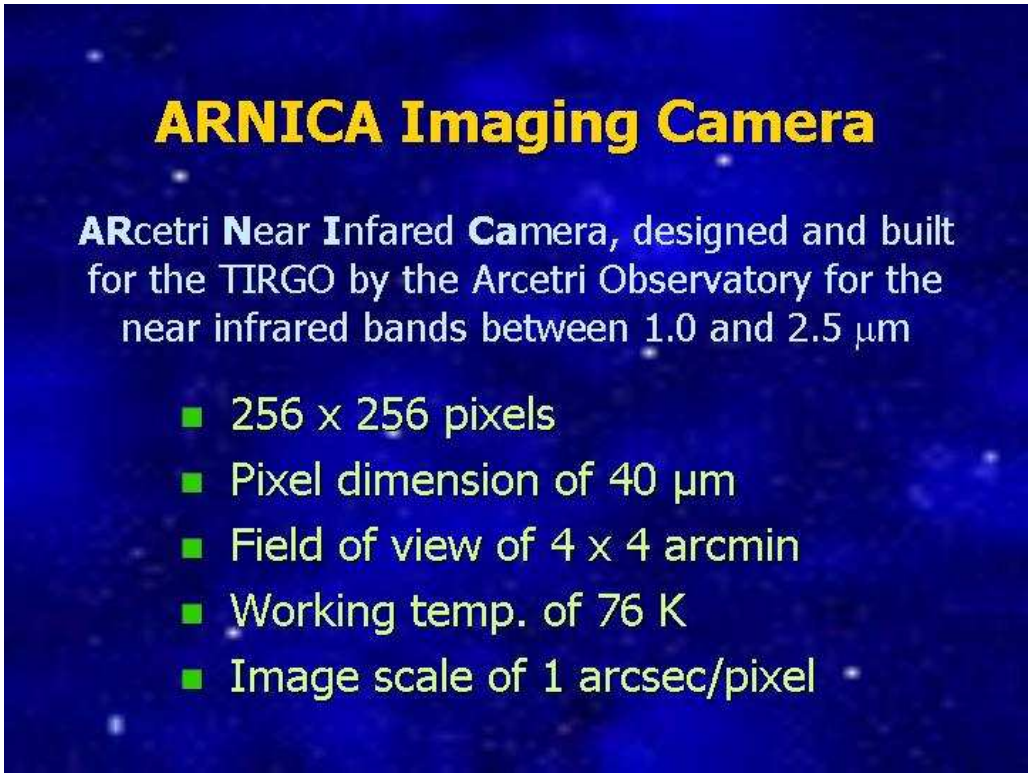
ARNICA Imaging Camera
ARcetri Near Infared Camera, designed and built for the TIRGO by the Arcetri Observatory for the near infrared bands between 1.0 and 2.5 μm
256 x 256 pixels
Pixel dimension of 40 μm
Field of view of 4 x 4 arcmin
Working temp. of 76 K
Image scale of 1 arcsec/pixel


Observing runs at TIRGO
18 – 24 December 2002 run
0219+428, 0235+164, 0851+202,
1226+023*, 1253-055*, 2200+420
7 – 14 March 2003 run
0851+202, 1226+023*, 1253-055*, 1510-089*
* Alan Marscher's program

Session II: Separating intrinsic and extrinsic intraday variability

IDV optical monitoring: What can we do? – C. M. Raiteri, M. Villata, on behalf of the WEBT collaboration

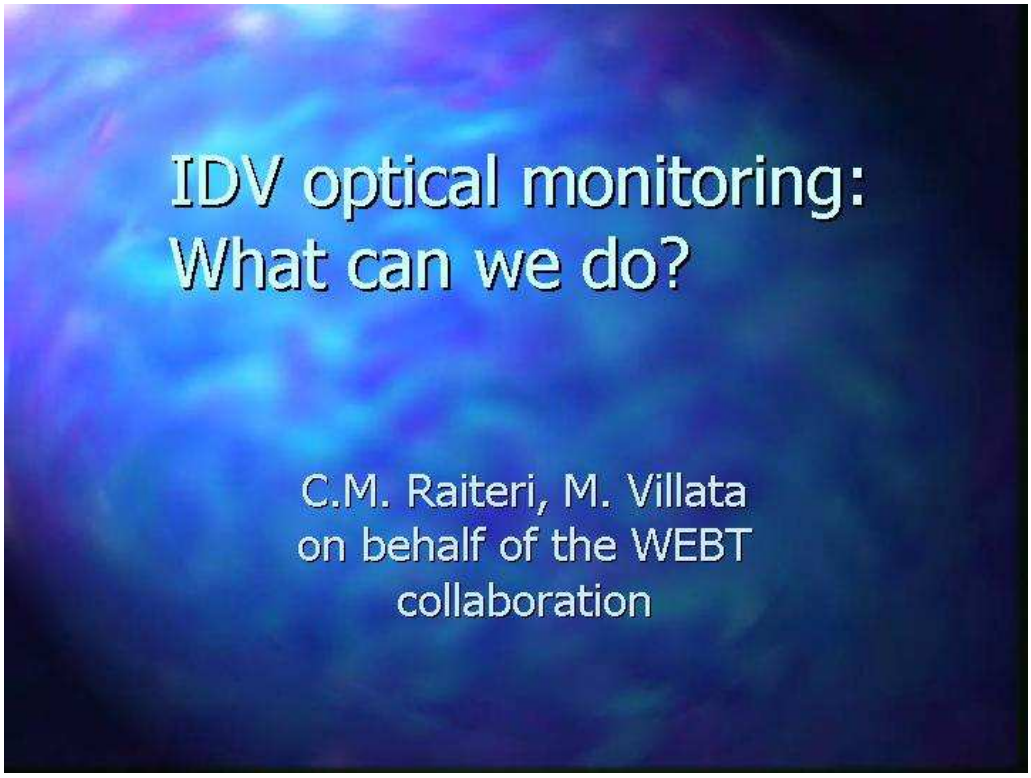

A single, medium size telescope

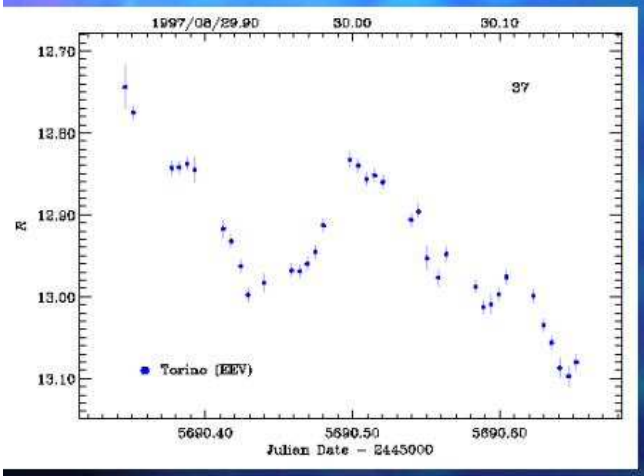

Observations of BL Lac on August 29-30, 1997 with the 1.05 m telescope of the Torino Observatory

Gaps due to *B*-band exposures

37 *R* and 7 *B* frames in 7.4 hours
Δt(*B*+*R*)~10 min
Δt(*R*)~12 min

A single, large size telescope

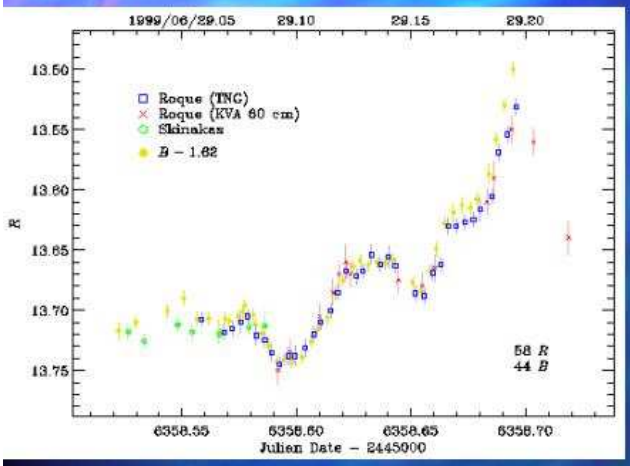

Observations of BL Lac on June 29, 1999 with the 3.58 m Telescopio Nazionale Galileo (TNG)

36 *B* and 36 *R* TNG frames in 3.3 hours
Δt(*B*+*R*)~2.8 min
Δt(*R*)~5.5 min

BUT: limited visibility period, weather-dependency, read-out time constraint, and difficulty in obtaining monitoring time

Fast photometry can overcome the latter two

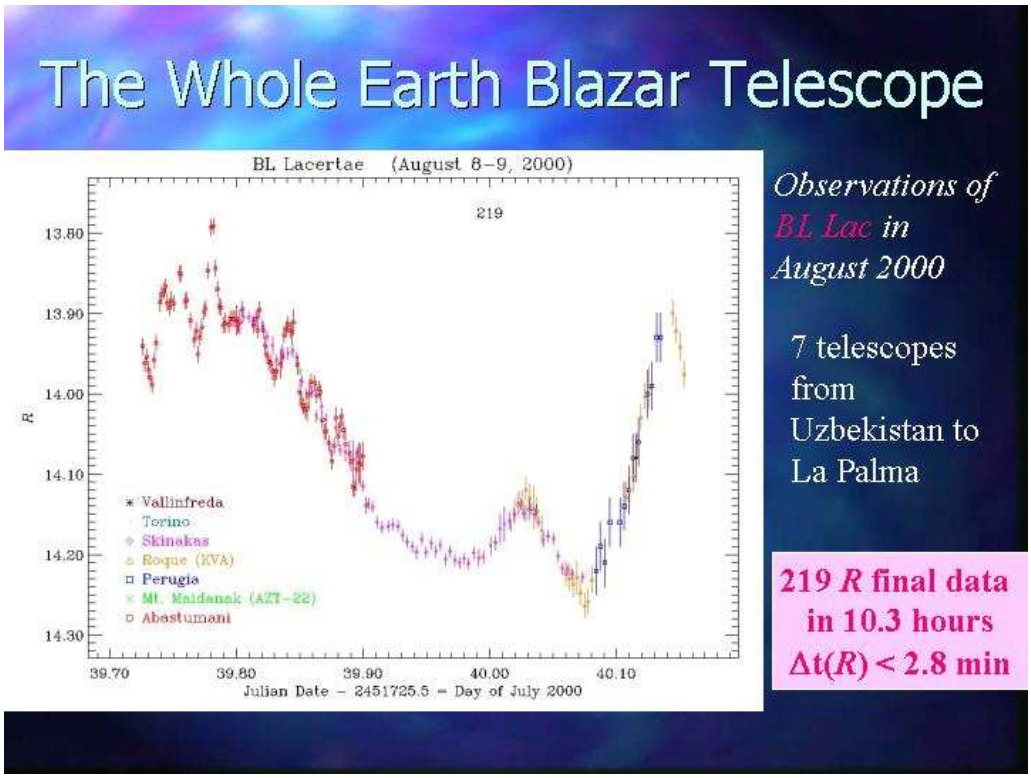
The Whole Earth Blazar Telescope
BL Lacertae (August 8–9, 2000)
219
R
13.80
13.90
14.00
14.10
14.20
14.30
39.70
39.80
39.90
40.00
40.10
Julian Date – 2451725.5 = Day of July 2000
Vallinfreda
Torino
Skinakas
Roque (KVA)
Perugia
Mt. Maidanak (AZT-22)
Abastumani
Observations of BL Lac in August 2000
7 telescopes from Uzbekistan to La Palma
219 R final data in 10.3 hours
Δt(R) < 2.8 min

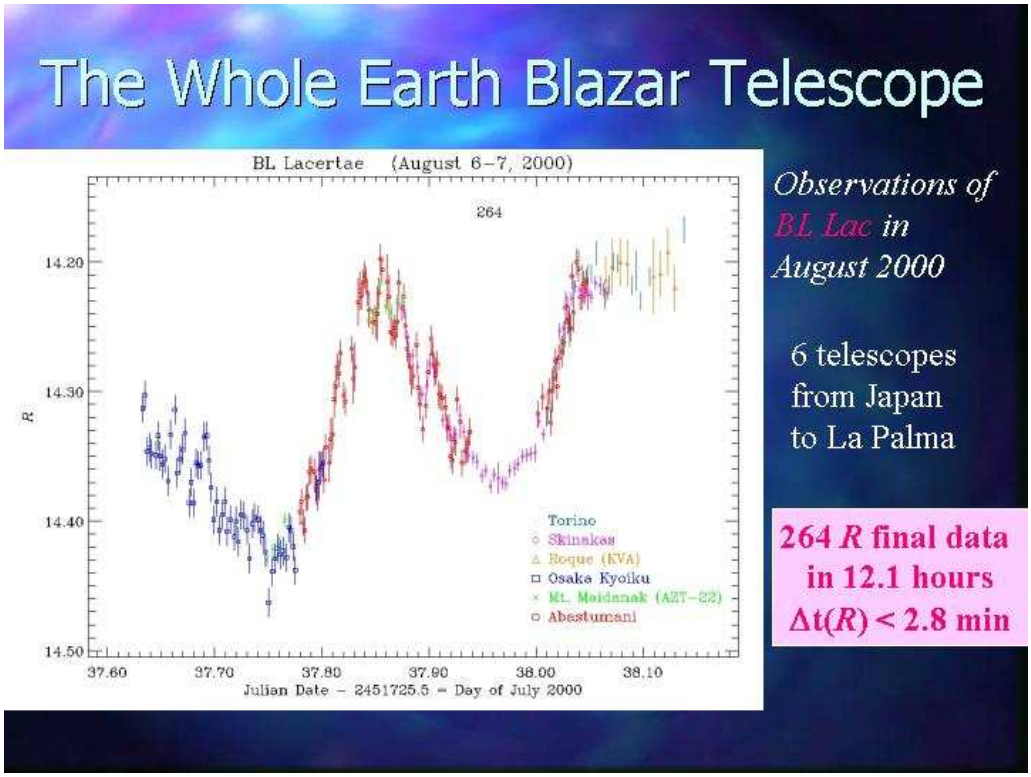
The Whole Earth Blazar Telescope
BL Lacertae (August 6–7, 2000)
264
R
14.20
14.30
14.40
14.50
37.60
37.70
37.80
37.90
38.00
38.10
Julian Date – 2451725.5 = Day of July 2000
Torino
Skinakas
Roque (KVA)
Osaka Kyoiku
Mt. Maidanak (AZT-22)
Abastumani
Observations of BL Lac in August 2000
6 telescopes from Japan to La Palma
264 R final data in 12.1 hours
Δt(R) < 2.8 min

The Whole Earth Blazar Telescope

Observations of BL Lac in August 2000

8 telescopes from Uzbekistan to Western Canada

172 *R* final data in 18.2 hours
Δt(*R*) < 6.3 min

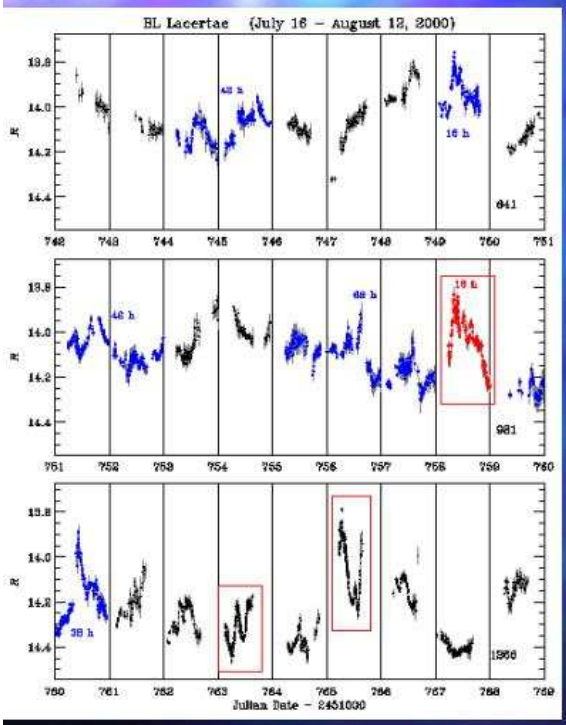

Observations of BL Lac during the core WEBT campaign 2000 (July 16-August 12)

19 telescopes from Japan to Wester Canada

Blue/red segments indicate the best covered periods (gaps<4 hours)

2888 *R* final data in 27 days
> 107 data/day
Δt(*R*) < 13 min

Problem: paucity of observers in the Pacific area

Conclusion:

The most efficient way to observe IDV in the optical band is to involve a large number of observers spread in longitude

Interpretation of intrinsic/extrinsic IDV – S. J. Wagner

Intra-Day Variability (IDV)

IDV: Variations on time-scales of 100 000 sec.

Radio-IDV at face value implies r ~ $\mathcal{D}$ 200 AU,
and thus very high photon densities.

Photon densities <=> brightness temperatures

$$T_B \propto D^2 \frac{S}{\nu^2} \left[\frac{1}{\Delta t_{obs}(1+z)} \right]^2 < T_{IC}$$

Limit to photon densities

Efficient particle acceleration leads to high u_{rad},
and thus to efficient IC scattering.

Self regulation through IC catastrophe

$$\frac{L_C}{L_S} = 0.5 \left(\frac{T}{10^{12}}\right)^5 \nu \quad [1 + 0.5 \left(\frac{T}{10^{12}}\right)^5 \nu]$$

Variability implies high photon-density/compactness.
Maximum value: log T ~ 12

The IDV problem:

IDV: Variations on time-scales of 100 000 sec.

$z \sim 1$, $S \sim 0.1$ Jy, $\nu \sim 5$ GHz

$$T_B \propto D^2 \frac{S}{\nu^2} \left[\frac{1}{\Delta t_{obs}(1+z)} \right]^2 < T_{IC}$$

Inferred brightness temperatures up to 10^{17} K,
i.e. >100000 above IC limit!

Possible solutions

$$T_B \propto D^2 \frac{S}{\nu^2} \left[\frac{1}{\Delta t_{obs}(1+z)} \right]^2 < T_{IC}$$

Concept wrong	Extrinsic mechanisms
Distances wrong	Non-cosmological redshifts
Fluxes wrong	Relativistic amplification
Diameters wrong	Geometry
Limit invalid	Ongoing IC catastrophes
Limit wrong	Radiation mechanism

Interstellar Scintillation:

Inhomogeneities in ISM lead to refractive distortions of EM waves (interstellar scintillation).

Flux density variations well studied in Pulsars.

Properties of IS screens not well constrained/understood

Unavoidable *contribution* to radio variability

Intrinsic variability?

Radio-optical IDV

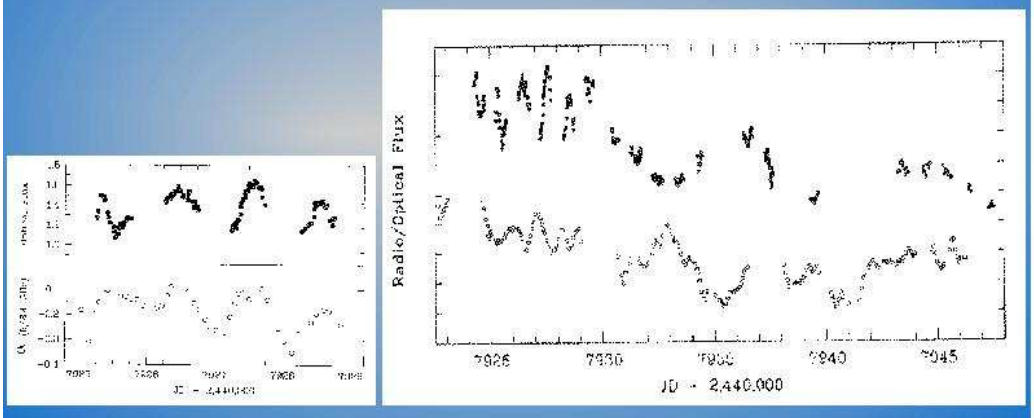

Is this a chance coincidence (not always correlated)?

Broad band correlations

Correlations between different energies and lags are not universal (and not even persistent within a single source)

Edelson et al., ApJ 438, 120

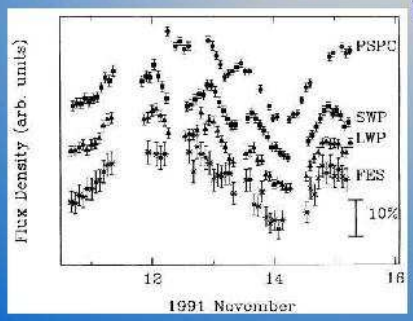

PKS 2155-304

Urry et al., ApJ, 476, 692

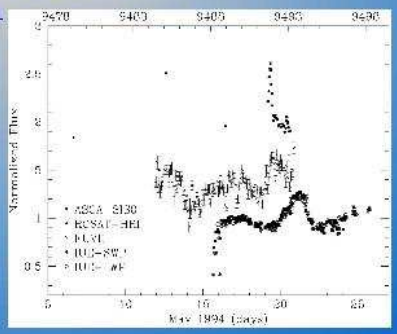

Broad band correlations

Correlations are not persistent.

This does NOT imply, that they are by chance.
Not all flares are similar.
There is steep spectral evolution.

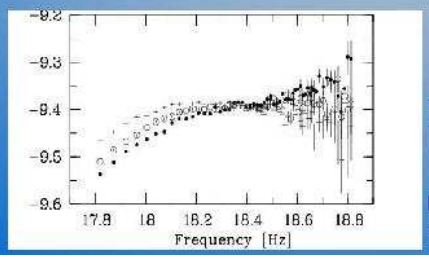

Mrk 501

Lamer & Wagner, 1999

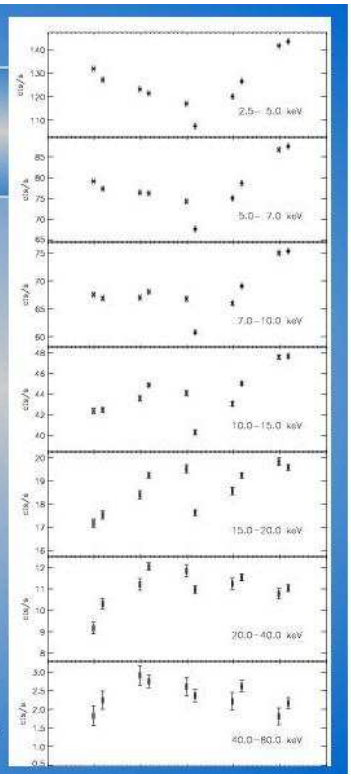

Separating ISS and intrinsic IDV

In very fast radio variations ISS can be tested:

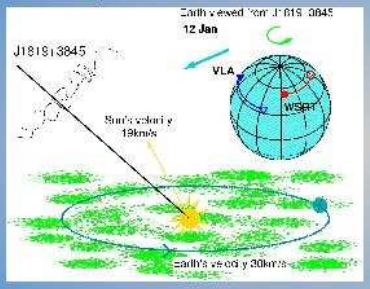

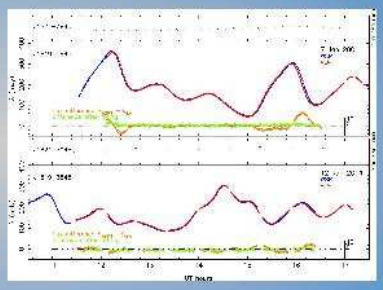

1.) annual variation (confirmed)
2.) lags between different stations (confirmed)
3) diffractive scintillation (probable)
in sources with little intrinsic variations

Time-scales of variability

Structure functions: $P = kt^N$
with break on time-scale
t ~ 100 ksec (~1 day)
over a wide frequency range
in many sources

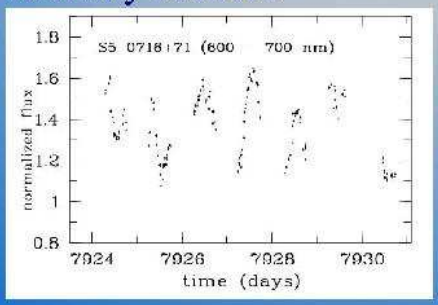

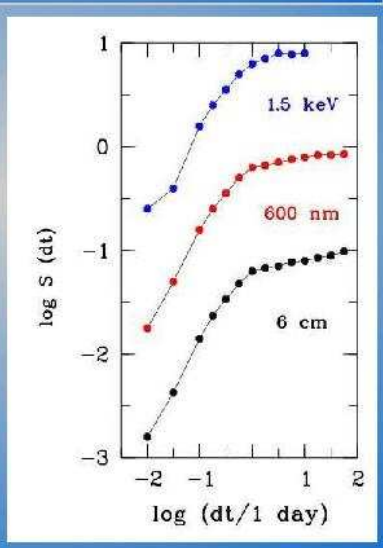

Intrinsic IDV dominates ?

Intrinsic IDV has similar characteristics throughout EM spectrum

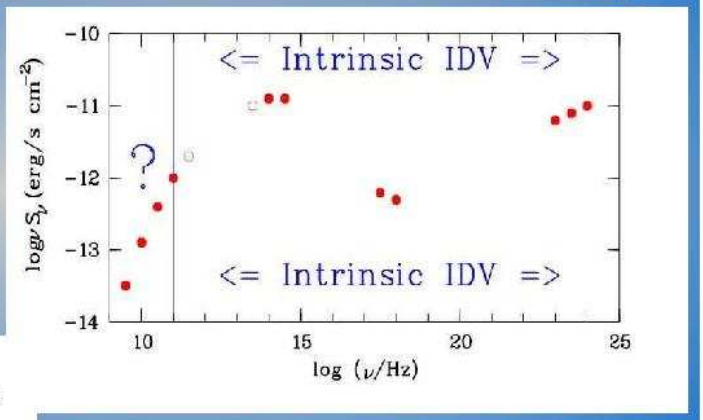

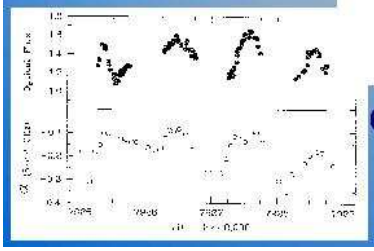

Can intrinsic radio IDV be avoided?

IDV photon density problem:

Extrinsic mechanisms:	Interstellar scintillation
Non-cosmological redshifts:	Stellar absorption lines
Geometry:	Camenzind, Qian, Salvati, Protheroe
Relativistic amplification:	$\mathcal{D} \sim 100$ required
	higher than observed energetics
	absorption
	(Begelmann, Sikora, & Rees)
Radiation mechanisms:	Coherence?
Ongoing IC catastrophe	Loss channels ?

Relativistic motion

Hypothesis (Rees, 1966, Woltjer, 1966):
relativistic potential related to relativistic outflow,
with resulting Doppler enhancement.

Higher fluxes, shorter timescales, smaller sizes
and higher apparent photon densities.
Prediction: Relativistic motion in jets.

Confirmation by VLBI: superluminal motion.

Problems with high Doppler factors

Maximum values in direct observations: ~20!
but...
Marscher et al. find up to ~50;
Jets might decelerate fast (Compton drag);
VLBI might not probe the jet flow;
fast spines of low rad. efficiency in slow VLBI jet;
etc.,
however:
self-absorption limit (Sikora et al.) [GRBs, PWN],
very high kinetic powers required [so what],
... etc. ... .

Compactness problem II

At high energies there is an analogous problem:
High energy photons (E>1 MeV) pair-annihilate on background field of soft photons.
Co-spatial high density photon fields of gamma-ray radiation and low-energy emission are opaque at high energies.
Fast variations require Doppler beaming

GeV: $\mathcal{D}$ ~ 1-10 (as in VLBI)
TeV: $\mathcal{D}$ ~ 50 (exceeding VLBI-$\mathcal{D}$ (~50))

Maximum photon densities ?

ISS also implies high brightness temperatures.
Precise determinations difficult (ISM properties), but log T ~ 13.5 -14 are in excess of ICC-limit.

Diffractive scattering suggest log T ~ 17

Extrinsic origins of variability: T ~ $\mathcal{D}$ (!)

ISS challenges the brightness temperature limit as much as IDV does.

Multi-frequency polarisation observations as tool for a better understanding of IDV – T. P. Krichbaum

Multi-Frequency Polarisation Observations as Tool for a better Understanding of IDV

Thomas P. Krichbaum, MPIfR, Bonn

Literature:

Qian S.J., Witzel A., Kraus A., Krichbaum T.P., & Zensus J.A., 2001, A&A 367, 770.

Qian S.J., Kraus A., Zhang X-Z., Krichbaum T.P., Witzel A., Zensus J.A., 2002, Chin.J. Astron. Astrophys., Vol.2, No.4, 325.

Rickett B.J., Kedziora-Chudczer L., & Jauncey D.L., 2002, ApJ 581, 103.

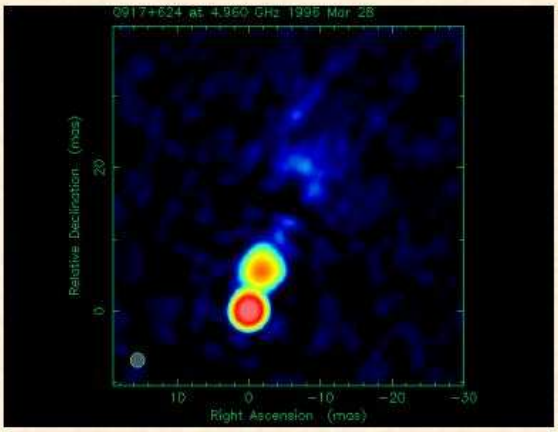

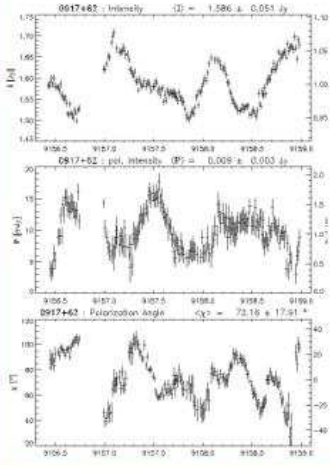

The IDV Quasar 0917+624 (z=1.446)

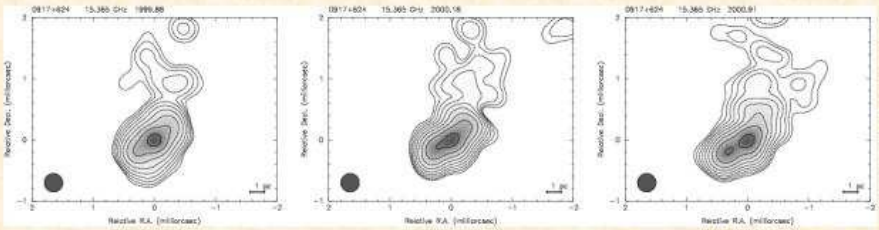

Krichbaum et al. 2002, PASA 19, 10.

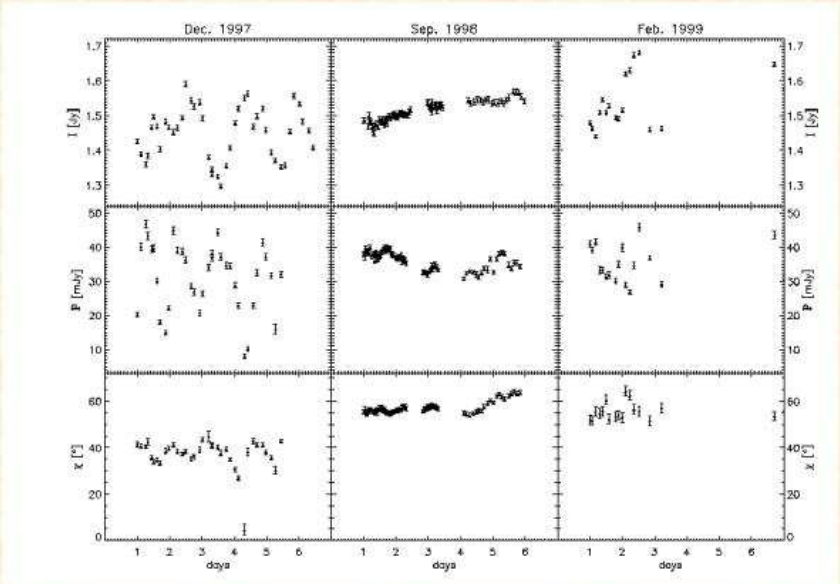

A change of the variability characteristics in the IDV source 0917+62

Kraus et al. 2000

Annual intensity variations due to orbital motion of Earth

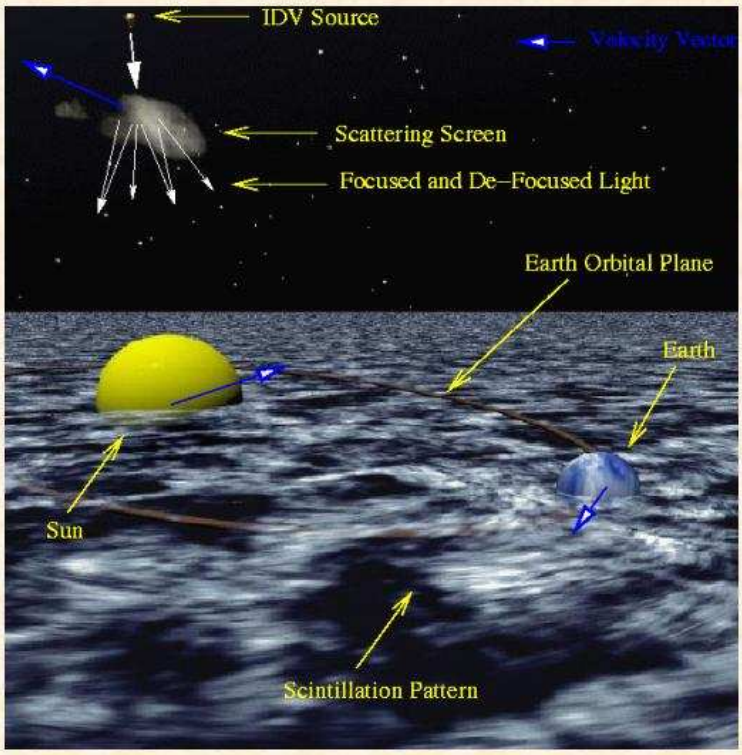

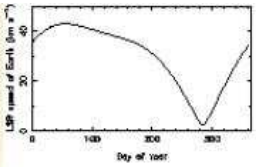

Earth velocity projected on 0917+62

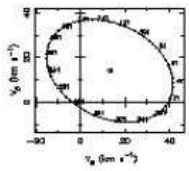

RA-DEC projection of velocity vector

Sept. 1998 (Krsua et al. 1999)

variability timescale vs. day of year

variability index vs. day of year

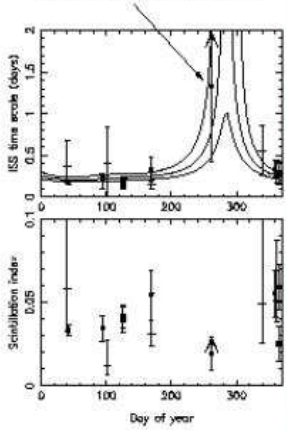

Rickett et al. 2001 (ApJL)

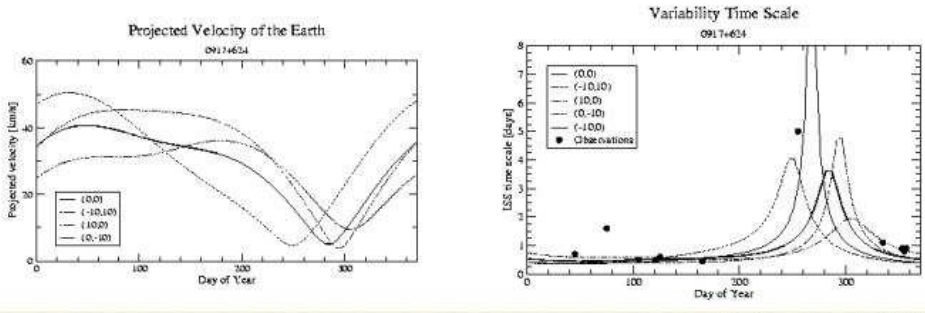

Fuhrmann et al. 2003

After more than 10 years of IDV, 0917+62 remains quite

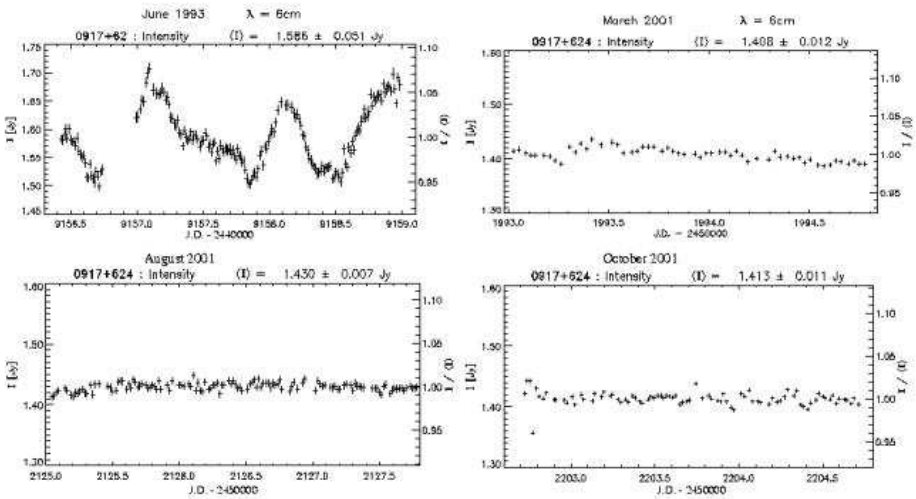

Fuhrmann et al. 2003

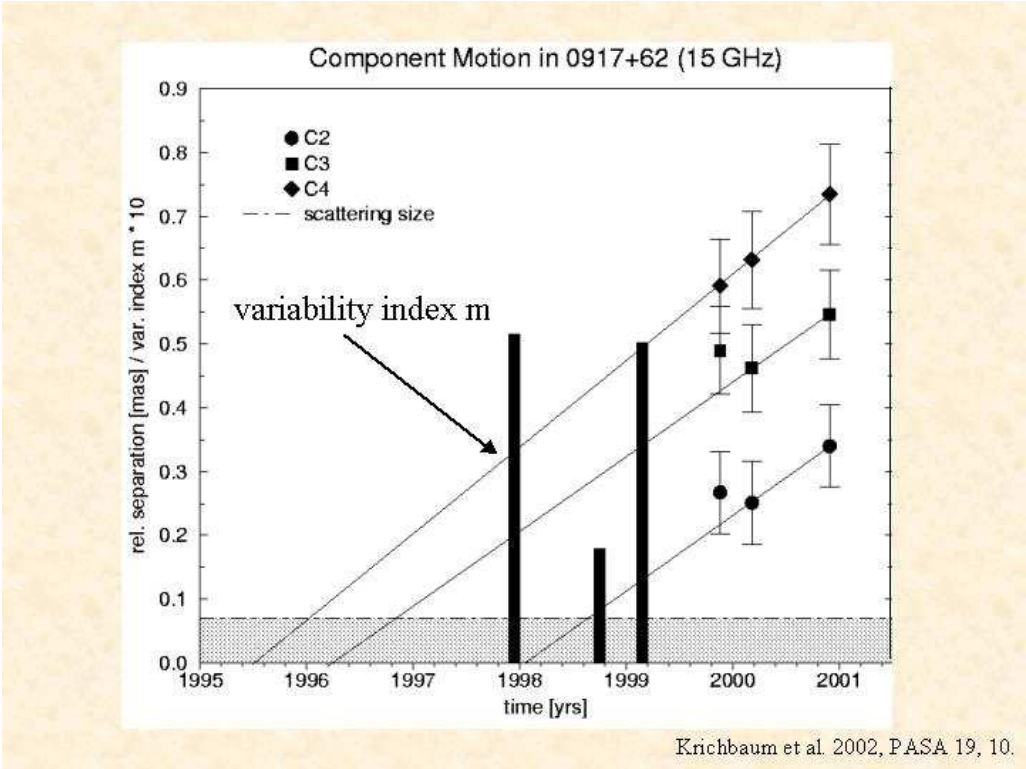

Krichbaum et al. 2002, PASA 19, 10.

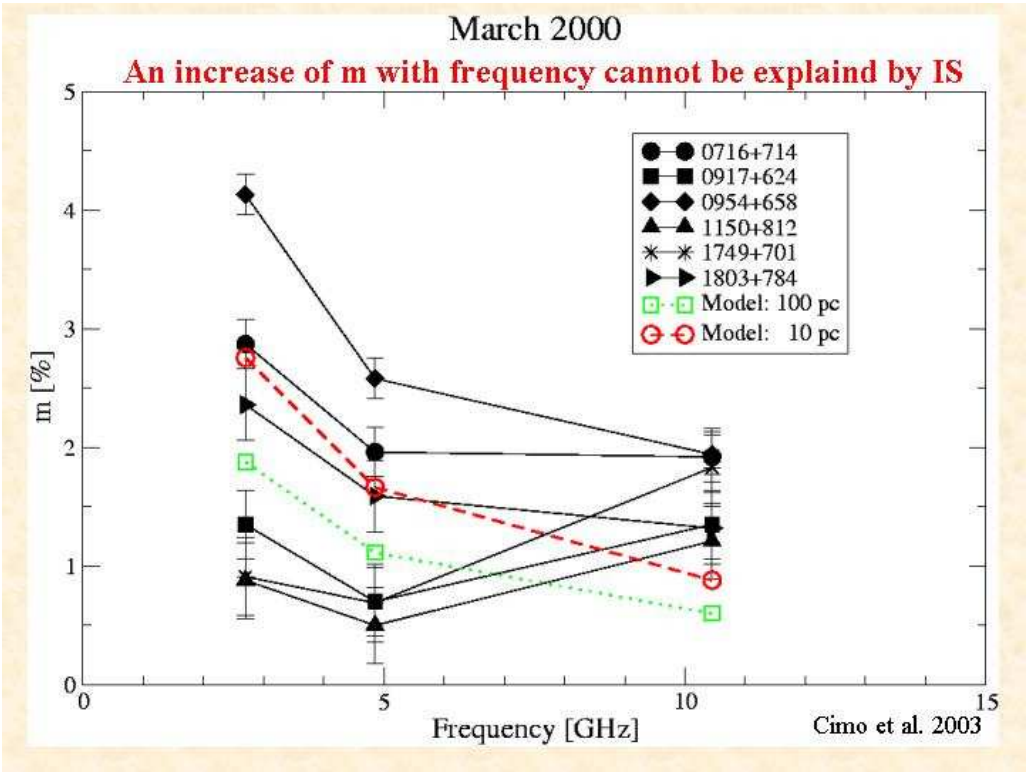

Example: IDV in 0917+62

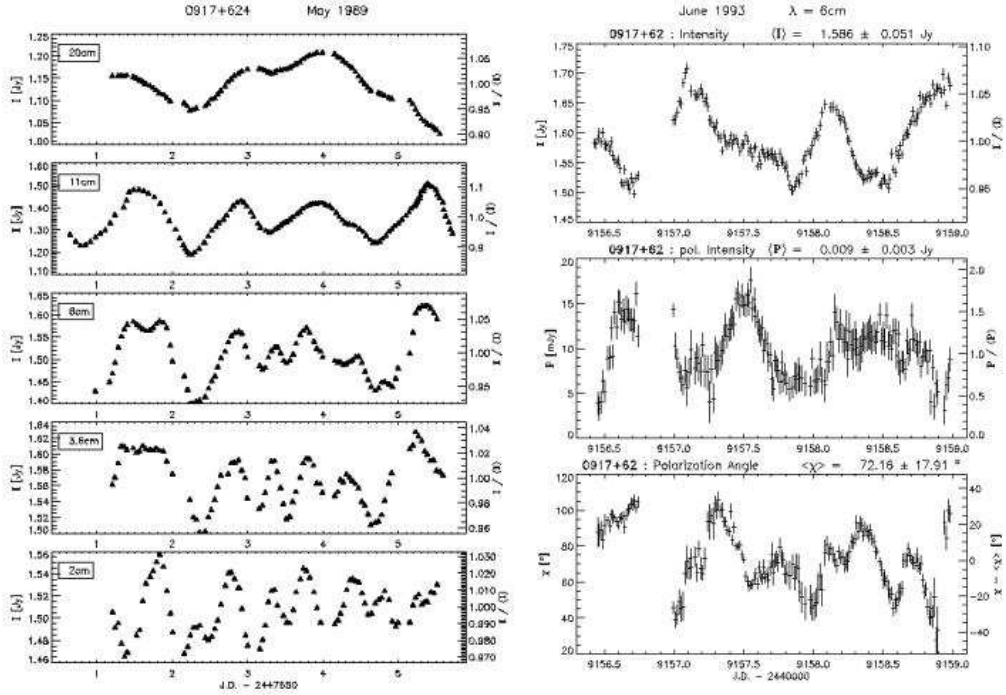

IDV of 0917+62 at 20 cm

May 1989, VLA + EB

- frequencies: 1.4, 2.7, 5, 8.3, 15 GHz
- sampling : ~ 1 hr
- m=5.7%, m_p=11.6%, Δpa=6-8 deg

Quirrenbach et al.2000, Qian et al. 2001

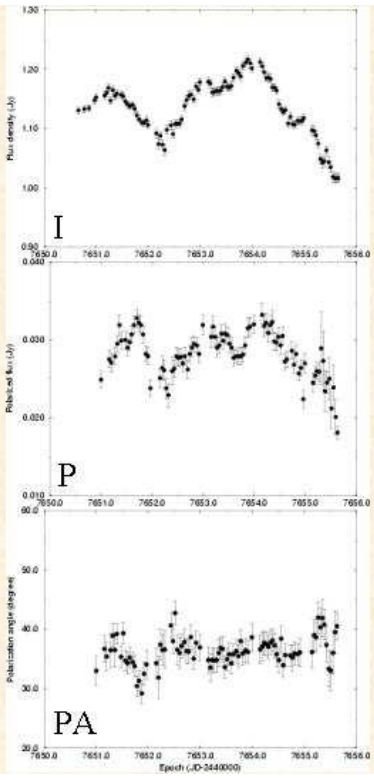

Polarisation and total Intensity are strongly correlated

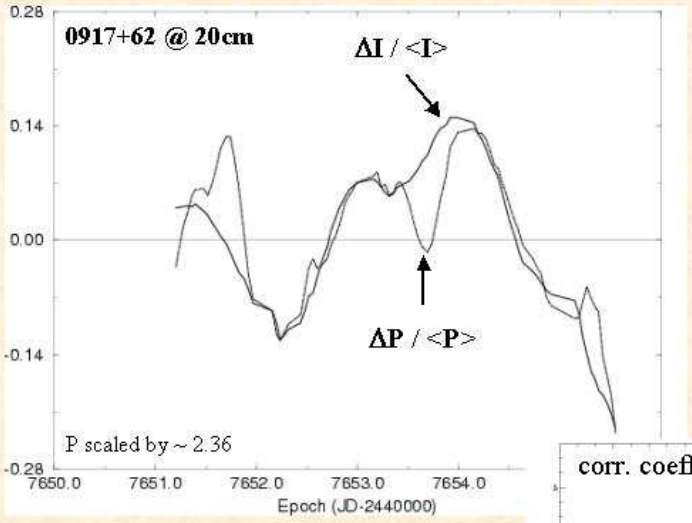

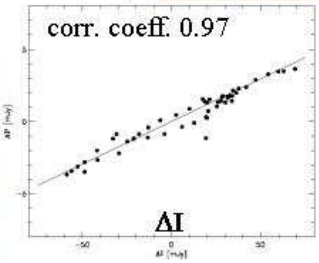

This proportionality implies that RISS might be at work. At shorter wavelength, however, we see correlations and anti-correlations between I & P !

Qian et al. 2001

I and P anti-correlate

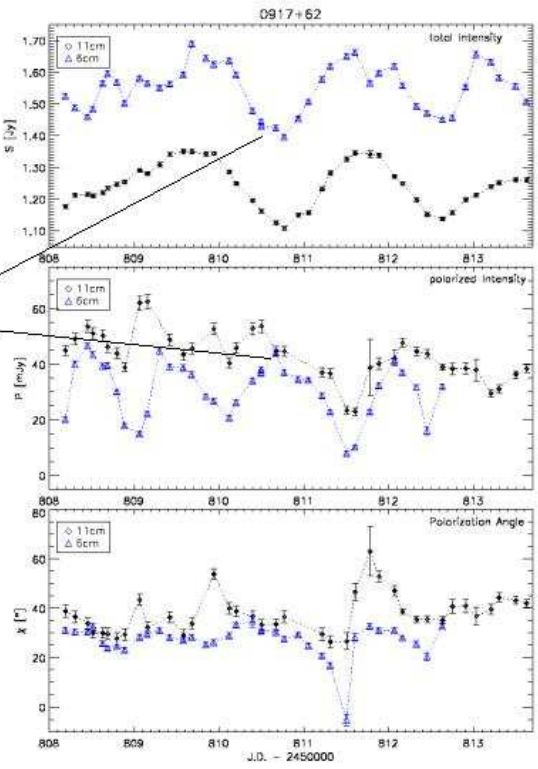

Multi-component modelling

2 component model:

one steady component

one variable component

$I(t) = I_0 + \Delta I(t)$ $\quad I_0 = I_{10}+I_{20}$
$Q(t) = Q_0 + \Delta I(t)\, m_{q2}$ $\quad Q_0 = I_{10}\, m_{q1} + I_{20}\, m_{q2}$
$U(t) = U_0 + \Delta I(t)\, m_{u2}$ $\quad U_0 = I_{10}\, m_{u1} + I_{20}\, m_{u2}$
$m_{q1} = p_1 \cos 2\chi_1$ $\quad m_{q2} = p_2 \cos 2\chi_2$
$m_{u1} = p_1 \sin 2\chi_1$ $\quad m_{u2} = p_2 \sin 2\chi_2$

The polarized flux is fitted,

but the polarization angle not.

→ need a third component

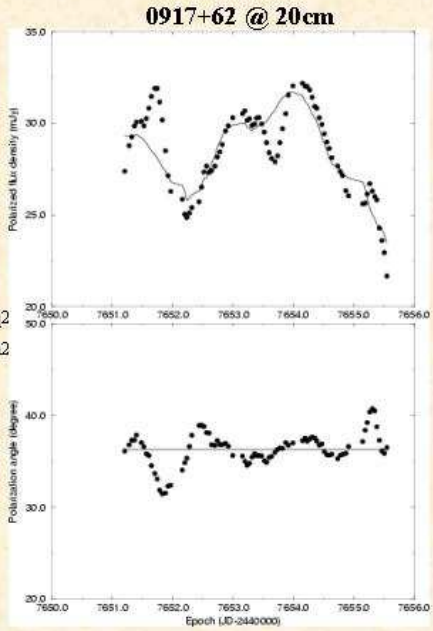

Qian et al. 2001

Multi-component modelling

2 component model:

one steady component

one variable component

$I(t) = I_0 + \Delta I(t)$ $\quad I_0 = I_{10}+I_{20}$
$Q(t) = Q_0 + \Delta I(t)\, m_{q2}$ $\quad Q_0 = I_{10}\, m_{q1} + I_{20}\, m_{q2}$
$U(t) = U_0 + \Delta I(t)\, m_{u2}$ $\quad U_0 = I_{10}\, m_{u1} + I_{20}\, m_{u2}$
$m_{q1} = p_1 \cos 2\chi_1$ $\quad m_{q2} = p_2 \cos 2\chi_2$
$m_{u1} = p_1 \sin 2\chi_1$ $\quad m_{u2} = p_2 \sin 2\chi_2$

The polarized flux is fitted,

but the polarization angle not.

→ need a third component

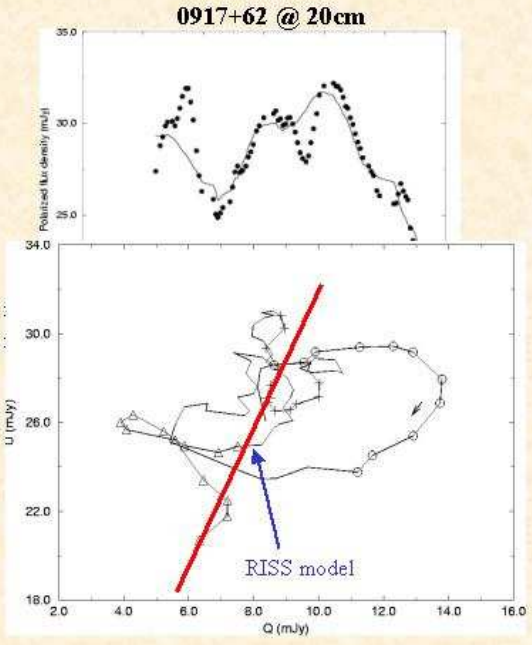

Qian et al. 2001

Multi-component modelling

3 component model:

one steady component

two variable components

$I(t) = I_0 + \Sigma I_2(t) + \Sigma I_3(t)$
$Q(t) = Q_0 + \Sigma I_2(t)\, m_{q2} + \Sigma I_3(t)\, m_{q3}$
$U(t) = U_0 + \Sigma I_2(t)\, m_{u2} + \Sigma I_3(t)\, m_{u3}$
time off set between $\Sigma I_2(t)$ and $\Sigma I_3(t)$

3 components fit much better

but still the PA - fit is not satisfactory.

→adding 4 or 5 components

doesn't help

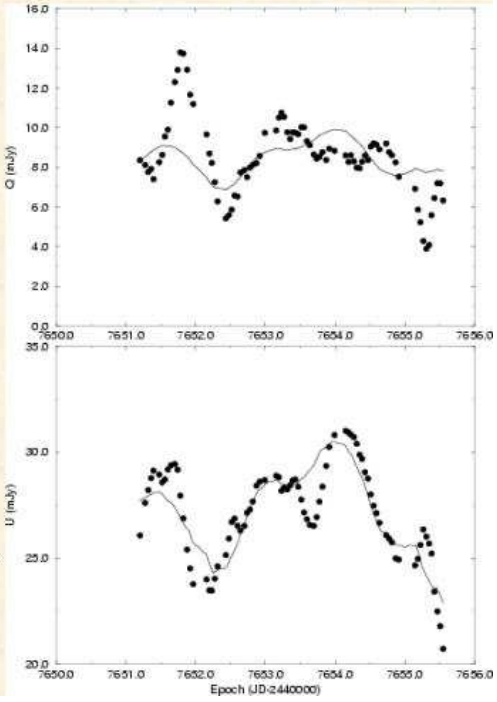

Multi-component modelling

3 component model:

one steady component

two variable components

$I(t) = I_0 + \Sigma I_2(t) + \Sigma I_3(t)$
$Q(t) = Q_0 + \Sigma I_2(t)\, m_{q2} + \Sigma I_3(t)\, m_{q3}$
$U(t) = U_0 + \Sigma I_2(t)\, m_{u2} + \Sigma I_3(t)\, m_{u3}$
time off set between $\Sigma I_2(t)$ and $\Sigma I_3(t)$

3 components fit much better

but still the PA - fit is not satisfactory.

→adding 4 or 5 components

doesn't help

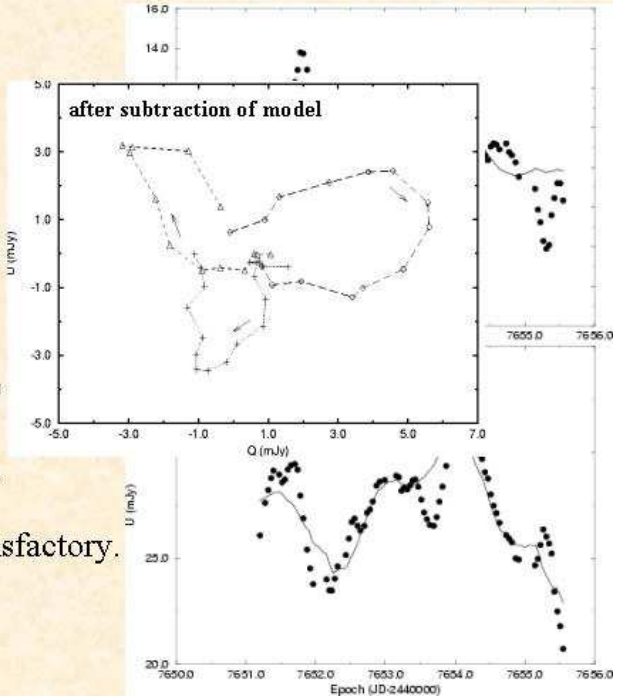

Multi-component modelling

S_2= 400 mJy, 120➲as, m=12%, ↖ = 0.63 days

S_3= 300 mJy, 65➲as, m=7.5%, ↖ = 0.34 days

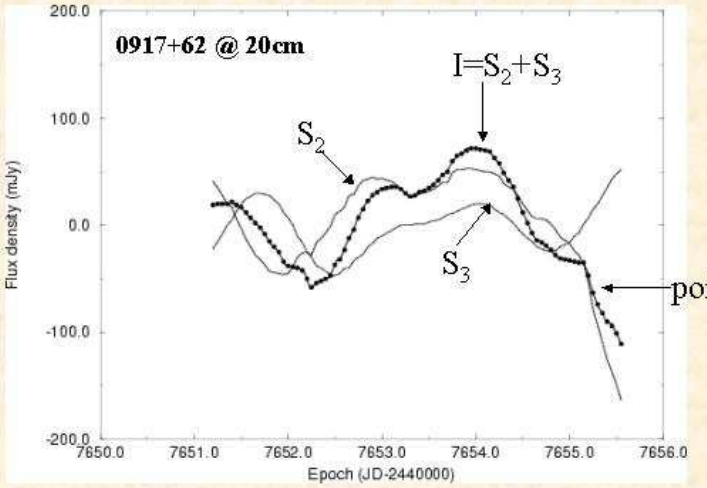

3 component model fits intensity very well

Qian et al. 2001

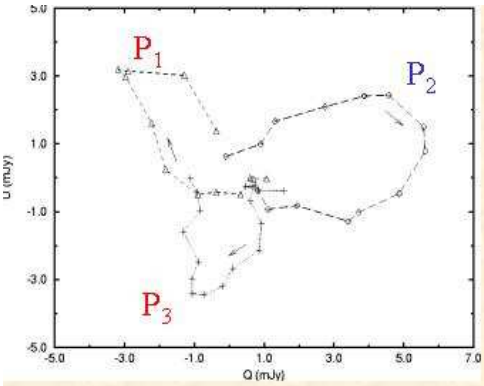

3 peaks in P_{res} of which two correlate with I and one anti-correlates. This cannot be explained by the same process !

Residual polarisation at 20cm after subtraction of 3 component RISS model

Qian et al. 2002

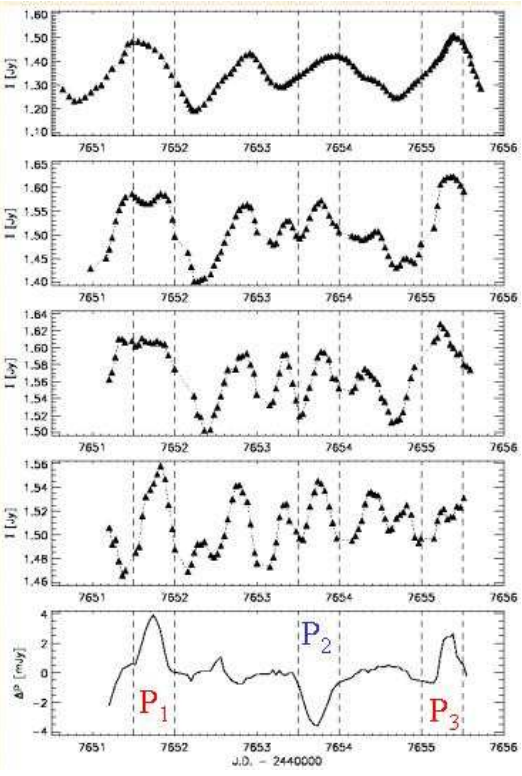

Rapid Intensity and Polarization Variations in PKS 0420-385

8.6 GHz, June 8-10, 1996

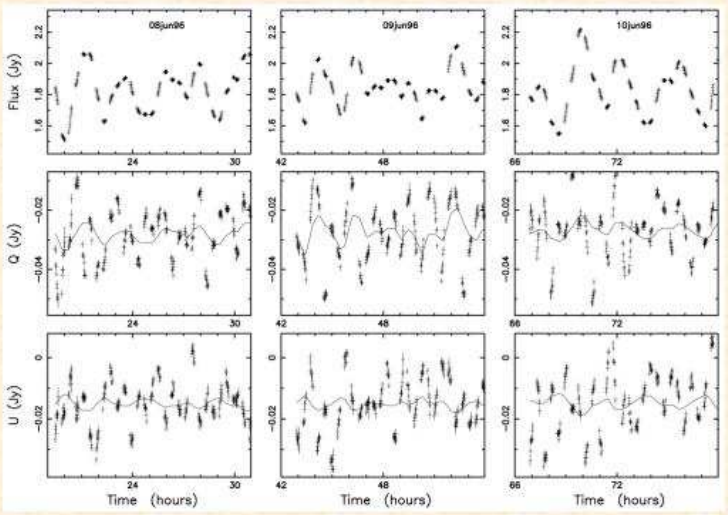

Line: Best fits of the variations in I to the variations in Q and U

Rickett et al. 2002, ApJ 581, 103

$$C_{II,t}(\tau) = \langle \Delta I(t)\Delta I(t+\tau)\rangle$$
$$C_{QQ,t}(\tau) = \langle \Delta Q(t)\Delta Q(t+\tau)\rangle$$
$$C_{UU,t}(\tau) = \langle \Delta U(t)\Delta U(t+\tau)\rangle$$
$$C_{IQ,t}(\tau) = \langle \Delta I(t)\Delta Q(t+\tau)\rangle$$
$$C_{IU,t}(\tau) = \langle \Delta I(t)\Delta U(t+\tau)\rangle$$
$$C_{QU,t}(\tau) = \langle \Delta Q(t)\Delta U(t+\tau)\rangle$$

two strongly polarized components

$T_B \sim 10^{13}$ K

~10 ➲as offset

screen distance 25 pc

velocity 36 km/s

anisotropy 1:4

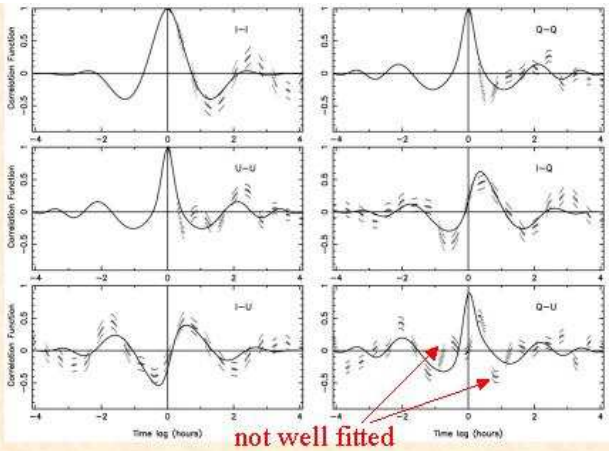

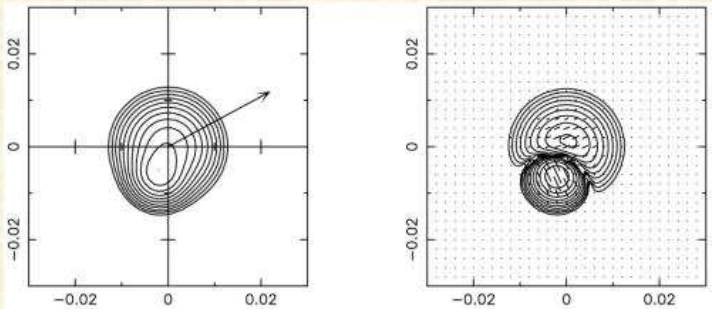

Rickett et al. 2002

3 polarized components

(17 variable parameters)

this fits the Q-U cross correlation (and therefore the polarisation angle)

note: the closer the screen, the lower T_B !

Rickett et al. 2002

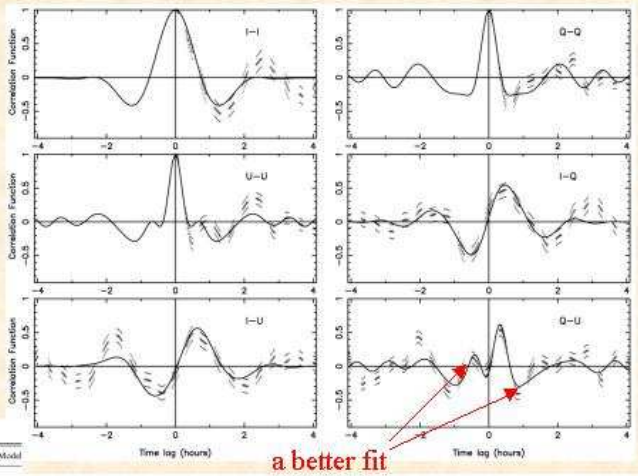

TABLE 3
MODEL PARAMETERS

Parameter	Two-Component Model	Three-Component Model
Screen distance L (pc)	25*	25*
Axial ratio R	0.25*	0.25*
ISS velocity V_{ISS} (km s^{-1})	36*	36*
Direction of ISS velocity ψ (deg)	28	11
Spectral exponent α	5/3*	5/3*
Total flux density S_{C1} (Jy)	0.38	0.48
FWHM θ_1 (μas)	15	30
Polarized flux density P_1 (Jy)	0.18	0.35
Polarized P.A. χ_1 (deg)	23	29
Total flux density component 2 S_{C2} (Jy)	0.19	0.024
FWHM θ_2 (μas)	9.4	19
Polarized flux density component 2 P_2 (Jy)	0.17	0.22
Polarized P.A. χ_2 (deg)	−65	63
Component 2 position $\delta_{x,2}$ (μas)	−1.9	−4
Component 2 position $\delta_{y,2}$ (μas)	−6	1.6
Total flux density S_{C3} (Jy)	0	0.091
FWHM θ_3 (μas)	...	19
Polarized flux density component 3 P_3 (Jy)	...	0.11
Polarized P.A. χ_3 (deg)	...	56
Component 3 position $\delta_{x,3}$ (μas)	...	11
Component 3 position $\delta_{y,3}$ (μas)	...	−2

NOTE.—The values with an asterisk were fixed in the fits. Angles are given relative to the minor axis of the scattering ellipse (defined in eq. [15]). Polarized position angles are defined as for the observations. Although the polarized flux densities for components 2 and 3 are greater than 70% of their individual total flux densities, the polarized brightness is everywhere less than 70% of the total brightness in these models, as displayed in Figs. 13 and 15. See text concerning the lack of uniqueness in the parameters.

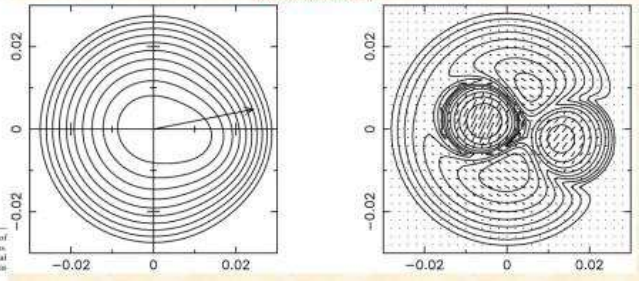

Summary

• a multi-component model consisting of stationary and scintillating component of different flux and size can explain the observed variations of total intensity and polarized flux at.

• highly polarized (10-70 %) sub-structure is required on mikro-arcsecond scales.

• the observed polarization angle variations cannot be explained in the Qian model (1 D) but likely is explained in the Rickett model (2 D, anisotropy).

• after subtraction of the model, the residual polarized flux shows 3 features, of which 2 correlated with the variations at higher frequencies. This could be explained by RISS.

• For one feature, the residual polarized flux anti-correlates with the variations at higher frequencies.

• In scintillation theory (Rickett, Walker) correlated or anti-correlated variations are possible. However a transition from correlated to anti-correlated would require a „coordinated variation" of at least 2 scintillating components.

• The observations could be also explained, if the polarized sub-structure changes on the time scale between „correlated" and „anti-correlated" (days) or by shock-in-jet models (e.g. Qian et al. 2002).

• Examination of CCFs for I, Q, U at different frequencies does help to disentangle scintillation effects from intrinsic variability.

Elimination of confusing sources in Cosmic Background Imager fields

– E. Angelakis, A. Zensus, T. Krichbaum, A. Kraus, A. Readhead, T. Pearson, R. Bustos, R. Reeves

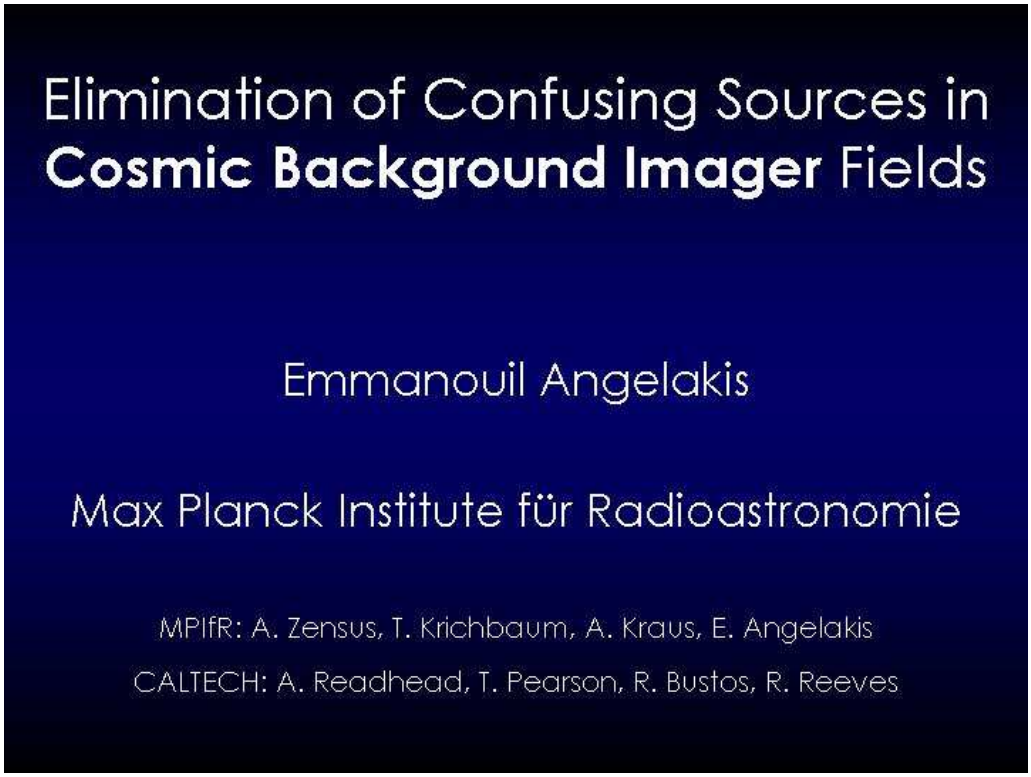

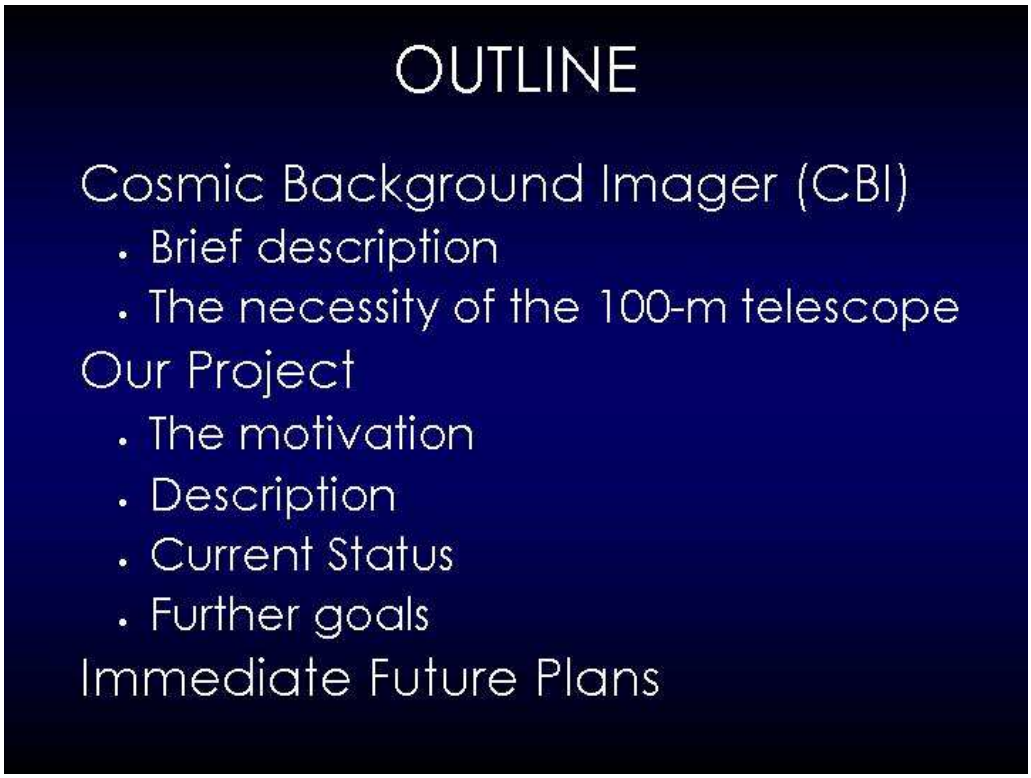
OUTLINE
Cosmic Background Imager (CBI)
• Brief description
• The necessity of the 100-m telescope
Our Project
• The motivation
• Description
• Current Status
• Further goals
Immediate Future Plans

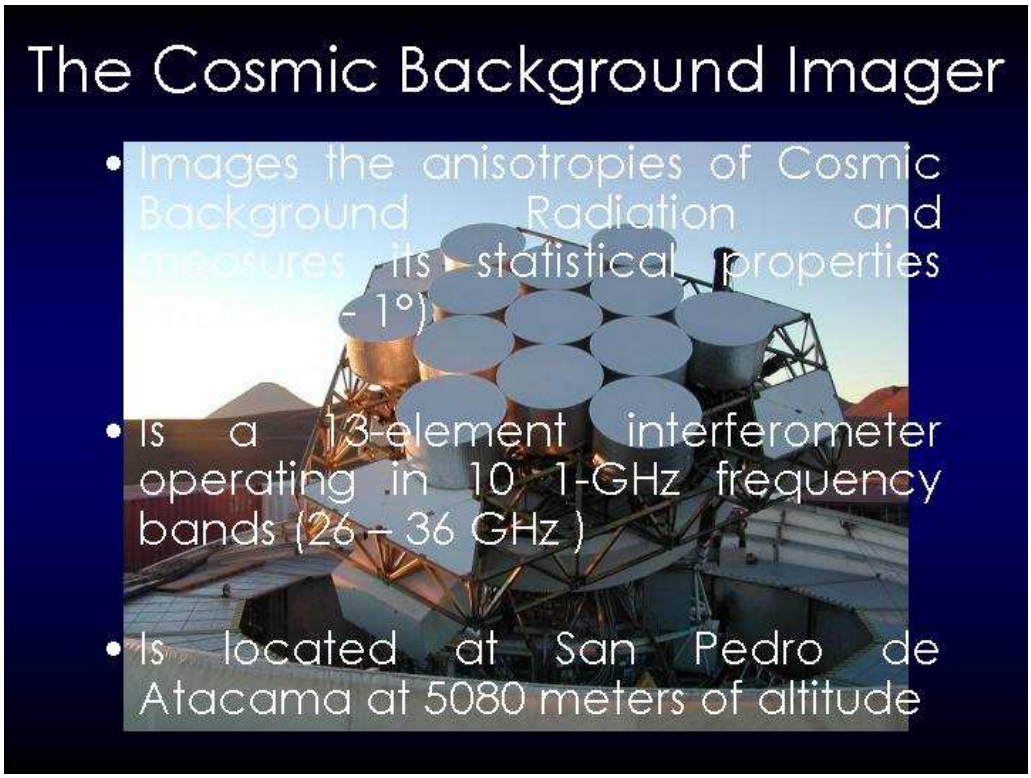
The Cosmic Background Imager
• Images the anisotropies of Cosmic Background Radiation and measures its statistical properties (scales ~ 1°)
• Is a 13-element interferometer operating in 10 1-GHz frequency bands (26 – 36 GHz)
• Is located at San Pedro de Atacama at 5080 meters of altitude

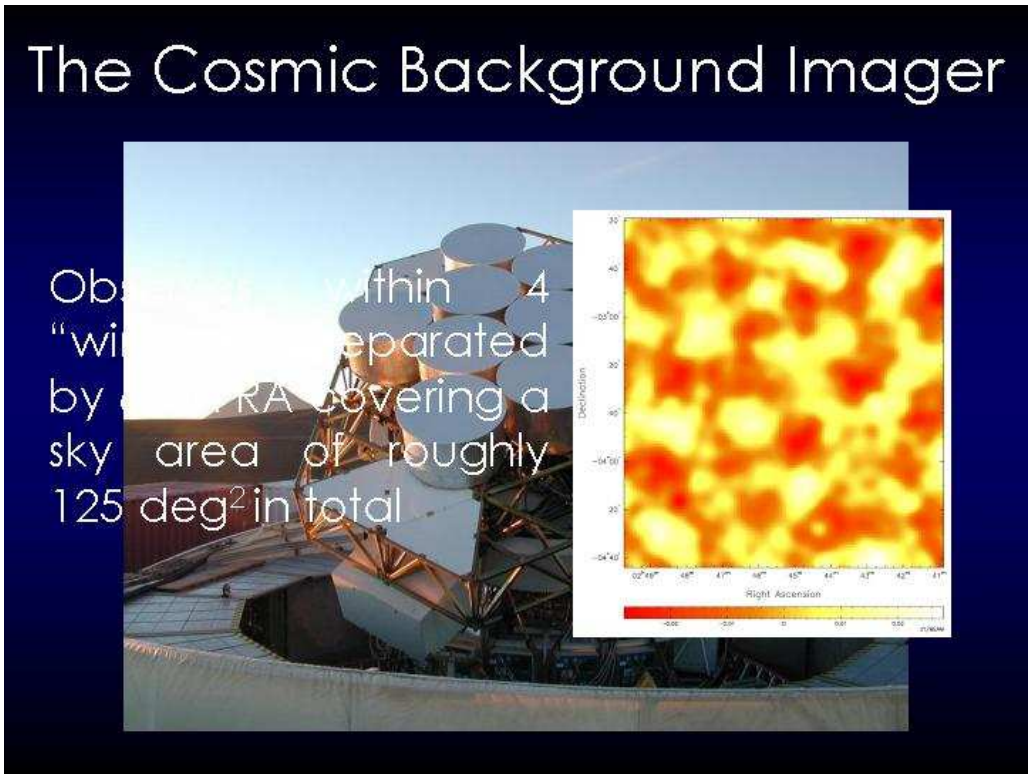
The Cosmic Background Imager
Declination
Right Ascension

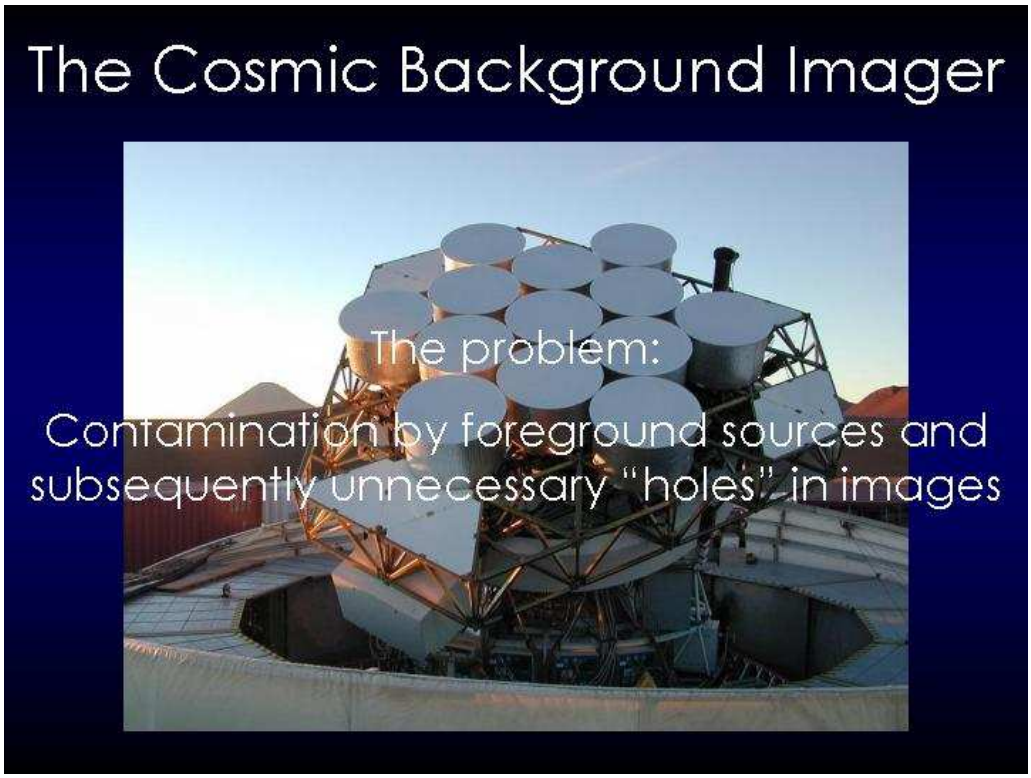
The Cosmic Background Imager
The problem:
Contamination by foreground sources and
subsequently unnecessary "holes" in images


Our Project: Motivation
The Solution:
Identify those sources and verify that they are NOT bright enough to "distort" the CMB image

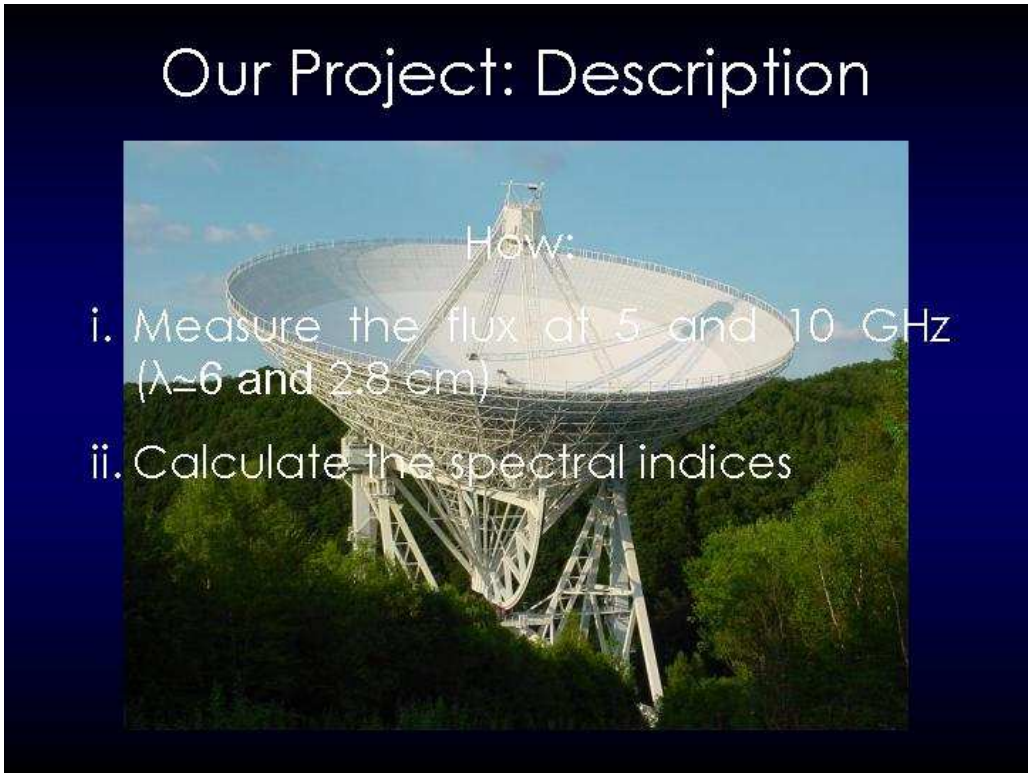
Our Project: Description
How:
i. Measure the flux at 5 and 10 GHz (λ≈6 and 2.8 cm)
ii. Calculate the spectral indices


Our Project: Description
Estimations:
• 37 sources/deg² with $S_{1.4GHz} > 3.4$ mJy
• Total field 125 deg² → 4500 sources
• Estimated observing time needed ≃ 400 h


Our Project: Description
The "on-off" technique has been implemented to subtract the "system noise"

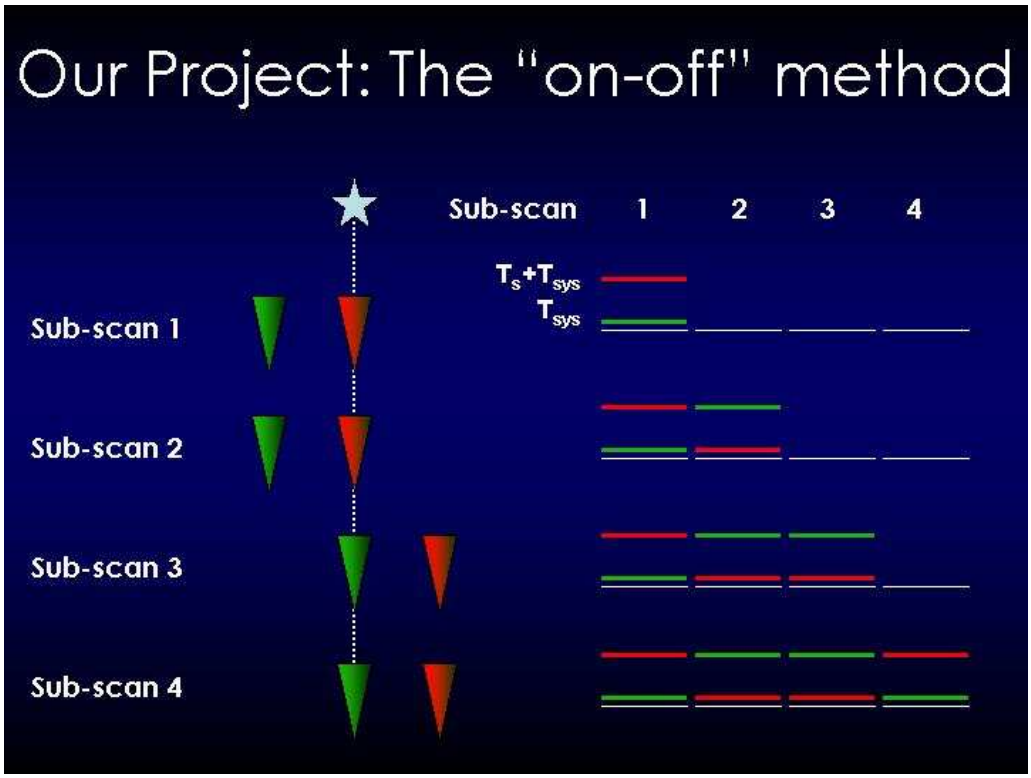
Our Project: The "on-off" method
Sub-scan 1 2 3 4
T_s+T_{sys}
T_{sys}
Sub-scan 1
Sub-scan 2
Sub-scan 3
Sub-scan 4

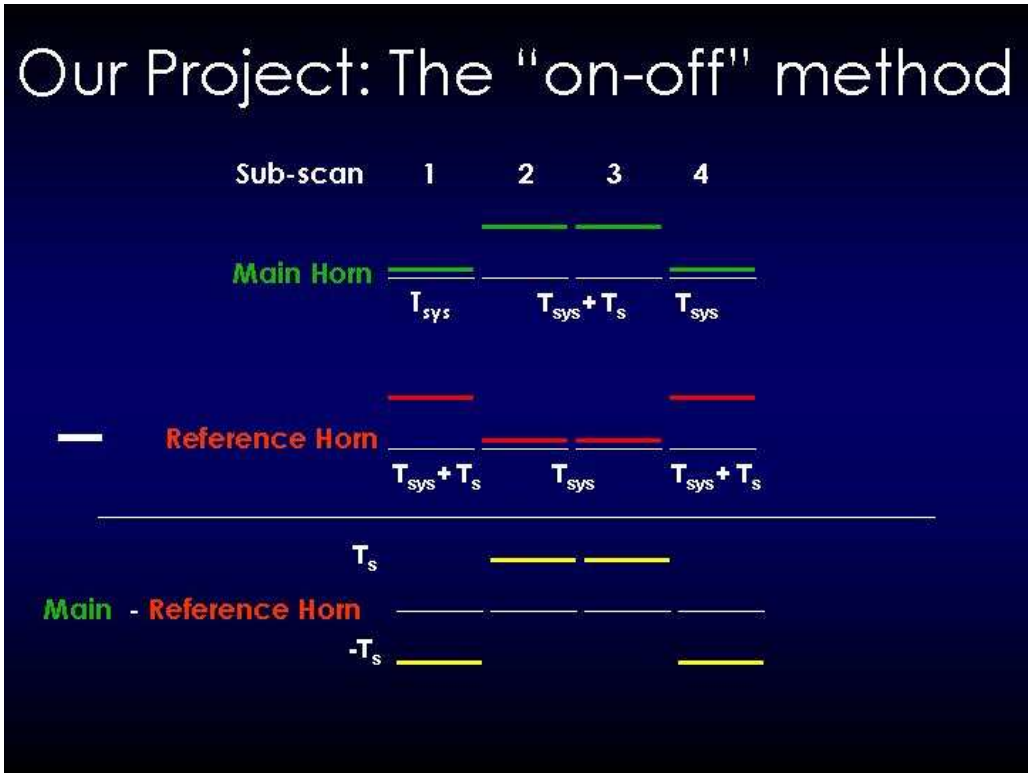
Our Project: The "on-off" method
Sub-scan 1 2 3 4
Main Horn
T_{sys} $T_{sys}+T_s$ T_{sys}
Reference Horn
$T_{sys}+T_s$ T_{sys} $T_{sys}+T_s$
T_s
Main - Reference Horn
$-T_s$

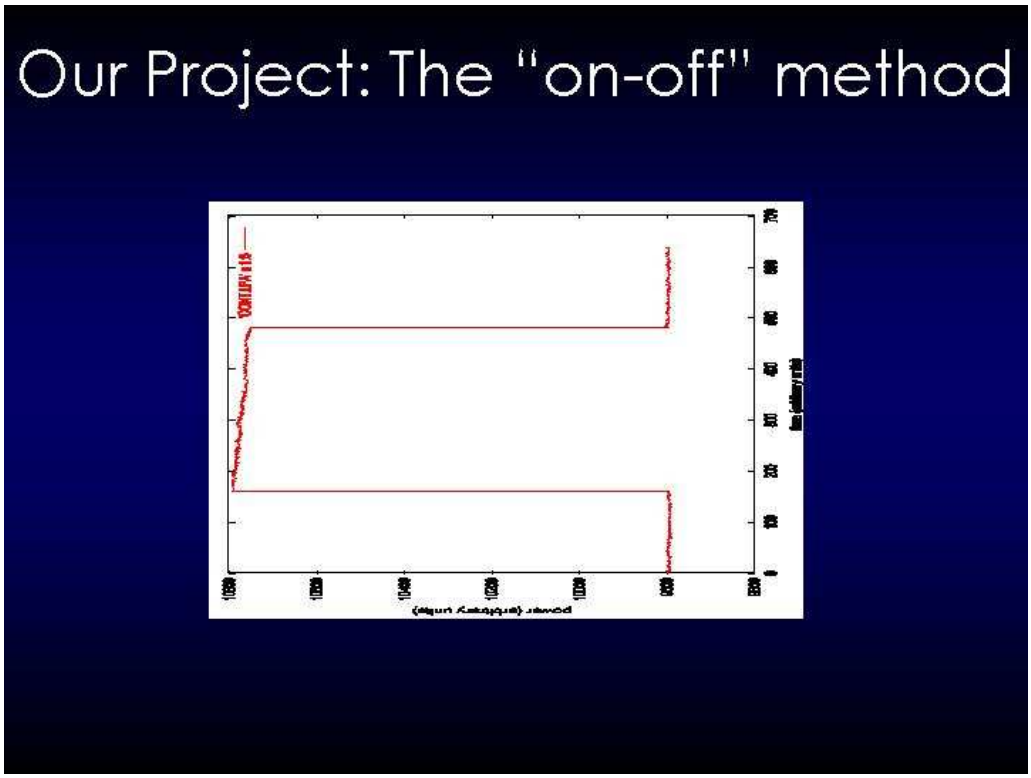
Our Project: The "on-off" method

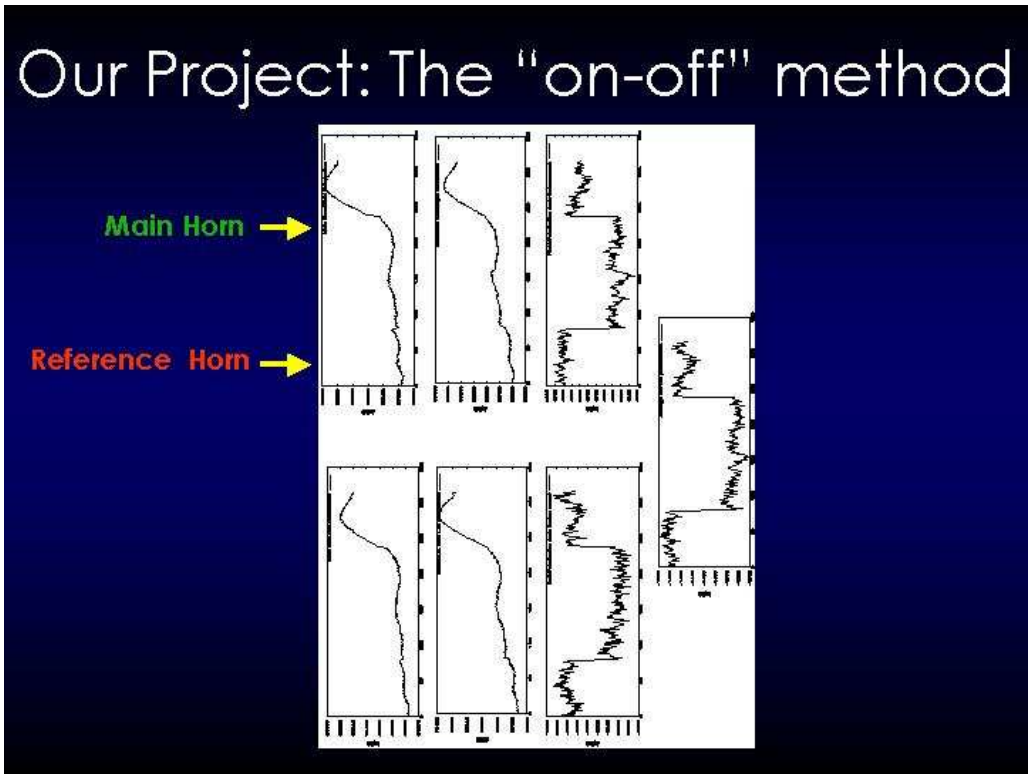
Our Project: The "on-off" method
Main Horn
Reference Horn

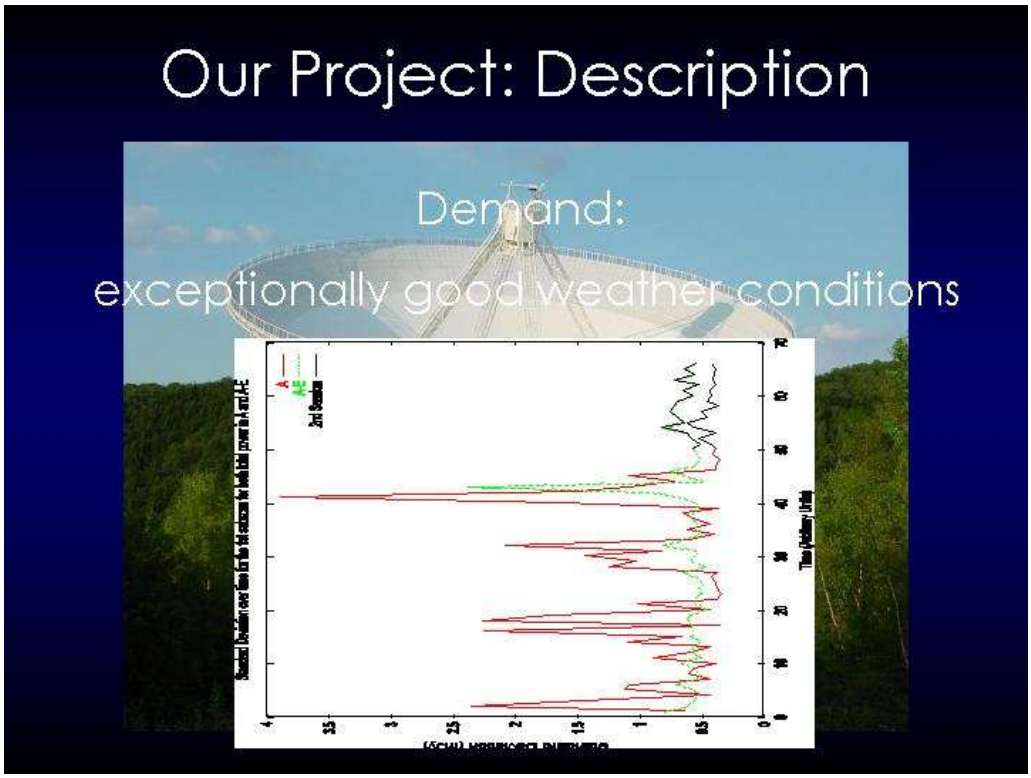
Our Project: Description
Demand:
exceptionally good weather conditions

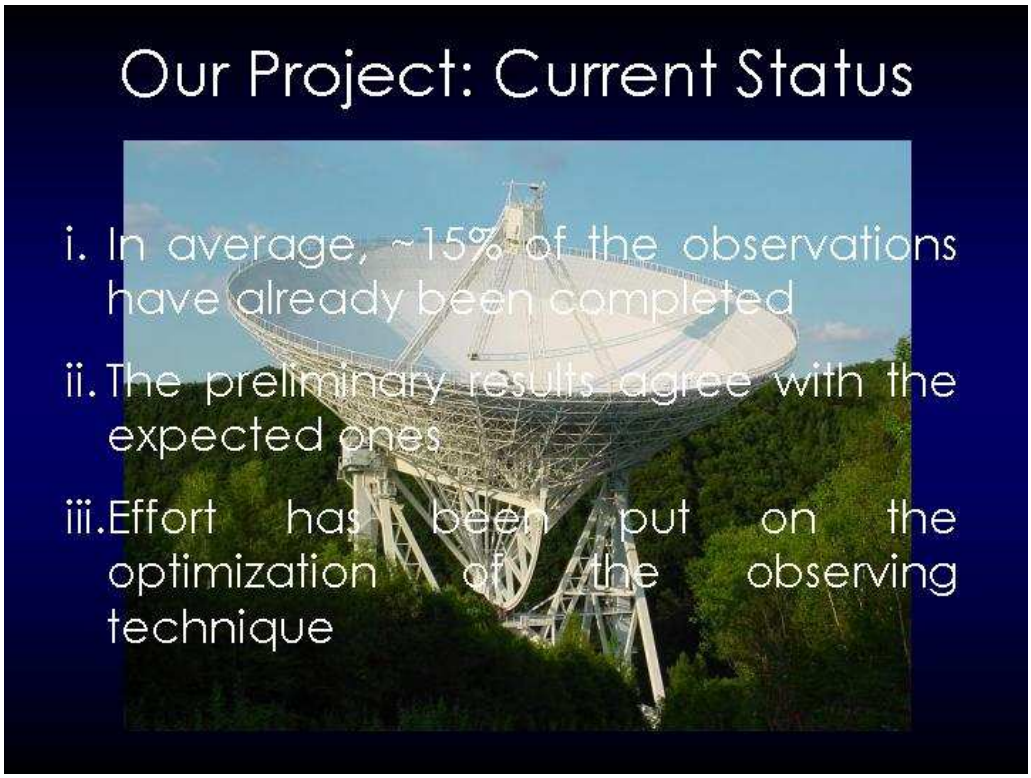
Our Project: Current Status
i. In average, ~15% of the observations have already been completed
ii. The preliminary results agree with the expected ones
iii. Effort has been put on the optimization of the observing technique


Our Project: Further Goals
i. Studying the spectral indices of a few thousand sources
ii. Radio sources statistics
iii. Intra-Day Variability candidates
iv. Detailed study of atmospheric influence on radio observations
v. And more…


Immediate Future Plans
i. Complete the first half of the observing sessions
ii. Keep on with the detailed data analysis
iii. Work on side projects in parallel

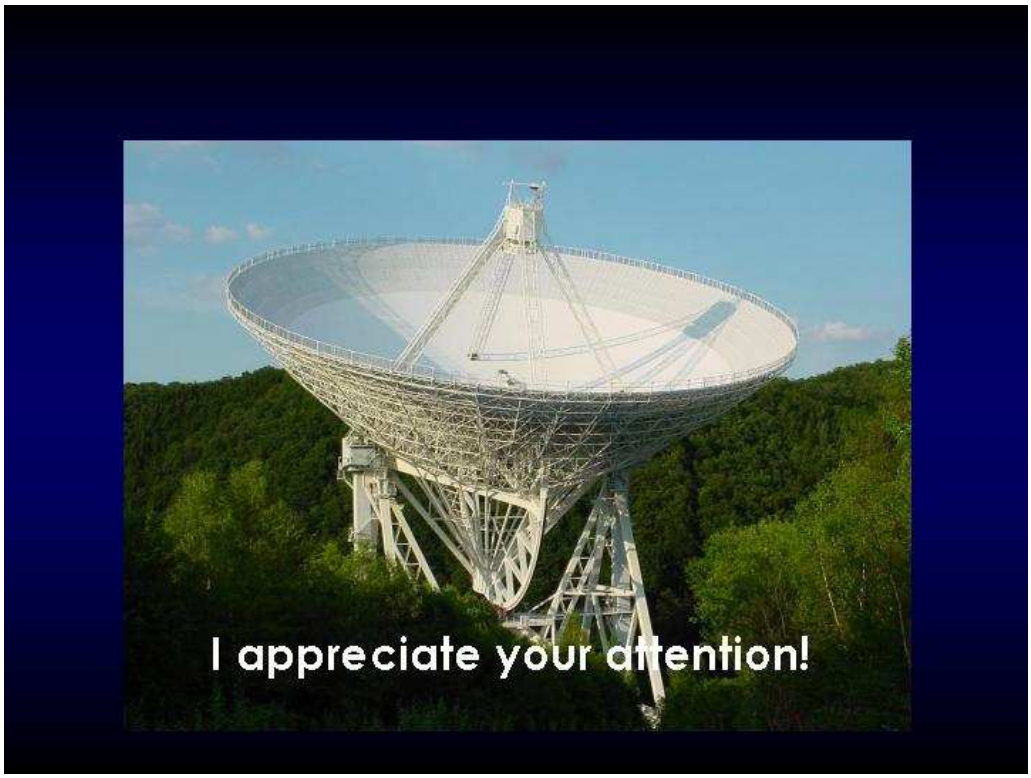
I appreciate your attention!

Session III: Variations of source structure and flux

Introduction to Session III: Variations of source structure and flux – M. Tornikoski

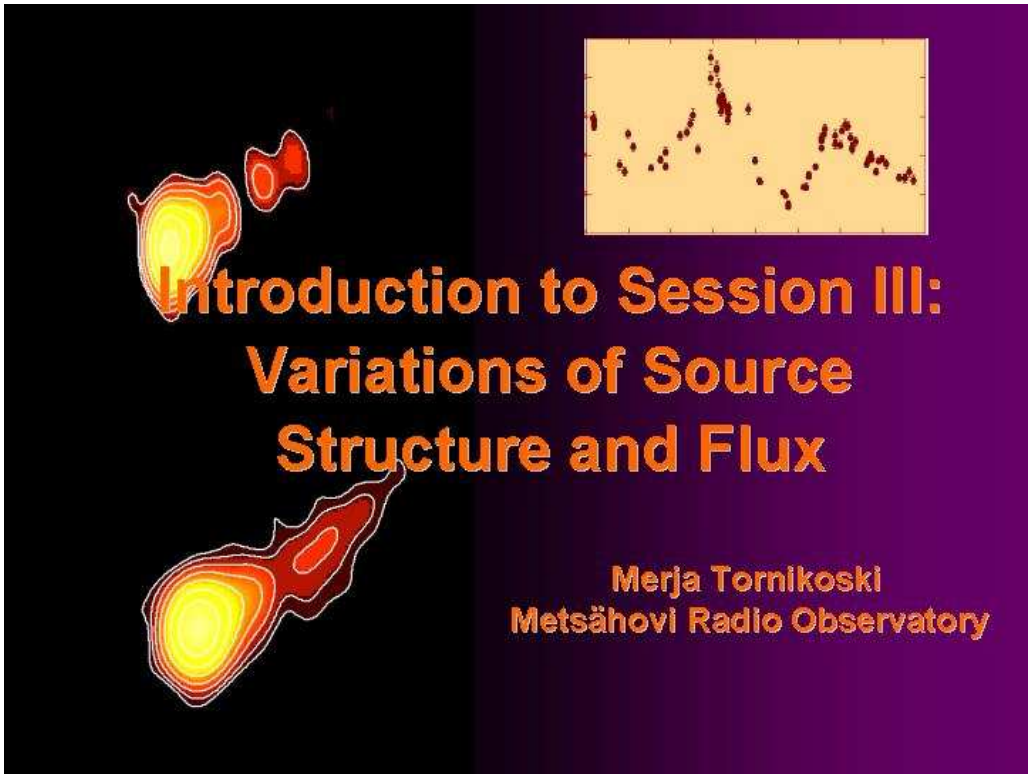

Goals

- High-resolution VLBI imaging.
- Long-term flux density monitoring at all wavebands.

Merja Tornikoski
Metsähovi Radio Observatory

Methods

- Dense monitoring & imaging.
- Flux databases.
- Multifrequency campaigns.
- Millimetre-VLBI.

Merja Tornikoski
Metsähovi Radio Observatory

Present situation

- Flux databases, multifrequency campaigns, flare alerts:
  ENIGMA multifrequency information web page.
- Multifrequency campaigns:
  Campaign session I & II on Tuesday.
- Millimetre-VLBI:
  Campaign session I & II on Tuesday.
- Also:
  analysis of existing data,
  individual flares, statistics, etc.: ongoing!

Merja Tornikoski
Metsähovi Radio Observatory

ENIGMA multifrequency data and campaign information web page

http://kurp.hut.fi/~mtt/enigma

1. Multifrequency campaigns: Past, present, future.
   - Epoch
   - Instruments
   - Contact person
   - (Past campaigns: status, whether additional data is needed, etc.)

Merja Tornikoski
Metsähovi Radio Observatory

2. Alerts about flaring blazars
- Object
- Observer, instrument, flux, comment
- A "FYI" alert or plea for data?

3. Data access information
- Instrument, frequency band(s)
- Source lists and other information
- Published: access, unpublished: contact person

Merja Tornikoski
Metsähovi Radio Observatory

See the following demonstration

and

help me update the info page

(+ help me keep it up to date)!

Merja Tornikoski
Metsähovi Radio Observatory

Radio variability of inverted-spectrum sources – M. Tornikoski, I. Torniainen

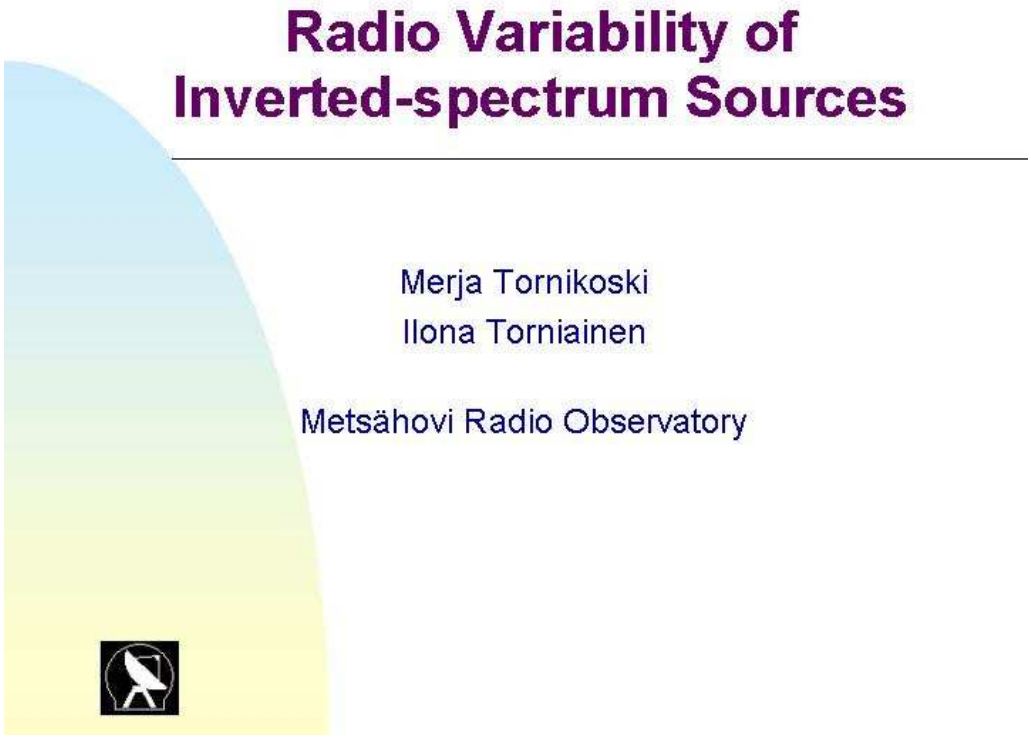

Inverted-spectrum sources

- GHz-peaked-spectrum (GPS) sources, in general:
  - $\nu_{turnover}$ > 1 GHz.
  - Compact.
  - GPS+CSS: the least variable class of compact extragal. objects.
  - Low optical polarization.
  - Superluminal motion appears to be rare.
  - GPS sources identified with QSOs have large z's.

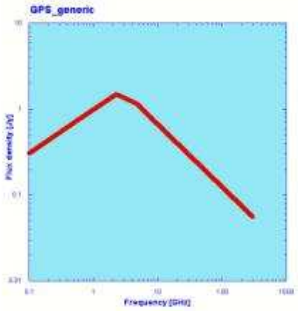

Merja Tornikoski
Metsähovi Radio Observatory

Our work: objectives

- Part of the Planck foreground science programme.
- Variability of known GPS sources.
- New GPS sources.
- Extreme-peaked sources.
- Variable flat-spectrum vs. "genuine" GPS sources.
- VLBI structure of high-peaked sources.

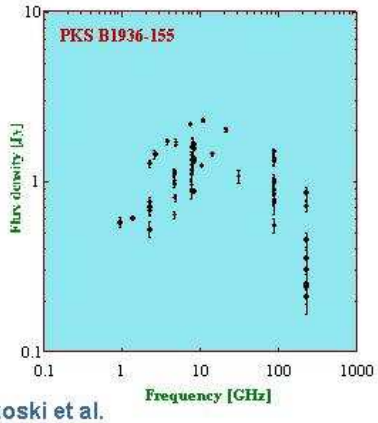

Tornikoski et al.
A&A 120, 2000

Merja Tornikoski
Metsähovi Radio Observatory

Samples

- "Bona fide GPS sources".
- GPS candidates.
- "Sometimes inverted spectra".

Southern sample + Northern sample
Long-term, multifrequency data.

- Comparison samples:
  GPS galaxies, CSS-galaxies.

Merja Tornikoski
Metsähovi Radio Observatory

"Bona fide GPS sources":
With long-term monitoring very few retain the convex shape!

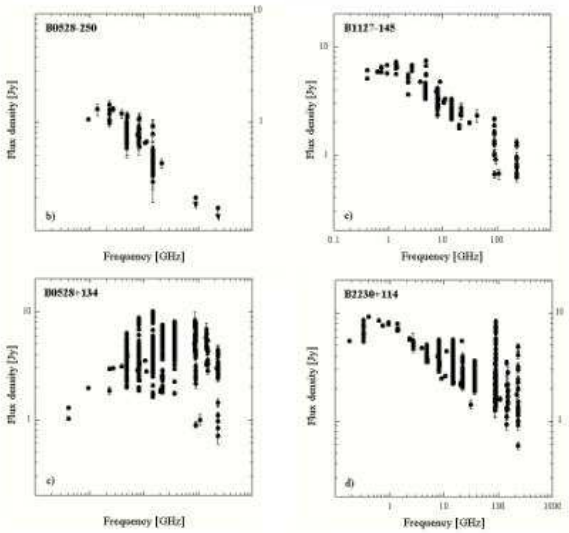

Merja Tornikoski
Metsähovi Radio Observatory

Effect of sparse data taking:

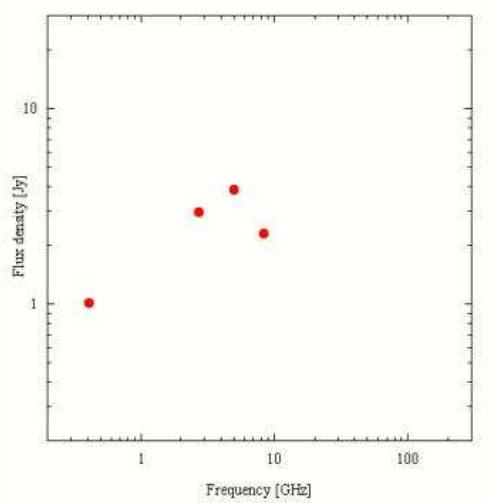

Merja Tornikoski
Metsähovi Radio Observatory

Effect of sparse data taking:

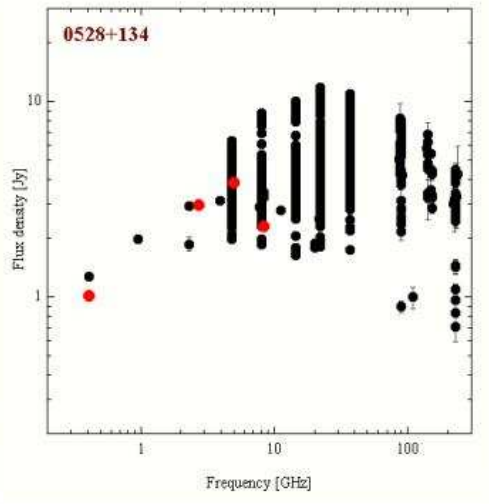

Merja Tornikoski
Metsähovi Radio Observatory

Only *very few* genuinely convex spectra!

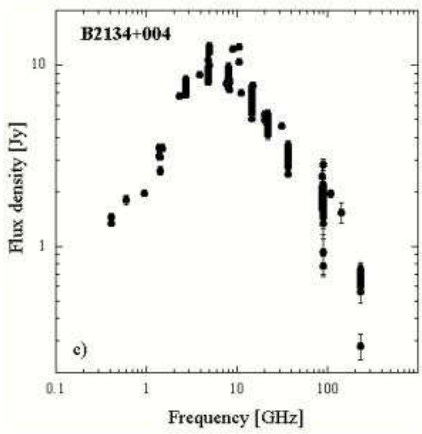

Merja Tornikoski
Metsähovi Radio Observatory

Torniainen & Tornikoski, in preparation for the A&A:

Lots of sources
with spectra inverted during flares!

- Considerable variability in the mm-domain.
- Turnover frequencies as high as >100 GHz.
- During quiescent state the spectra remain flat or even falling.
- Probably a large number of such sources have been excluded from high-frequency studies and thus have not been identified yet!
- Note: much less time is spent in the active state!

Merja Tornikoski
Metsähovi Radio Observatory

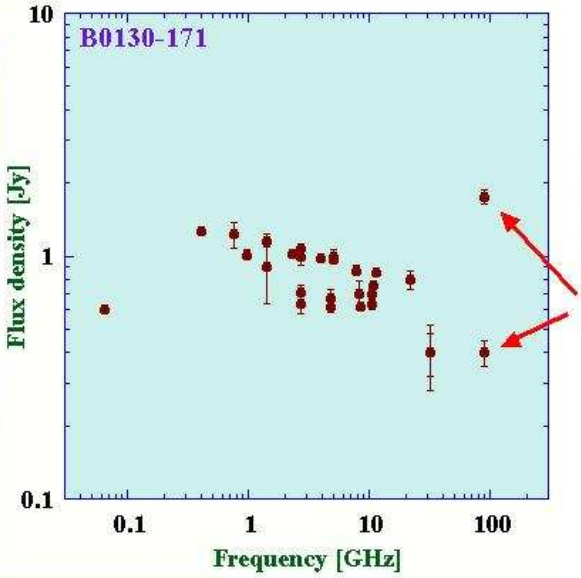

Sometimes
few-epoch observations
can reveal the true (?)
variability!
(Time btw the 2
90 GHz data points
= 14 years!)

Merja Tornikoski
Metsähovi Radio Observatory

Radio properties of BL Lacs, Intermediate BL Lacs (IBL)

Goals:

- Systematically study the mm-properties of BLOs.
- Is there a continuity from subsample to subsample?
- Are there radio silent BLOs?
- Can radio weak BLOs be radio loud at times?
- How does this all fit within the framework of the unifying scheme?

Original source sample:
Veron-Cetty & Veron 2000: 462 BLOs

Merja Tornikoski
Metsähovi Radio Observatory

Results

- By July 2003: Observed 385 out of 398 equatorial to Northern BLOs = 96.7%.
- For many of them, only one-epoch so far!
- 37 GHz detection limit ca. 0.3 Jy.
- Detections:
  ALL: 130 / 385; 34%
  RBL: 49 / 56; 88%
  IBL: 41/125; 33%
  XBL: 28 / 103; 27%

Note: Some objects do not belong to any of the subclasses, sometimes several classifications are assigned to one object.

Merja Tornikoski
Metsähovi Radio Observatory

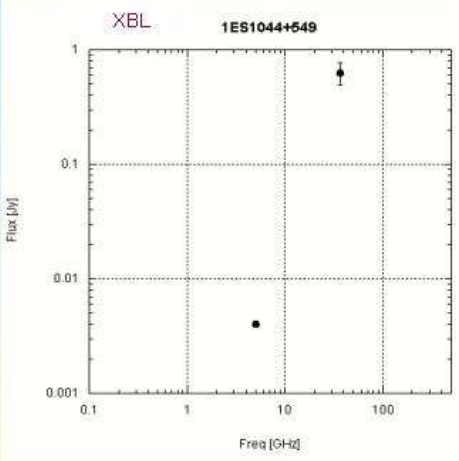

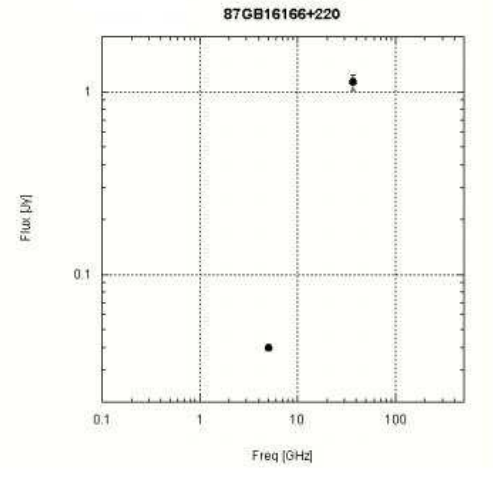

Merja Tornikoski
Metsähovi Radio Observatory

BLO -- conclusions

- More than 1/3 of all objects, ca. 1/3 of XBLs detected (S > 250-300 mJy) in one- or few-epoch observations.
  (→ detectable also with Planck-satellite!)
- Several highly inverted spectra.
- Variability?

Merja Tornikoski
Metsähovi Radio Observatory

Conclusions

- Only very few genuinely convex spectra.
- Lots of sources with spectra that can sometimes be inverted, many of them are faint at low radio frequencies.
- A large number of sources that can be bright in the mm-domain have earlier been excluded from source samples.

→ Number of AGNs that can be bright in the mm-domain probably larger than expected?

Merja Tornikoski
Metsähovi Radio Observatory

Quasi-periodic changes in the parsec-scale jet of the quasar 3C 345. A high resolution study using VSOP and VLBA – J. Klare, J. A. Zensus, A. Witzel, T. P. Krichbaum, A. P. Lobanov, E. Ros

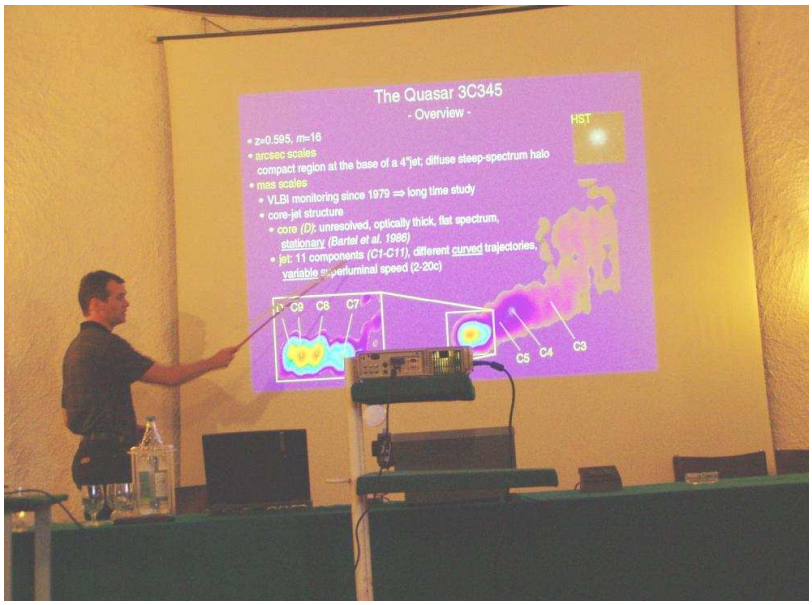

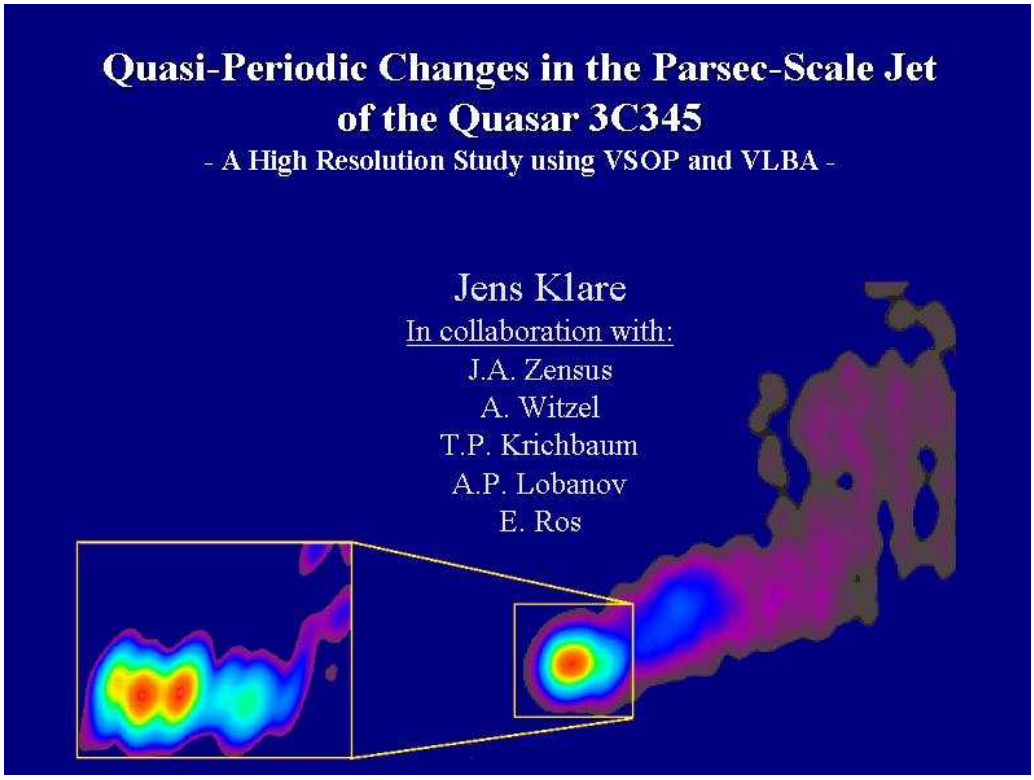

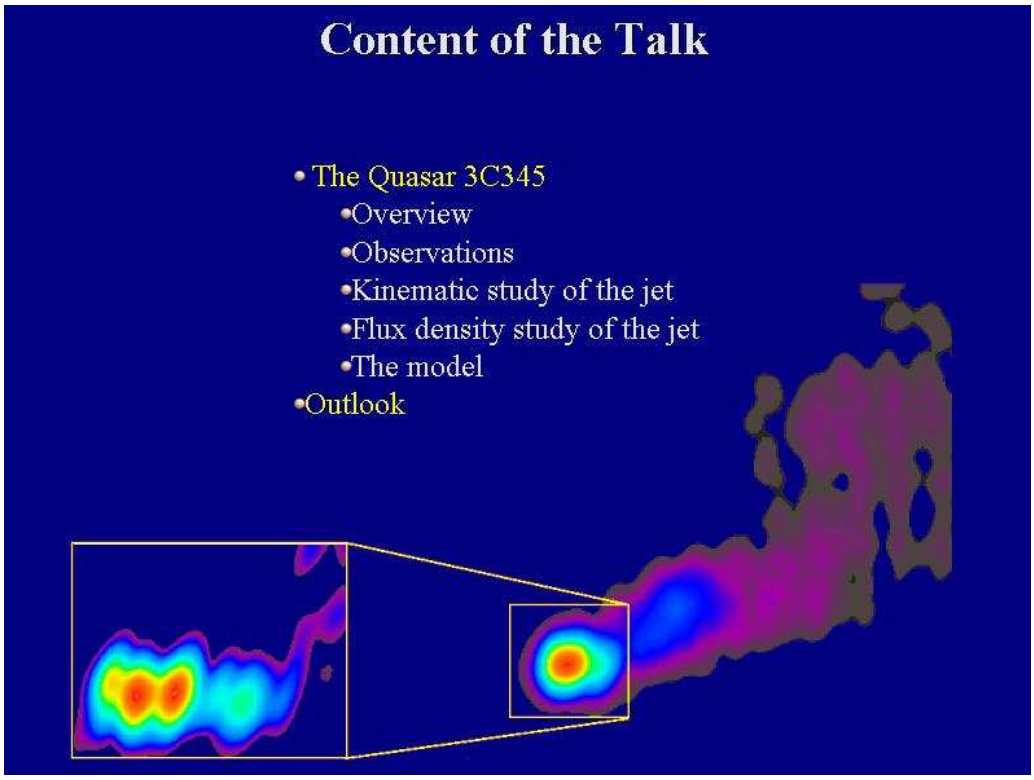
Content of the Talk
• The Quasar 3C345
•Overview
•Observations
•Kinematic study of the jet
•Flux density study of the jet
•The model
•Outlook

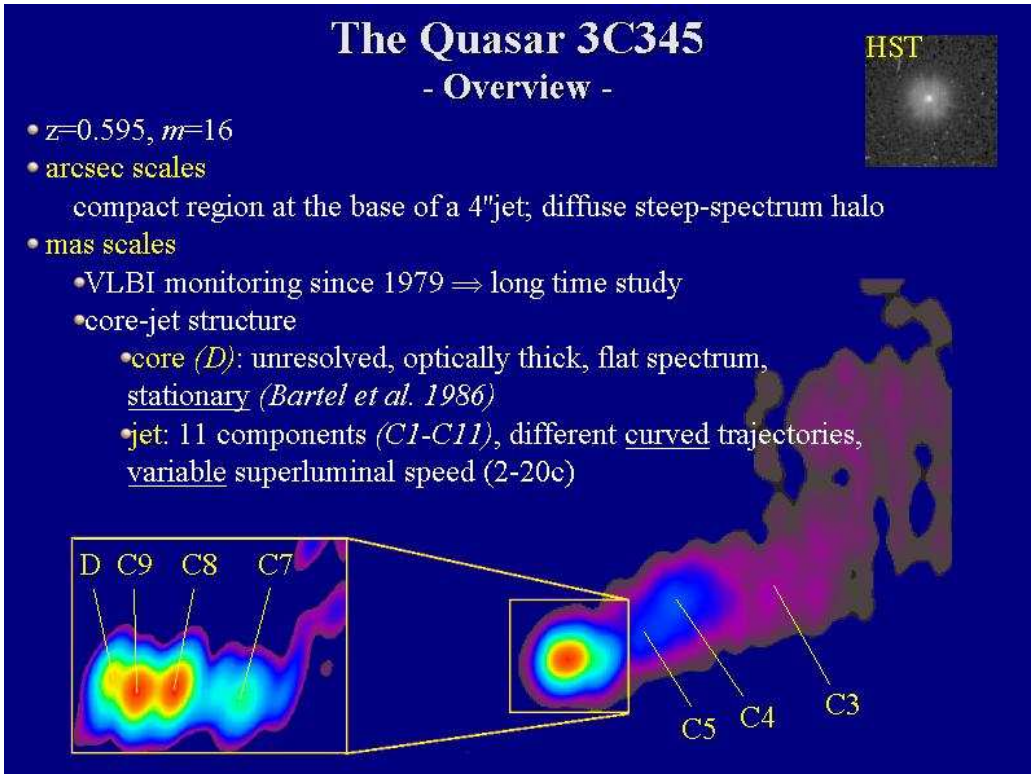
The Quasar 3C345
- Overview -
HST
• z=0.595, m=16
• arcsec scales
compact region at the base of a 4"jet; diffuse steep-spectrum halo
• mas scales
•VLBI monitoring since 1979 ⇒ long time study
•core-jet structure
•core (D): unresolved, optically thick, flat spectrum, stationary (Bartel et al. 1986)
•jet: 11 components (C1-C11), different curved trajectories, variable superluminal speed (2-20c)
D C9 C8 C7
C5 C4 C3

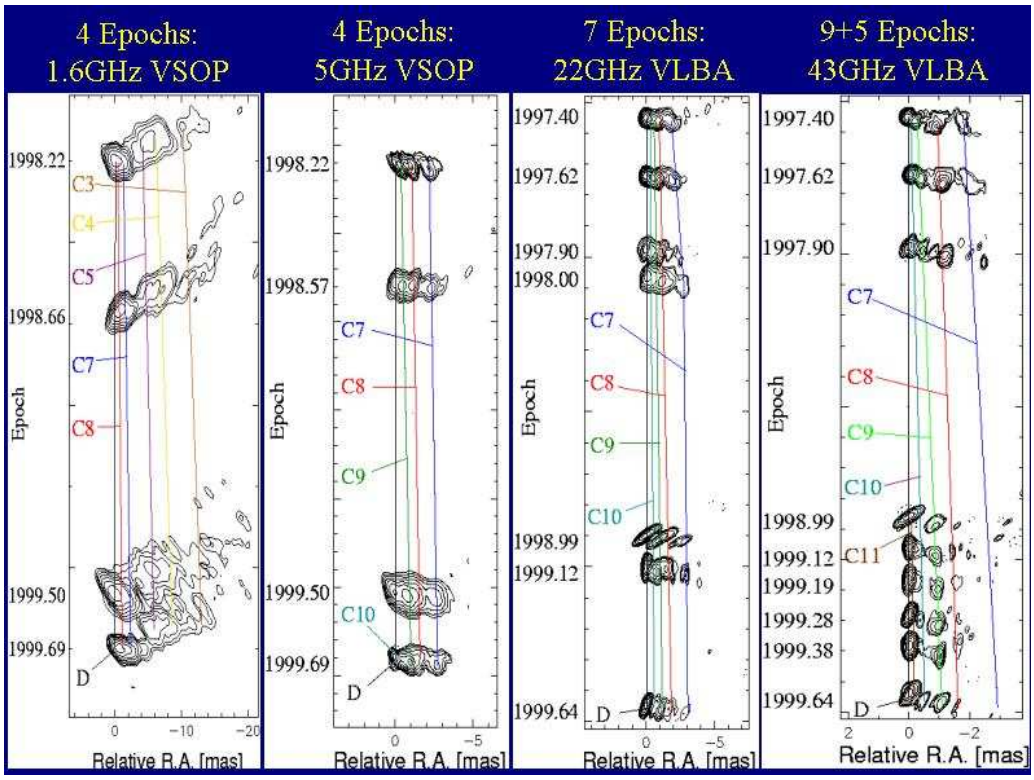
4 Epochs:
1.6GHz VSOP
4 Epochs:
5GHz VSOP
7 Epochs:
22GHz VLBA
9+5 Epochs:
43GHz VLBA
Epoch
Relative R.A. [mas]
C3
C4
C5
C7
C8
C9
C10
C11
D

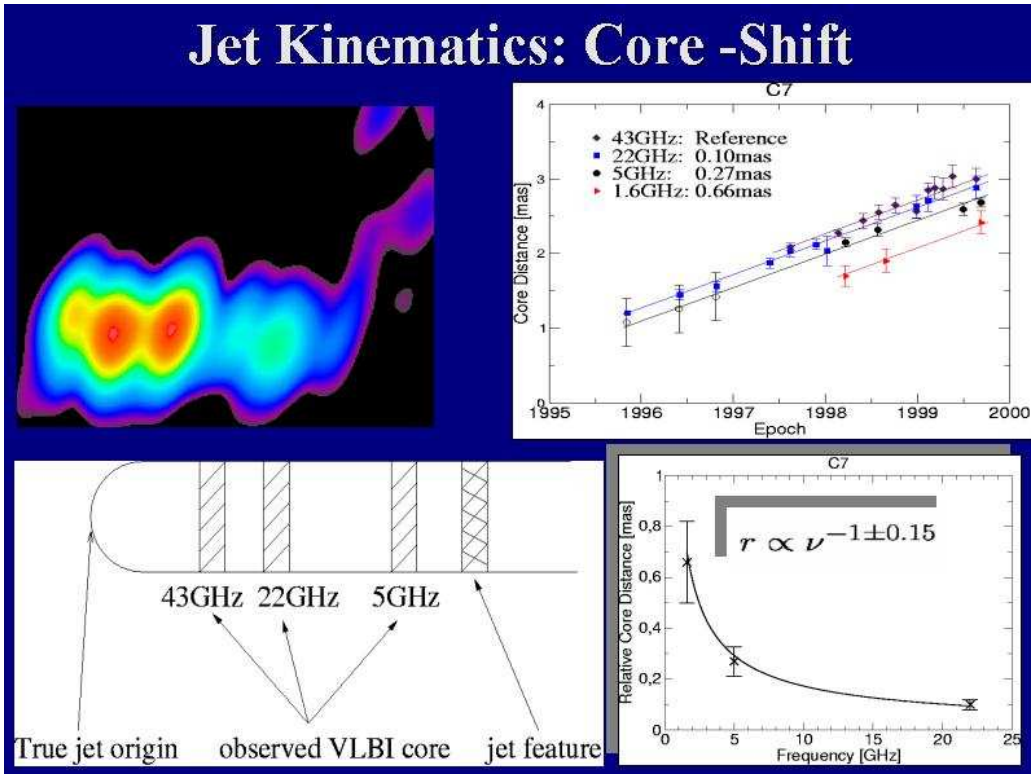
Jet Kinematics: Core -Shift
C7
43GHz: Reference
22GHz: 0.10mas
5GHz: 0.27mas
1.6GHz: 0.66mas
Core Distance [mas]
Epoch
43GHz 22GHz 5GHz
True jet origin
observed VLBI core
jet feature
Relative Core Distance [mas]
$r \propto \nu^{-1\pm0.15}$
Frequency [GHz]

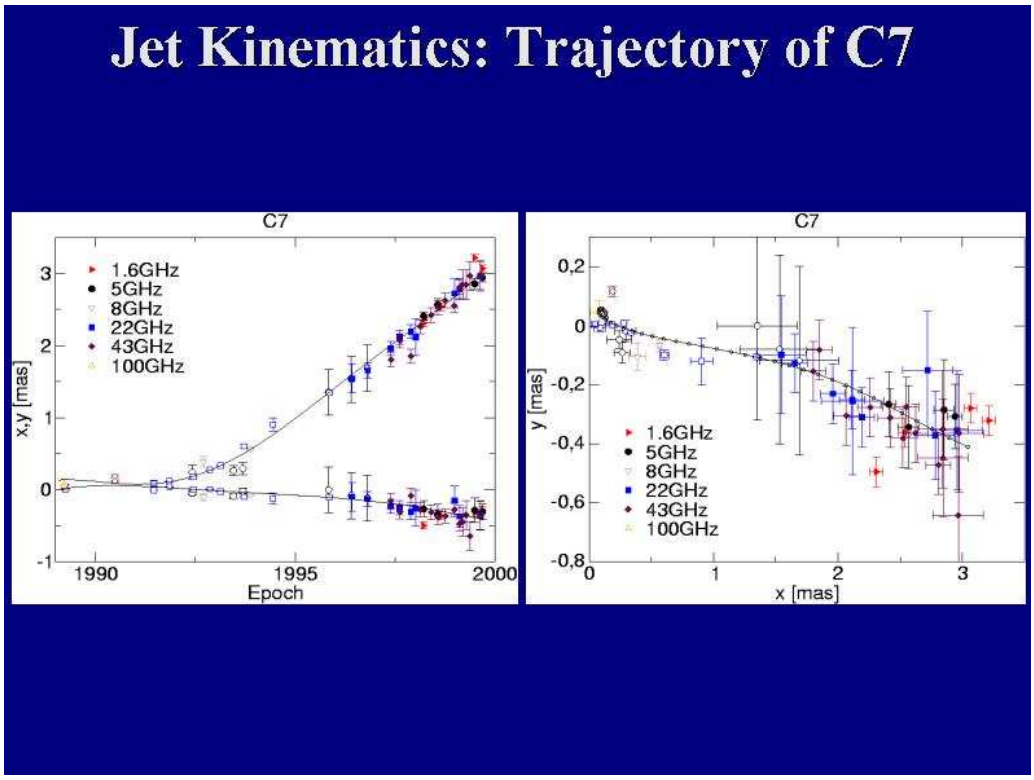
Jet Kinematics: Trajectory of C7
C7
1.6GHz
5GHz
8GHz
22GHz
43GHz
100GHz
x,y [mas]
Epoch
C7
y [mas]
x [mas]

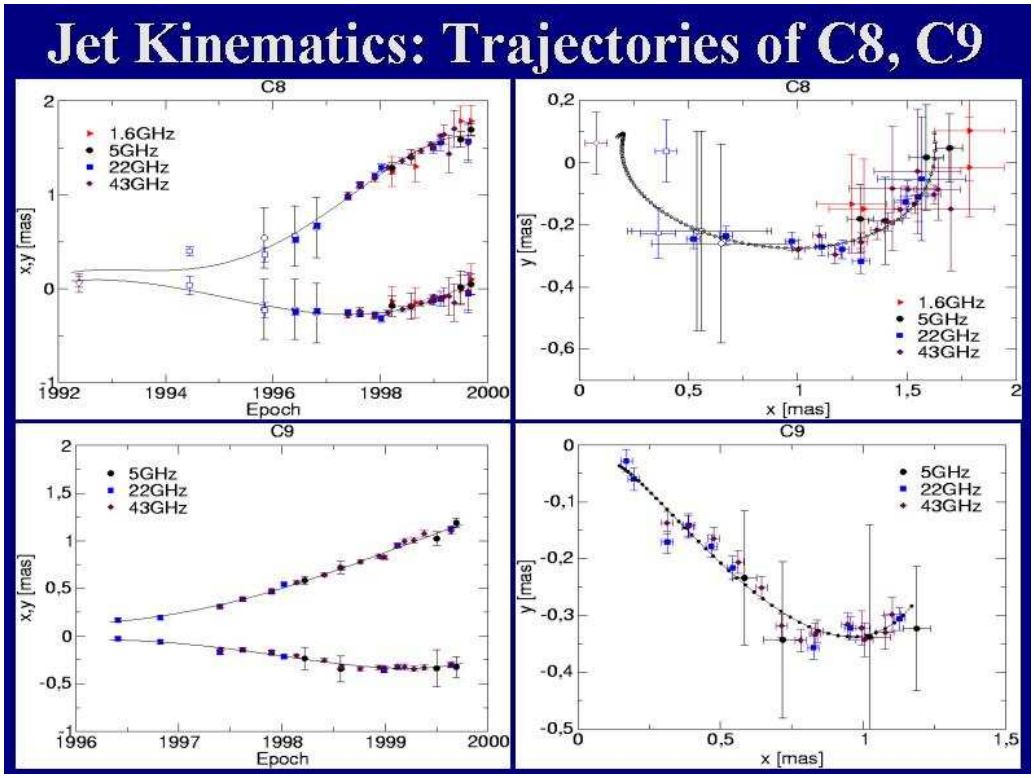
Jet Kinematics: Trajectories of C8, C9
C8
1.6GHz
5GHz
22GHz
43GHz
x,y [mas]
Epoch
C8
y [mas]
x [mas]
C9
5GHz
22GHz
43GHz
x,y [mas]
Epoch
C9
y [mas]
x [mas]

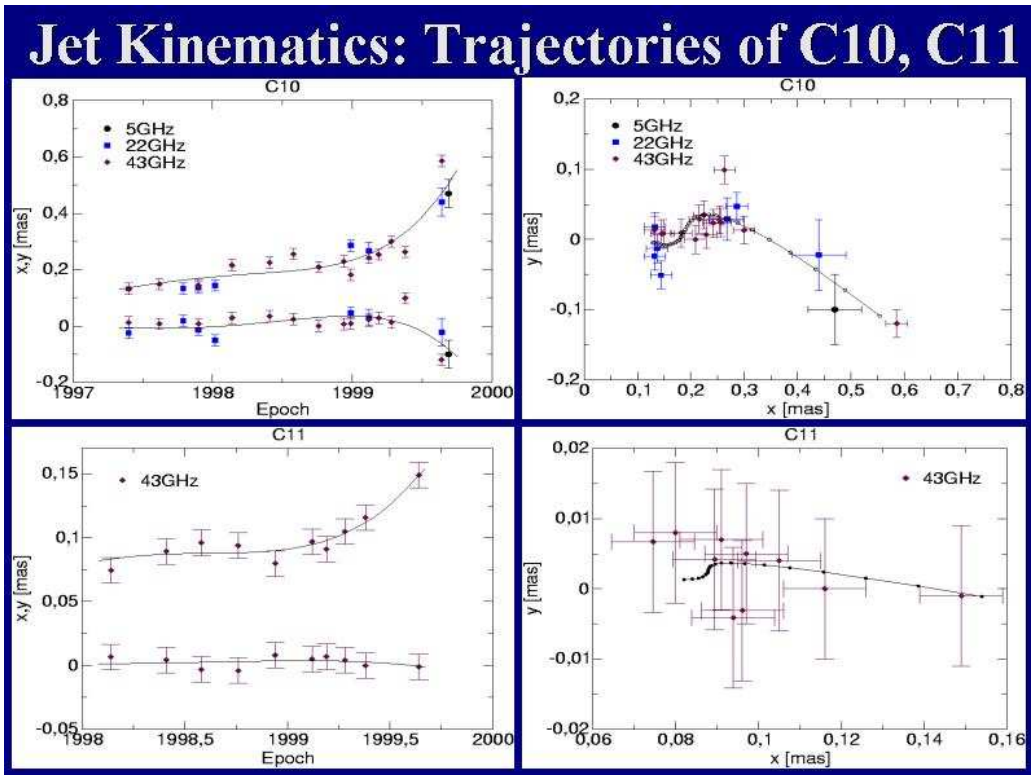
Jet Kinematics: Trajectories of C10, C11
C10
5GHz
22GHz
43GHz
x,y [mas]
Epoch
y [mas]
x [mas]
C11
43GHz

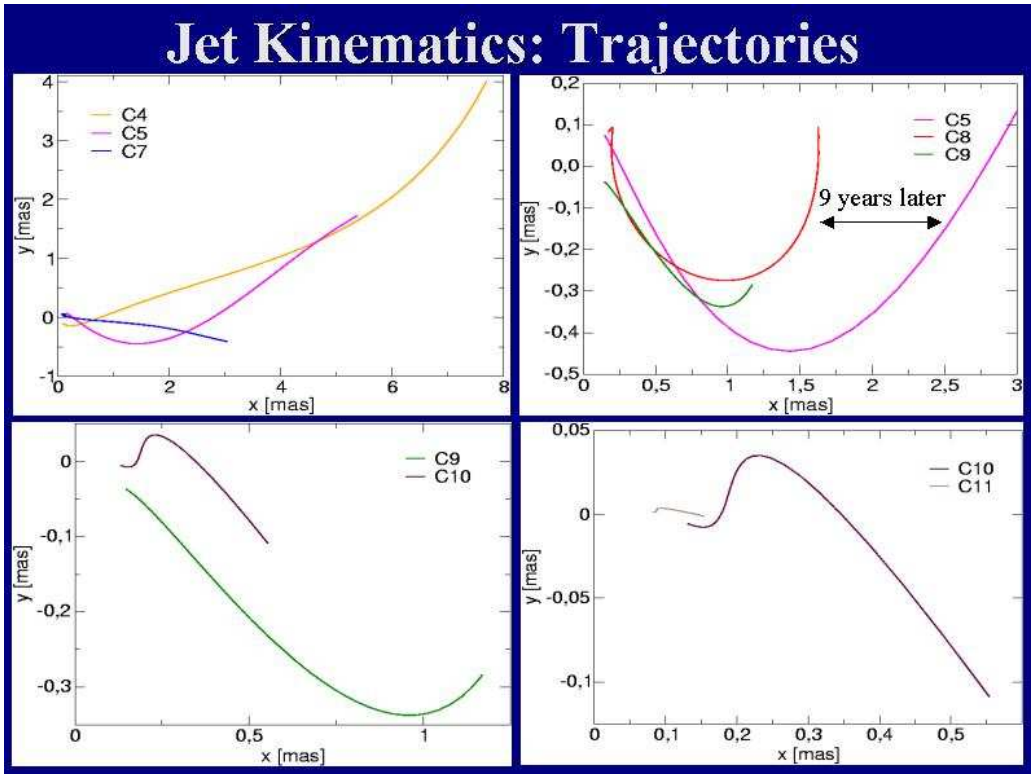
Jet Kinematics: Trajectories
C4
C5
C7
C8
C9
9 years later
C10
C11
y [mas]
x [mas]

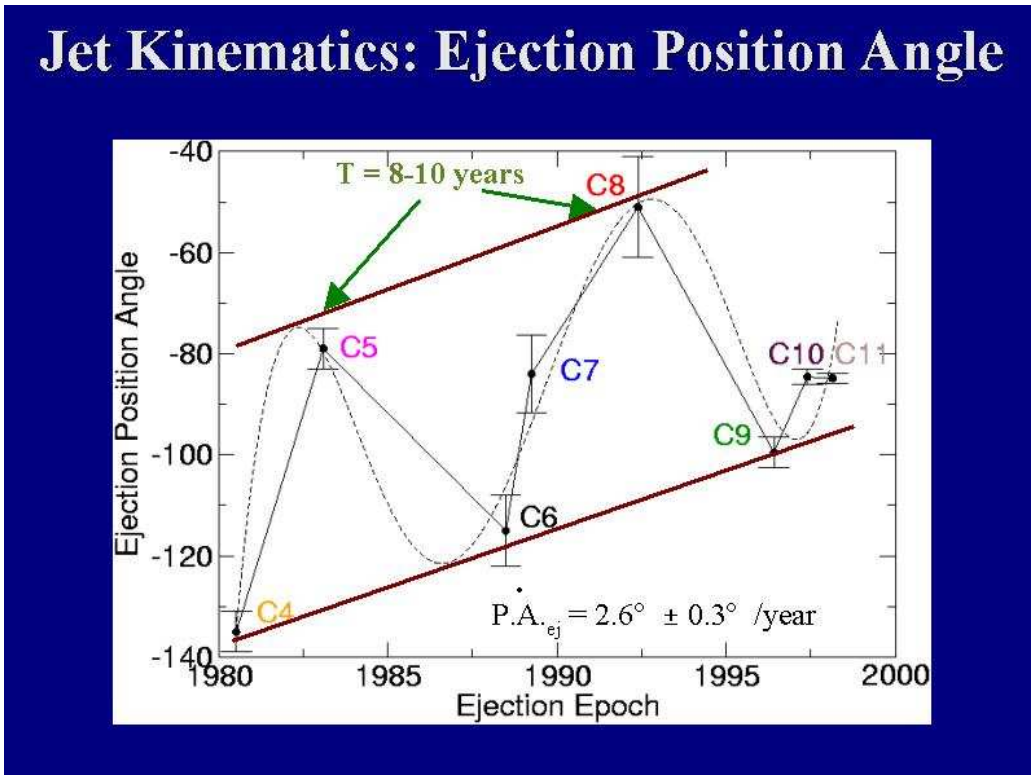
Jet Kinematics: Ejection Position Angle
T = 8-10 years
C8
C5
C7
C10
C11
C9
C6
C4
P.A.ej = 2.6° ± 0.3° /year
Ejection Position Angle
Ejection Epoch
-40
-60
-80
-100
-120
-140
1980
1985
1990
1995
2000

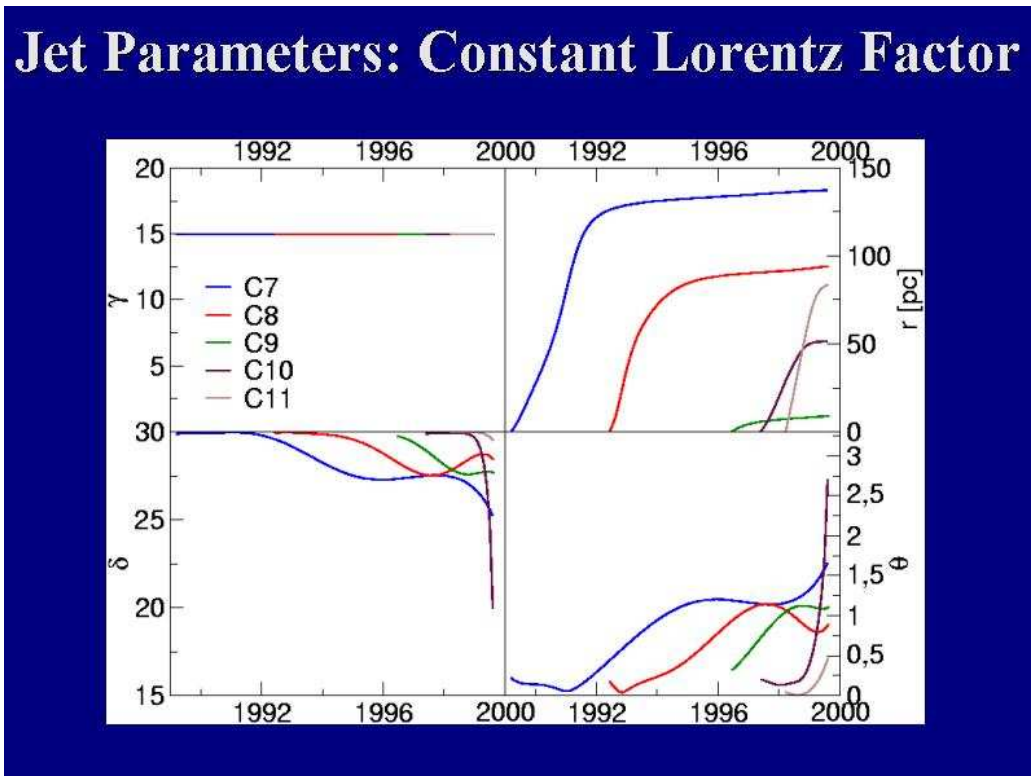
Jet Parameters: Constant Lorentz Factor
C7
C8
C9
C10
C11
γ
δ
θ
r [pc]
1992
1996
2000

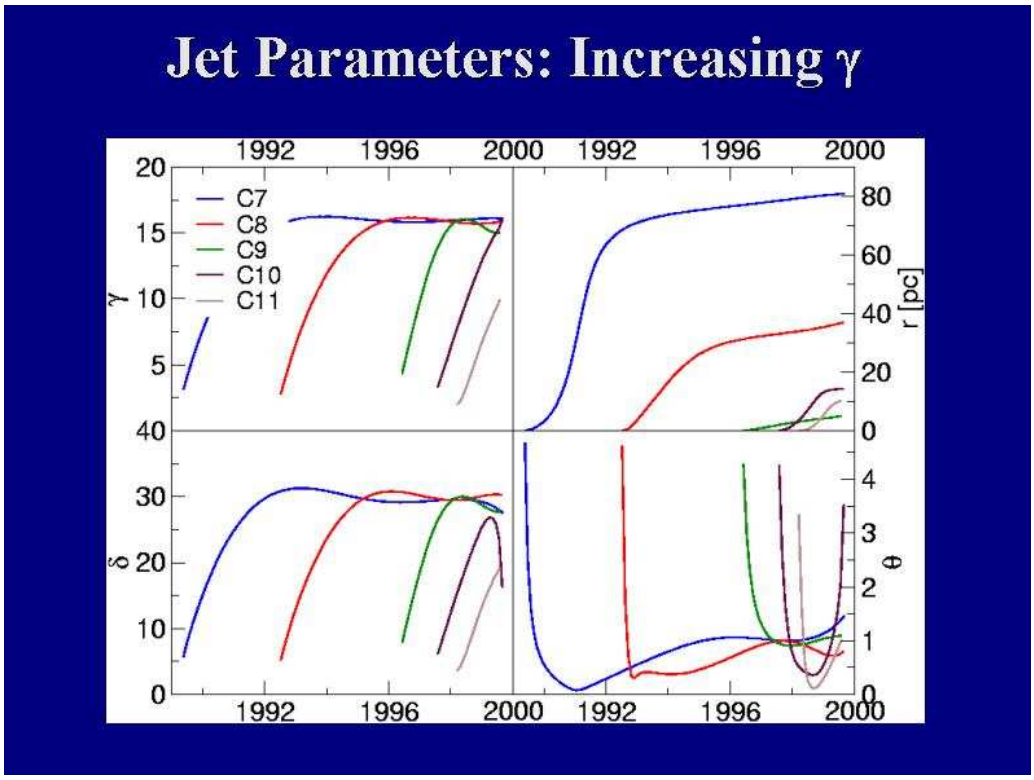
Jet Parameters: Increasing γ
1992
1996
2000
C7
C8
C9
C10
C11
γ
δ
θ
r [pc]

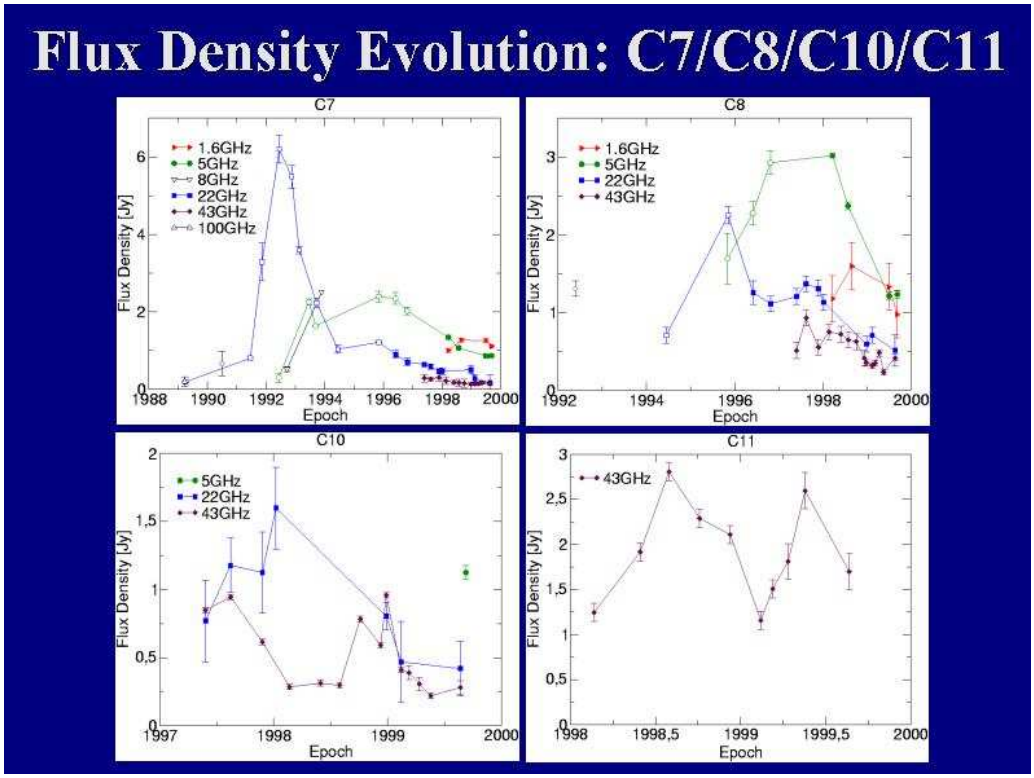
Flux Density Evolution: C7/C8/C10/C11
C7
1.6GHz
5GHz
8GHz
22GHz
43GHz
100GHz
C8
C10
C11
Flux Density [Jy]
Epoch

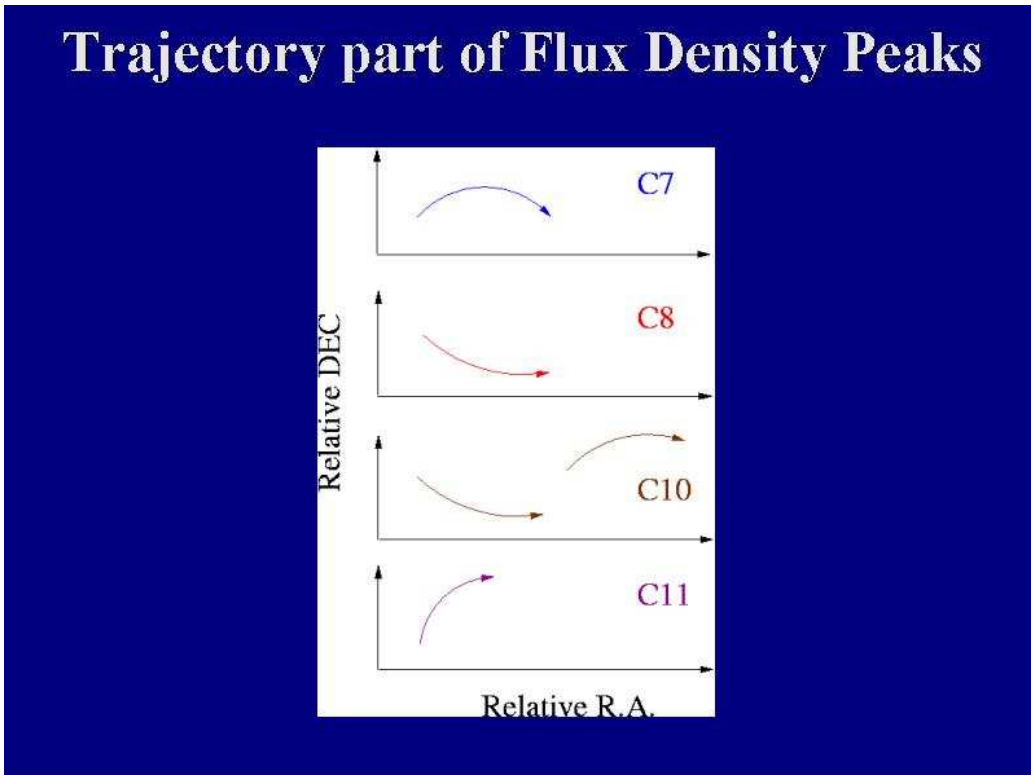
Trajectory part of Flux Density Peaks
C7
C8
C10
C11
Relative DEC
Relative R.A.

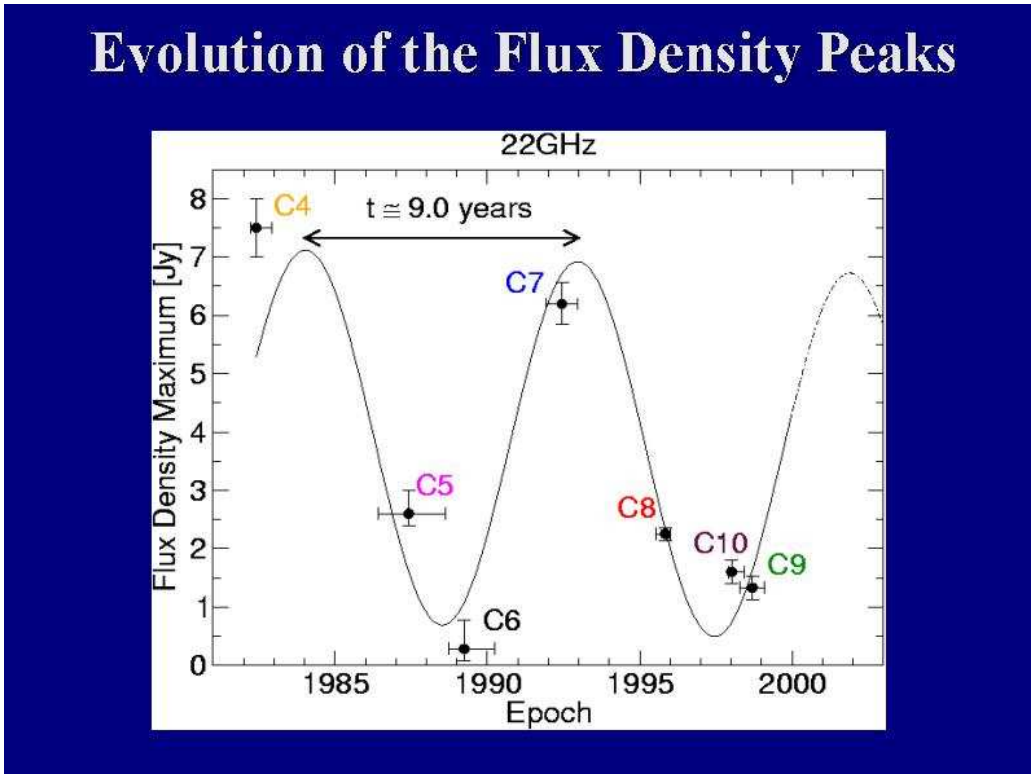
Evolution of the Flux Density Peaks
22GHz
C4
t ≅ 9.0 years
C7
C5
C8
C10
C9
C6
Flux Density Maximum [Jy]
0
1
2
3
4
5
6
7
8
1985
1990
1995
2000
Epoch

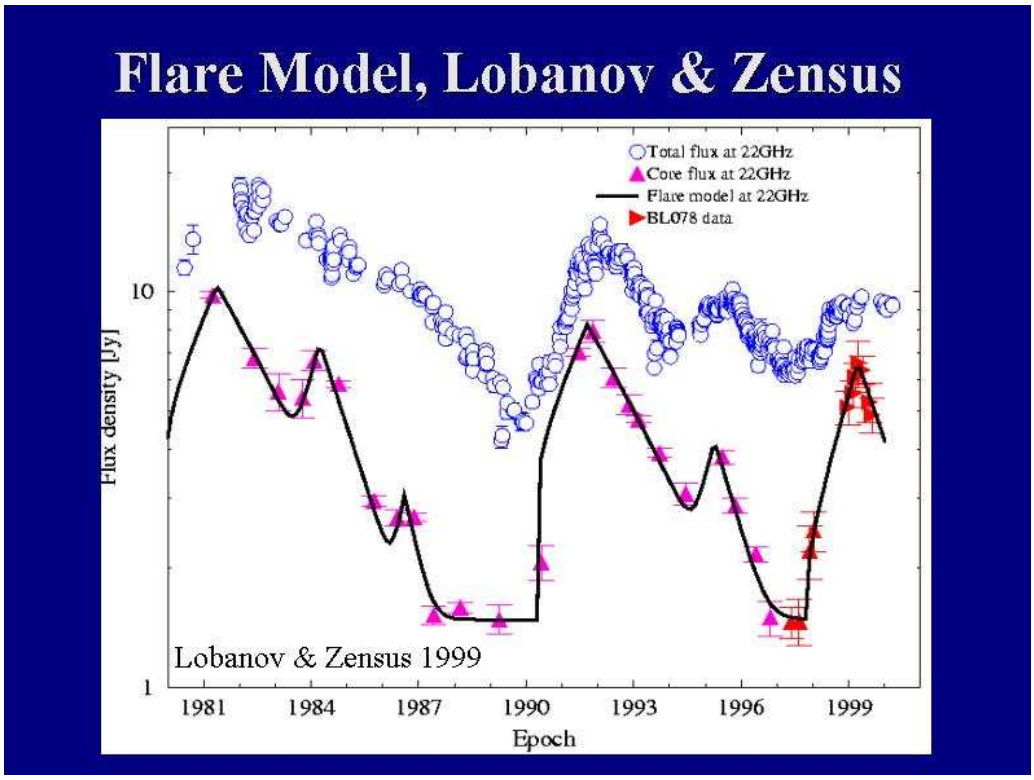
Flare Model, Lobanov & Zensus
Total flux at 22GHz
Core flux at 22GHz
Flare model at 22GHz
BL078 data
Flux density [Jy]
10
1
Lobanov & Zensus 1999
1981
1984
1987
1990
1993
1996
1999
Epoch

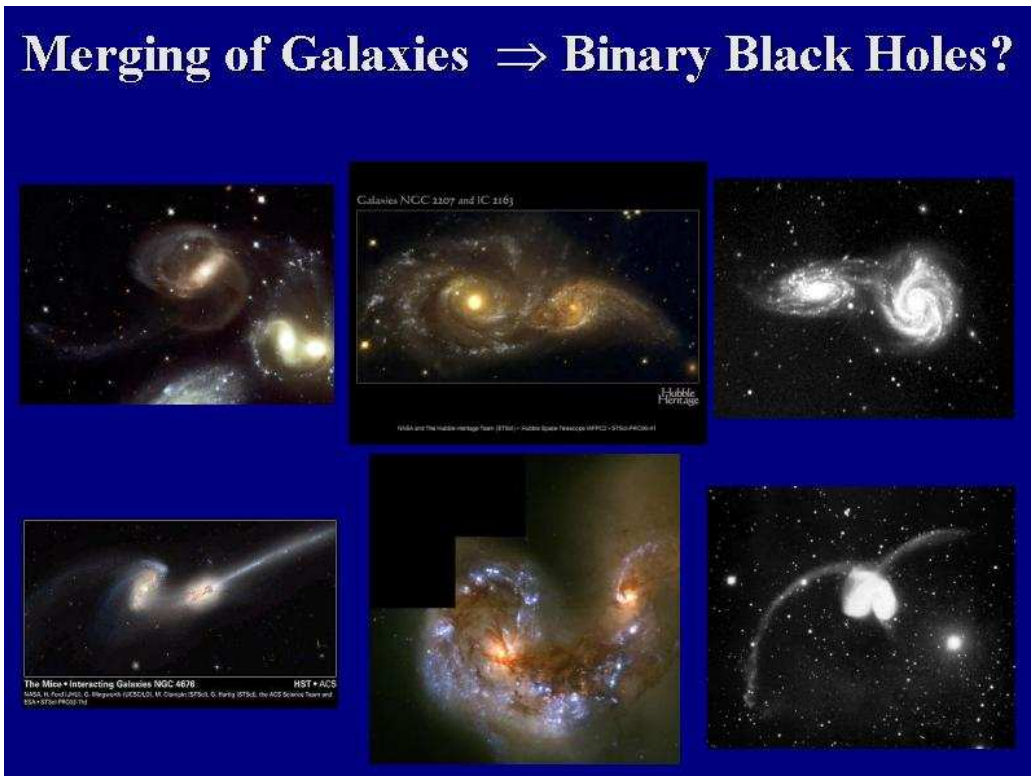
Merging of Galaxies ⇒ Binary Black Holes?
Galaxies NGC 2207 and IC 2163
The Mice • Interacting Galaxies NGC 4676
HST • ACS

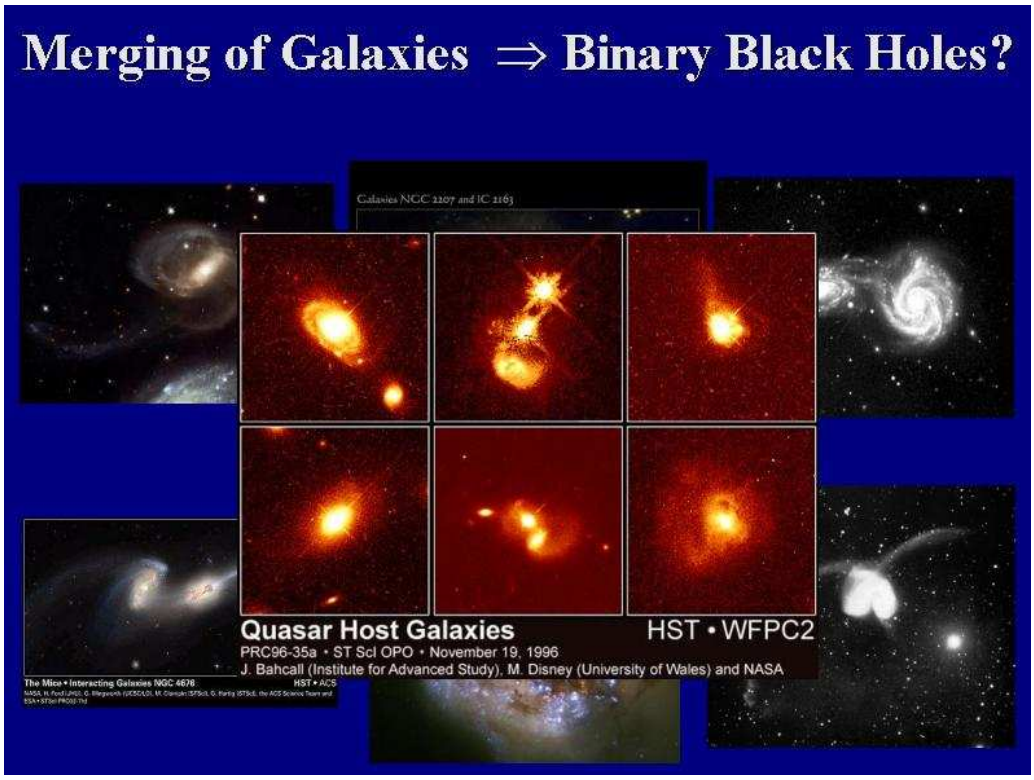
Merging of Galaxies ⇒ Binary Black Holes?
Quasar Host Galaxies
HST • WFPC2
PRC96-35a • ST ScI OPO • November 19, 1996
J. Bahcall (Institute for Advanced Study), M. Disney (University of Wales) and NASA

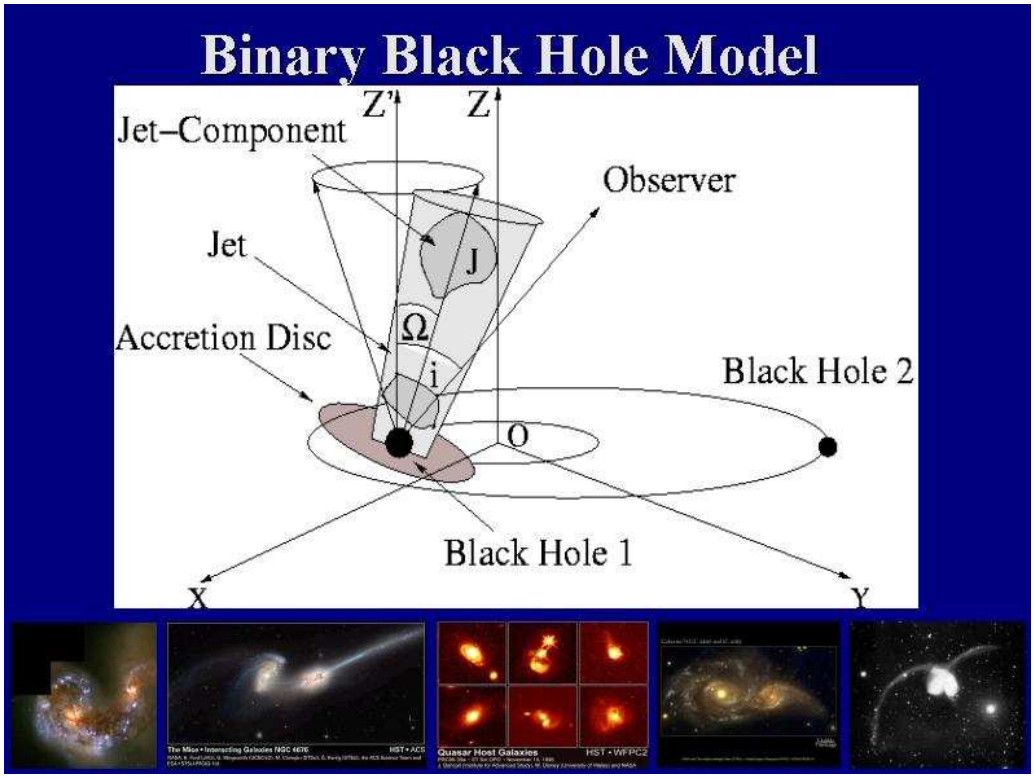
Binary Black Hole Model
Jet–Component
Z'
Z
Observer
Jet
J
Ω
Accretion Disc
i
Black Hole 2
O
Black Hole 1
X
Y

Binary Black Hole Model

Binary Black Hole model of Lobanov & Roland 2002:
C7: Kinematic and flux density evolution

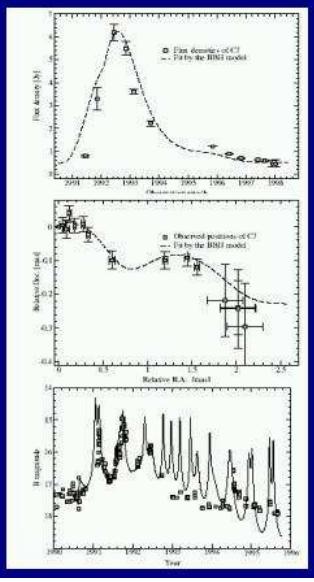

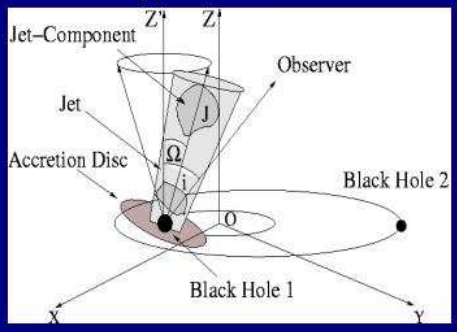

Parameter	Rest Frame
M_1	$1.5 \cdot 10^9 M_\odot$
M_2	$1.0 \cdot 10^9 M_\odot$
T_{orb}	~ 170 years
T_{prec}	~ 125 years
orbital major axis	0.64 pc

Binary Black Hole Model

Binary Black Hole model results of Lobanov & Roland 2002
compared with the observed periodicity

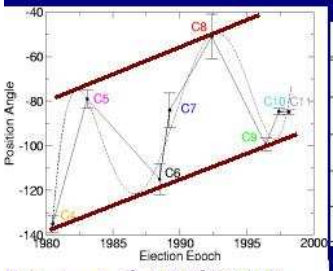

P.A.ej = 2.6° ± 0.3°/ year

Parameter	Rest Frame
M_1	$1.5 \cdot 10^9 M_\odot$
M_2	$1.0 \cdot 10^9 M_\odot$
T_{orb}	~ 170 years
T_{prec}	~ 125 years
orbital major axis	0.64 pc

P.A.prec = 2.9°/year

Peak-to-peak:
Obs: Δ P.A.$_{ej}$ = 26° ± 7°
BBH: Δ P.A.$_{ej}$ = 30°

C5-to-C8:
Obs: Δ P.A.$_{ej}$ = 28° ± 14°
BBH: Δ P.A.$_{ej}$ = 27°

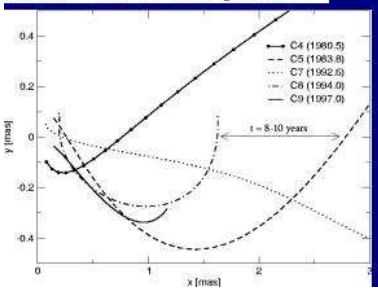

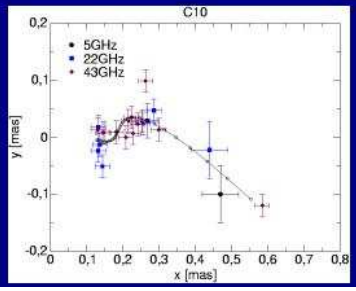

Results

1. Three new ejected jet components C9, C10 and C11.
2. Different component trajectories but similarity of the C5 and C8 trajectory: Equivalent points are about 8-10 years later for C8 than for C5.
3. Component ejection angles vary: Quasi-periodicity of 8-10 years. Long-term variation of $P.A._{ej} = 2.6° \pm 0.3°$ / year
4. Acceleration of the jet components. Lorentz factor rises from 3 to 16.
5. Doppler factor rises from 5 to 30.
6. Angle to the line of sight changes down to: $3.5° > \Theta > 0.2°$.
7. Component flux density peaks due to Doppler boosting.
8. Component flux density peaks show quasi-periodicity with a period of about 9 years.
9. Observations match with Binary Black Hole model of Lobanov & Roland 2002: Precession period in observers frame: 125 years (2.9° / year)
10. Rotation of jet or accretion disc: 8-10 years

Outlook

1. Continue VLBI monitoring to pursue our intensive study of this particular quasar.
2. Several observations have been made at $\lambda = 3$ mm to supplement our extensive study at core distances smaller than 100 μarcsec. Proposed: **Global mm-VLBI Array** observations => Angular resolution ~ 50 μarcsec

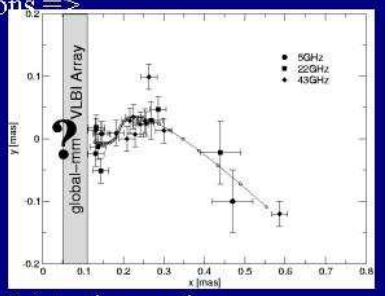

3. Test the stationarity of the core: Phase-referencing program started with the VLBA to the nearby quasar NRAO 512 (~ 0.5° apart) at 7 mm and 3 mm in 2002.
4. Test Binary Black Hole model with jet components C8 and C9.

Structure variability in 0716+714 – U. Bach, T. P. Krichbaum, S. Britzen, E. Ros, A. Witzel, J. A. Zensus

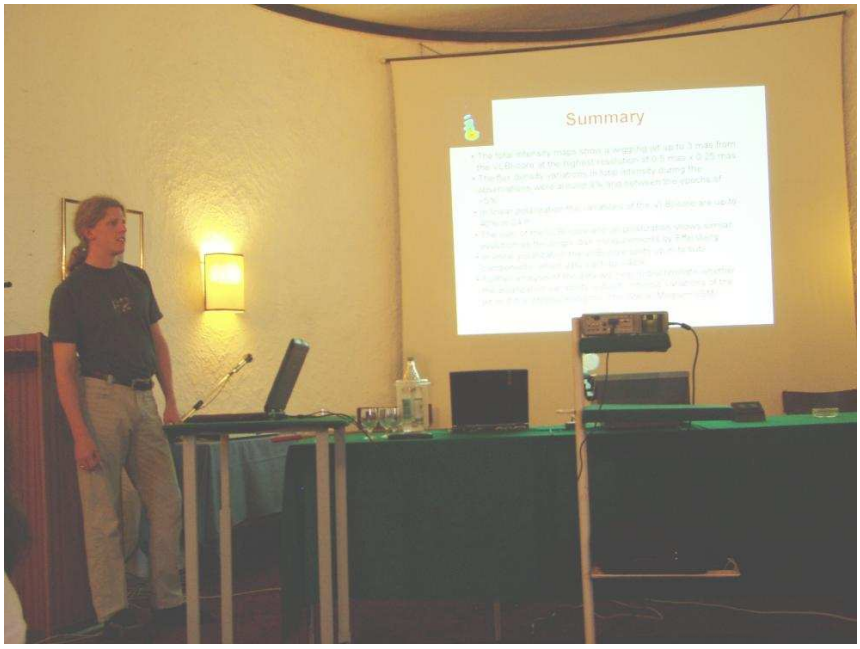

Structure variability in 0716+714

Uwe Bach

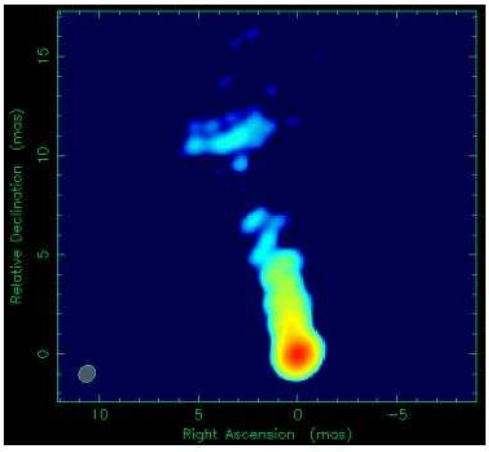

in collaboration with:
T.P. Krichbaum, S. Britzen, E. Ros, A. Witzel and J.A. Zensus

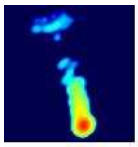

Facts about 0716+714

- S5 blazar and one of the most active BL Lac objects.
- Extremely variable on time scales from hours to months.
- Yet no known redshift. Optical imaging however suggests an redshift of $z > 0.3$.
- Intraday variable (IDV) in the radio bands.
- Very flat radio spectrum, extending up to at least 350 GHz.
- Correlated variability over wide ranges of the electromagnetic spectrum.
- VLBI studies covering more than 20 years show a core-dominated evolving jet extending to the north.
- VLBI jet is oriented at 90° with respect to the VLA jet.

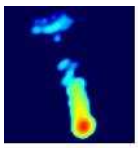

Observations

Our analysis is based on 26 epochs:

- 4 epochs at 5 GHz between 1992 and 1999 from the CJF-Survey (Britzen et al. 1999).
- 1 VSOP observation at 5 GHz from 2000 (own data).
- 3 epochs at 8.4 GHz from between 1994 and 1999 (Ros et al. 2000).
- 2 epochs at 8.4 GHz from 1994 and 1995 (own data).
- 5 epochs at 15 GHz between 1994 and 2001 from the VLBA 2 cm-Survey (Kellermann et al. 1998; Zensus et al. 2002).
- 7 epochs at 22 GHz between 1995 and 1997 (Jorstad et al. 2001).
- 4 epochs at 22 GHz between 1992 and 1996 (own data).

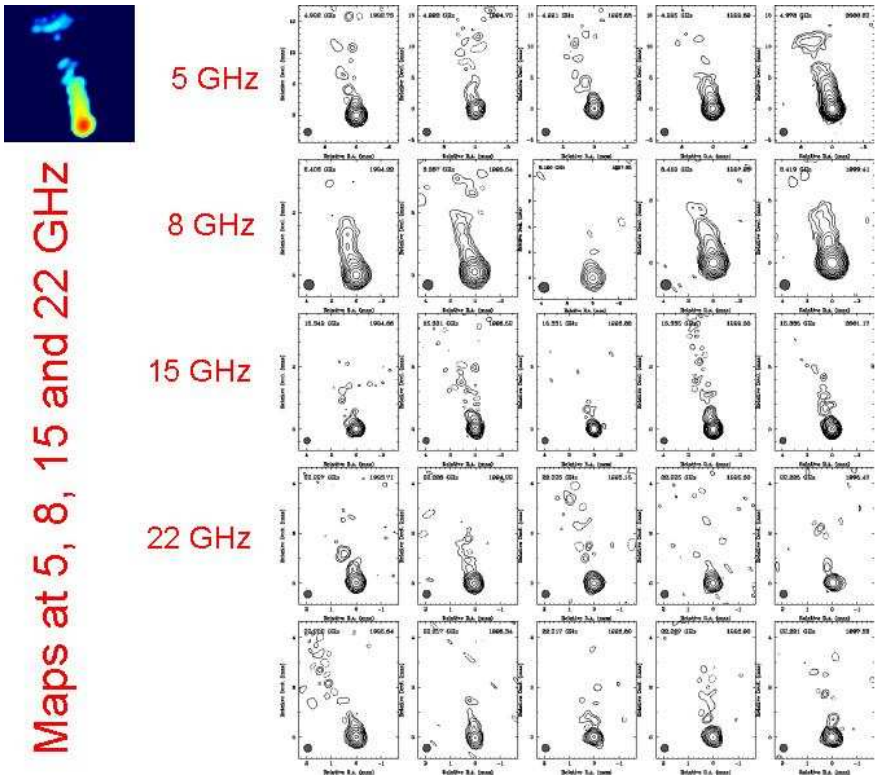
Maps at 5, 8, 15 and 22 GHz
5 GHz
8 GHz
15 GHz
22 GHz

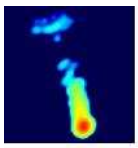

The Model

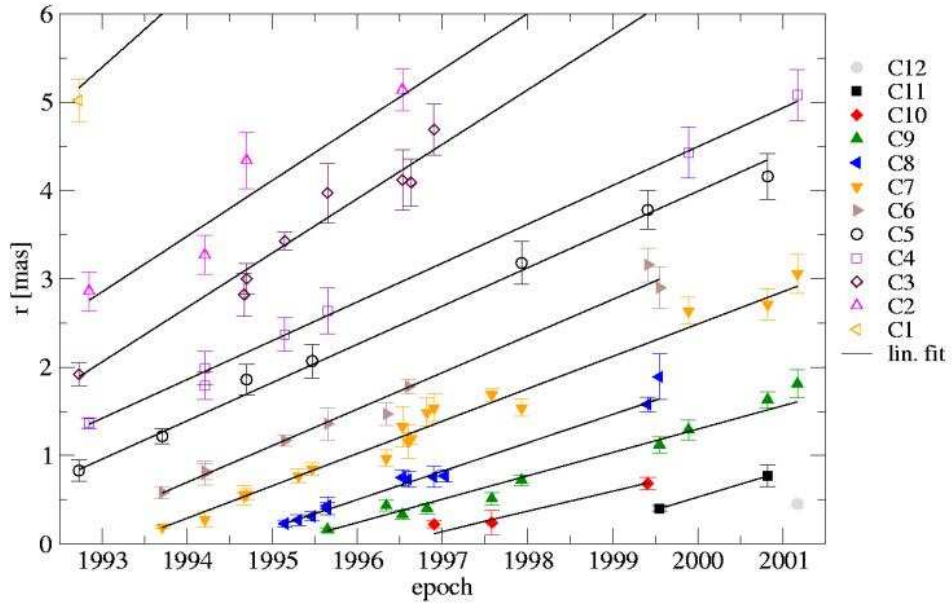
r [mas]
epoch
0
1
2
3
4
5
6
1993
1994
1995
1996
1997
1998
1999
2000
2001
C12
C11
C10
C9
C8
C7
C6
C5
C4
C3
C2
C1
lin. fit

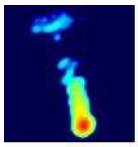

Component Summary

Comp	#	μ [mas/yr]	$\beta_{\rm app}$	Ejection date
C1	4	0.857 ± 0.125	14.29 ± 2.09	1986.71 ± 1.32
C2	5	0.631 ± 0.097	10.51 ± 1.62	1988.48 ± 0.96
C3	8	0.616 ± 0.040	10.27 ± 0.67	1989.66 ± 0.34
C4	7	0.440 ± 0.013	7.32 ± 0.22	1989.77 ± 0.13
C5	7	0.433 ± 0.015	7.22 ± 0.26	1990.79 ± 0.16
C6	9	0.414 ± 0.018	6.90 ± 0.29	1992.32 ± 0.14
C7	17	0.366 ± 0.010	6.11 ± 0.17	1993.21 ± 0.06
C8	11	0.321 ± 0.011	5.35 ± 0.18	1994.44 ± 0.06
C9	10	0.265 ± 0.015	4.41 ± 0.24	1995.09 ± 0.11
C10	3	0.240 ± 0.024	4.01 ± 0.41	1996.54 ± 0.24
C11	2	0.291 ± 0.029	5.11 ± 0.51	1998.18 ± 0.31

$z = 0.3$, $H_0 = 70\,\mathrm{km\,s^{-1}\,Mpc^{-1}}$ and $q_0 = 0.5$.

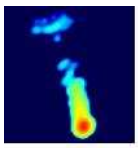

Kinematics and Geometry

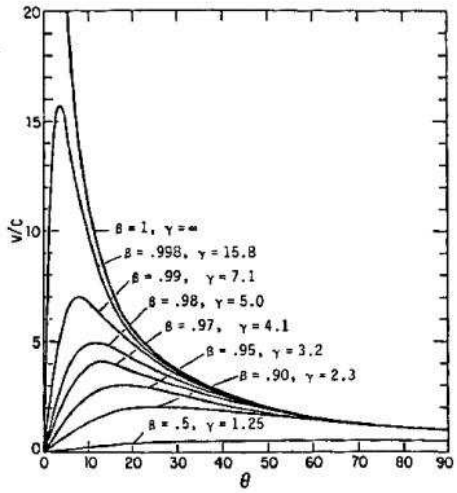

Using $\beta_{\rm app} = 10.3$ (C3) and adopting

$$\beta_{\rm app} = \frac{\beta \sin\theta}{1 - \beta\cos\theta}$$

we find

$$\gamma_{\rm min} = \sqrt{1 + \beta_{\rm app}^2} = \mathbf{10.3}$$
$$\theta_{\rm max} = \mathbf{5.6^\circ}$$

which corresponds to a Doppler factor of:

$$\delta = [\gamma(1 - \beta\cos\theta))]^{-1} \approx \mathbf{10.3}$$

The Doppler factor is maximized at $\theta \to 0$, which yields:

$$\delta_{\rm max} = 2\gamma = \mathbf{20.6}$$

But for IDV $\delta \approx 30 - 50$:

$$\gamma \approx \mathbf{16.1 - 25.6}$$
$$\theta \approx \mathbf{1.0^\circ - 0.4^\circ}$$

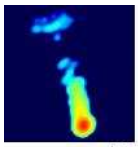

Doppler factor vs. apparent velocity

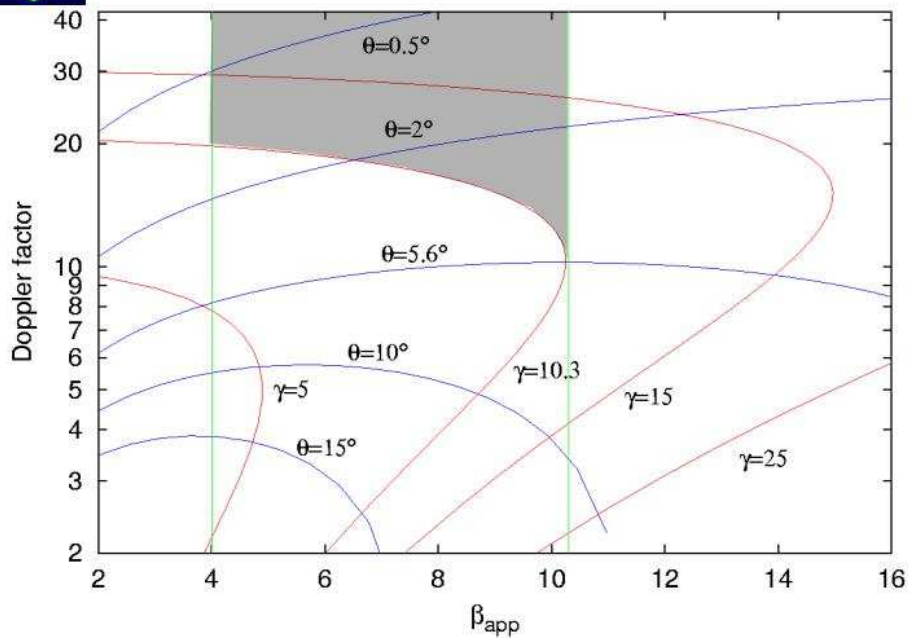

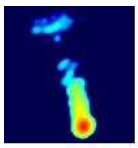

Variation of the ejection angle

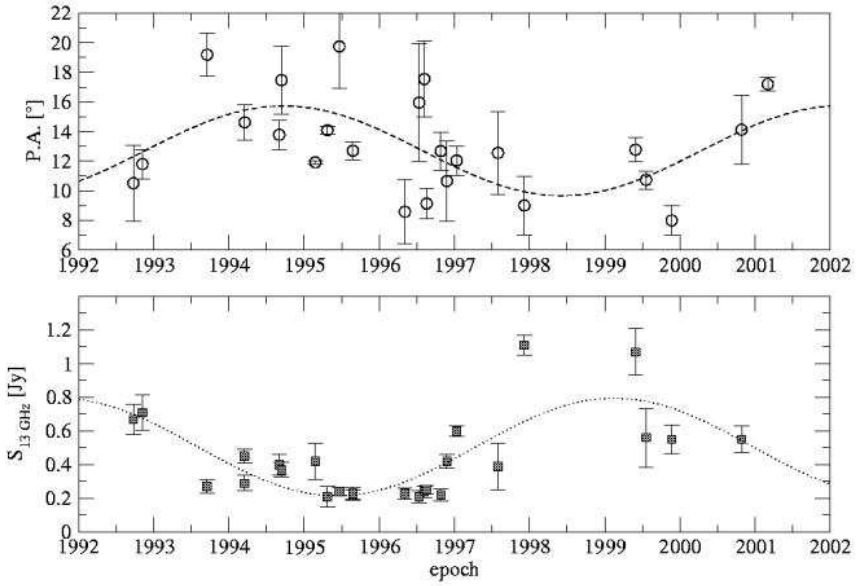

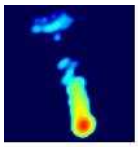

Radio light-curves

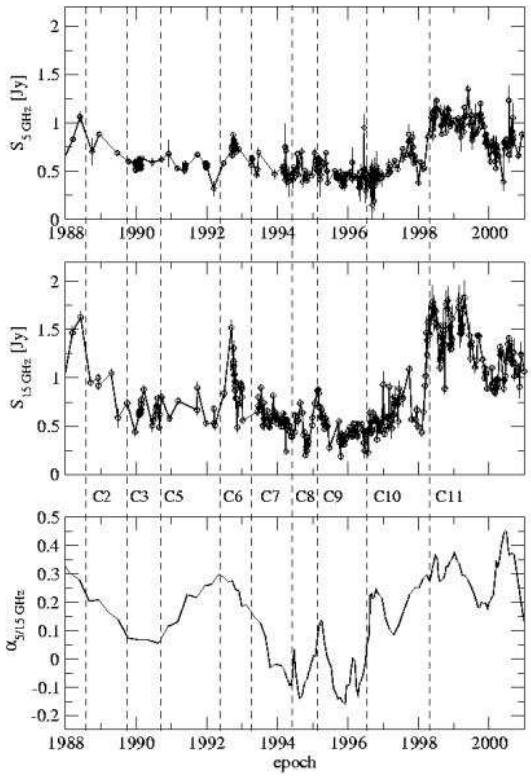

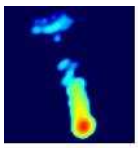

Summary

- We reanalyzed 26 epochs of VLBI data at 5, 8, 15 and 22 GHz.
- We obtained:
  - a satisfactory model for the motion of the components, where the components move with an average of ~7 c.
  - a lower limit for the Lorentz Factor of ~10.3.
  - a maximum angle to the line of sight of ~5.6°.
  - but more probable are g > 15 and q < 2°, which correspond to a Doppler factor > 20.

  - We found a periodic variation of the ejection angle of ~6° in ~7 years, which seems to correlate with the VLBI core flux density.
  - The ejection angle of new components shows a weak correlation with the radio light curves at cm-wavelengths and the spectral index.

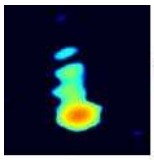

VSOP observations of 0716+714

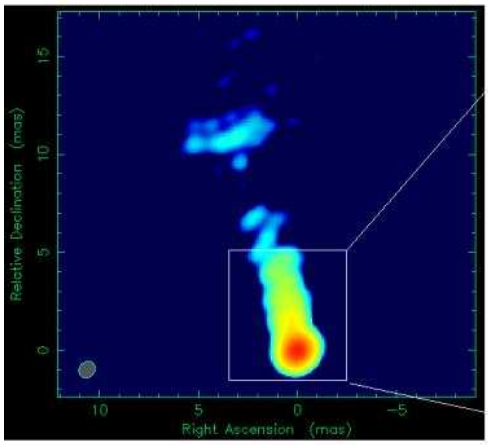

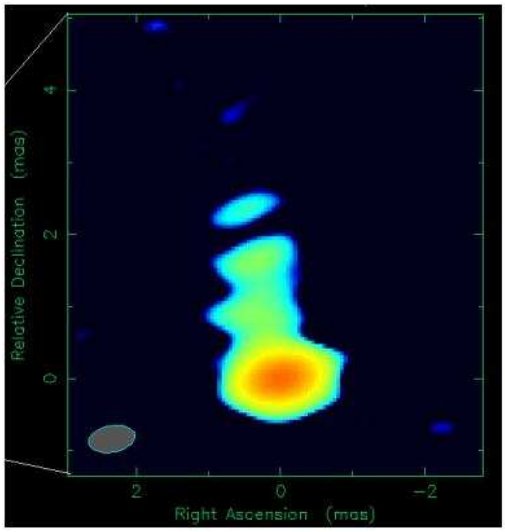

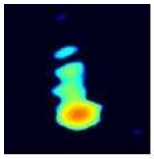

Observations

- 3 epochs (16 h) with 12 ground-stations (VLBA, Effelsberg & VLA) and the HALCA satellite.
- Separations of 6 days and 1 day.
- Nearly identical uv-coverage.
- ~0.25 mas resolution at 5 GHz.
- Simultaneous pointing scans in Effelsberg.

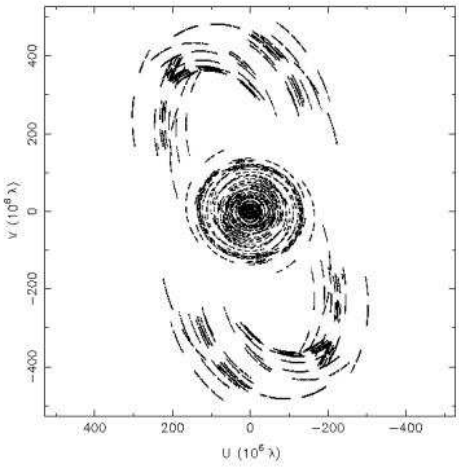

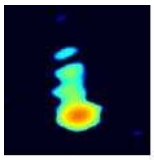

Ground-array Maps

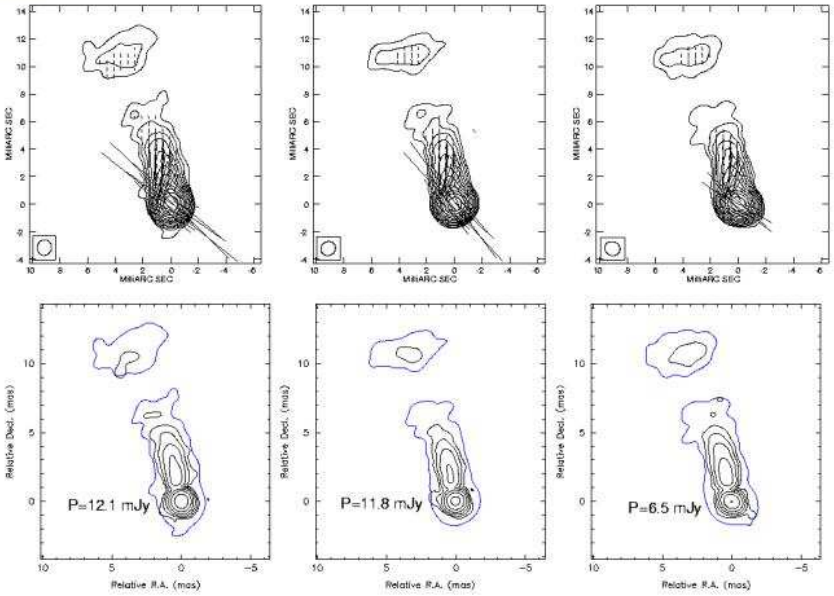

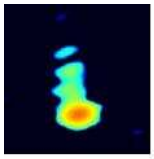

Ground-array Profile

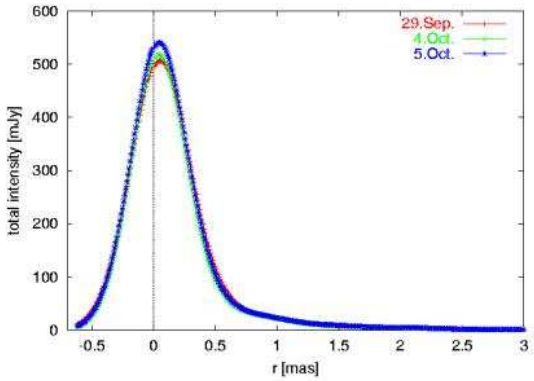

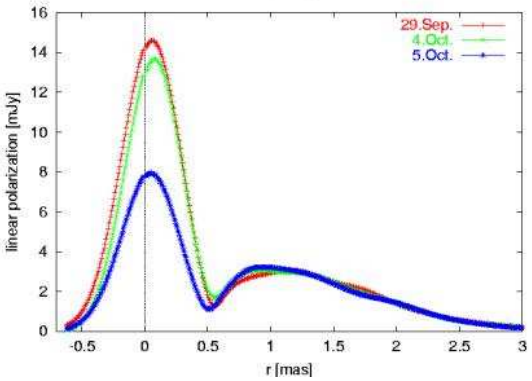

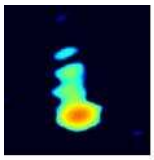

VLBI vs. single dish

A2: 29. Sep 2000

		I [mJy]	ΔI [mJy]	P [mJy]	ΔP [mJy]	φ [°]	Δφ [°]	P_{tot} [mJy]	ΔP_{tot} [mJy]	φ_{tot} [°]	$\Delta\varphi_{tot}$ [°]
VLBI	Core	525.0	18.0	12.1	1.2	49.4	4.1	17.0	9.2	27.3	15.3
	Jet	45.6	3.2	7.4	0.7	-10.8	5.6				
Effelsberg		763.0	12.0					21.0	2.1	23.4	2.1

A4: 4. Oct 2000

		I [mJy]	ΔI [mJy]	P [mJy]	ΔP [mJy]	φ [°]	Δφ [°]	P_{tot} [mJy]	ΔP_{tot} [mJy]	φ_{tot} [°]	$\Delta\varphi_{tot}$ [°]
VLBI	Core	497.0	14.0	11.8	1.2	40.7	4.0	17.3	9.4	21.3	12.0
	Jet	44.4	3.9	7.3	0.7	-11.2	5.8				
Effelsberg		736.0	12.0					22.0	2.2	18.6	2.2

A5: 5. Oct 2000

		I [mJy]	ΔI [mJy]	P [mJy]	ΔP [mJy]	φ [°]	Δφ [°]	P_{tot} [mJy]	ΔP_{tot} [mJy]	φ_{tot} [°]	$\Delta\varphi_{tot}$ [°]
VLBI	Core	506.0	10.0	6.5	1.0	52.7	5.2	12.0	7.3	19.1	12.1
	Jet	43.9	2.7	7.5	0.7	-9.5	5.4				
Effelsberg		740.0	11.0					16.0	1.6	13.3	2.2

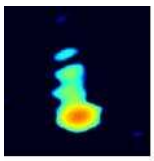

VSOP Maps

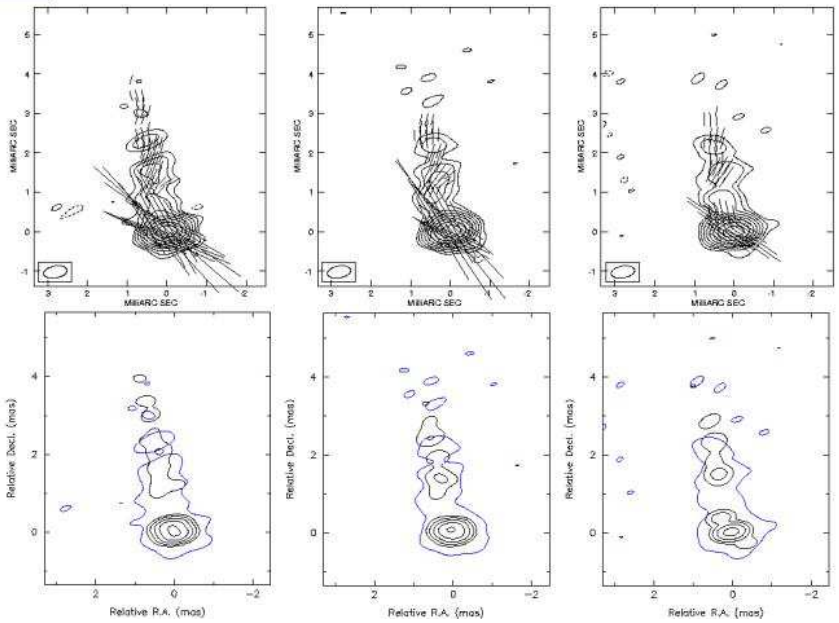

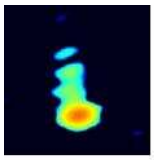

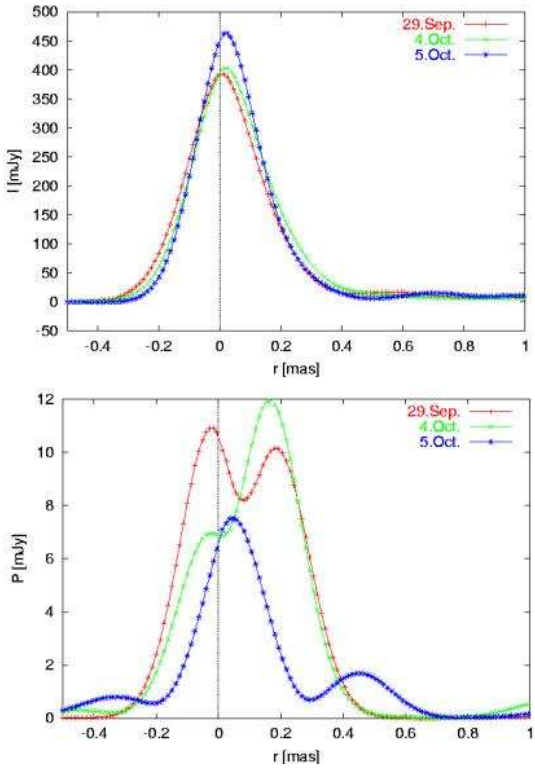

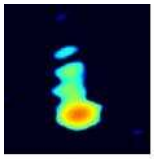

Summary

- The total intensity maps show a wiggling jet up to 3 mas from the VLBI-core at the highest resolution of 0.5 mas x 0.25 mas.
- The flux density variations in total intensity during the observations were around 4% and between the epochs of ~5%.
- In linear polarization the variations of the VLBI-core are up to 40% in 24 h.
- The sum of the VLBI-core and jet polarization shows similar evolution as the single dish measurements by Effelsberg.
- In linear polarization the VLBI-core splits up in to sub-components, which vary each by ~40%.
- Further analysis of the data will help to discriminate whether the polarization variability is due to intrinsic variations of the jet or if it is introduced by the Inter Stellar Medium (ISM).

The new 11 Jy radio outburst of NRAO 150: VLBI study at the resolution limit

I. Agudo, U. Bach, T. P. Krichbaum, W. Alef, D. Graham, M. Bremer, H. Ungerechts, M. Grewing, H. Teräsranta, A. Witzel, J. A. Zensus

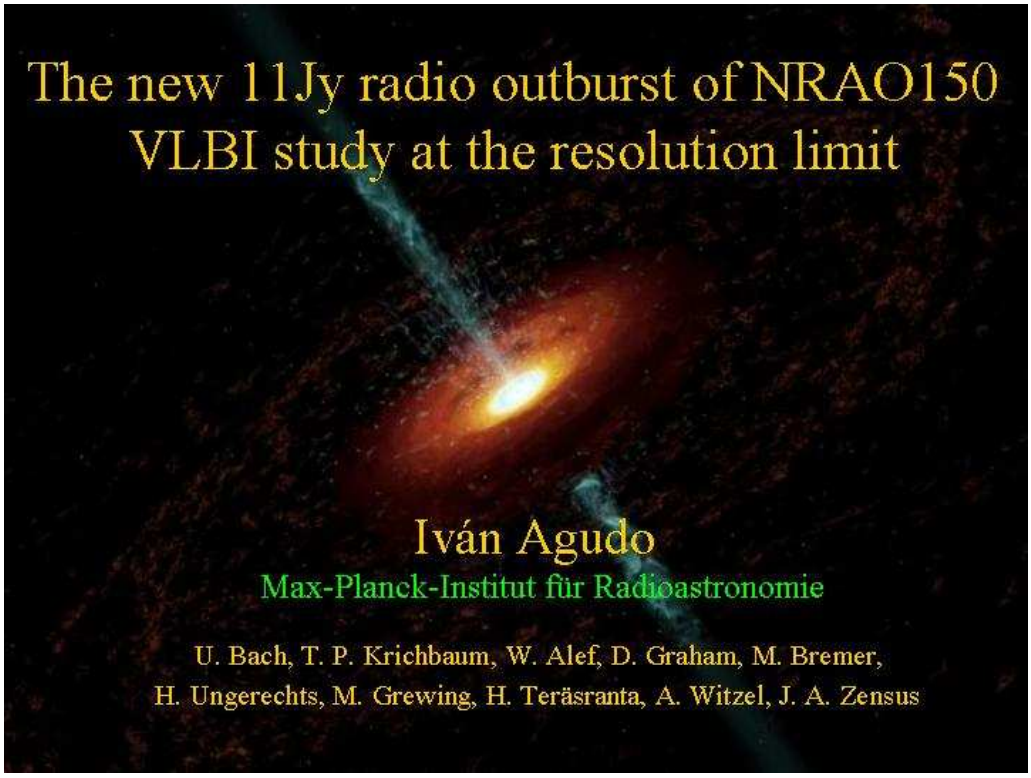

Overview of the Talk:

- Introduction
- Single dish radio monitoring
- The VLBI study
- Summary
- Future work

Introduction

- No optical identification
- Probably due to extinction or source confusion in the galactic plane
- Galactic latitude ~ 1°
- Studied since 1960 (first VLBI observations by Clark et al. 1968)
- cm-VLBI shows a jet extended up to 30 mas to the North-East (Kellermann et al. 1998)
- No X ray observations up to nov

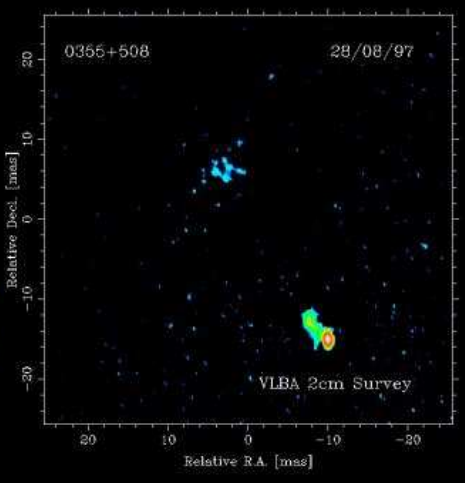

Kellermann et al. 1998

Single dish monitorings: UMRAO

- Second historical outburst
- Dramatic EVPA differences between frequencies
- Highly inverted spectrum during the last 5 years
- Extreme opacity effects

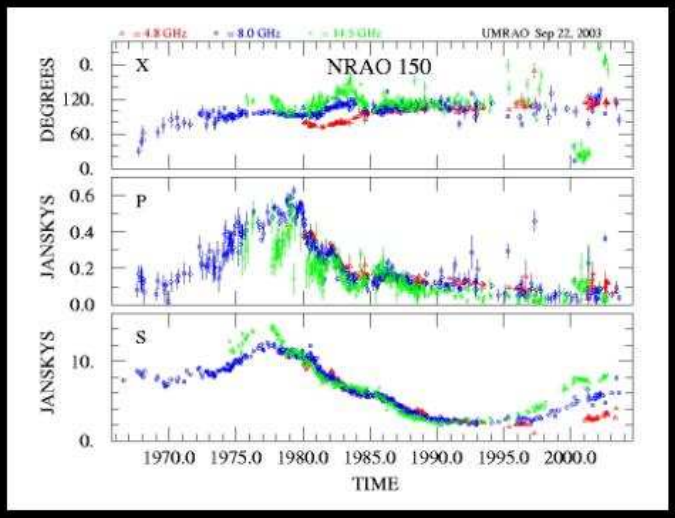

M. Aller 2003, private communication

Single dish monitorings: Metsähovi

- Second outburst even higher at 22 and 37 GHz. Up to 11-12 Jy!

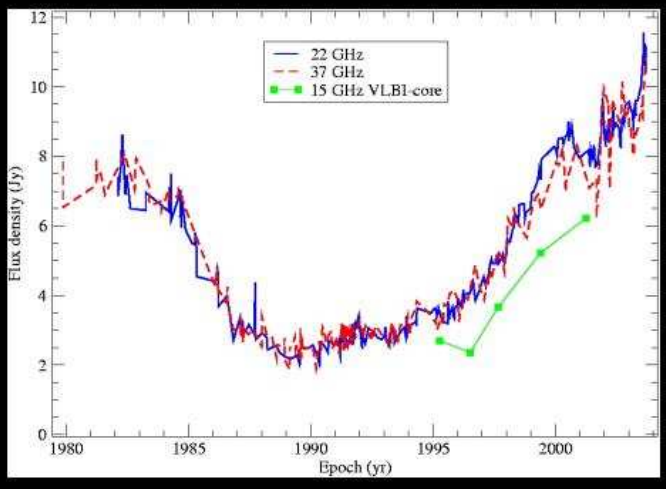

- Long term variation superimposed on shorter time scale (weeks) flares of ~1 Jy
- Correlation with the 15 GHz VLBI core flux evolution
- Long term variations seem to be produced in the 15 GHz VLBI core.

H. Teräsranta 2003, private communication

Single dish monitorings: Metsähovi and Pico Veleta

- Evidence of correlation of short time scale flares at all the frequencies.
- Possible correlation with the flux evolution of the 86 GHz VLBI core.
- 1 Jy flares produced in the very inner jet?

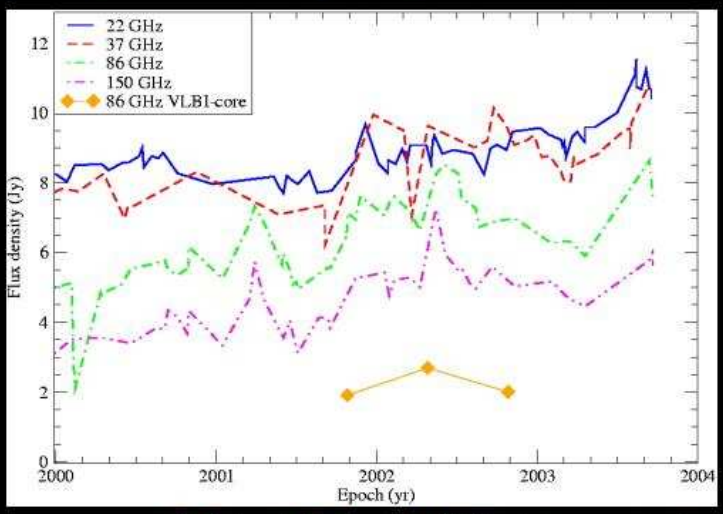

H. Teräsranta, H. Ungerechts 2003, private communication

The VLBI study

- Analysis of the 15 GHz VLBI images from the 2 cm VLBA survey.
- Leads to source structure variability study with ~0.5 milliarcsecond resolution
- Observing epochs:

  Feb. 1994 (5 GHz)
  Apr. 1995
  Jul. 1996
  Aug. 1997
  May 1999
  Mar. 2001

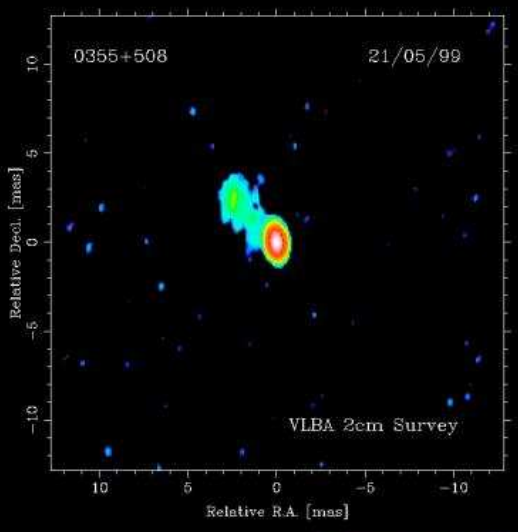

Kellermann et al. 1998

The VLBI study: Evidence of moving helical pattern

- A helical pattern seems to move along the jet at ~0.25 mas/yr

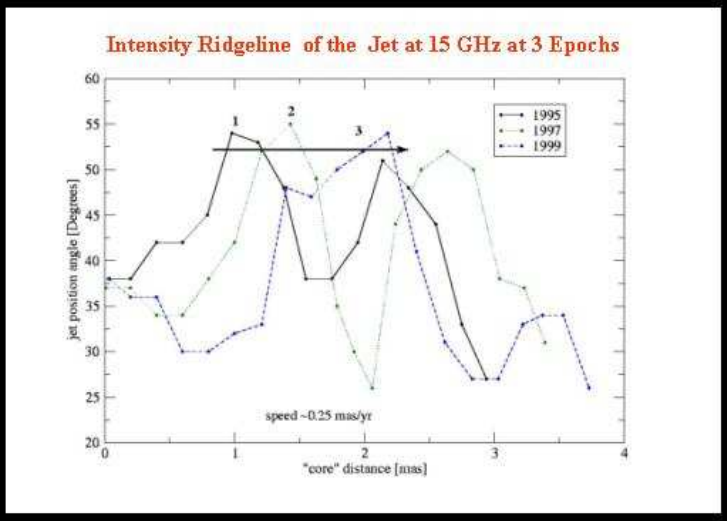

The VLBI study: Evidence of moving helical pattern

- On the other hand, fast jet components seem to separate from the core with ~ 0.6 mas/yr.
- If this is confirmed, it will be the second time that a helical pattern is observed to move at ~1/2 of the component speed (fluid speed?). See Krichbaum et al. (2001)
- Comparison of these two different kinematical scheme could help to extract information about plasma physical parameters through comparison with Kelvin-Helmholtz instabilities theory.

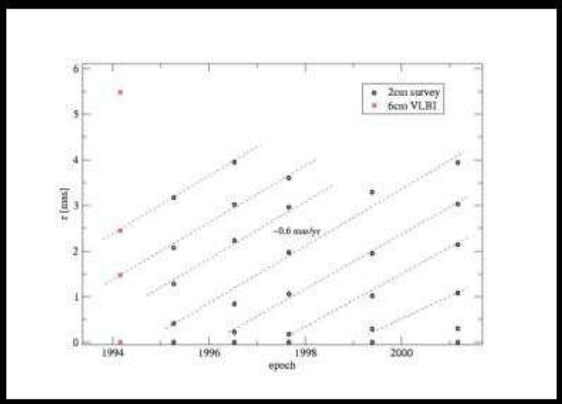

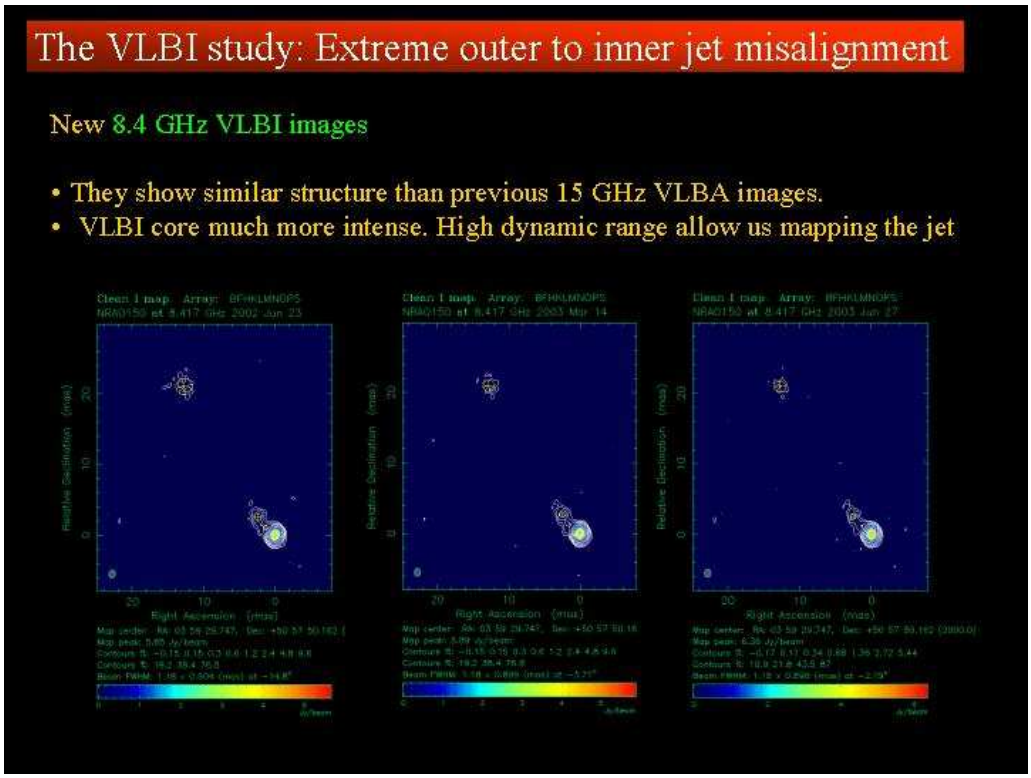
The VLBI study: Extreme outer to inner jet misalignment
New 8.4 GHz VLBI images
• They show similar structure than previous 15 GHz VLBA images.
• VLBI core much more intense. High dynamic range allow us mapping the jet

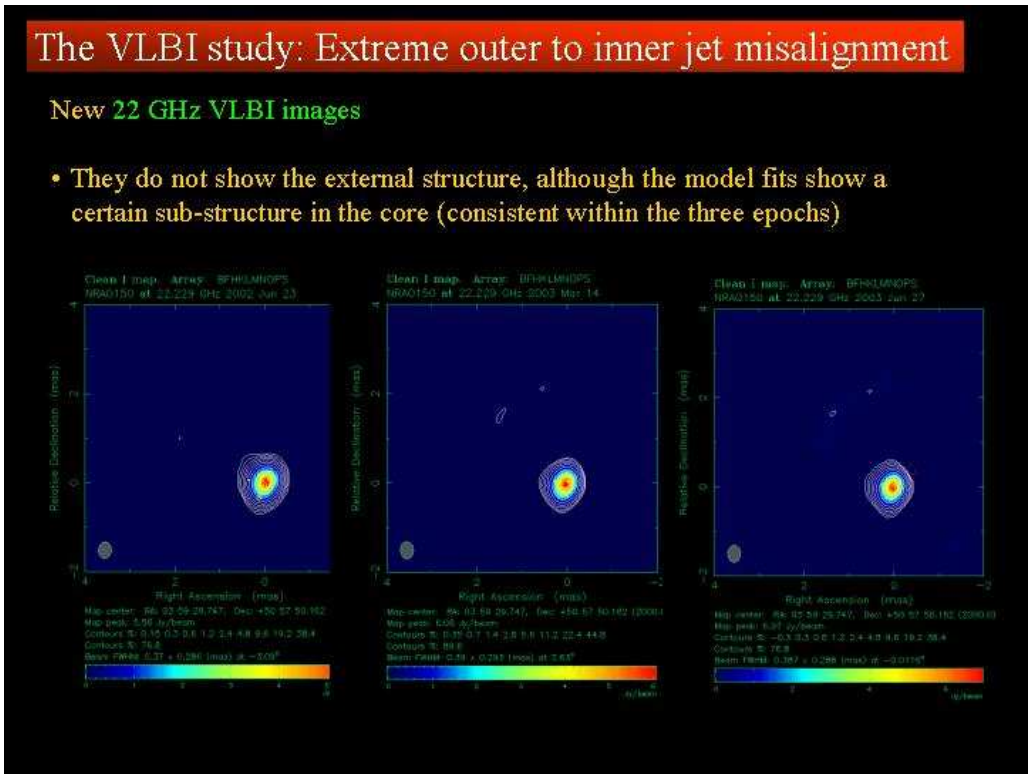
The VLBI study: Extreme outer to inner jet misalignment
New 22 GHz VLBI images
• They do not show the external structure, although the model fits show a certain sub-structure in the core (consistent within the three epochs)

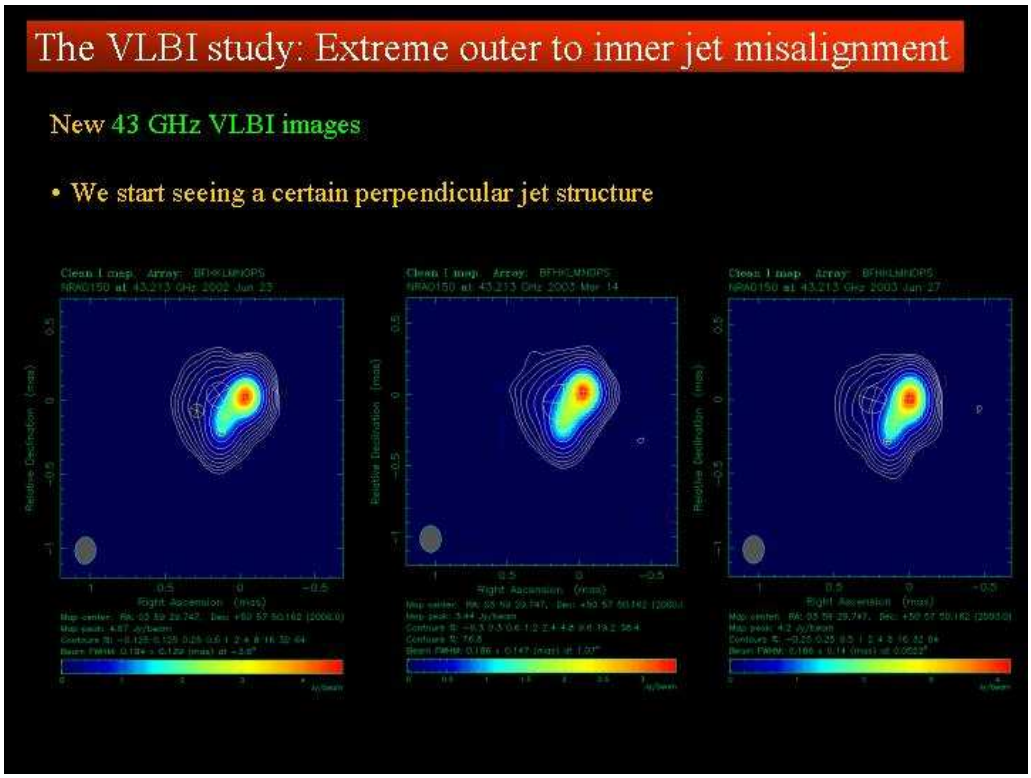
The VLBI study: Extreme outer to inner jet misalignment
New 43 GHz VLBI images
• We start seeing a certain perpendicular jet structure

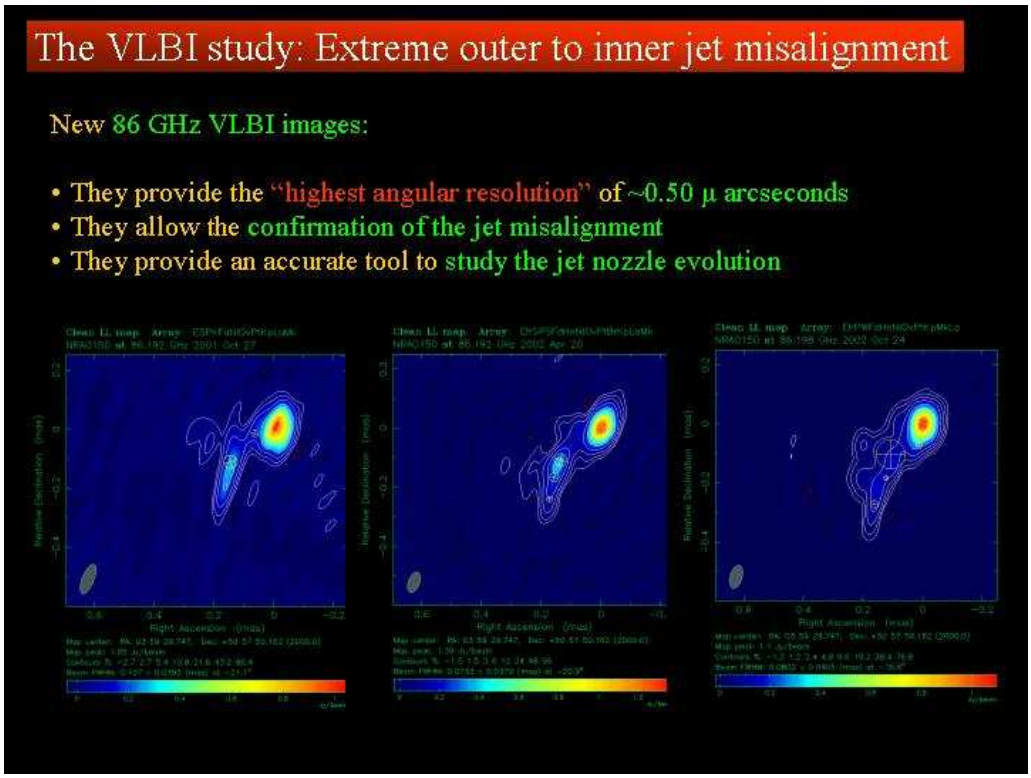
The VLBI study: Extreme outer to inner jet misalignment
New 86 GHz VLBI images:
• They provide the "highest angular resolution" of ~0.50 μ arcseconds
• They allow the confirmation of the jet misalignment
• They provide an accurate tool to study the jet nozzle evolution

The VLBI study: Extreme outer to inner jet misalignment

- New multi frequency VLBI images clearly show the extreme misalignment within the 0.5 mas inner jet structure.
- This could be related with the previous evidence for helical structures

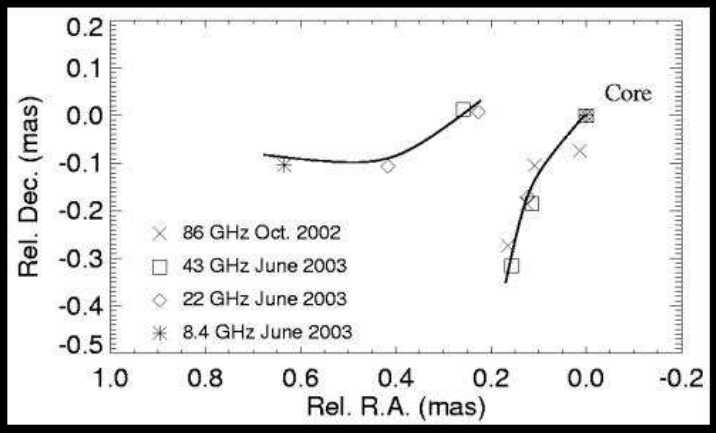

86, 43, 22 and 8.4 GHz VLBI model fits

The VLBI study: Extreme outer to inner jet misalignment

86 GHz VLBI model fits

- New 86 GHz VLBI images show evidence of jet position angle changing.
- This finding further supports the evidence of helical jet structure.
- Jet nozzle precession could explain the main jet phenomenology.

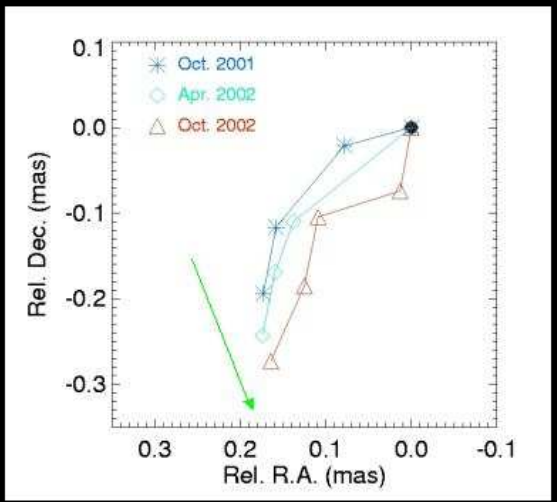

Summary

- NRAO150 shows evidence of a moving helical pattern
- It also show an extreme misalignment between the inner and outer jet
- There is new evidence of inner jet position angle changing
- Also a relatively regular (probably periodic) long term flux density evolution
- All the pieces of evidences suggest a PRECESSING JET
- If all the evidences are confirmed, we will be able of to extract important information about plasma properties and hopefully about the central engine (through precession models)
- For that, we will need a source distance measurement.
- X-ray spectra could give a distance measurement.

Future work

- Calibration and analysis of the 8.4, 22 and 43 GHz polarization VLBA images, corresponding to the shown images.
- New proposals for 86 GHz VLBI and 43, 22 and 15 GHz polarimetric VLBA observations have been sent the last 1st of October.
- Continuation of the multi-frequency and polarimetric VLBI evolution study.
- Continuation of the single dish monitoring.

New results from millimeter VLBI at 3, 2 and 1 mm wavelength. Present status and future possibilities – T. P. Krichbaum

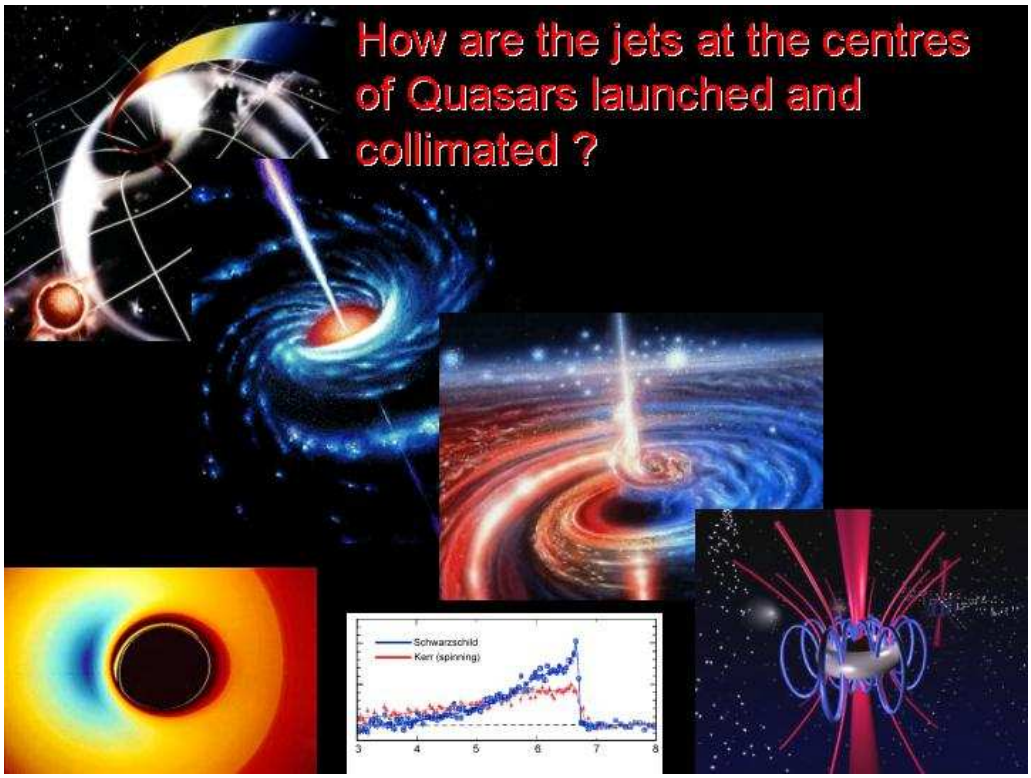
How are the jets at the centres of Quasars launched and collimated ?
Schwarzschild
Kerr (spinning)
3
4
5
6
7
8

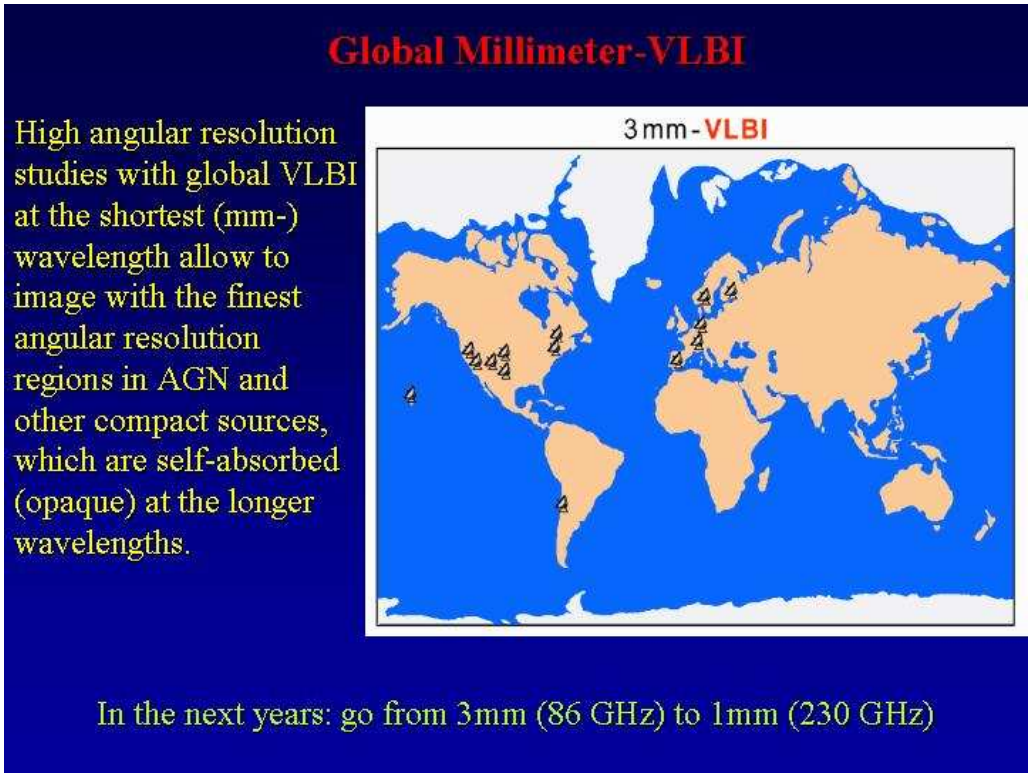
Global Millimeter-VLBI
High angular resolution studies with global VLBI at the shortest (mm-) wavelength allow to image with the finest angular resolution regions in AGN and other compact sources, which are self-absorbed (opaque) at the longer wavelengths.
3mm-VLBI
In the next years: go from 3mm (86 GHz) to 1mm (230 GHz)

Angular and Spatial Resolution of mm-VLBI

λ	ν	θ	z=1	z=0.01	d=10kpc
3 mm	86 GHz	50 μas	0.46 pc	14.3 mpc	2.4 μpc
2 mm	147 GHz	30 μas	0.28 pc	8.6 mpc	1.5 μpc
1.3 mm	230 GHz	18 μas	0.17 pc	5.1 mpc	0.9 μpc

these scales correspond to a few ten to hundred Schwarzschild radii, depending on distance and black hole mass !

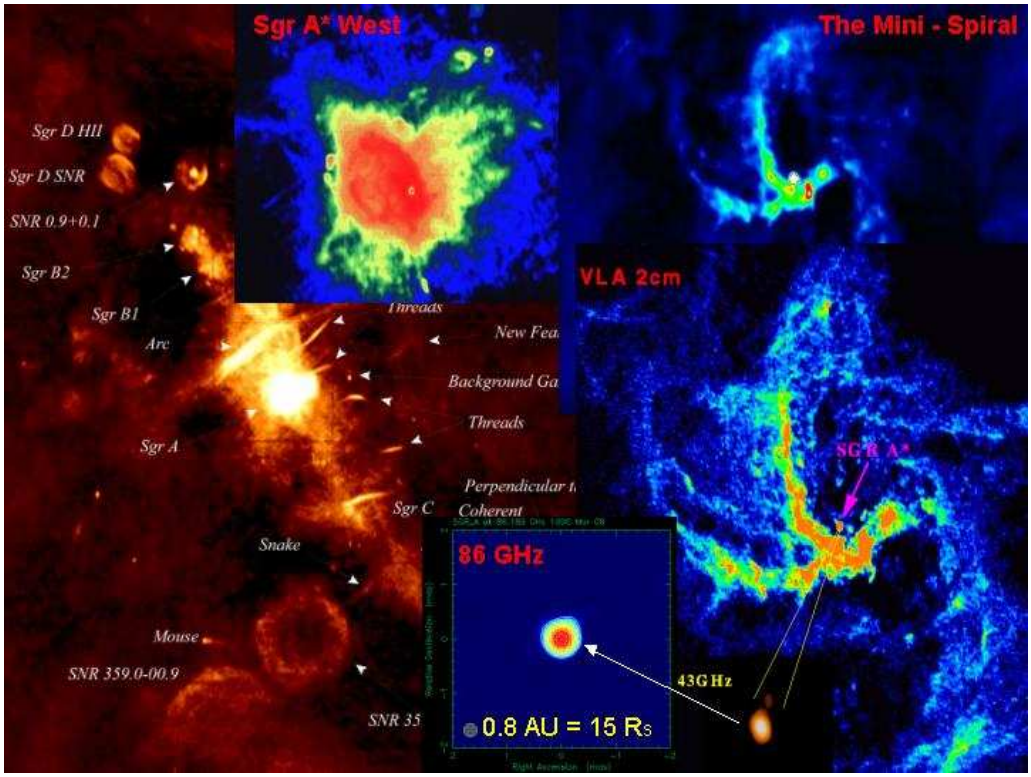

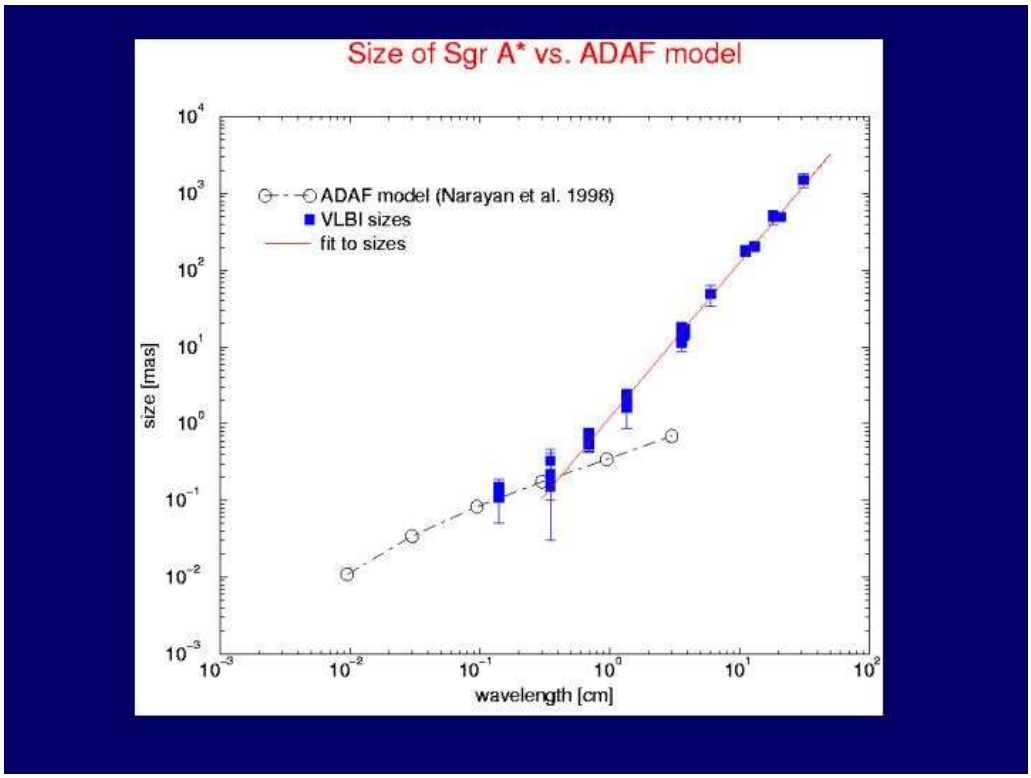
Size of Sgr A* vs. ADAF model
ADAF model (Narayan et al. 1998)
VLBI sizes
fit to sizes
size [mas]
wavelength [cm]

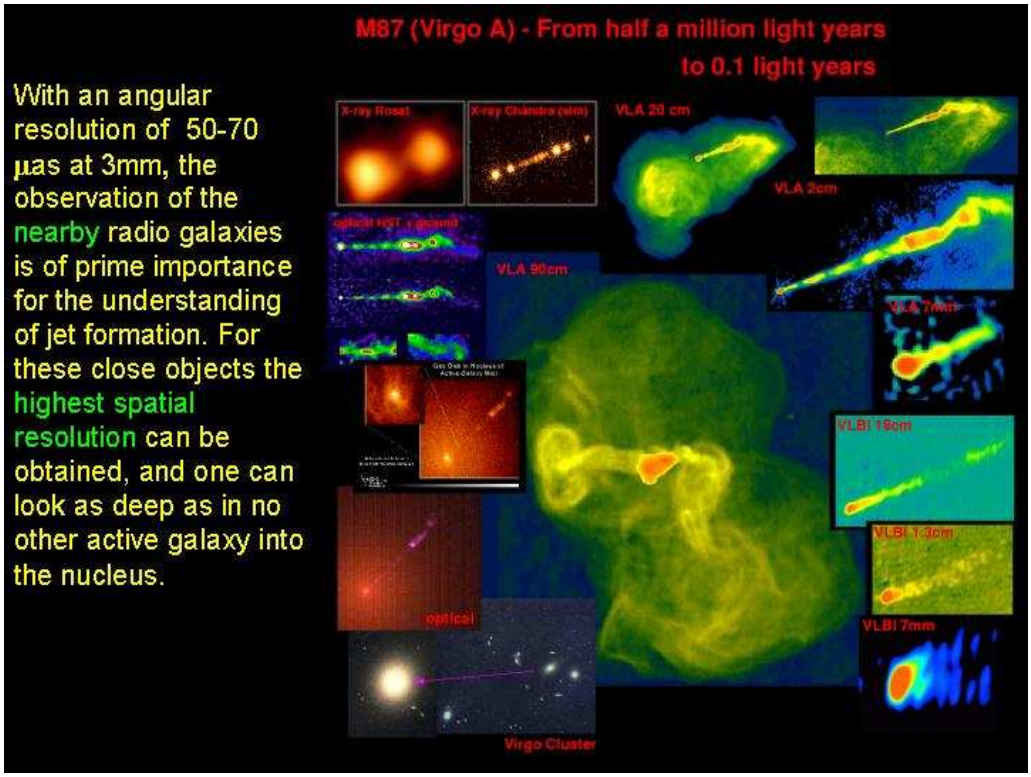
With an angular resolution of 50-70 μas at 3mm, the observation of the nearby radio galaxies is of prime importance for the understanding of jet formation. For these close objects the highest spatial resolution can be obtained, and one can look as deep as in no other active galaxy into the nucleus.
M87 (Virgo A) - From half a million light years to 0.1 light years
VLA 20 cm
VLA 2cm
VLA 90cm
VLA 7mm
VLBI 18cm
VLBI 1.3cm
VLBI 7mm
optical
Virgo Cluster

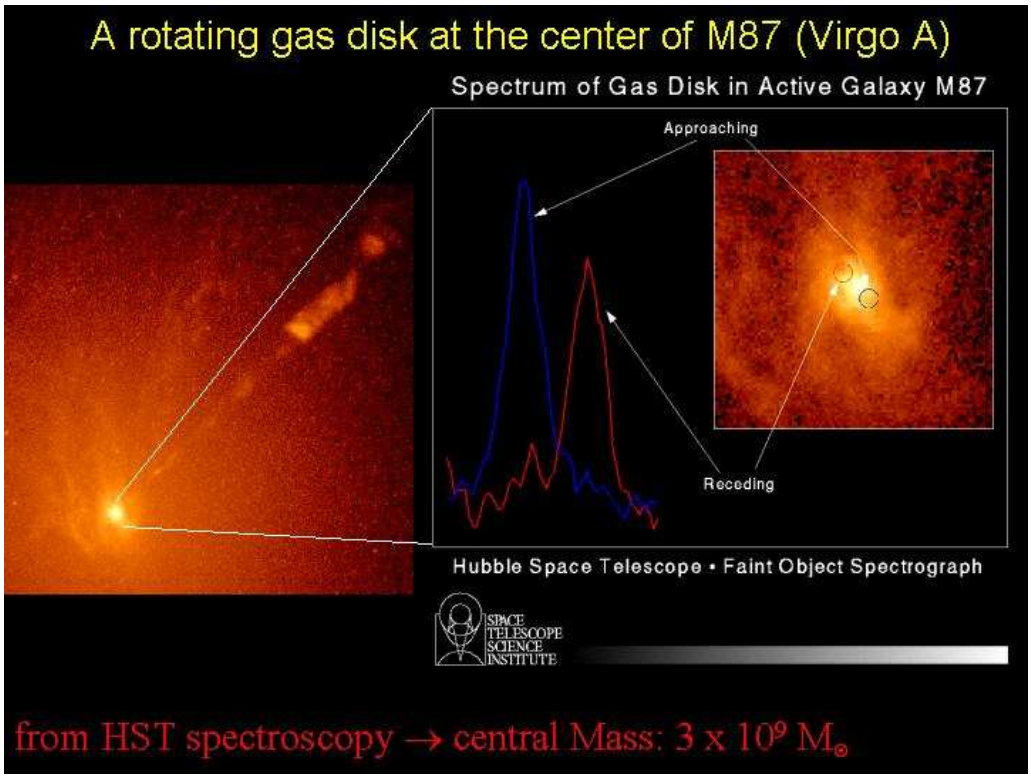
A rotating gas disk at the center of M87 (Virgo A)
Spectrum of Gas Disk in Active Galaxy M87
Approaching
Receding
Hubble Space Telescope • Faint Object Spectrograph
SPACE TELESCOPE SCIENCE INSTITUTE
from HST spectroscopy → central Mass: 3 x 10⁹ M⊙

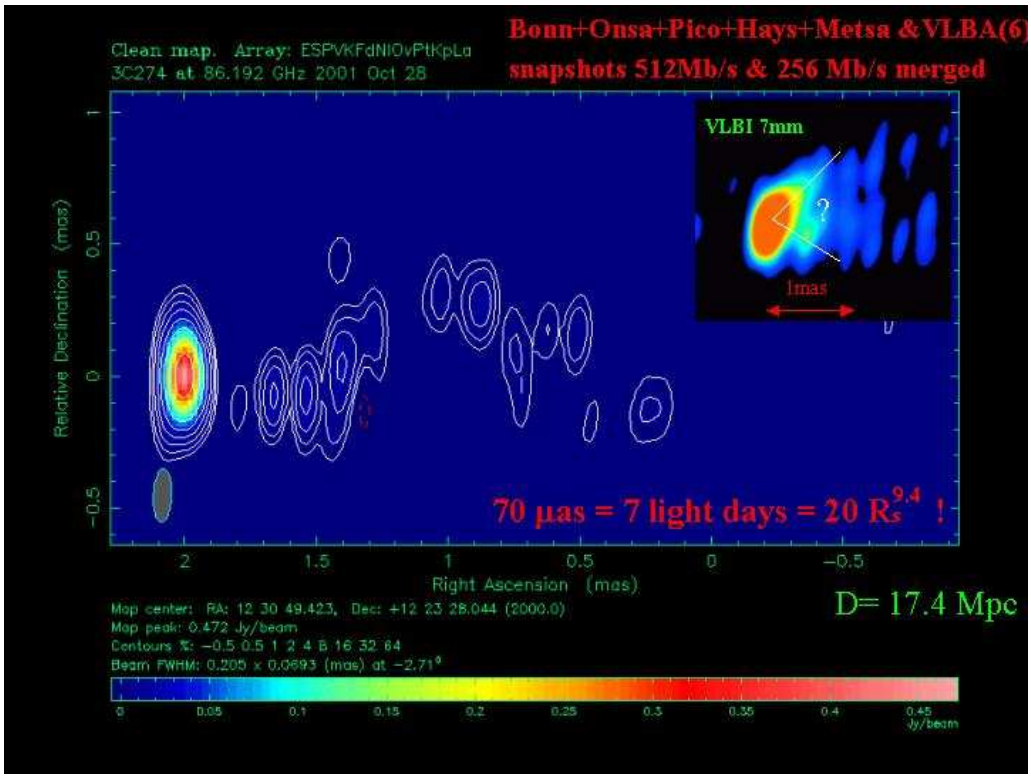
Clean map. Array: ESPVKFdNlOvPtKpLo
3C274 at 86.192 GHz 2001 Oct 28
Bonn+Onsa+Pico+Hays+Metsa &VLBA(6)
snapshots 512Mb/s & 256 Mb/s merged
VLBI 7mm
1mas
70 μas = 7 light days = 20 Rs^9.4 !
Relative Declination (mas)
Right Ascension (mas)
D= 17.4 Mpc
Map center: RA: 12 30 49.423, Dec: +12 23 28.044 (2000.0)
Map peak: 0.472 Jy/beam
Contours %: -0.5 0.5 1 2 4 8 16 32 64
Beam FWHM: 0.205 x 0.0693 (mas) at -2.71°
Jy/beam

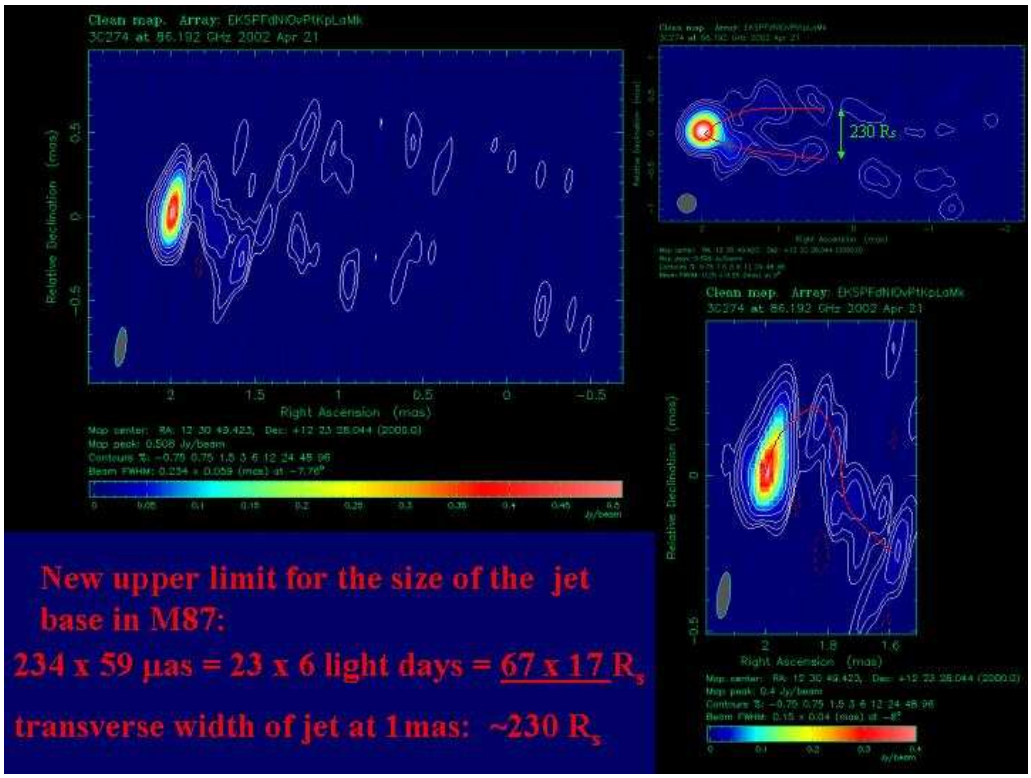
Clean map. Array: EKSPFdNOvPtKpLoMk
3C274 at 86.192 GHz 2002 Apr 21
Relative Declination (mas)
Right Ascension (mas)
230 Rs
New upper limit for the size of the jet base in M87:
234 x 59 μas = 23 x 6 light days = 67 x 17 Rs
transverse width of jet at 1 mas: ~230 Rs

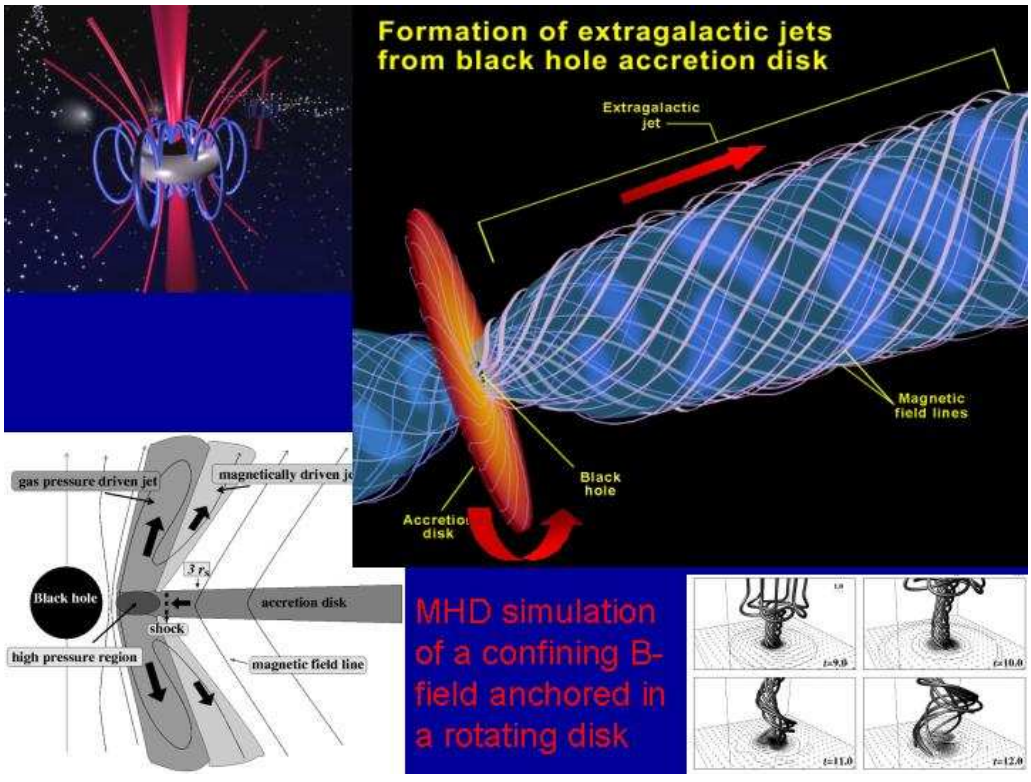
Formation of extragalactic jets from black hole accretion disk
Extragalactic jet
Magnetic field lines
Black hole
Accretion disk
gas pressure driven jet
magnetically driven jet
Black hole
accretion disk
shock
high pressure region
magnetic field line
MHD simulation of a confining B-field anchored in a rotating disk

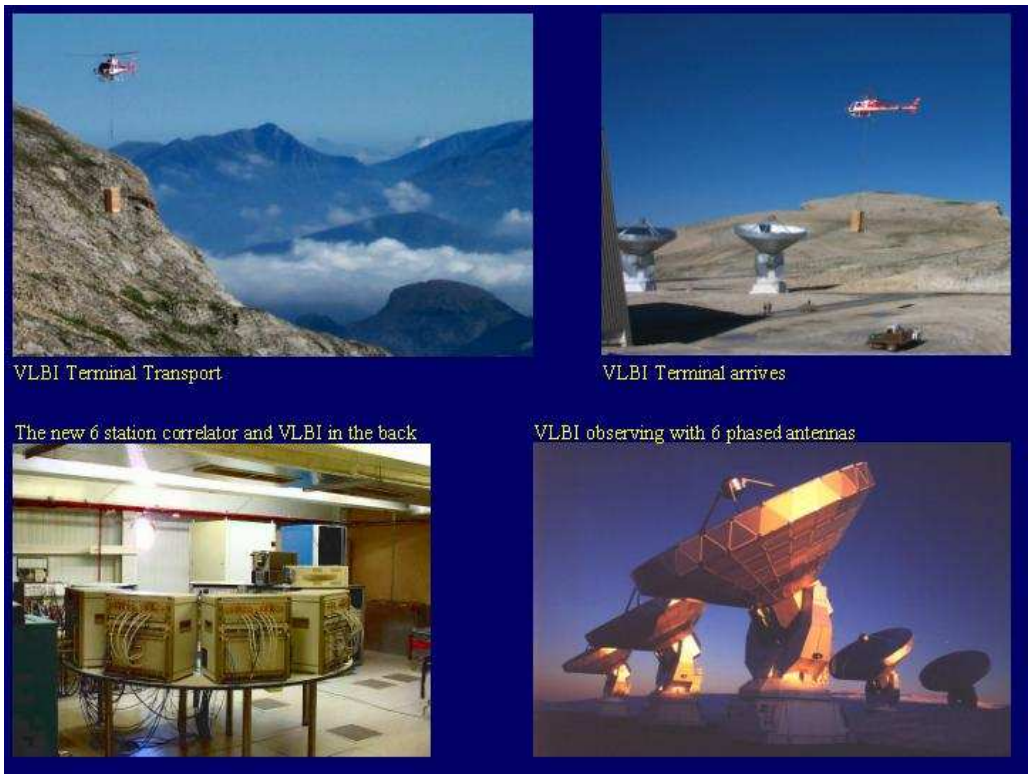
VLBI Terminal Transport
VLBI Terminal arrives
The new 6 station correlator and VLBI in the back
VLBI observing with 6 phased antennas


New: The Global Millimeter VLBI Array
45 Micro-Arcseconds resolution at 86 GHz
The Antennas:
• 100m Effelsberg, Germany
• 6x15m Plateau de Bure, France
• 30 m Pico Veleta, Spain
• 20 m Onsala, Sweden
• 15 m Metsähovi, Finland
• 8 x 25 m VLBA, USA
The Global mm-VLBI Array
http://www.mpifr-bonn.mpg.de/globalmm

Antenna Properties at 86 GHz						
Station	Country	Diameter [m]	Zenith Tsys [K]	Gain [K/Jy]	App.Eff. %	SEFD [K]
Effelsberg	Germany	100	130	0.14	7	930
Plateau de Bure	France	31	120	0.18	65	670
Pico Veleta	Spain	30	120	0.14	55	860
Onsala	Sweden	20	250	0.053	45	4720
Metsähovi	Finland	14	300	0.017	30	17650
VLBA(8)	USA	25	120	0.03	17	400
Future:						
GBT	Va,USA	100	100	1.0	35	100
Nobeyama	Japan	45	100	0.17	30	590
Noto	Italy	25	100	0.09	30	1100
CARMA	Ca,USA	35	100	0.14	50	710
LMT	Mexico	50	100	0.14	40	720
Yebes	Spain	40	100	0.13	30	770
APEX	Chile	12	100	0.03	70	3300
ALMA	Chile	64x12	100	1.8	70	55

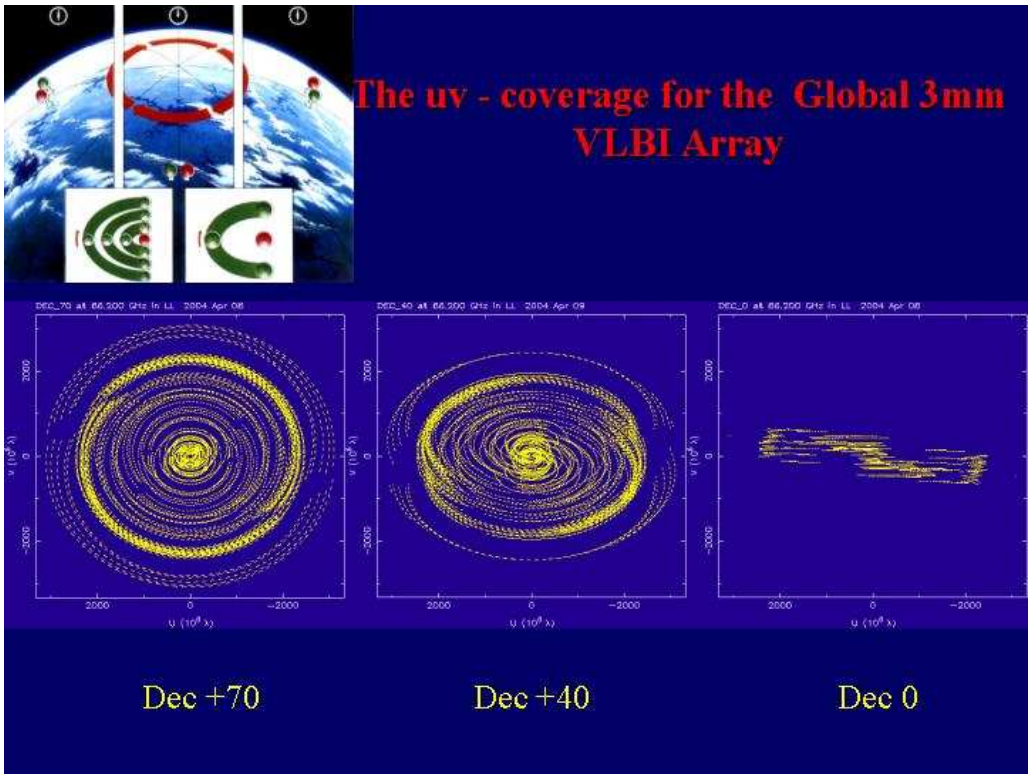

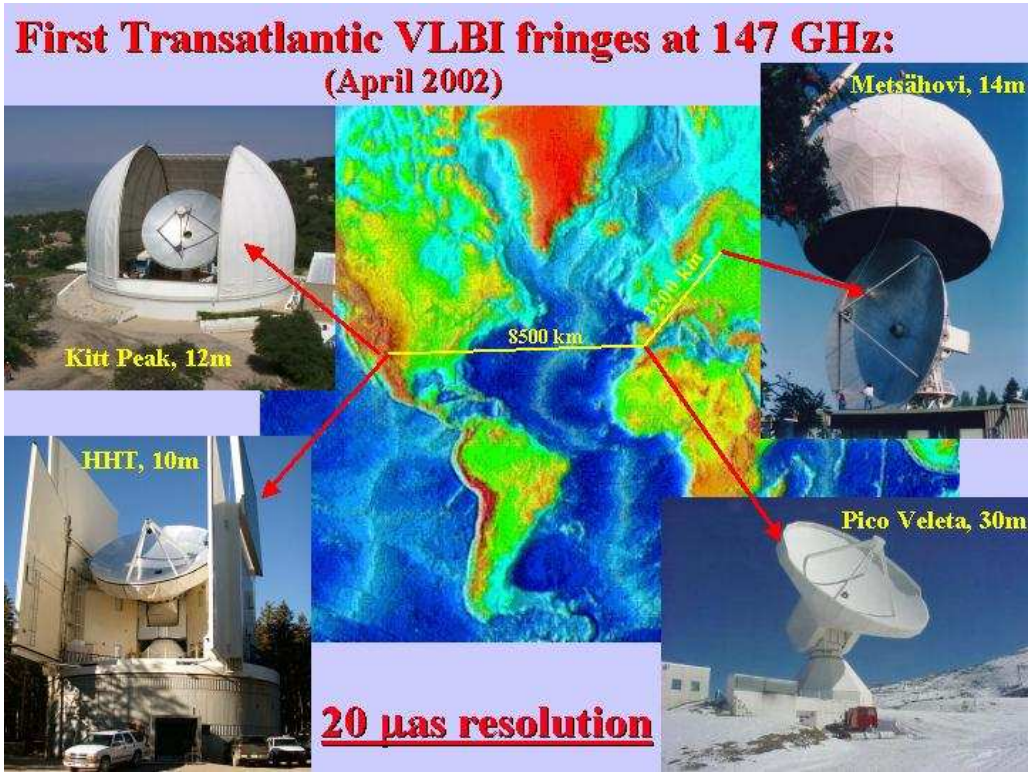

The SNR´s of the transatlantic VLBI detections at 147 GHz
(April 2002)

Source	Flux [Jy]	HHT-KP	HHT-PV	KP-PV	MET-PV
NRAO150	6.5	19	7	6	
0420-014	5.7	13	5?	5?	
3C279	21.1	49	75	20	10
1633+382	7.3	23	23	13	
3C345	4.7	7	6?	5?	
3C454.3	8.8	15	6?	5?	

Sources detected on the short baseline HHT-KP:
0133+476, 3C273, NRAO530, SgrA*, 1921-293, BL Lac, 2255-282

: detected : marginally detected on long baselines

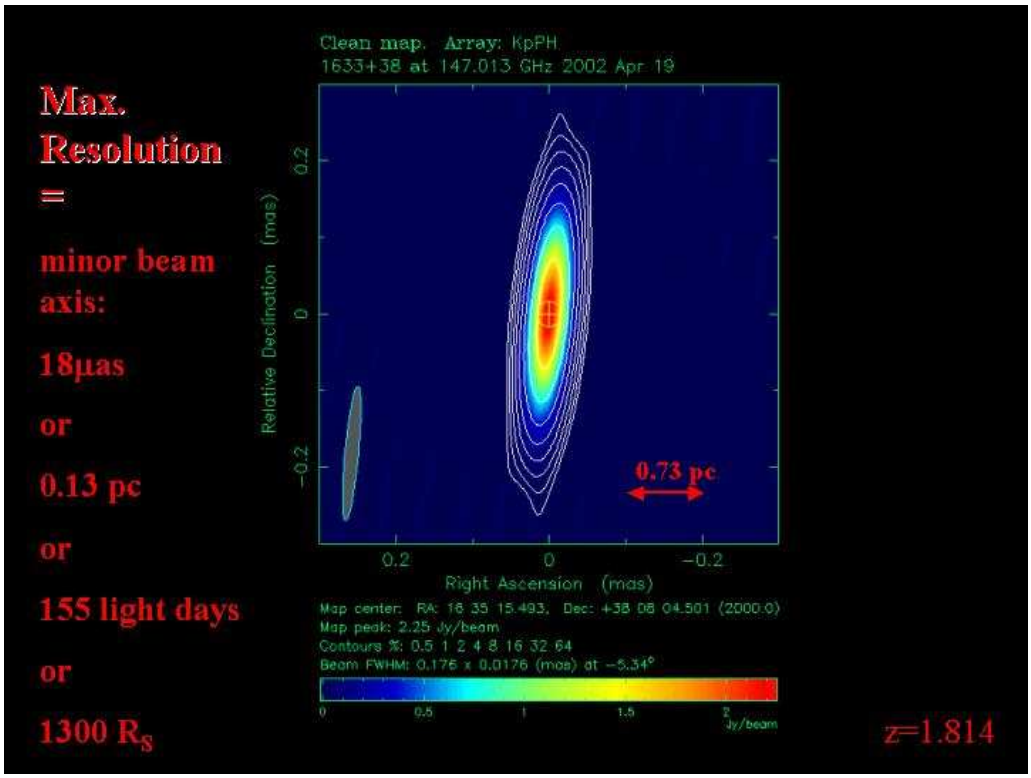
Max. Resolution =
minor beam axis:
18μas
or
0.13 pc
or
155 light days
or
1300 R_S
Clean map. Array: KpPH
1633+38 at 147.013 GHz 2002 Apr 19
Relative Declination (mas)
Right Ascension (mas)
0.73 pc
Map center: RA: 16 35 15.493, Dec: +38 08 04.501 (2000.0)
Map peak: 2.25 Jy/beam
Contours %: 0.5 1 2 4 8 16 32 64
Beam FWHM: 0.176 x 0.0176 (mas) at −5.34°
Jy/beam
z=1.814

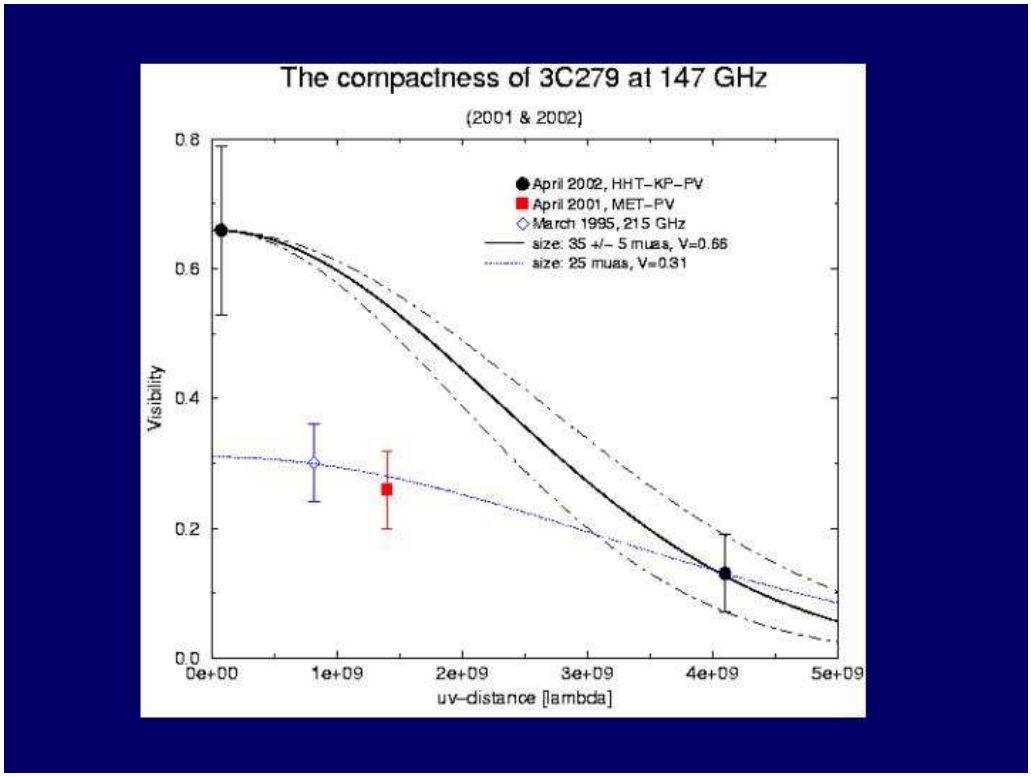
The compactness of 3C279 at 147 GHz
(2001 & 2002)
April 2002, HHT-KP-PV
April 2001, MET-PV
March 1995, 215 GHz
size: 35 +/- 5 muas, V=0.66
size: 25 muas, V=0.31
Visibility
uv-distance [lambda]

Are the Quasar Nuclei spatially resolved ?

Source	z	S_tot [Jy]	S_corr [Jy]	FWHM [muas]	T_B 10E12 [K]	size [pc]
3C279	0.536	21.1	14.0	34	0.7	0.20
1633+382	1.814	7.3	4.9	33	0.3	0.24

$$\theta_{\min} \geq \sqrt{\frac{1.22 \cdot S}{\nu^2} \cdot \frac{1}{T_B^{\max}}}$$

for $T_B^{\max} \leq 10^{12}\,\mathrm{K} \rightarrow \theta_{\min} \geq 10 - 20\,\mu as$

$(17 \leq \theta \leq 33\,\mu as$ **for 1633+382**$)$

$(27 \leq \theta \leq 34\,\mu as$ **for 3C279**$)$

First transatlantic VLBI fringes at 230 GHz (1.3 mm)

April 2003, 512 Mbit/s

HHT – PV

$SNR_{max} = 7.3$

PdBI – PV

$SNR_{max} = 25$

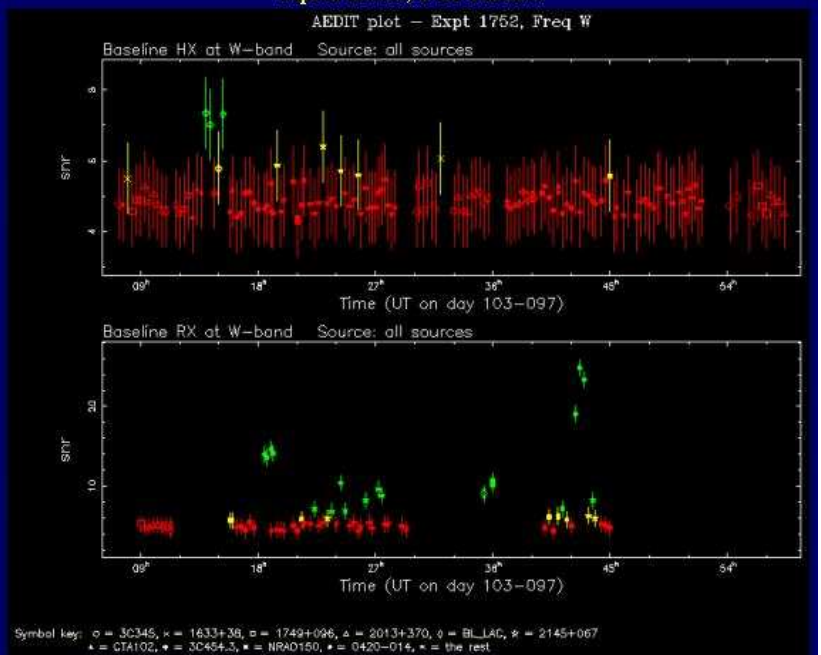

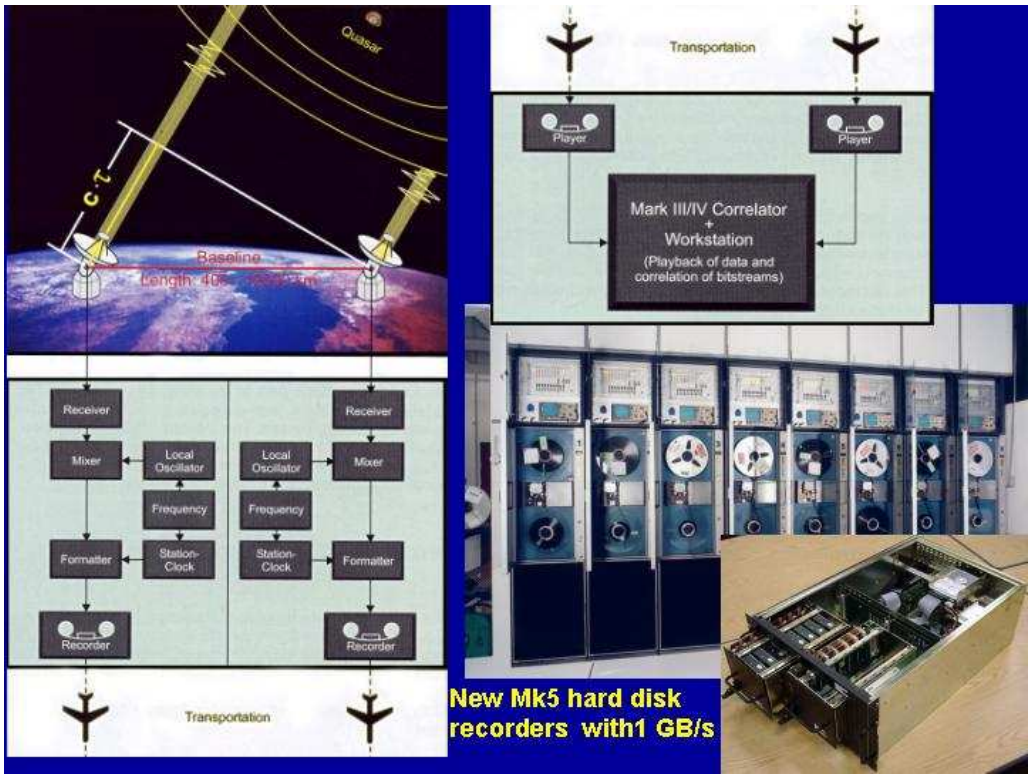

Signal-to-Noise ratios of the 230 GHz detections:

short baselines: ≤25
long baseline: 6-7

Two sources detected at 6.4 Gλ (32 μas):

3C454.3 and 0716+714

for 3C454.3 (z=0.859)

$\nu' = 428$ GHz, life time $B\gamma^2 = 3.6\ 10^5$,

$\Theta \leq 16$ μas = 0.1 pc = 1050 R_S^9,

SSA: $B \leq 1$ G $\rightarrow \gamma \geq 600$

Source	PdBI - PV	HHT - PV
NRAO150	10.7	
3C120	8.2	
0420-014	24.9	
0736+017	7.1	
0716+714	6.8	6.4 ?
OJ287	10.4	
1055+018		
3C273	8.2	
3C279	9.6	
NRAO530		
SgrA*		
3C345		
1633+382		
1749+096		
2013+370		
BL Lac	9.0	
2145+067		
CTA102		
3C454.3		7.3

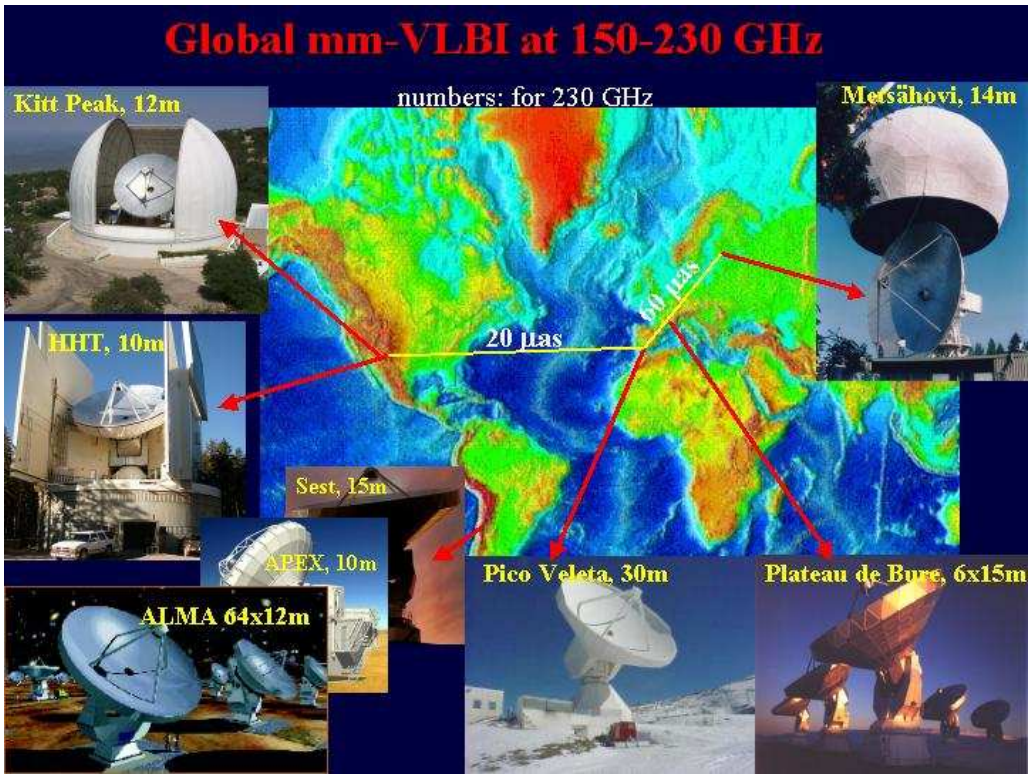

Conclusion

- 3mm: The new Global 3mm VLBI Array improves the imaging sensitivity by a factor of 3 – 4 (USE IT !)
- 2mm & 1mm: new hard disc recording and new antennas will allow imaging with a resolution of a few 10 micro-arcseconds
- M87: core size is smaller than expected (17 Rs); how to collimate jets on such small scales, BH rotation, Kerr metric ?
- SgrA*: need southern antenna(s) to image event horizont

Optical and radio variability of the BL Lac object 0109+224 – S. Ciprini, G. Tosti, C. M. Raiteri, M. Villata, H. Teräsranta, M. A. Ibrahimov, G. Nucciarelli, L. Lanteri, H. D. Aller

0109+224 Characteristics

Compact radio-loud source GC 0109+224 (S2 0109+22). (Green Bank radio survey list C, Davis 1971; Pauliny-Toth et al. 1972). Other most used names: TXS 0109+224, RX J0112.0+2244, EF B0109+2228, 2E 0109.3+2228, RGB J0112+227 - *[B0109+224, J0112+2244]*

Optical identification in 1976 (Owen & Mufson 1977), first measure of a strong mm emission (>1.5 Jy at 90 GHz) and inclusion in the BL Lacs family

Continuous featureless optical spectrum (Wills & Wills 1979) and spectrophotometric observations compatible with a single power-law (Falomo et al. 1994)

Intermediate optical behaviour between the large-amplitude variability BL Lacs and the smaller-amplitude blazars/AGNs (Pica 1977)

Host galaxy unresolved in NTT observations (Falomo 1996) and UKIRT (K-band) observations (Wright et al. 1998) - Suggested redshift: z>0.4 (Falomo 1996)

II Enigma Meeting - Stefano Ciprini Oct.12 2003

0109+224 Characteristics

No evidence for a thermal component in the far-infrared–optical SED (Impey & Neugebauer 1988).

Optical flux and the polarization variable on different timescales, including intranight variations (Sitko et al. 1985; Mead et al. 1990; Valtaoja et al. 1991).

Strong variable degree (5%-30%) and direction of the linear polarization (Takalo 1991; Valtaoja et al. 1993). No clear correlation between flux level and polarization (Valtaoja et al. 1993).

Near-infrared flux variations smaller than in the optical one (Fan 1999).

Variable radio flux, degree of polarization and position angle. Flat average spectrum (classical BL Lac object).

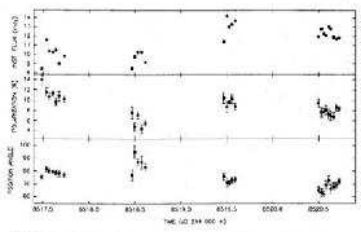

Fig. 6. Intranight variations of the polarization, position angle and flux plotted for four sequential nights as a function of time

Valtaoja et al. 1993

II Enigma Meeting - Stefano Ciprini Oct.12 2003

0109+224 Characteristics

VLA pc scale at 5 GHz reveals a compact core with a secondary component.
Less luminous and/or beamed than the 1-Jy sample of BL Lacs (Bondi et al. 2001)
Same mas structure in VLBA images at 2 and 8 GHz (Fey & Charlot 2000)

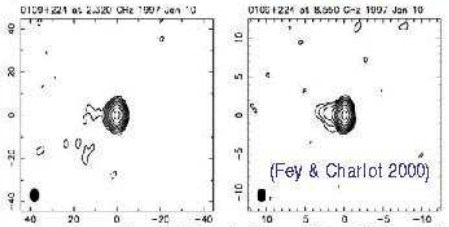

Contour plots at radio *S* and *X* bands. The scale is in milliarcseconds

kpc scale: a faint one-sided collimated radio jet, about 2 arcsec long (Wilkinson et al. 1998), largely misaligned with the pc-scale inner region (~> high-power low peaked BL Lac, LBL).

Included in the 200-mJy blazar sample (March˜a et al. 1996). Intermediate BL Lac between HBL and LBL (Bondi et al. 2001)

Regular radio monitoring by the University of Michigan Radio Astronomy Obs. (UMRAO, USA, at 4.8 GHz, 8 GHz, and 14.5 GHz, 24-years monitoring) and Metsähovi Radio Observatory (Finland, 22 GHz and 37 GHz, 19-years monitoring).

II Enigma Meeting - Stefano Ciprini Oct.12 2003

0109+224 Characteristics

Included in the Whole Year Blazar Telescope source list (WYBT; Tosti et al. 2002, R-band opt. Long-term monitoring, born from the WEBT collab. (Villata et al. 2000, 2002).

Bright X-ray point source ($\nu F_\nu(1\ \mathrm{keV}) \gtrsim 10^{-13}\ \mathrm{erg\ cm^{-2}\ s^{-1}}$)
HEAO-1 pointing (Della Ceca et al. 1990), detections of Einstein Obs. (Owen et al. 1981), EXOSAT (Maraschi & Maccagni 1988; Giommi et al. 1990; Reynolds et al. 1999), and ROSAT (Neumann et al. 1994; Brinkmann et al. 1995; Kock et al. 1996; Reich et al. 2000). Member of the RGB (ROSAT All-Sky Survey-Green Bank) catalog (Laurent-Muehleisen et al. 1999), an intermediate blazar sample.

In the diagnostic diagram $\alpha_{\text{rad-Opt}}$-$\alpha_{\text{Opt-X}}$ (Padovani & Giommi 1995), 0109+224 appears close to a prototype of intermediate blazars like W Com (ON 231, B2 1219+28), (Dennett-Thorpe & Marchã 2000)

GC 0109+224 was not detected in gamma-rays by EGRET (Fichtel et al. 1994), with a rather low upper limit.

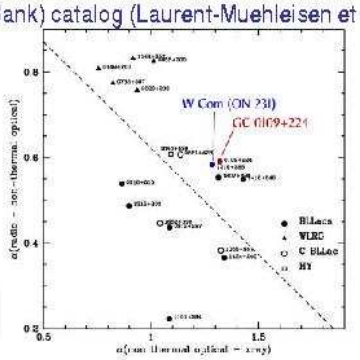

II Enigma Meeting - Stefano Ciprini Oct.12 2003

Comparison stars optical photometric calibrations

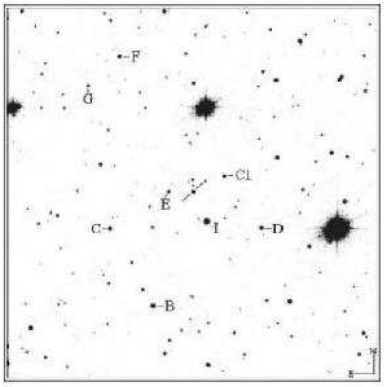

Fig. 1. Finding chart with a field of 15′×15′ centered on GC 0109+224 (elaborated from a frame of the Digitized Sky Survey). Calibration of stars D, C1, I, E is reported in Table 1. Stars B C F G belong to the photometric sequence calibrated by Miller et al. (1983).

BVR_cI_c Johnson-Cousins photometric calibration of comparison stars in the field of GC 0109+224.

star	R.A. (J2000.0)	Dec. (J2000.0)	$U^{(1)}$ (mag)	B (mag)	V (mag)	R_c (mag)	I_c (mag)
D	01 11 53.4	+22 43 17.9	15.48	15.19 ± 0.06	14.45 ± 0.05	14.09 ± 0.05	–
C1	01 12 00.5	+22 45 22.3	–	16.30 ± 0.10	15.38 ± 0.07	14.72 ± 0.06	14.22 ± 0.08
I	01 12 05.2	+22 43 30.7	13.51	13.25 ± 0.06	12.51 ± 0.05	12.11 ± 0.04	11.76 ± 0.04
E	01 12 10.6	+22 44 40.3	15.78	16.01 ± 0.08	15.29 ± 0.07	14.94 ± 0.05	14.61 ± 0.07

(1) U values by Miller et al. (1983)

Source Magnitude by differential photometry with respect to comparison stars in the same field. (Johnson-Cousins photometric system, see, e.g. Bessel 1979)

Calibrations derived from several photometric nights at the Perugia and Torino Observatories using Landolt standards. (for observing and reduction details see e.g. Fiorucci & Tosti (1996), Fiorucci et al. (1998), Villata et al. (1998), and Raiteri et al. (1998).

II Enigma Meeting - Stefano Ciprini Oct.12 2003

Historical light curve

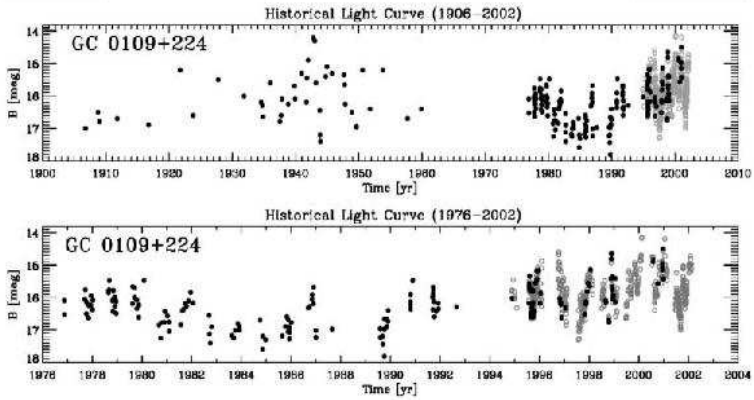

Fig. 3. The historical light curve of GC 0109+224 in B band (black dots) reconstructed from the literature (Pica 1977; Pica et al. 1980; Puschell & Stein 1980; Zeki et al. 1981; Moles et al. 1983; Pica et al. 1988; Xie et al. 1988a; Xie et al. 1988b; Mead et al. 1990; Sillanpää et al. 1991; Takalo 1991; Xie et al. 1992; Valtaoja et al. 1993; Falomo et al. 1994; Xie et al. 1994; Katajainen et al. 2000). Data after 1994 are almost entirely from this paper. B magnitudes derived from R_c values by using the mean $B-R_c$ index are added to improve sampling (grey circles); the maximum error for these estimates is about 0.3–0.4 mag. Pre-1960 values have original errors of 0.1 mag and represent photographic magnitudes (see text). Error bars are not represented for clarity.

II Enigma Meeting - Stefano Ciprini Oct.12 2003

Historical light curve

1906–now: empty gap in 1960–1975. Original non-corrected data reported, (pre-1961 values could be overestimated by 0.2–0.3 mag). Pre-1961 data mainly by Heidelberg plates (Zekl et al. 1981) and Harvard plates (Pica 1977). 1976-1988 data mainly obtained by Rosemary Hill Obs. Florida (Pica et al. 1988). Data after 1994 almost entirely from Perugia and Torino observatories (comparison with some V data from Tuorla, Katajainen et al. 2000, reveals a good agreement).

Largest brightness variation occurred in 1942–1943, (Bmag-phot 14.2, steep decline of 3.07 mag during 1 year). A comparable brightness level was reached again only in the flares of 1990s. 1944-1996: source never observed brighter than B = 15, (this could be due to poor sampling). In 1981–1990 the object remained in a low state around B = 17 (except for 2 observed flares). August 1989 the source brightness fell down to B = 18.42, minimum value ever observed (Takalo 1991).

In the post-1994 better sampled light curve obtained with our data, we see a general brighter mean B value (15.8), again comparable with the 1920–1960 period, and some flare events. Variations of 2.5 mag in less than one year are common.

II Enigma Meeting - Stefano Ciprini Oct.12 2003

Our optical photometric monitoring

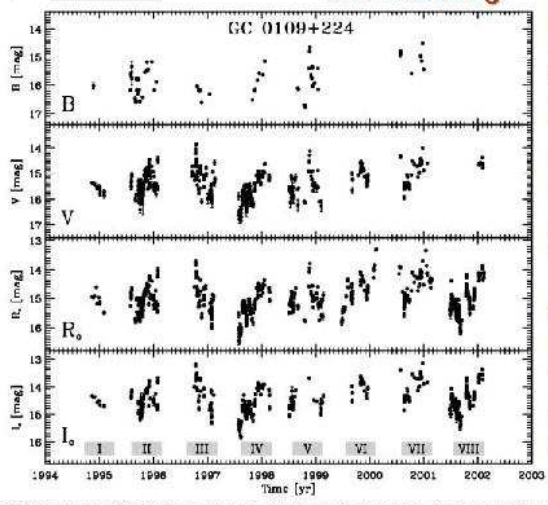

Perugia Obs. 1994-2002, B(few),V,R,I data

Torino Obs. 1995-1999 B,V,R data

Mt. Maidanak Obs. Dec2000 U,B,V,R,I data

8 observing seasons, 7 years 1542 photometric points,

Our improved sampling recorded also the larger (and faster) optical flares

Six main optical outbursts (weeks/month scale), variability mode placed between the flickering and the shot noise.

II Enigma Meeting - Stefano Ciprini Oct.12 2003

Colour indexes: general trends

NUMBER OF DATA PER OBSERVATORY

Obs.	U	B	V	R_c	I_c	Tot.	Period
Perugia	0	5	309	568	434	1316	Nov. 94-Feb. 02
Torino	0	56	41	96	0	193	Jul. 95-Jan. 99
Maid.	5	7	7	7	7	33	Dec. 00
Total	5	68	357	671	441	1542	

SAMPLING AND FLUXES

	B	V	R_c	I_c
Start date [JD-2 449 000]	679	669	669	669
End date [JD-2 449 000]	2908	3309	3318	3309
Mean gap in data [day]	33.2	6.7	3.9	6.0
Longest time gap [day]	357	352	244	244
Mean flux [mJy]	2.39	2.88	3.38	4.47
Max. flare flux [mJy]	7.85	11.66	16.16	15.10
Max/Min flux ratio	6.87	10.90	15.28	14.63
Absorption coeff. [mag]	0.161	0.124	0.100	0.073

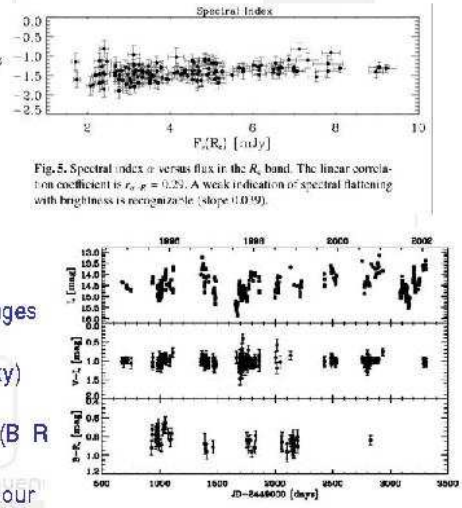

Fig. 5. Spectral index α versus flux in the R_c band. The linear correlation coefficient is $r_{\alpha,F} = 0.29$. A weak indication of spectral flattening with brightness is recognizable (slope 0.039).

Fig. 4. Temporal behaviour of the I_c magnitude (upper panel) and of $V - I_c$ (middle panel) and $B - R_c$ (lower panel) colour indexes.

Color indexes reveal spectral shape changes during flux variations. Here galaxy color interference is neglected (faint host galaxy)

Data dispersion around the mean values (B R = 0.83 and V I = 1.00). No correlation nor general trends. Rather achromatic behaviour in long timescales.

II Enigma Meeting - Stefano Ciprini Oct.12 2003

Variability loops in optical flares

During optical flares chromatic behaviour appears evident. The degree of correlation between spectral index and the flux sheds light on the non-thermal emitting processes (synchrotron in the optical).

Soft-hard-soft signature: common pattern (not the unique one) in X-ray flares. Spectral slope flattens when source luminosity increases. The more intense is the energy release, the higher is the particles energy. Loops, hysteresis cycles in the scatter plot between spectral index and flux. Acceleration mechanism tends to work with almost fixed populations of particles, spectral slope controlled by the radiative cooling, so that the information about changes in the injection rate of accelerated particles propagates from high to low energies (see e.g., Kirk et al. 1998; Georganopoulos & Marscher 1998, Kirk & Mastichiadis 1999)

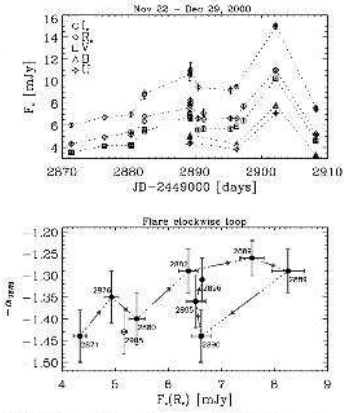

Fig. 6. Evolution of the optical spectrum of GC 0109+224 as a function of the flux in the R_c band during the double-peaked flare of November 22 – December 29, 2000. The loop formed by points connected by arrows corresponds to the first peak. In the subsequent major peak the flux achieves $F_c(R_c) = 11.04$ mJy and the spectral index $\alpha = 1.09$ on day 2902 (this point is out of the plot, for clarity), and then drops rapidly to the base value $F_c(R_c) = 5.15$ mJy, $\alpha = 1.39$, on day 2908 (empty circle in the plot).

II Enigma Meeting - Stefano Ciprini Oct.12 2003

Variability loops in optical flares

Variability loops, during isolated flares are recognizable not only in the X-ray emission, but also in the optical one, once sampling is sufficient to trace the patterns well (and also in the case of a LBL/intermediate blazar like GC 0109+224).
Clockwise loop comes out from the double-peaked flare of Nov22-Dec29, 2000 and from the isolated flare of Oct14–Dec4, 1998.

Double-peaked flare of Oct1-Oct24, 1996 shows an anticlockwise loop due to the first peak superimposed to a second clockwise loop due to the second peak. This could be a nice signature of the superimposition of a second flare on a previous one. Anticlockwise loops less common (cooling times comparable to acceleration times)

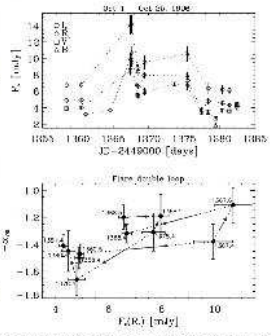

Fig. 8. Evolution of the optical spectrum of GC 0108+224 as a function of the flux in the *R*, band during the double-peaked flare of October 1-25, 1996. An anticlockwise loop due to the first peak is superimposed to a second clockwise loop due to the second peak. This might be a general and nice signature of flares superimposition.

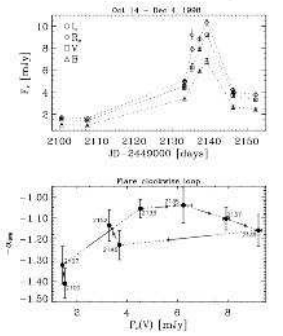

Fig. 7. Evolution of the optical spectrum of GC 0109+224 as a function of the flux in the *V* band during the isolated flare of 14 October – 4 December 1998. A well-defined clockwise loop is traced evidencing, one more time, that the spectrum gets softer when the source gets fainter.

Optical timescales of 0109+224

Three standard methods optimized for unevenly sampled datasets, applied to give a quantitative statistical description of the optical time variability of GC 0109+224: structure function (*SF*), discrete correlation function (*DCF*), and discrete Fourier transform in the Lomb-Scargle implementation (periodogram).

Indications of recurrent time scales of variability, from a dozen days to a few years.

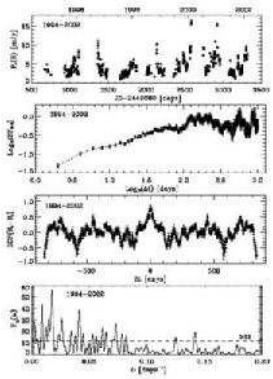

Fig. 9. The 1994–2002 *R*, flux light curve, its structure function (data bin: 1 day, *SF* bin: 2 days), discrete correlation function (data bin: 1 day, *DCF* bin: 4 days), and periodogram ($\omega = 2\pi f$). The dashed line indicates the 99% significance threshold.

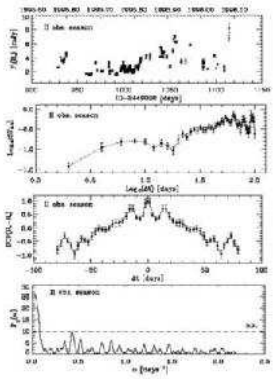

Fig. 10. The II observing season (July 1995 – January 1996) *R*, flux light curve, its structure function (data bin: 1 day, *SF* bin: 2 days), discrete correlation function (data bin: 1 day, *DCF* bin: 3 days), and periodogram ($\omega = 2\pi f$). The dashed line indicates the 99% significance threshold.

Optical timescales of 0109+224

Scales of about 25–40 days and 1.2, 1.9 years were found several times, and the time scale of 6.4 years is similar to the variability period recognized in AO 0235+16 (Raiteri et al. 2001). Slopes in the *SF* were reliably determined, but the *SF* plateau can be recognized only for the best sampled light curves. The values of imply a variability mode between the flickering and the shot noise.

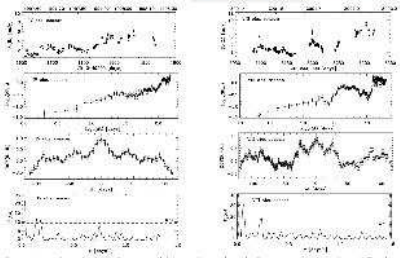

Table 3. Summary of all the time scales revealed by the statistical analysis (when possible) performed with the structure function (*SF*), the discrete correlation function (*DCF*), and the Lomb-Scargle periodogram (P_{LS}). Columns report: (1) observing period, (2) period length, (3) time scales estimated by visual inspection, (4) time scales calculated by deep drops in the *SF*, (5) *SF* slope, (6) time scales deduced from the *SF* transition to the plateau, (7) time scales estimated from the *DCF* peaks, (8) time scales derived from the peaks of the periodogram.

Obs. period	Duration [days]	*VET* [days]	$SF\,T_{eff}$ [days]	*SF* slope β	$SF\,T_{tr}$ [days]	$DCF\,T_{pk}$ [days]	P_{LS} *T* [days]
1976-2002 (*)	26y	...	320,1.2y,1.9y,6.5y	0.55 ± 0.06	...	340,1.2y,2.1y	1.0y,1.2y,2.0y,6.4y
1994-2002 (*)	7.3y	320, 1.2y	327,1.2y,1.9y	0.57 ± 0.02	128	1.2y,1.9y	150,1.0y,1.9y
II season	186	120	12,18,74	0.68 ± 0.06	...	13	14
III season	131	...	38,64	0.57 ± 0.09	...	68	70
IV season	210	45	130	0.70 ± 0.04	122	42	35, 45
V season	230	...	54	0.72 ± 0.08	...	54	...
VI season	235	...	88	...	...	...	87
VII season	220	40	40	1.05 ± 0.08	...	38,95	...
VIII season	255	24	26, 104	0.73 ± 0.09	40	26,88,104	27,111

† Time scales followed by "y" are expressed in years.

II Enigma Meeting - Stefano Ciprini

Radio-optical flux correlations?

Optical flares are clearly much faster with respect to the radio-mm bands. Some particularly large optical outbursts do not have obvious counterparts at mm and radio.

The radio light curves appear well correlated at the different frequencies, around the zero lag.

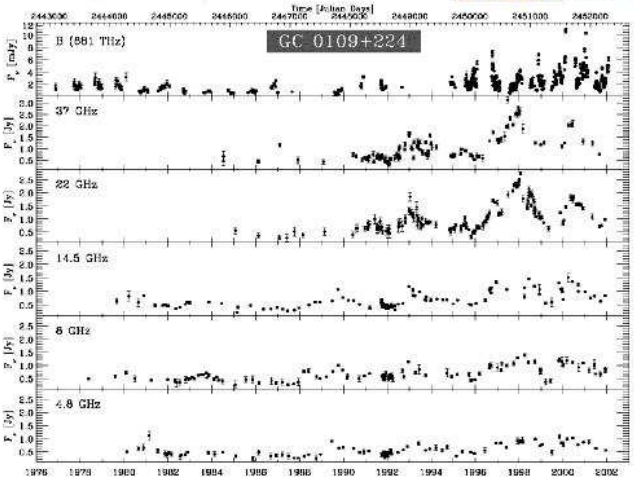

Figure 1. The complete radio–optical density flux light curves of GC 0109+224. The optical observations are historical, and Perugia Obs. (Italy) data (the post-1994 data points), reported in the original or extrapolated Johnson B band (see for details Ciprini et al. 2003a). The high sampled data at 37 and 22 GHz are from Metsähovi (Finland), and the 14.5 GHz, 8 GHz, 4.8 GHz data are from the long term monitoring of the UMRAO (USA). This source clearly exhibit a higher mean flux level, and an enhanced activity in the radio–mm after 1992, and in the optical after 1994, even if the optical sampling before this year is insufficient to record faster (and usually larger) flares.

II Enigma Meeting - Stefano Ciprini Oct.12 2003

Radio-optical flux correlations?

Radio-optical cross-correlation peaks, found in all the bands around the lag of 2.1-2.4 years, are extended and have low values (ZDCCF < 0.62). Complexity, spread and low values of the correlation peaks, impossibility to visually recognize the lags, their large values, the very different duty-cycles, and especially such long delays, suggest that there is not a real correlation, and no physical meaning in the two-year lag. Other shorter radio-optical delays around 33, 190, and 500 days are not significant because they are found with very small correlation coefficients. Previous lags hinted are based only on correlations with 3-years optical data (Hanski et al.2002).

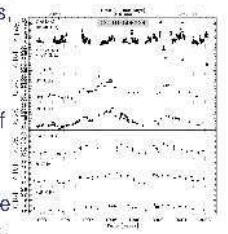

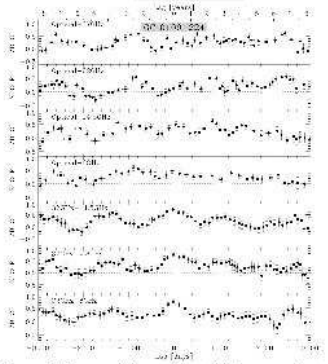

Figure 3. Cross correlation calculation with the z-transformed discrete correlation function (ZDCF, Alexander 1997). Due to the different timescales for the duty cycles in the radio and optical, and to gaps mainly of data in the optical, no strong evidence of a real correlation is found. Weak peaks in the cross-correlations [ZDCCF coefficient ≈ 0.5 – 0.6] are found around a lag of 801 days (also positive in the optical–22GHz correlations, see text). On the other hand, the lines of the various radio frequencies appear well correlated, as expected, with a peak around the zero lag.

Radio variability mode

The ZDACF and first-order SF shapes give a fluctuation mode between the flickering and the shot noise: $P(f) = 1/f^{\alpha}$, with $1.39 < \alpha < 1.65$. A similar behaviour was found also for the optical emission ($1.57 < \alpha < 2.05$) of this source. This power spectrum is characteristic of a random walk, stochastic relaxation processes

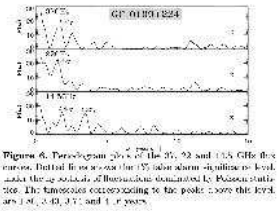

Figure 4. The auto-correlations of the radio flux curves, calculated with the ZDCF. These do not show any relevant feature, except for broad and weak ($ZDACF \geq 0.6$) peaks around the timescale of 3.14-4.06 years (at 14.5 GHz), and around 3.53-4.80 years (at 37 GHz). From 37 GHz to 14.5 GHz, the ZDACF profile resembles to a shot noise, with a single bump in the correlation curve within the 2000 days timescale (semi-amplitude ≈ 2.7 years).

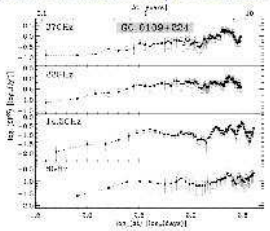

Figure 5. The first order structure functions (SF) of the radio density flux light curves, in logarithmic scale. For the 37 GHz flux curve, the mean slope index of the steep part of the SF is $\beta = 0.48 \pm 0.09$, and for the 22 GHz curve $\beta = 0.55 \pm 0.05$ (bins size used is 60 days for both). For the 14.5 GHz curve the SF mean slope is $\beta = 0.09 \pm 0.14$, and for the 8 GHz data $\beta = 0.52 \pm 0.04$, 250 days the bin size used). The time scales corresponding to steeper drops in the SF are of 3.4-3.8 and 7.0-7.6 years. The shorter lags at which one sees a flattening in the curves are around 1.1 - 1.3 years.

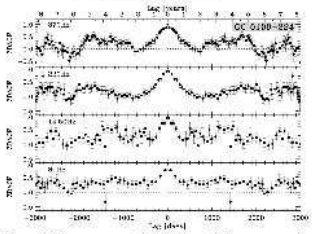

Multiwavelength data

Multiwavelength overall SED data points out a synchrotron peak in the frequency range around the near-IR, optical (possibly near-UV?) range. This strengthens the assumption that GC 0109+224 is an LBL or intermediate blazar, (as suggested for example in Laurent-Muehleisen et al. 1999; Dennett-Thorpe et al. 2000; Bondi et al. 2001). Rather low EGRET upper limit, no data available to check the presence of the high-energy (i.e. IC) emission component.

Table 1. Some properties and fluxes of GC 0109+224. (1) optical counterpart *Hipparcos* coordinates (Zacharias et al. 1999); (2) redshift lower limit (Falomo 1996); (3) 92 cm flux density (Douglas et al. 1996); (4) 20 cm flux density (Owen et al. 1980); (5) mean flux densities from this work; (6) 37 GHz flux from Metsähovi; (7) 1.2 mm Mambo-IRAM detection (Bertoldi 2002); (8) IRAS far-IR flux at 60 μm (Impey & Neugebauer 1988); (9) mid-IR flux in L band (O'Dell et al. 1978); (10) mean optical flux in R Cousins band (Ciprini et al. 2003a); (11) mean optical flux in B Johnson band from historical light curve (Ciprini et al. 2003a); (12) optical (B band) min and max degree of linear polarization (Valtaoja et al. 1993; Takalo 1991); (13) X-ray flux at 2 keV by Einstein Observatory (HEAO-2) IPC and MPC instruments (Owen et al. 1981; Ledden & Odell 1985; Maraschi et al. 1986); (14) X-ray flux at 1 keV by CMA instrument on EXOSAT (Maraschi & Maccagni 1988; Giommi et al. 1990; Reynolds et al. 1999); (15) X-ray flux at 1 keV by PSPC instrument of ROSAT (Neumann et al. 1994; Brinkmann et al. 1995; Reich et al. 2000) and spectral index (Kock et al. 1996; Laurent-Muehleisen et al. 1999); (16) flux limit above 100 MeV by EGRET (see Tab. 2), (Fichtel et al. 1994).

Quantity	Value	Epoch	Ref.
R.A. (J2000.0)$_{opt}$	01h 12m 05.8238s	...	(1)
Dec (J2000.0)$_{opt}$	−22° 44' 38.796"		(1)
z	> 0.4	...	(2)
F_ν(0.305 GHz)	0.278 ± 0.021 Jy		(3)
F_ν(1.494 GHz)	0.36 ± 0.2 Jy	Jan79	(4)
<F_ν(4.8 GHz)>	0.50 Jy	Feb80-Dec01	(5)
<F_ν(8 GHz)>	0.87 Jy	May78-Dec01	(5)
<F_ν(14.5 GHz)>	0.66 Jy	Sep79-Dec01	(5)
<F_ν(22 GHz)>	1.07 Jy	Jan85-Dec01	(5)
<F_ν(37 GHz)>	1.05 Jy	Jul84-Aug01	(5)
F_ν(87 GHz)	2.06 ± 0.09 Jy	2000 Apr 28	(6)
F_ν(250 GHz)	3.22 ± 0.06 Jy	2000 Mar 29	(7)
F_ν(60 μm)	188 mJy	1983	(8)
F_ν(3.5 μm)	11.8 mJy	Jan77	(9)
<F_ν(0.64 μm)>	3.8 ± 0.2	Nov94-Feb02	(10)
<F_ν(0.44 μm)>	2.4 ± 0.3	Nov78-Feb02	(11)
$P(B)_{min/max}$	0.7% / 29.69 %	...	(12)
F_ν(2 keV)	0.15 μJy	Jul 1979	(13)
F_ν(1 keV)	0.21 μJy	Aug 1984	(14)
F_ν(1 keV)	0.26 ± 0.08 μJy	Aug 1990	(15)
α_X	1.06 ± 0.25	Aug 1990	(15)
F_ν(> 100 MeV)	< 0.01 nJy	1992	(16)

Table 2. EGRET viewing periods (v.p.) and flux upper limits (u.l.) of GC 0109+224. Related quasi-simultaneous radio and optical fluxes from this work are also reported in the Table when available. References: (a) EGRET integral flux density upper limit above 100 MeV (first EGRET catalog, phase 1) for three v.p. (Fichtel et al. 1994); (b) the only simultaneous optical data available (Valtaoja et al. 1993), points out a low brightness and polarization degree 0.20 ± 0.81; (c) u.l. given by the summed exposure of phase 1 pointings, and the other EGRET v.p. of the GC 0109+224 region on phase 3 and cycle 4 (1994-96) (Hartman et al. 1999). Any new pointing of the region was done during the EGRET phase 2 (Nov.1992-Sept.1993, Thompson et al. 1995). During EGRET cycle 8, at least one more pointing was available (2000, Apr 18-Apr 25) but our source was on the edge of the field of view. Throughout all the EGRET v.p. the source had a relatively low (sub-Jy) radio emission.

EGRET v.p.	Start-End Date	F_γ(> 100MeV) [ph cm^{-2} s^{-1}]	Ref.	Optical obs. epoch	F_{opt} [mJy]	Ref.	Radio obs. epoch	F_{rad} [Jy]
0020....	1992 Apr 23 - Apr 28]			...	...		1992 Apr 26	$F_{14.5}$ = 0.48 ± 0.08
0280....	1992 May 07 - May 14] ⇒	< 6.0 × 10^{-8}	(a)	...	...		1992 Apr 29	F_{22} = 0.59 ± 0.13
0370....	1992 Aug 20 - Aug 27]			1992 Aug 28	0.94 ± 0.08	(b)	1992 May 06	$F_{14.5}$ = 0.83 ± 0.01
...				...	...		1992 Sep 01	F_{22} = 0.84 ± 0.03
3170....	1994 Feb 17 - Mar 01]			...	...		1994 Mar 15	F_{22} = 0.78 ± 0.11
4250....	1996 Jul 25 - Aug 08] ⇒	< 5.6 × 10^{-8}	(c)	...	...		1996 Jul 20	F_{22} = 0.75 ± 0.04
...	...	...		...	...		1996 Aug 04	F_{22} = 0.83 ± 0.05
...	...	...		...	...		1996 Aug 06	F_{22} = 0.91 ± 0.06

II Enigma Meeting - Stefano Ciprini Oct.12 2003

The SED of 0109+224

Only old X-ray ROSAT-PSPC (F_x=0.26 ± 0.08 μJy, Kock et al. 1996) EXOSAT-CMA and *Einstein* flux data point. These very few detections seem to suggest that the highest energy synchrotron tail is emitted in the soft-X ray band (-> LBL/intermediate blazars).

IRAS: 188 mJy at 60 micron

IRAM-Mambo detected a flux of about 3.1-3.3 Jy at 250 GHz.

EGRET u.l. (first cycle, Fichtel et al.1994) above 100 MeV:

$F_\gamma < 6\times10^{-8}$ photons cm^{-2} s^{-1}

Low optical brightness and the small radio fluxes (sub-Jansky radio fluxes in this EGRET viewing period.

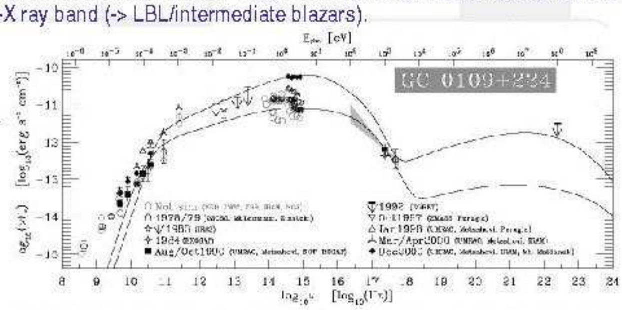

Figure 7. The SED of GC 0109+224 assembled with the available multi-wavelength data (open and filled symbols), upper limits (arrows), and ROSAT slope ... at different epochs. Two SSC model fit attempts (black lines) are used, for a low emission state and an high state. The SED is consistent with a pure smooth synchrotron continuum, peaking between the near IR, optical, near UV, range. EGRET upper limit above 100 MeV is rather low. There is no evidence of gamma-ray emission bump, and the few X-ray detections suggests a downward trend. Data are grouped for no-simultaneous epochs with the same symbol, instruments or references are indicated in parentheses. Data from this work (UMRAO, Metsähovi and Perugia observatories), NED database, from (Owen et al. 1980, OSC80), Mt. Lemmon (Puschell & Stein 1980), from (Fan 1999, F99) and (Neser et al. 2000, N00), Einstein IPC (Owen et al. 1981; Ledden & Odell 1985), IRAS (Impey & Neugebauer 1988, IN88), EXOSAT CMA (Maraschi & Maccagni 1988; Giommi et al. 1990; Reynolds et al. 1999), NOT (Valtaoja et al. 1993), ROSAT PSPC (Neumann et al. 1994; Brinkmann et al. 1995; Kock et al. 1996; Reich et al. 2000), EGRET (Fichtel et al. 1994; Hartman et al. 1999), 2MASS (Skrutskie et al. 1997), IRAM Mambo (Bertoldi 2002) and Mt. Maidanak (Ciprini et al. 2003a). The two lines referring to the SSC fit attempts for the flaring state of December 2000 and the low state around the ROSAT detection on 1990 are performed with the following parameters. August/October 1990 low state γ_{min} = 60, γ_{max} = 1.7 × 10^6, γ_{break} = 5 × 10^3, p_1 = 2.4, p_2 = 2.5, ξ = 0.015, B = 0.45Gauss, R = 9.5 × 10^{16}cm, $\mathcal{D}$ = 13. December 2000 high state: γ_{min} = 25, γ_{max} = 5 × 10^5, γ_{break} = 7 × 10^3, p_1 = 2.1, p_2 = 2.2, ξ = 0.015, B = 1 Gauss, R = 8.5 × 10^{15}cm, $\mathcal{D}$ = 15. Redshift z = 0.4 is assumed (Falomo 1996).

II Enigma Meeting - Stefano Ciprini Oct.12 2003

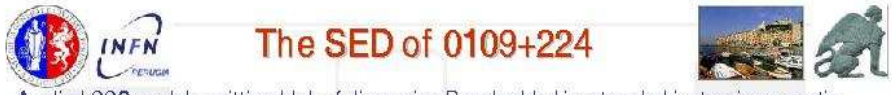

The SED of 0109+224

Applied SSC model: emitting blob of dimension R embedded in a tangled isotropic magnetic field of mean intensity B, subjected to a continuous injection of shocked relativistic electrons with a break power law energy distribution, exponentially damped:

$$Q_{inj}(\gamma) = Q_0 \gamma^{-p} \exp(-\gamma/(k\gamma_{max}))\ [\mathrm{cm}^{-3}\ \mathrm{s}^{-1}]$$

Region moving almost aligned with our line of sight

$$\mathcal{D} = ((1+z)\Gamma(1-\beta\cos\theta))^{-1}$$

The IC spectrum results from the interaction of the distribution with the synchrotron photon field. The produced spectra were transformed to the frame of the observer respect to jet direction), using the relativistic Doppler beaming/bulk factor.

SED data and modelling allude to a synchrotron peak ranging between the near-IR, for the quiescent states, and the optical (perhaps also near-UV) bands for the flaring states. As a classical BL Lac, the SED is represented well with leptonic SSC models. Therefore, with simple scaling considerations, the IC emission can be seen as the upshifted synchrotron component. Near-IR-optical peak can predict a possible IC peak in GeV gamma-ray energies (e.g. Stecker et al. 1996) $(\nu_{GeV} F_{GeV})/L_{IC} \simeq (\nu_{opt} F_{opt})/L_{syn}$

Lsyn and B intensity might be high for this object, reducing the IC dominance. However the strong mm flux, the peak of the SED in near-IR-optical bands, and the brightness in X-ray frequencies, might suggest the possibility of gamma-ray emission. $U_{rad}/U_B = L_{IC}/L_{syn}$

II Enigma Meeting - Stefano Ciprini Oct.12 2003

Conclusions

Obtained, collected and analyzed the largest amount of radio-optical data ever published on GC 0109+224. Some results are found, but also open questions are arisen.

Over 20 years of radio (UMRAO and Metsähovi) and optical data (last 7-years improved sampled optical data of by Perugia and Torino Observatories)

Reconstructed the overall SED. No EGRET detection and no hints of a high-energy (e.g. IC) spectral component (very-very few data beyond optical frequencies).

GC 0109+224 can produce strong outburst at high radio frequencies (2-3 Jy at freq. > 20 GHz), but can remain relatively quiet at low frequencies for long periods.

Radio and optical flux density variability characterized by intermittent behaviour, not regular alternation of relatively large amplitude flares, and flickering phases, varying over all timescales sampled (days, months, years). Relatively fast drops of the flux.

II Enigma Meeting - Stefano Ciprini Oct.12 2003

Conclusions

Optical flares clearly much faster with respect to the radio-mm bands. Some particularly large optical outbursts do not have obvious counterparts at mm and radio wavelengths (different emitting components, duty cycles, more rapid cooling at higher frequencies).

No evidence for long term periodic variations with fixed period, but only weak hints of typical timescales in the ranges of 3.2-4.5 years in the radio. No evidence for long term periodic variations in the optical but hints of typical-recurrent timescales from a dozed days to a few years.

Rather achromatic long-term optical variations. Short-term optical flares at least in some cases follow the "flatter when brighter" feature. 3 optical flares sampled almost sufficiently show clear hysteresis loops (as usually found when analyzing the X-ray flux behaviour of blazars). Radiative cooling of a single population of accelerated electrons is dominating in larger and faster optical flares in this cases.

Variability mode between flickering and the shot noise, i.e. $P(f) = 1/f^{\alpha}$, with α 1.2/1.3 < 1.8/2.0, i.e. the power spectrum is characteristic of a random walk, both in the optical and in the radio (common behaviour in blazars).

II Enigma Meeting - Stefano Ciprini Oct.12 2003

Conclusions

Synchrotron emission possibly dominant, (as suggested by the high polarization degree, absence of emission lines) Also our homogeneous SSC modelling suggests a relatively high magnetic field and synchrotron luminosity, diminishing the inverse self-Compton radiation, (warning!: multiwavelength data insufficient to constrain hypotheses)

GC 0109+224, suffers from substantial lack of data in mm, sub-mm, and infrared (as usual) bands, and high energy observations beyond the optical. High energy gamma-ray predictions from optical and X-ray fluxes suffer uncertainties also with pure SSC models (e.g. Boettcher et al. 2002 for W Com).

However the suggested high millimeter brightness, and synchrotron emission peaked at near-IR-optical frequencies, could imply a GeV gamma-ray radiation detectable by the next-generation of gamma-ray space telescopes. (integral scheduling by Pian et al.)

An increased observing effort for this source, especially at millimeter, X-ray bands and beyond, together with a better optical monitor is suggested.

II Enigma Meeting - Stefano Ciprini Oct.12 2003

References

Ciprini S., Tosti G., Raiteri C. M., Villata M., Ibrahimov M. A., Nucciarelli G., & Lanteri, L. 2003, Astronomy & Astrophysics, 400, 487

Ciprini S., Fiorucci M., Tosti G., & Marchili N. 2003, in High Energy Blazar Astronomy, L. O. Takalo, & E. Valtaoja eds., ASP Conf. Series, 299, 265

Ciprini S., Tosti G., Teräsranta H. & Aller H. D. 2003, Mon. Not. Royal Astron. Soc., submitted

A multiwavelength study of the OJ 287 variability – N. Marchili, M. Villata, C. M. Raiteri, G. Tosti, S. Crapanzano, L. Lanteri, H. D. Aller, M. F. Aller, H. Teräsranta

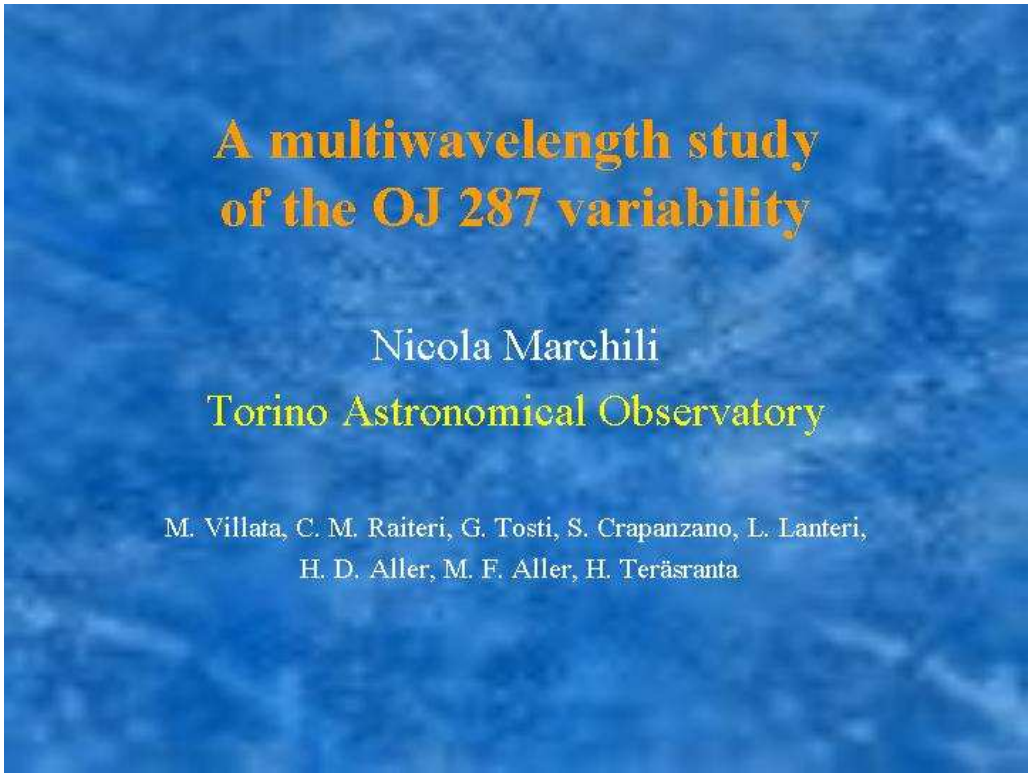

A multiwavelength study of the OJ 287 variability

- construction of light curves;
- temporal analysis of radio data by means of DCF and periodogram;
- temporal analysis of optical data, with particular attention to the most recent data;
- cross radio-optical correlation.

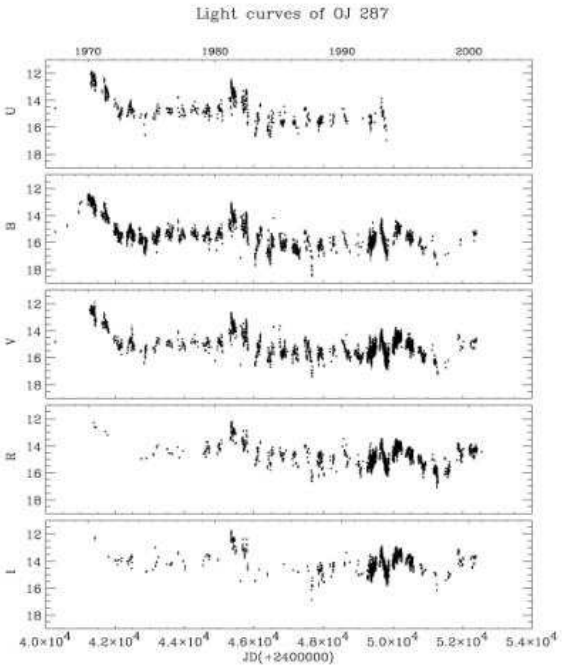

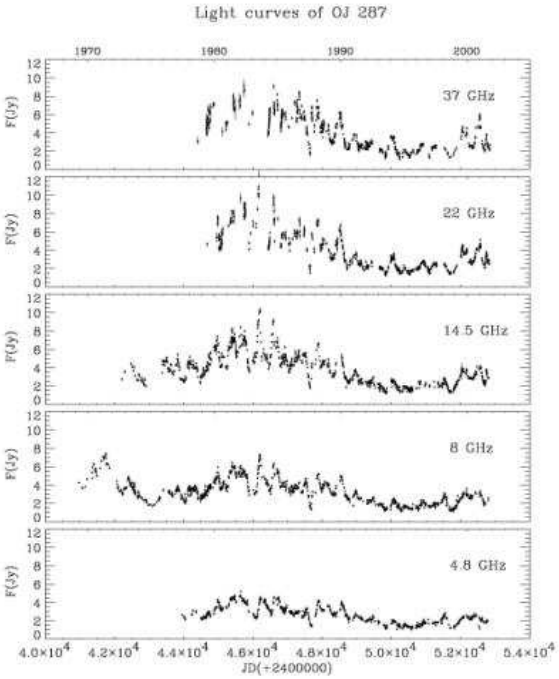
Light curves of OJ 287
1970
1980
1990
2000
37 GHz
22 GHz
14.5 GHz
8 GHz
4.8 GHz
F(Jy)
4.0×10^4
4.2×10^4
4.4×10^4
4.6×10^4
4.8×10^4
5.0×10^4
5.2×10^4
5.4×10^4
JD(+2400000)

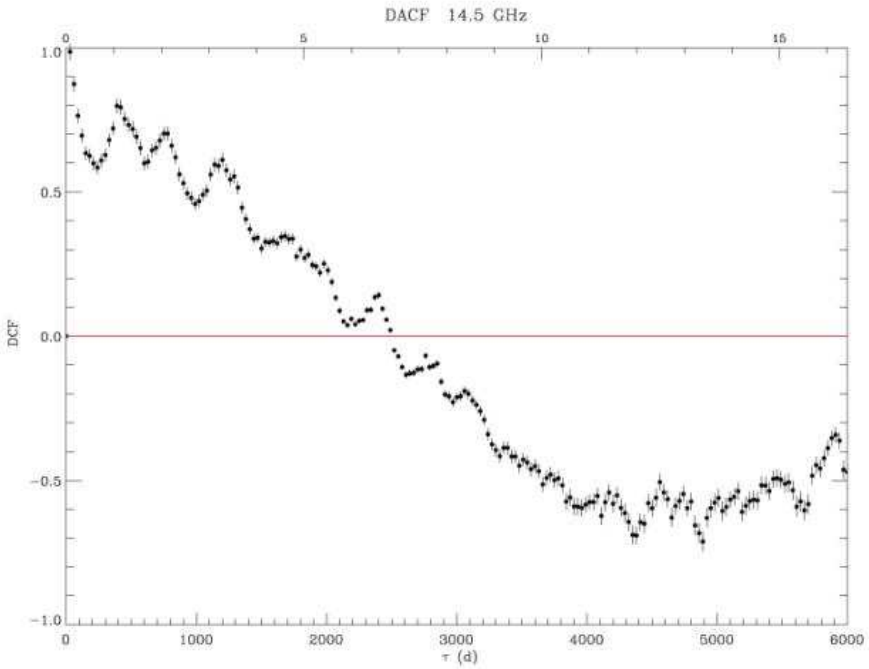
DACF 14.5 GHz
DCF
τ (d)

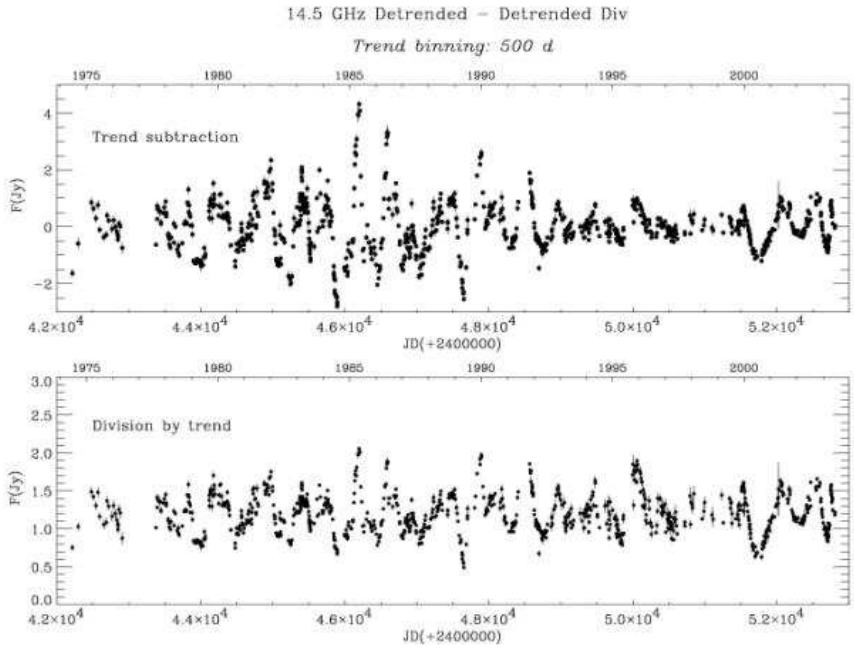
14.5 GHz Detrended – Detrended Div
Trend binning: 500 d
Trend subtraction
Division by trend
F(Jy)
JD(+2400000)

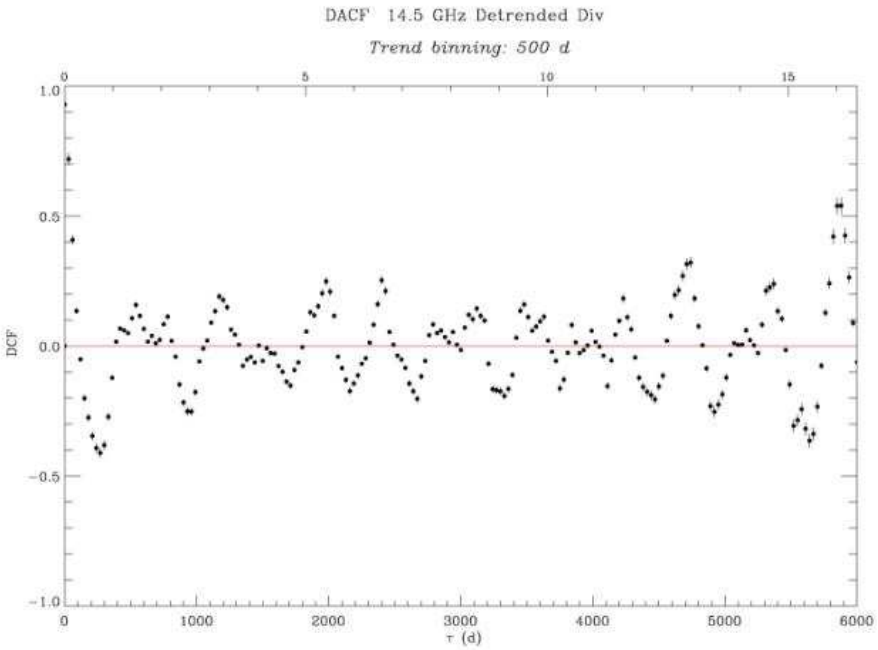
DACF 14.5 GHz Detrended Div
Trend binning: 500 d
DCF
τ (d)

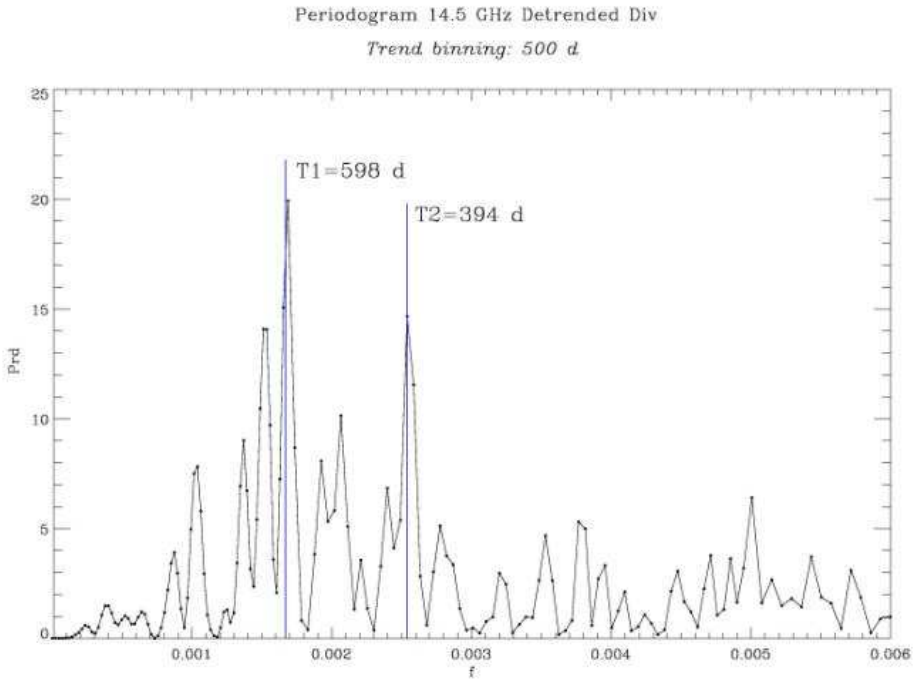
Periodogram 14.5 GHz Detrended Div
Trend binning: 500 d
T1=598 d
T2=394 d
Prd
f
0
5
10
15
20
25
0.001
0.002
0.003
0.004
0.005
0.006

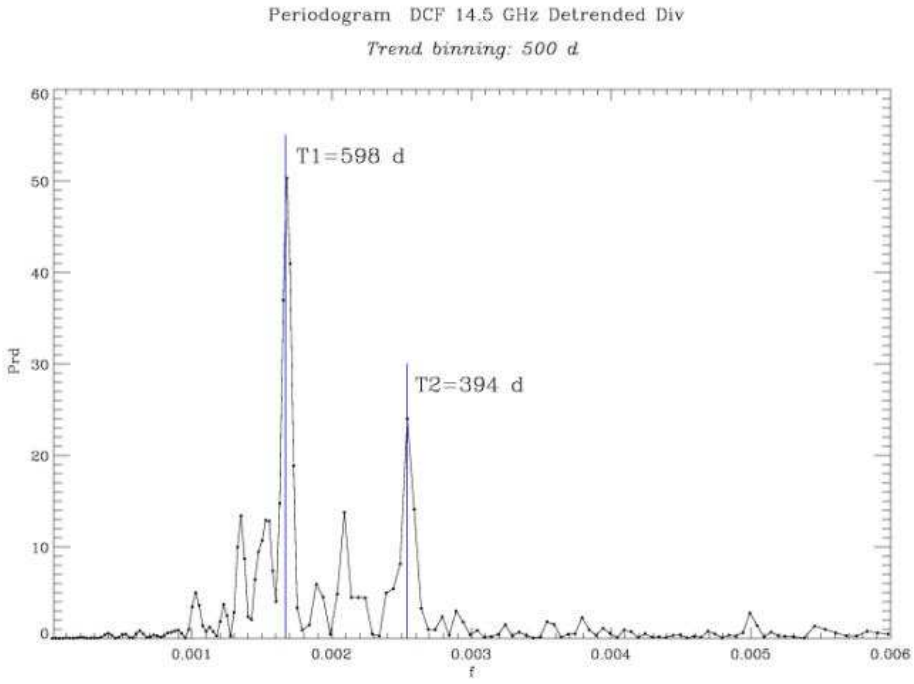
Periodogram DCF 14.5 GHz Detrended Div
Trend binning: 500 d
T1=598 d
T2=394 d
Prd
f
0
10
20
30
40
50
60
0.001
0.002
0.003
0.004
0.005
0.006

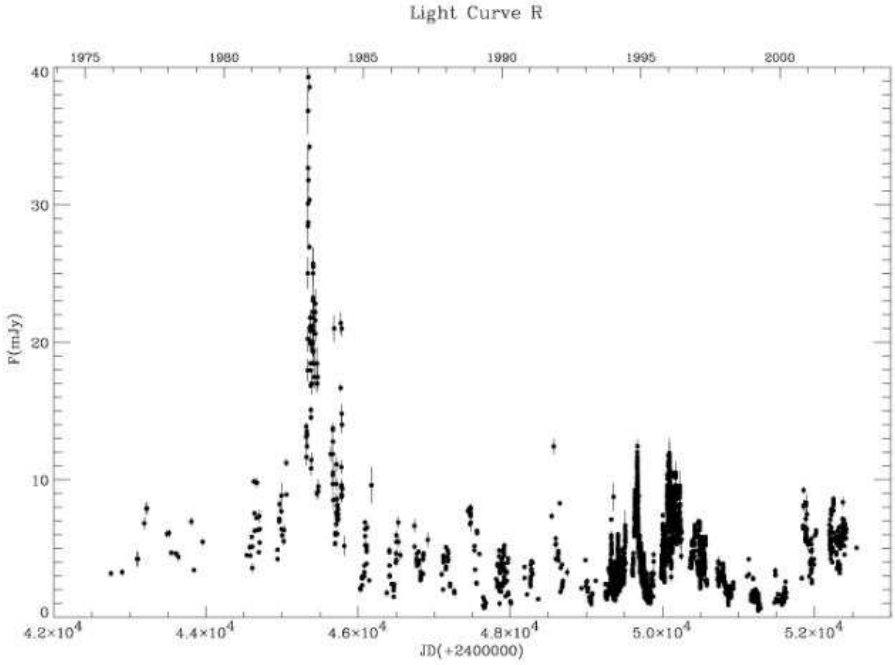
Light Curve R
1975
1980
1985
1990
1995
2000
40
30
20
10
0
F(mJy)
4.2×10^4
4.4×10^4
4.6×10^4
4.8×10^4
5.0×10^4
5.2×10^4
JD(+2400000)

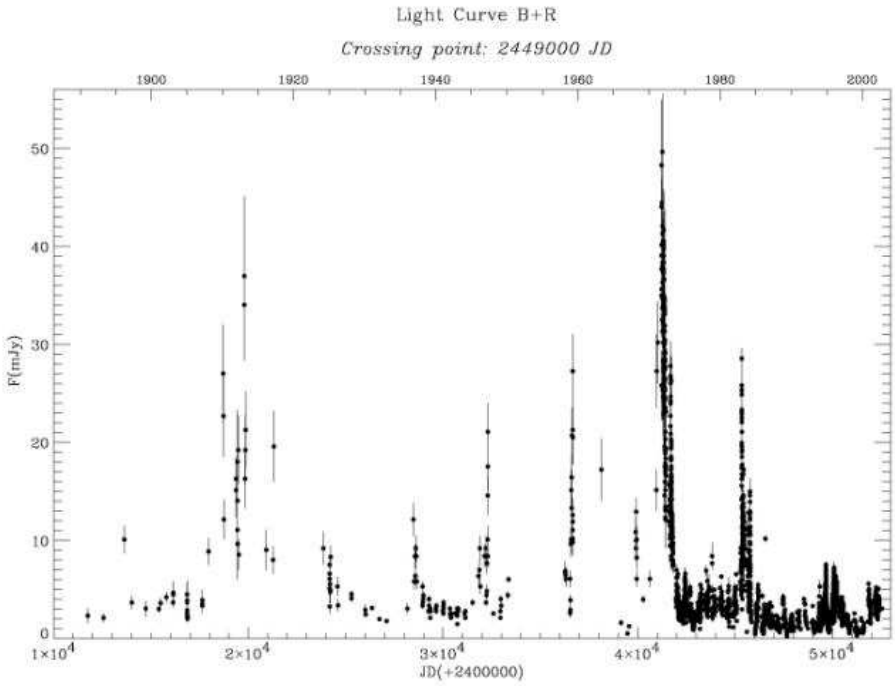
Light Curve B+R
Crossing point: 2449000 JD
1900
1920
1940
1960
1980
2000
50
40
30
20
10
0
F(mJy)
1×10^4
2×10^4
3×10^4
4×10^4
5×10^4
JD(+2400000)

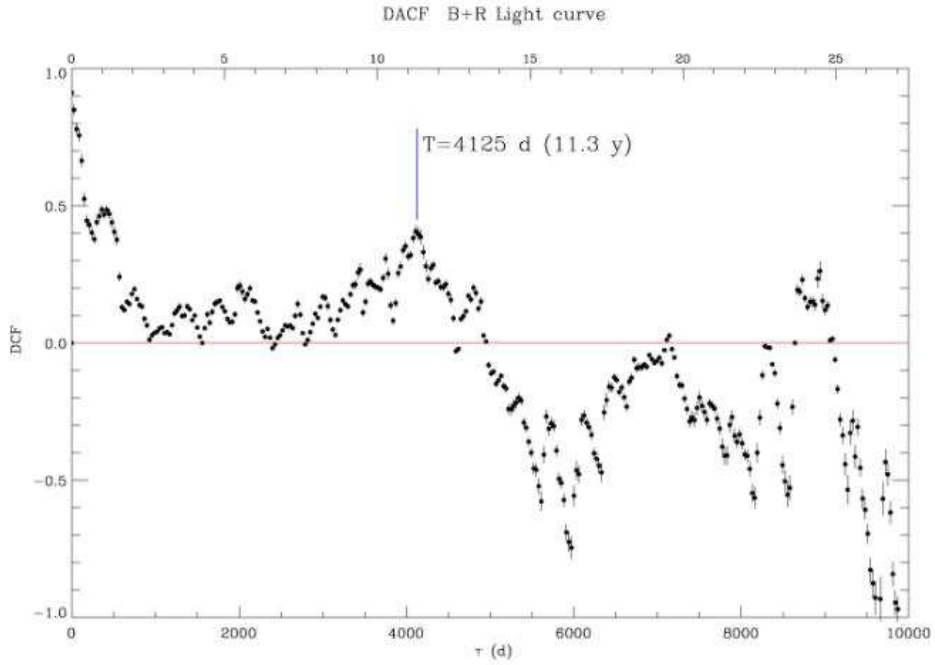
DACF B+R Light curve
T=4125 d (11.3 y)
DCF
τ (d)

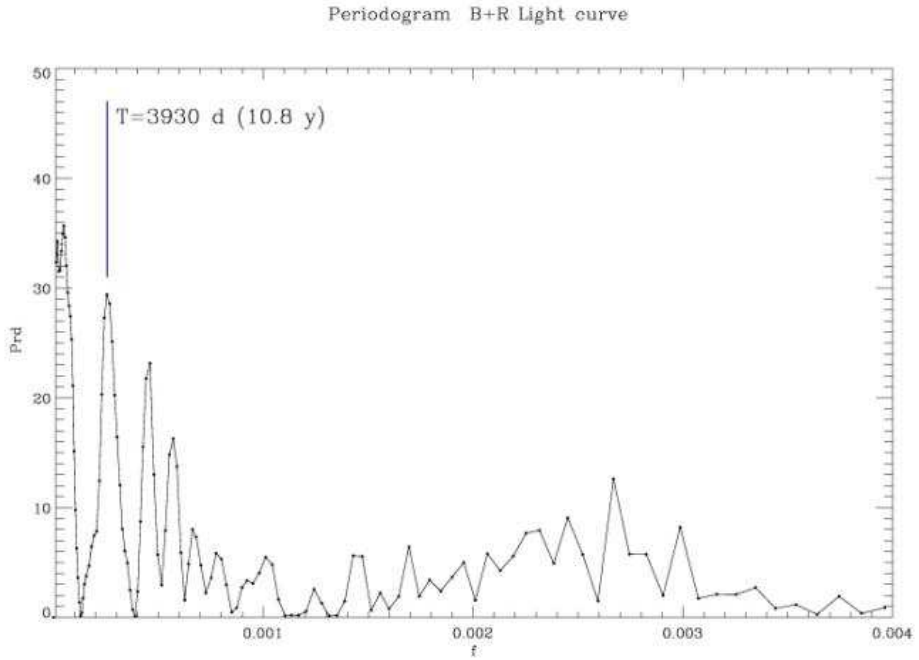
Periodogram B+R Light curve
T=3930 d (10.8 y)
Prd
f

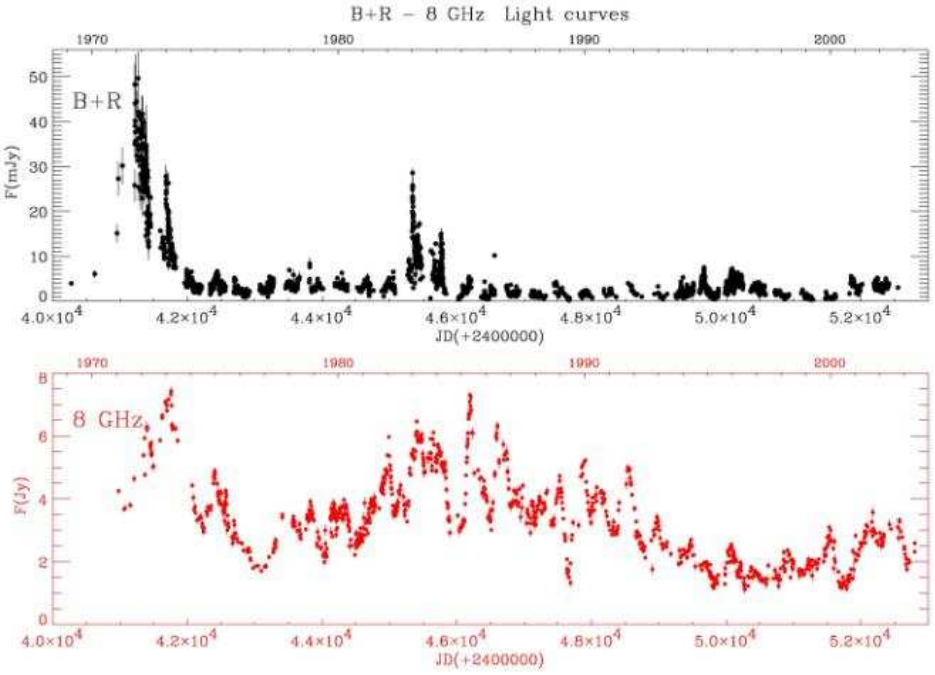
B+R – 8 GHz Light curves
B+R
F(mJy)
8 GHz
F(Jy)
JD(+2400000)

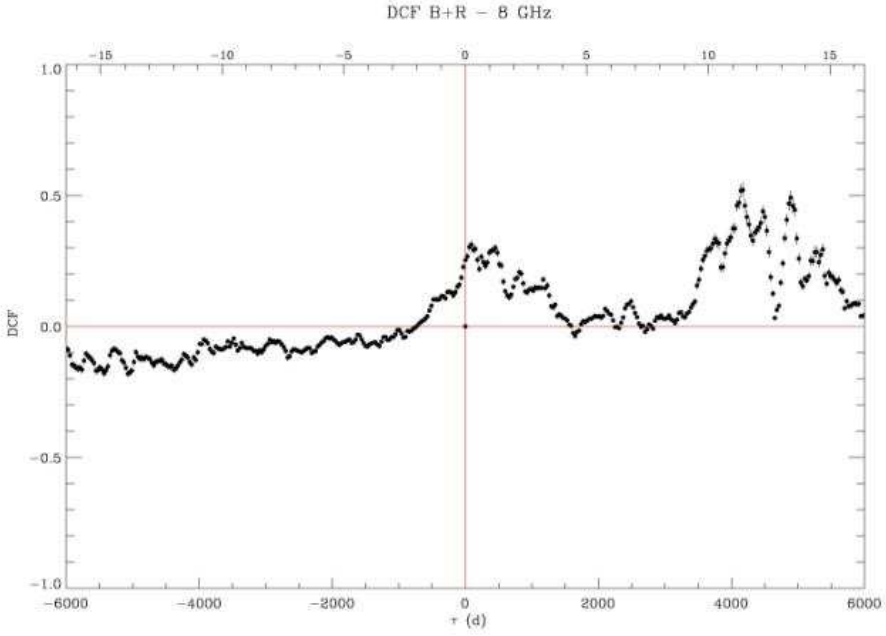
DCF B+R – 8 GHz
DCF
τ (d)

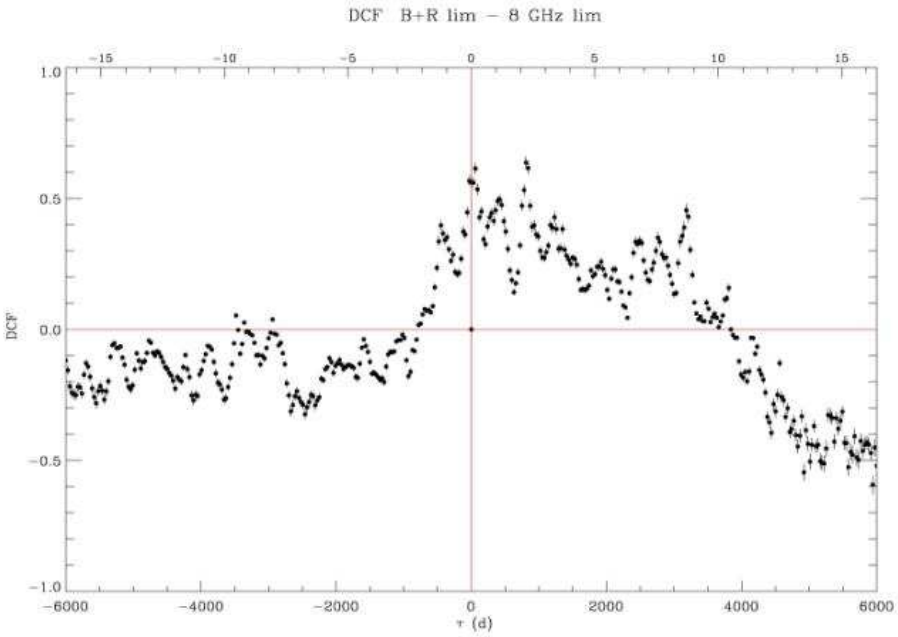

Conclusions:

- - we have collected data for the construction of light curves at all the monitored frequencies;
- - we have found some indications for the presence of a ~600 day periodicity in the radio light curves, adopting a preliminary detrending procedure;
- - we have found a broad period of correlation between optical and radio data, with the maximum peak around 800 days.

Radio spectra of X-ray selected BL Lacs (the good old EMSS) – A. Wolter

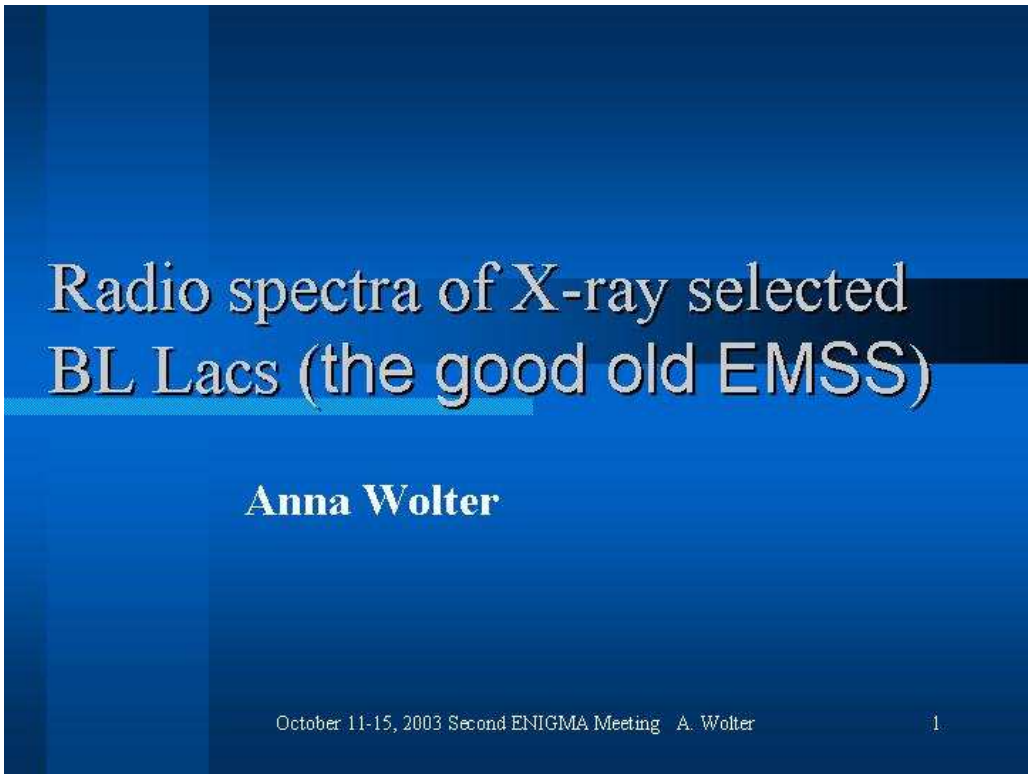

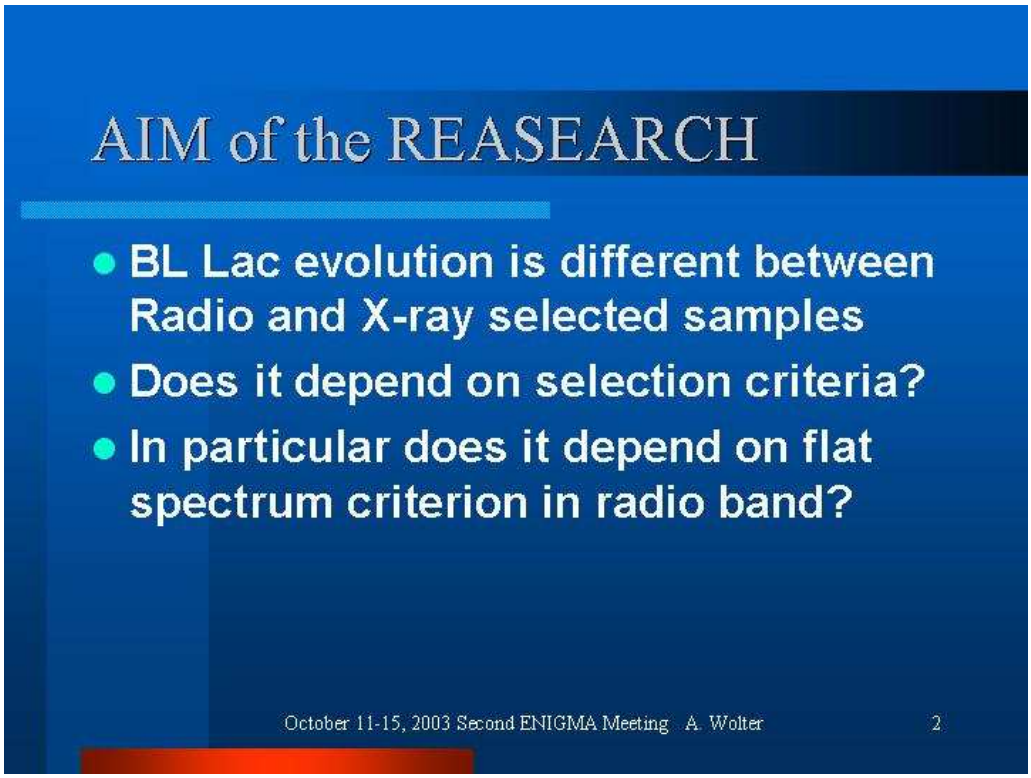
AIM of the REASEARCH
BL Lac evolution is different between Radio and X-ray selected samples
Does it depend on selection criteria?
In particular does it depend on flat spectrum criterion in radio band?
October 11-15, 2003 Second ENIGMA Meeting A. Wolter
2

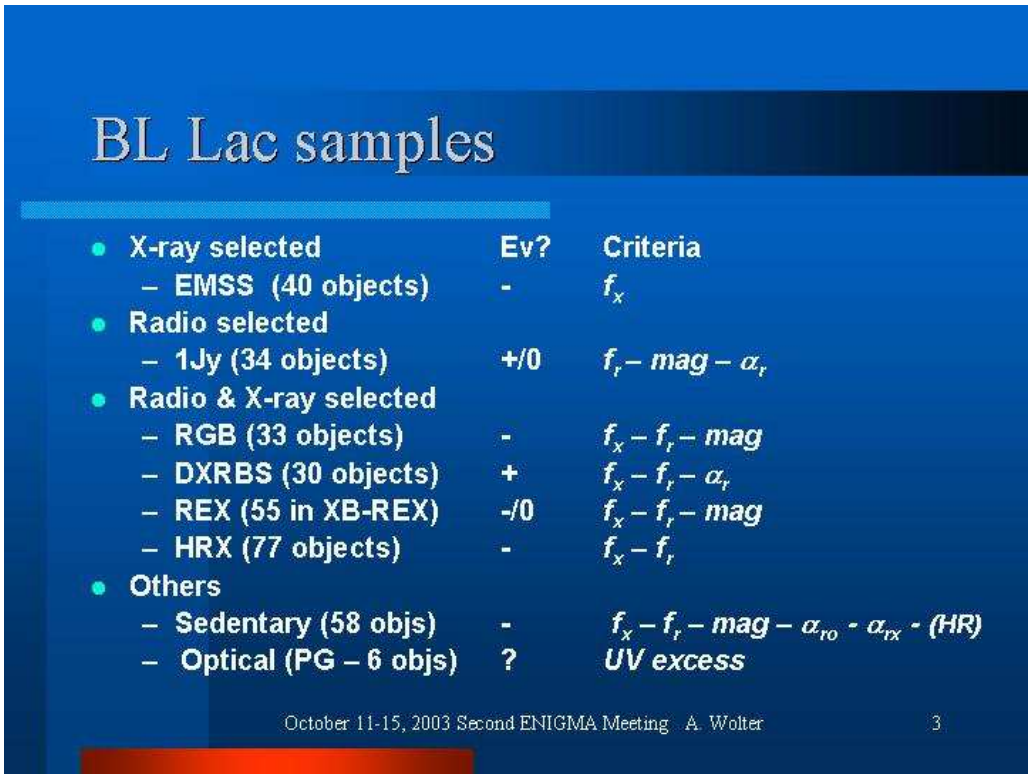
BL Lac samples
X-ray selected
– EMSS (40 objects)
Radio selected
– 1Jy (34 objects)
Radio & X-ray selected
– RGB (33 objects)
– DXRBS (30 objects)
– REX (55 in XB-REX)
– HRX (77 objects)
Others
– Sedentary (58 objs)
– Optical (PG – 6 objs)
Ev?
-
+/0
-
+
-/0
-
-
?
Criteria
f_x
f_r – mag – α_r
$f_x - f_r$ – mag
$f_x - f_r - \alpha_r$
$f_x - f_r$ – mag
$f_x - f_r$
$f_x - f_r$ – mag – α_{ro} - α_{rx} - (HR)
UV excess
October 11-15, 2003 Second ENIGMA Meeting A. Wolter
3

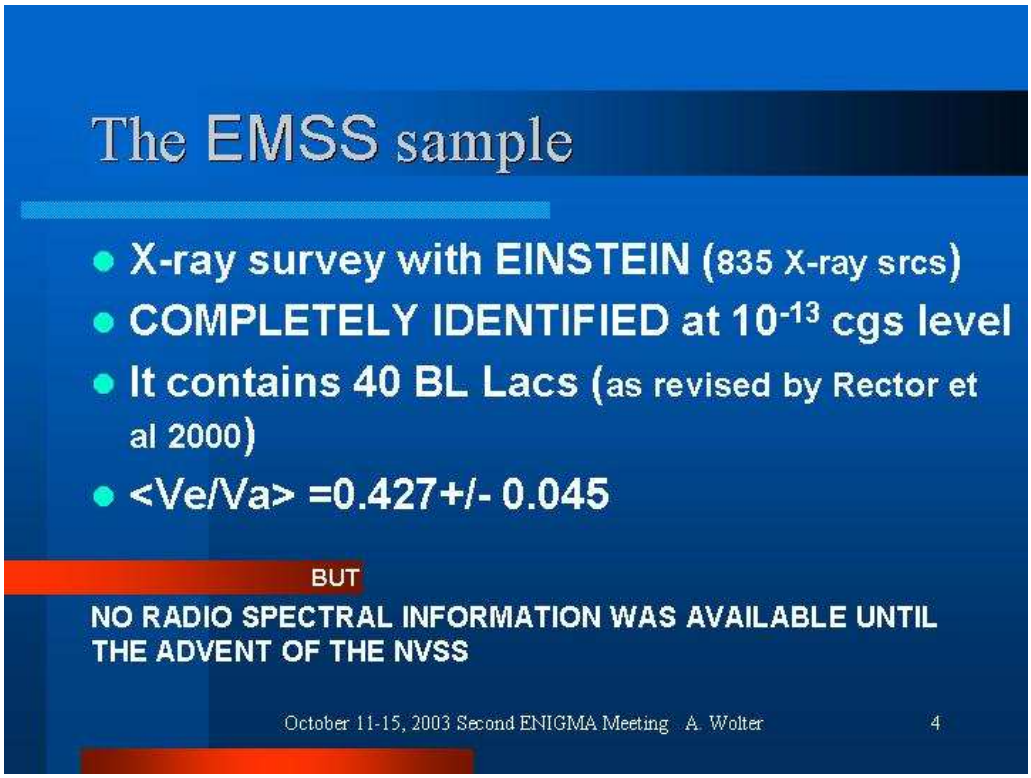
The EMSS sample
X-ray survey with EINSTEIN (835 X-ray srcs)
COMPLETELY IDENTIFIED at 10-13 cgs level
It contains 40 BL Lacs (as revised by Rector et al 2000)
<Ve/Va> =0.427+/- 0.045
BUT
NO RADIO SPECTRAL INFORMATION WAS AVAILABLE UNTIL THE ADVENT OF THE NVSS
October 11-15, 2003 Second ENIGMA Meeting A. Wolter 4

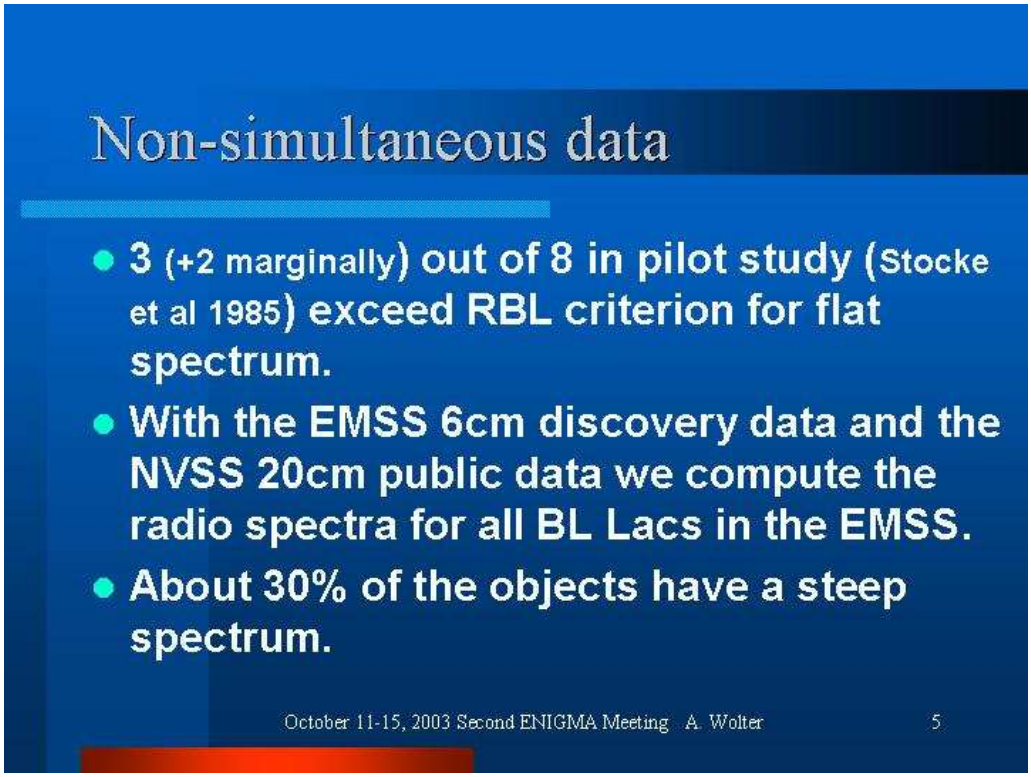
Non-simultaneous data
3 (+2 marginally) out of 8 in pilot study (Stocke et al 1985) exceed RBL criterion for flat spectrum.
With the EMSS 6cm discovery data and the NVSS 20cm public data we compute the radio spectra for all BL Lacs in the EMSS.
About 30% of the objects have a steep spectrum.
October 11-15, 2003 Second ENIGMA Meeting A. Wolter 5

VLA Observations

- We obtaine SIMULTANEOUS [C/D config.] multifrequency radio observation for 26 of the EMSS BL Lacs
- $\delta > -20^{o}$ assures 100% identification
- $F_{6cm} > 1$ mJy assures detection in all VLA bands (L=20cm, C=6cm, X=3.6cm)
- 22 srcs observed in June 2000 + 4 srcs published in Stocke (1985)

October 11-15, 2003 Second ENIGMA Meeting A. Wolter 6

SPECTRA

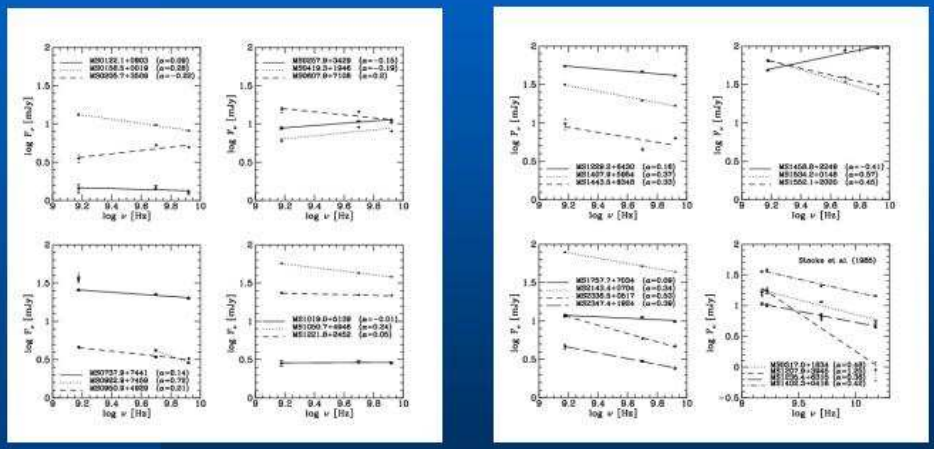

October 11-15, 2003 Second ENIGMA Meeting A. Wolter 7

Steep or not?

Simultaneous

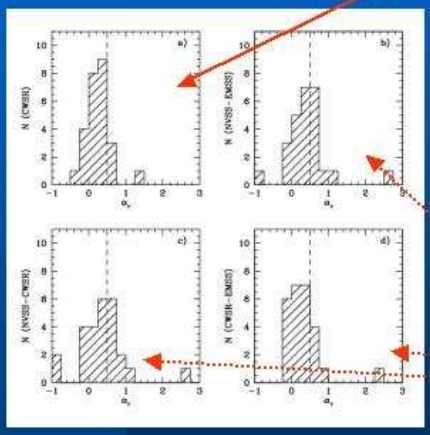

- Distribution of α_r for the 26 srcs.
- 15.4% steep s. spectra
- 23-39% steep non-s. spectra

Non-simultaneous

October 11-15, 2003 Second ENIGMA Meeting A. Wolter 8

Core-to-extended flux

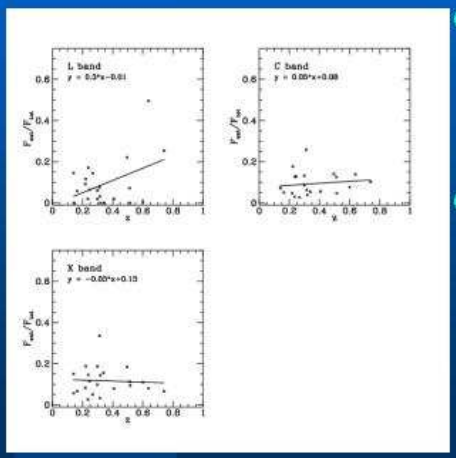

- These plots show the presence of an extended component (visible at 20cm)
- This might explain why the non-sim. data are "steeper" – Observation with less resolved VLA configuration (D) at 20cm.

October 11-15, 2003 Second ENIGMA Meeting A. Wolter 9

Extended component

- there is no redshift dependence of the detection of the extended component. (slope is 0.41+/- 0.39 consistent with 0).

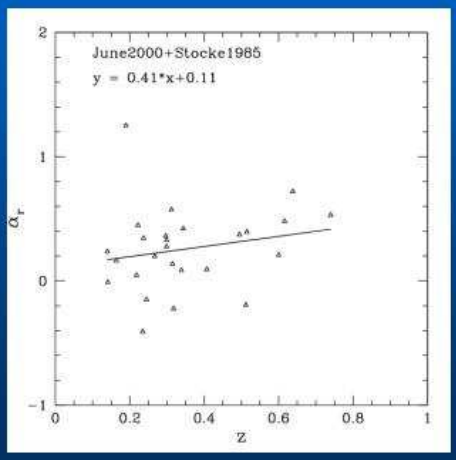

October 11-15, 2003 Second ENIGMA Meeting A. Wolter 10

Differences btw. STEEP and FLAT srcs

- Redshift, Luminosity and Core dominance
- Z,Lx: lower
- R: marginal

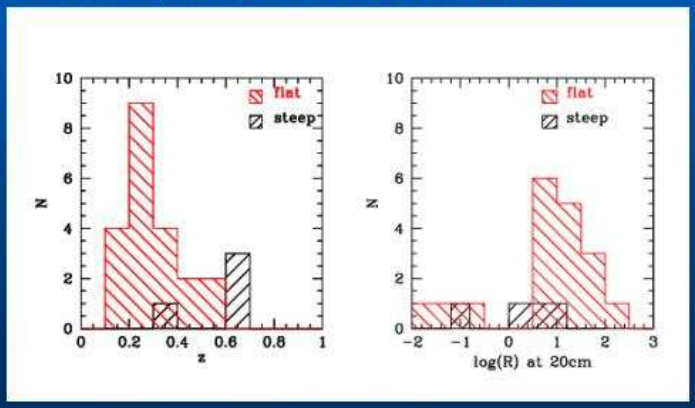

October 11-15, 2003 Second ENIGMA Meeting A. Wolter 11

Steep spectrum EVOLUTION

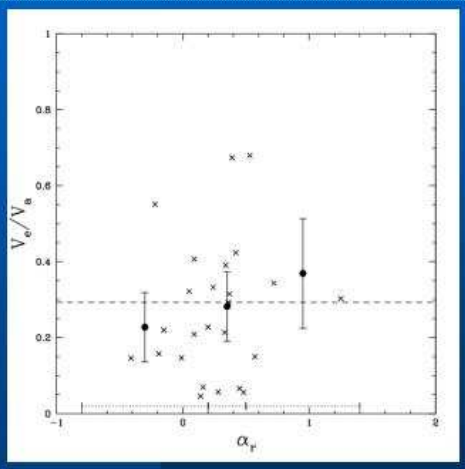

- The spatial distribution DOES not depend on the radio spectrum.
- The STEEP spectra do not carry a VERY NEGATIVE evolution.
- Mildly less negative

October 11-15, 2003 Second ENIGMA Meeting A. Wolter 12

Conclusion

- A large fraction of BL Lacs show a steep spectrum. (15-40% depending on conditions of observation)
- These objects are missed in radio surveys that need an α_r selection to avoid radio galaxies.
- However, the steep srcs have similar properties than flat srcs.

In particular:

- the spectral selection is not responsible for the different evolution properties of RBL and XBL.

October 11-15, 2003 Second ENIGMA Meeting A. Wolter 13

Session IV: Radiation processes at high energies

Chandra observations of QSO jets – F. Tavecchio

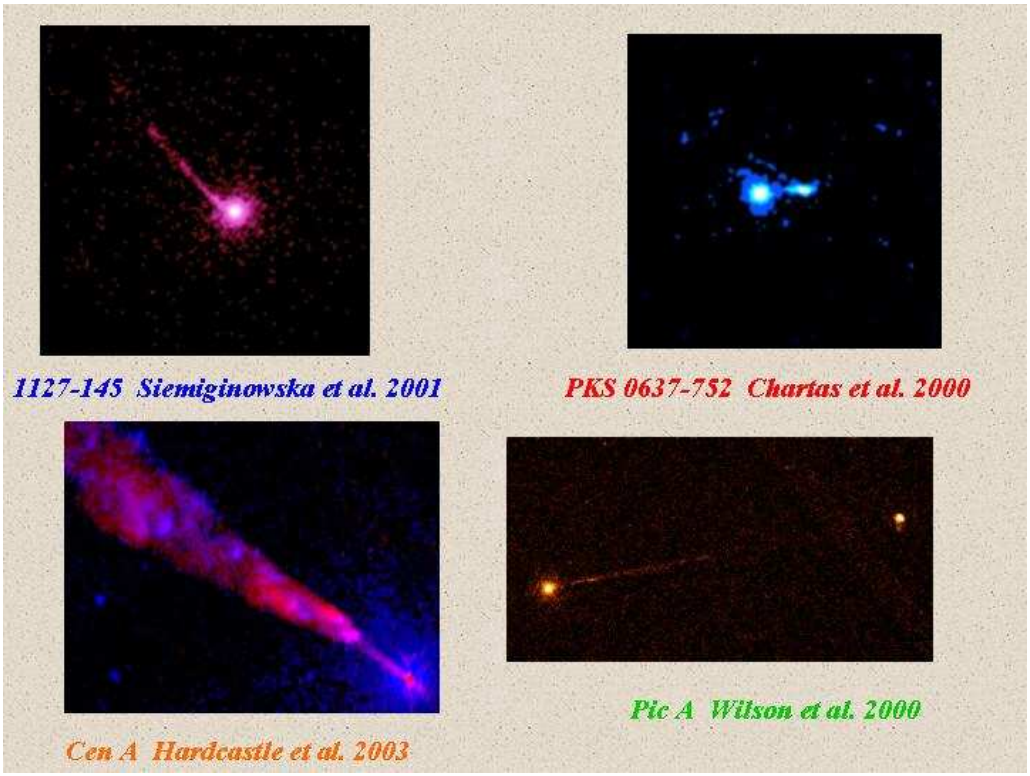

Producing X-rays in large-scale jets

Powerful sources (QSOs)

~~Synchrotron~~ ~~SSC~~ ~~thermal~~ → IC/CMB

Schwartz et al. 2000

Tavecchio et al. 2000
Celotti et al. 2001

Low power sources (radiogalaxies)

Synchrotron e.g Worrall et al. 2001, 2002

SSC e.g. Wilson et al. 2000

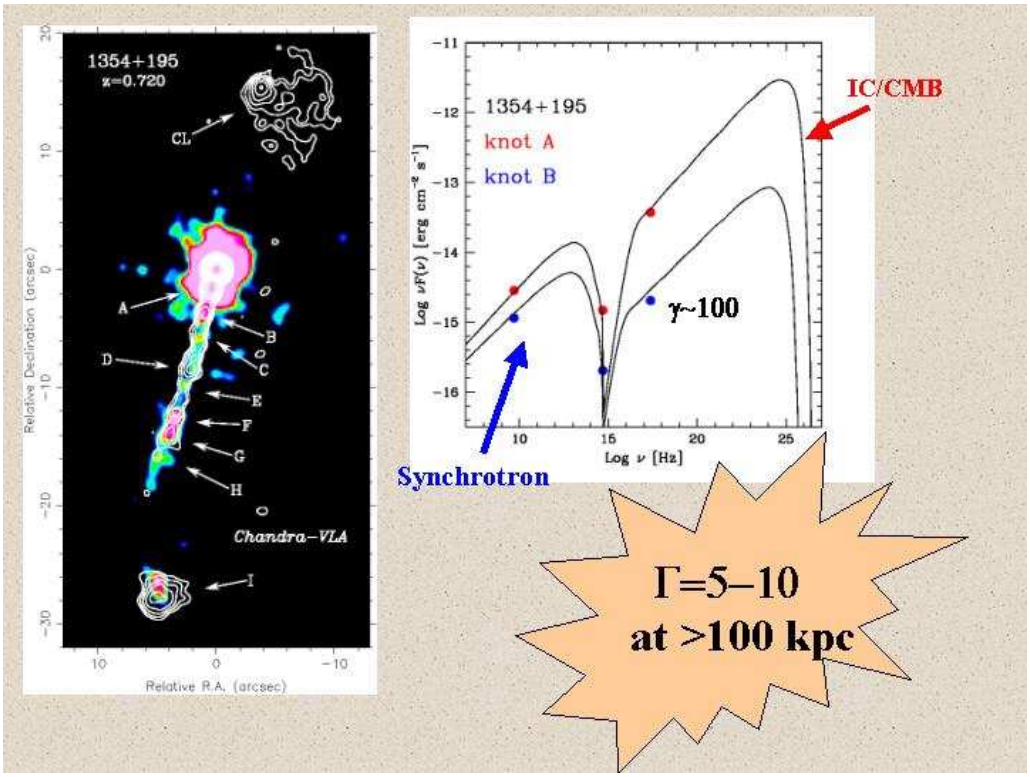
1354+195
z=0.720
CL
A
B
C
D
E
F
G
H
I
Chandra–VLA
Relative Declination (arcsec)
Relative R.A. (arcsec)
1354+195
knot A
knot B
IC/CMB
γ~100
Synchrotron
Log νF(ν) [erg cm⁻² s⁻¹]
Log ν [Hz]
Γ=5–10
at >100 kpc

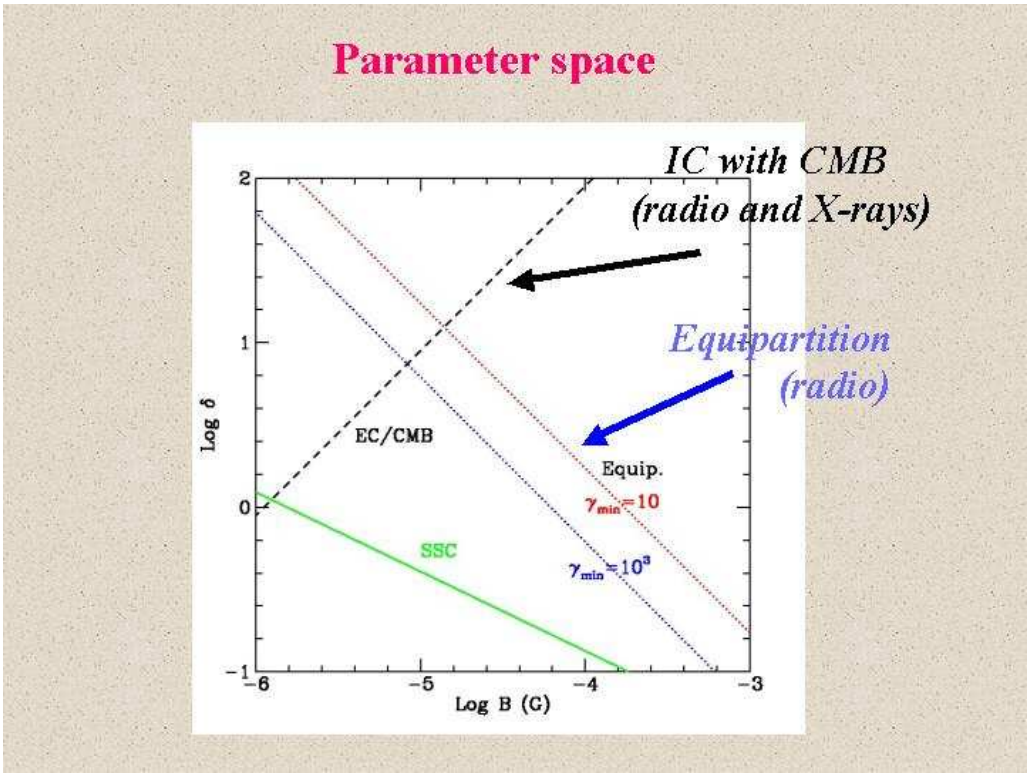
Parameter space
IC with CMB
(radio and X-rays)
Equipartition
(radio)
EC/CMB
Equip.
γmin=10
γmin=10³
SSC
Log δ
Log B (G)

A Chandra-HST survey of jets

17 "radio selected" jets

10 with X-rays (59%)

10 with optical

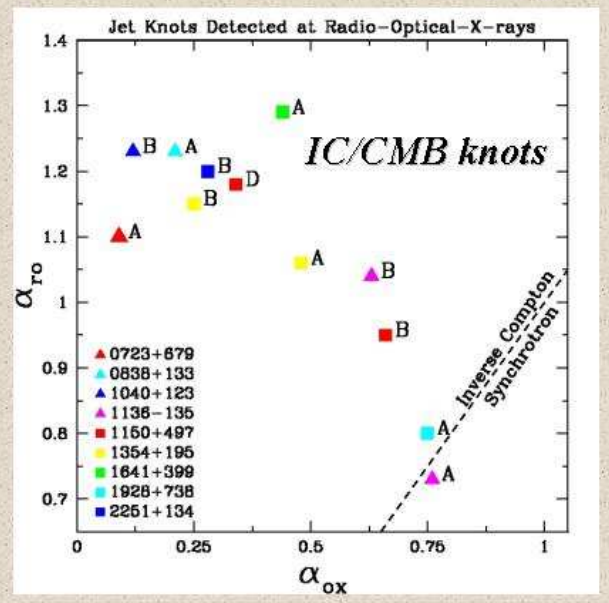

Sambruna et al. 2001
Sambruna et al. 2003

From subpc to kpc-scale

Blazars and Chandra: physical quantities at (very) different scales!

Example: 1510-089 (z=0.361)

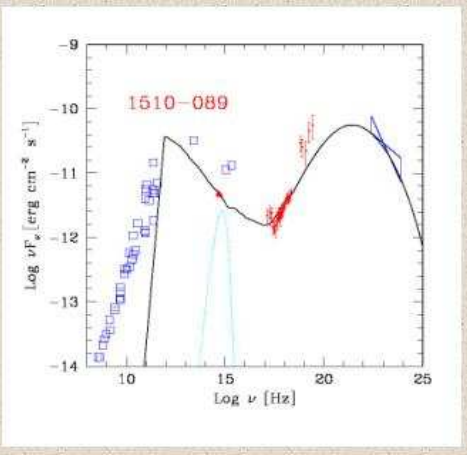

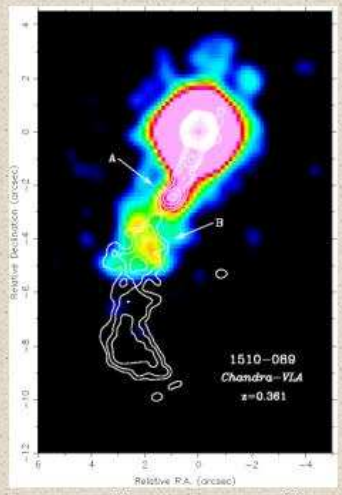

B=2G; R=3x10^{16} cm

B=0.6x10^{-5} G; R=2x10^{22} cm

Deep images

1136-135
1150+497

Synchrotron to Compton transition?

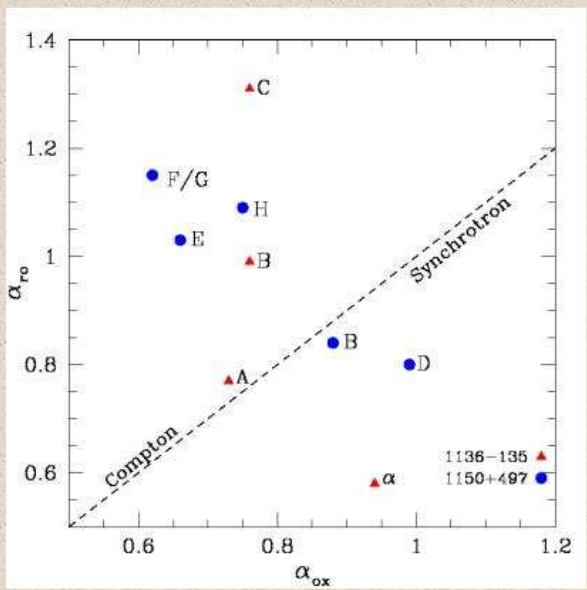

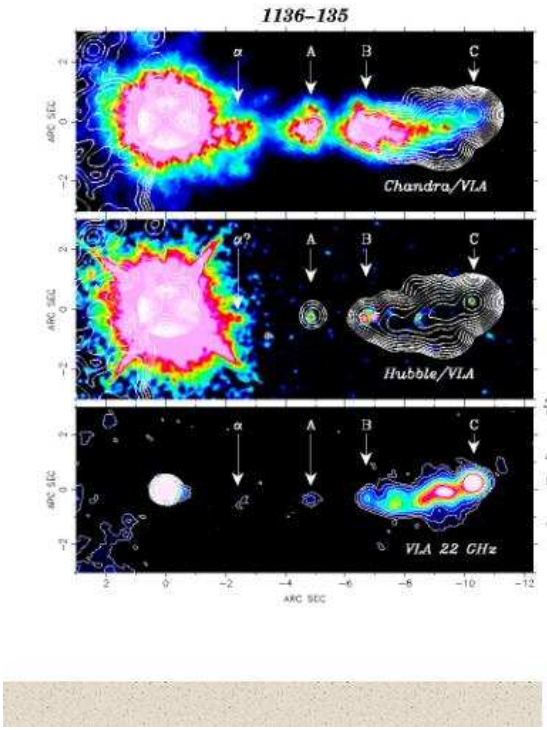
1136–135
α
A
B
C
Chandra/VLA
α?
Hubble/VLA
VLA 22 GHz
ARC SEC

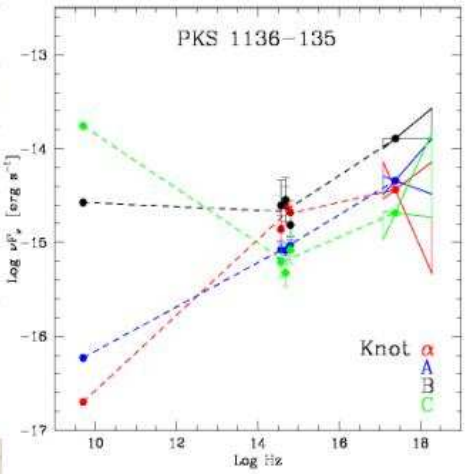
PKS 1136−135
Knot α
A
B
C
Log Hz

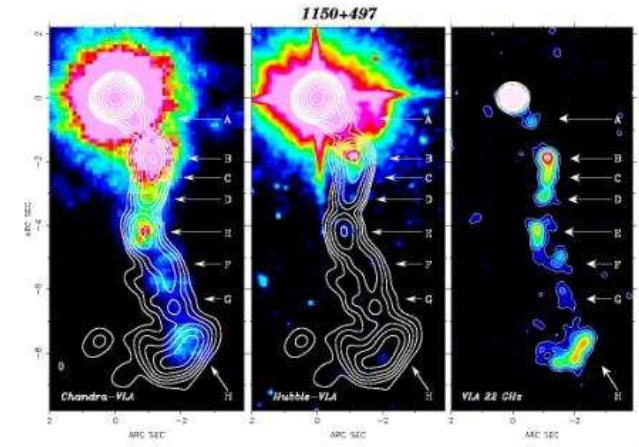
1150+497
A
B
C
D
E
F
G
H
Chandra–VLA
Hubble–VLA
VLA 22 GHz
ARC SEC

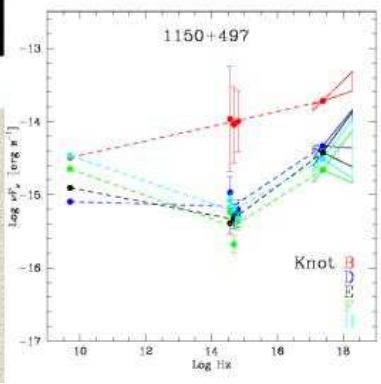
1150+497
Knot B
D
E
F
Log Hz

Clumps in jets?

Problem: the X-ray emitting electrons *cannot cool* inside the knot even including adiabatic losses!

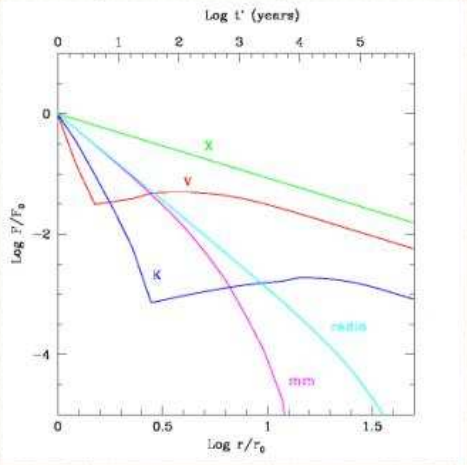

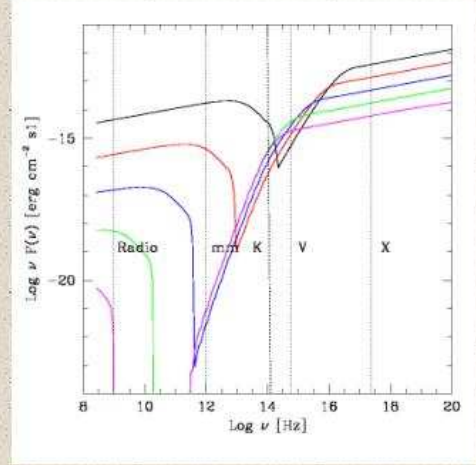

Tavecchio, Ghisellini & Celotti 2003

A possible solution

Several compact regions overpressured with respect to the external plasma (instabilities, clouds, entrained material, reconnection sites)

→ expansion

→ very efficient adiabatic losses

Consequence: expected variability in knots (~month)

New evidences:

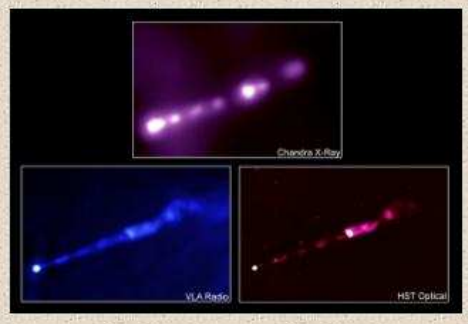

Several knots in M87 are variable!
(Harris et al. 2003)

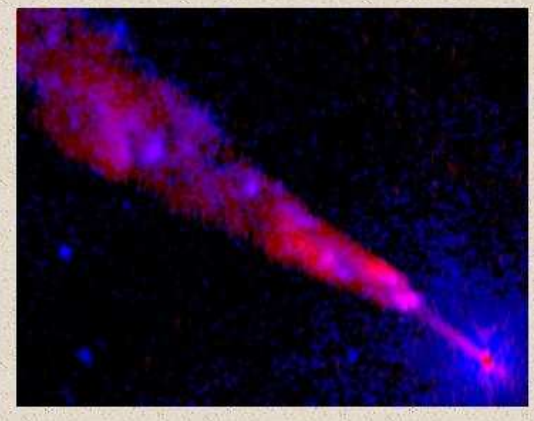

Cen A shows compact X-ray/radio knots
(Hardcastle et al. 2003)

Summary

The IC/CMB model works well for powerful jets in QSO

Deep pointings reveal synchrotron to IC transition along the jet

Comparison of Blazar-outer jet properties

Low E electrons cannot cool: clumps!

PCA observations of Mkn 421 – D. Emmanoulopoulos, S. Wagner, I. Papadakis

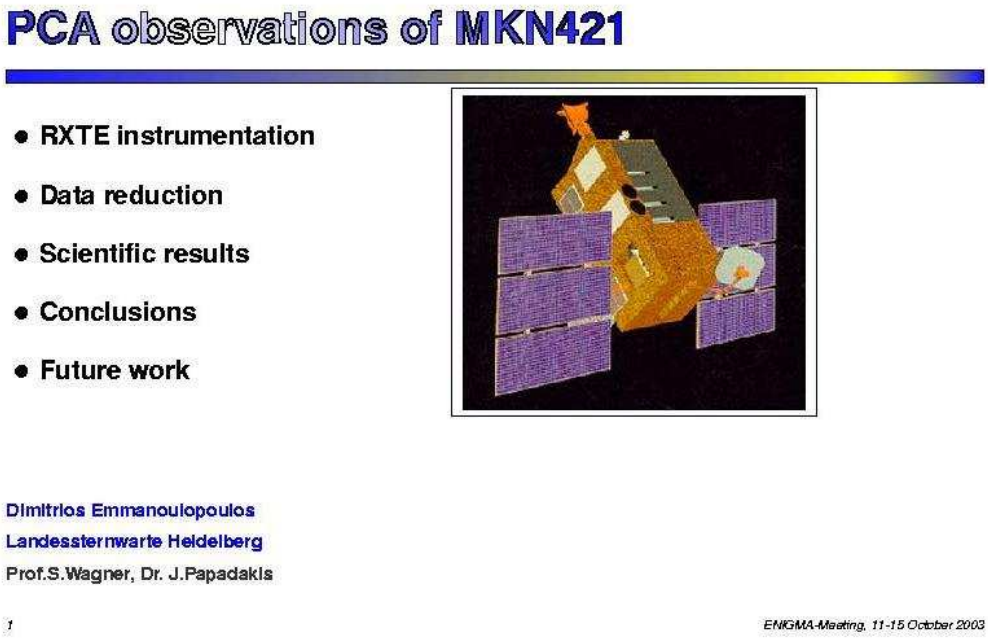

RXTE instrumentation

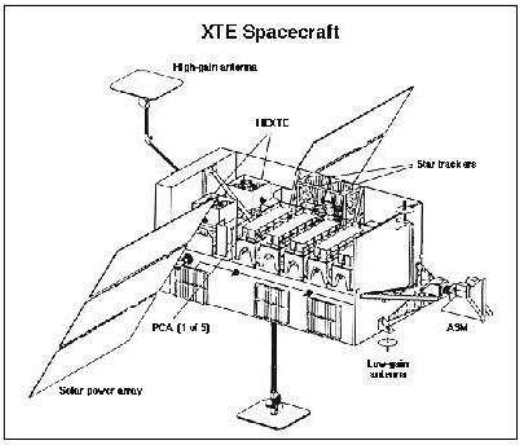

- PCA → 2-60keV
- HEXTE → 15-200keV
- ASM

2 ENIGMA-Meeting, 11-15 October 2003

PCA

INSTRUMENTATION PROPERTIES

Energy range:	2 - 60 keV
Energy resolution:	<18 % at 6 keV
Time resolution:	1 μ sec
Spatial resolution:	collimator with 1 degree FWHM
Detectors:	5 proportional counters
Collecting area:	3100 cm^2 at 6keV
Layers:	1 Propane veto
	3 Xenon, each split into two
	1 Xenon veto layer
Sensitivity:	0.1 mCrab
Background:	90 mCrab

3 ENIGMA-Meeting, 11-15 October 2003

Data reduction

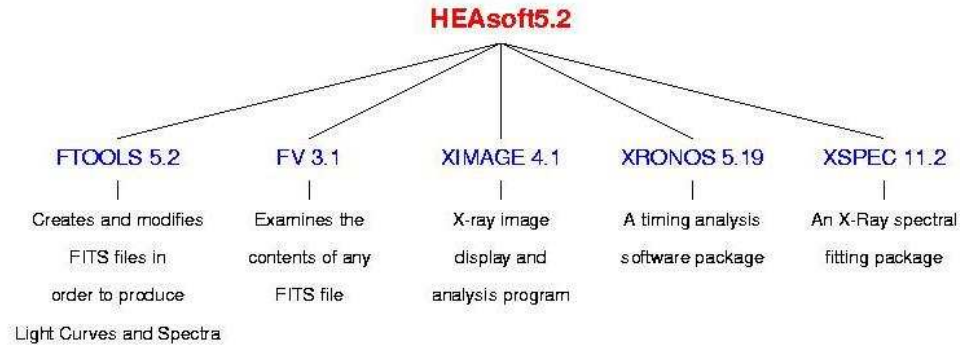

4 ENIGMA-Meeting, 11-15 October 2003

Procedure

- **STANDARD-2 configuration**→ 16 seconds binning. The pulse-height histograms have 129 channels and are accumulated from "good"xenon events (i.e. those which survive background rejection)
- **GTI files**→ ELV$>10^{o}$ (elevation angle) Time Since SAA $>$30min (time since south Atlantic anomaly) Offset $<0.02^{o}$ (pointing position)
- **Background files**→ PCABACKEST

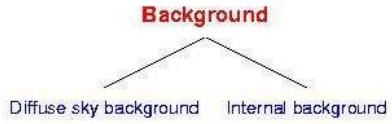

PCABACKEST estimates the variable,internal component of the background but also is capable of adding a constant term to approximate the diffuse sky background.

- **Production of Scientific results** → Light Curves and Spectra.

5 ENIGMA-Meeting, 11-15 October 2003

Scientific results

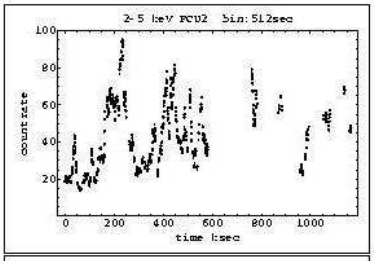

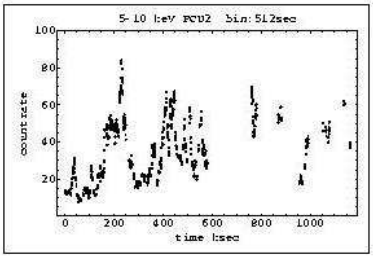

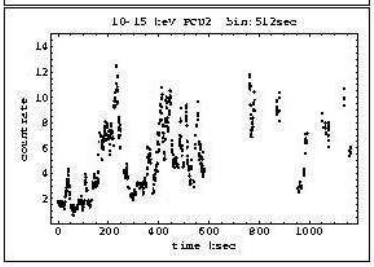

- Two well defined daily flares ~1 day .
- The daily flares show substructures with time scales of 4ksec.
- Additional variability between the large flares.

6 *ENIGMA-Meeting, 11-15 October 2003*

Scientific results

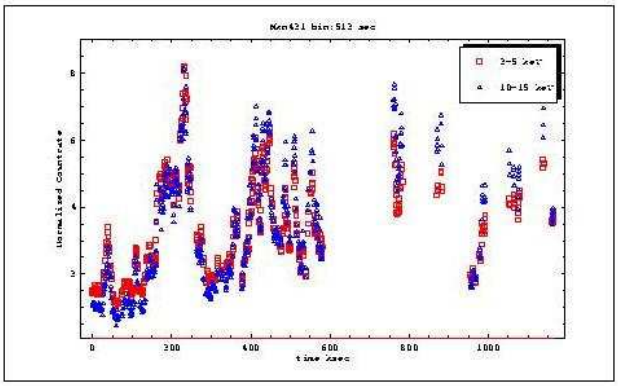

- The amplitude of variations in the 10-15keV band is shifted and especially in the short time flares is larger.
- The flares in the two bands are well correlated. Time lags ~ 1ksec.

7 *ENIGMA-Meeting, 11-15 October 2003*

Structure function analysis

Definition of the first order Structure Function (for a finite sequence of measurements):

$$S_x(\lambda) = \frac{1}{N(\lambda)} \sum_{n=1}^{N} w(i)\, w(i+\lambda) \left[x(t+\lambda\Delta t) - x(t)\right]^2$$

where $N(\lambda) = \sum w(i)\, w(i+\lambda)$ and $w(i)$ is the weighting factor equals to 1 if a measurement exists for the i_{th} interval, 0 otherwise (*Simonetti et al. Ap.J. 296,1985*).

For *self-affine* processes the **SF** obeys the following power-law scaling with λ

$$S(\lambda) = \lambda^{2H} S(1)$$

where **H** (Hurst Exponent) is the characteristic scaling exponent (*Osborne, Provenzale Physica D 35, 357 1989*) .

- **H > 0.5** long-range correlations, an increasing trend in the past implies an increasing trend in the future.
- **H=0.5** the increments are not correlated.
- **H=0** white noise.

8 ENIGMA-Meeting, 11-15 October 2003

Structure function analysis for Mkn421

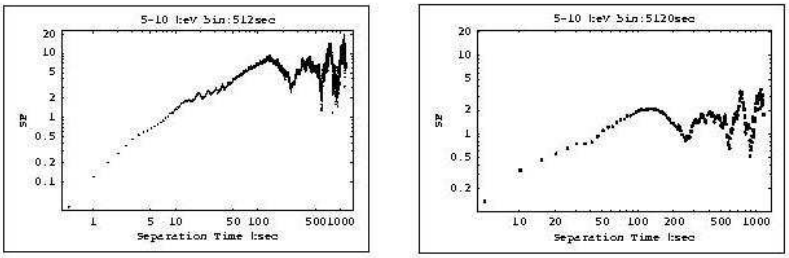

- The observed breaks are at ~ 130ksec = 1.5days (0.5 day Tanihata, et al. 2001 Apj,563,569).
- Around the break the SF (bin:512) is steeper than the SF (bin:5120).

9 ENIGMA-Meeting, 11-15 October 2003

Structure function analysis for Mkn421

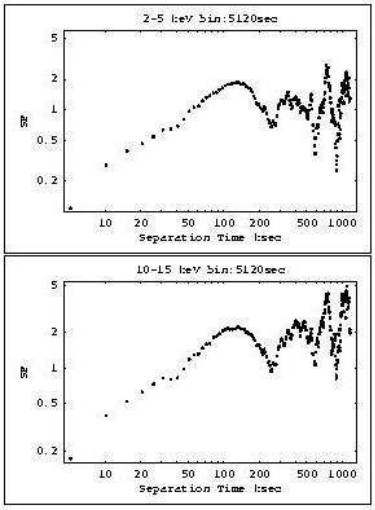

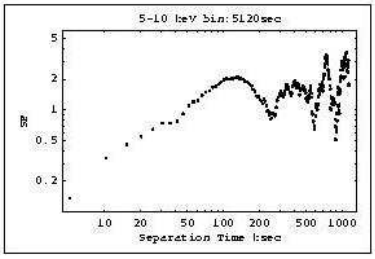

- SF (bin:5120) flattens around 30-45ksec as the energy band is increasing.

10 ENIGMA-Meeting, 11-15 October 2003

Structure function analysis for Mkn421

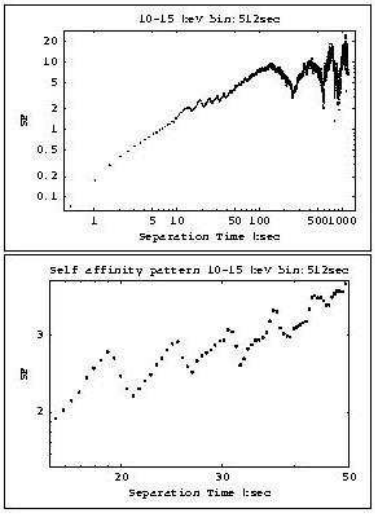

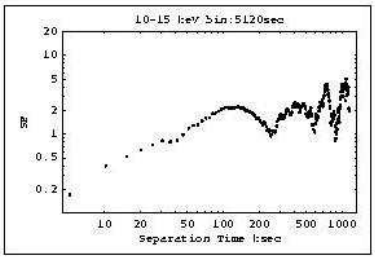

- SF (bin:512) has around 30-45ksec characteristics structures with shapes similar to this of the entire structure function (probable self-affinity).
- The slope between 0-130ksec is 1.2, steeper than the "white noise".

11 ENIGMA-Meeting, 11-15 October 2003

Long Look observations of Mkn421

- Akerlof ⟶2/4/97-3/6/97
- Madejski ⟶ 18/4/98-8/5/98
- Remillard ⟶ 26/2/98-25/7/98
- Montigny ⟶ 24/3/98-13/4/98
- Sambruna ⟶ 5/2/00-8/5/00
- Fossati ⟶ 18/3/01-1/4/01
- Instrument ⟶ PCU2
- Gain correction ⟶ Cassiopeia A
- Count rates rescaling ⟶ epoch3 (15/4/96)-(22/3/99)

12 ENIGMA-Meeting, 11-15 October 2003

Long Look observations of Mkn421

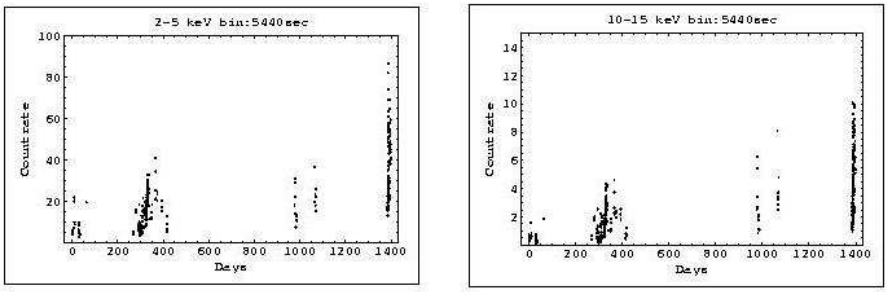

The observations cover the period between (2/4/97-1/4/01), almost 1460 days.

13 ENIGMA-Meeting, 11-15 October 2003

Conclusions

- PCA's high time resolution help us to probe special X-ray characteristics in very short time scales.
- The break in the Structure Function of Mkn421 is not totally in agreement with previous observations.
- The shortest time binning (512sec) has revealed characteristic structures in the time properties of the X-ray flux.
- The long look observations of Mkn421 revealed an increase in the average X-ray flux.

Future work

- Work on the spectra.
- Investigation of the characteristic patterns in the SF from the side of time series analysis.
- Production of the hardness ratio for various energy bands in order to find loops.
- Comparison of our results with that of other Blazars (Mkn501).

Session V: Particle acceleration in MHD outflows

Particle acceleration in MHD outflows

– A. Mastichiadis, on behalf of the Athens team

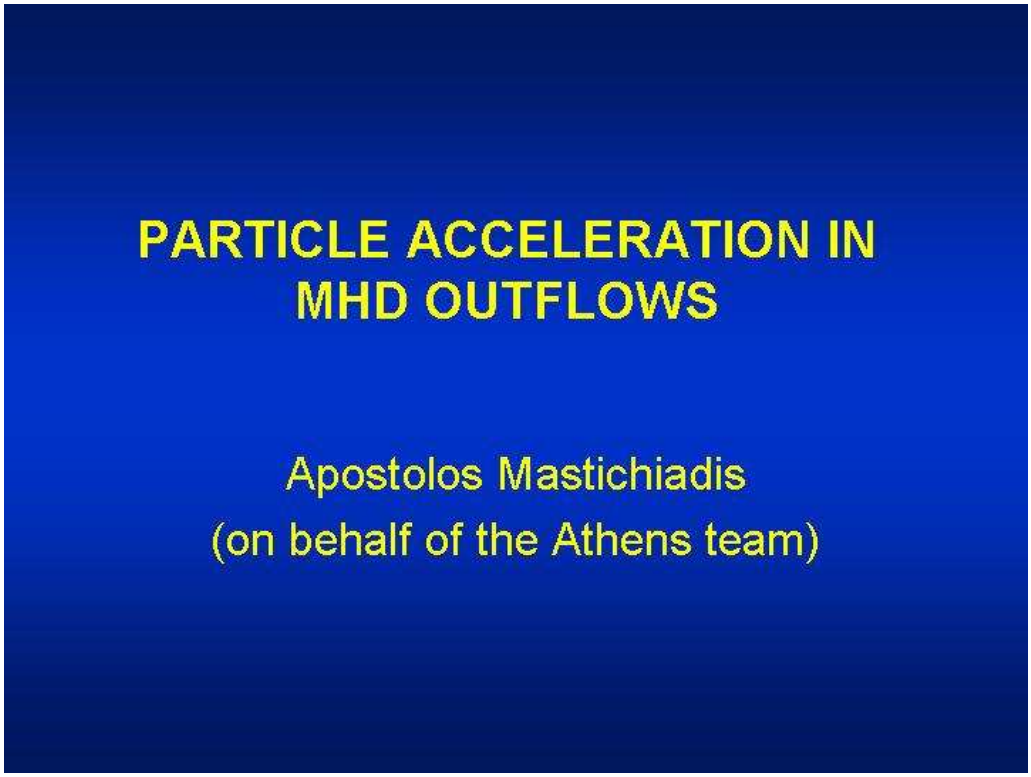

ENIGMA ACTIVITIES: THE PAST

- Paper from Heidelberg/Athens (+ external collaborators)

  ``Modelling the TeV gamma-ray spectra of two low-redshift AGN: Mkn 421 and Mkn 501''

  A. Konopelko, A. Mastichiadis, J. Kirk, O.de Jager, F. Stecker, ApJ in press

THE PRESENT
Signatures of acceleration in the X-ray observations of Mkn 421

- Phase One: Analysis of archival X-ray observations of Mkn 421 (D. Emmanoulopoulos, S. Wagner, J. Papadakis) → soft/hard time lags, hardness ratios, etc
- Phasis Two: Detailed comparisons with the model of Kirk, Rieger & Mastichiadis (1997) which includes particle acceleration and cooling in a two-zone picture (Athens/HD/?)
- Phasis Three: Inclusion of SSC emission and losses

THE NEAR FUTURE
Particle acceleration at shocks formed in relativistic outflows

- Shock formation in a two-component outflow (Bogovalov & Tsinganos 2003)
  → flow speeds, B-fields, angles determined
  → apply diffusive acceleration theory at oblique shocks with one free parameter, the acceleration timescale (Athens/HD/?)

→→A two-component model for jets from source+disk

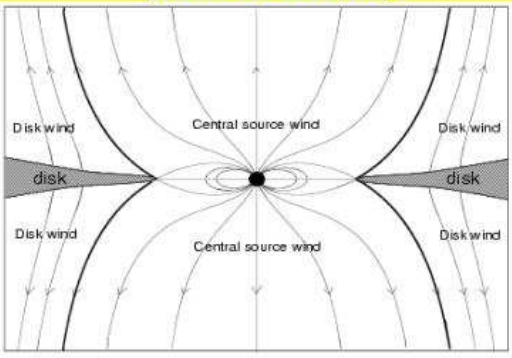

Recent numerical simulations and analytical models of magnetically collimated plasma outflows from a uniformly rotating central gravitating object and/or a Keplerian accretion disk have shown that relatively low mass and magnetic fluxes reside in the produced jet. Observations however indicate that in some cases, as in jets of YSO's, the collimated outflow carries higher fluxes than these simulations predict. A solution to this problem is proposed by the above model where jets with high mass flux originate in a central source which produces a noncollimated outflow provided that this source is surrounded by a rapidly rotating accretion disk. The relatively faster rotating disk produces a collimated wind which then forces all the enclosed outflow from the central source to be collimated too. This conclusion is confirmed by self-consistent numerical solutions of the full set of the MHD equations.

Far Zone :
Poloidal magnetic lines of outflow :
(at intervals of equal magnetic flux)
Before rotation starts – After rotation started
Note compression of inner flow and formation of a shock.

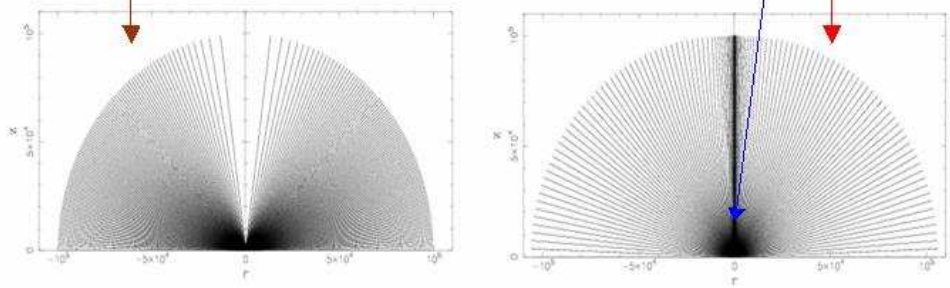

Confinement of stellar wind by a disk-wind

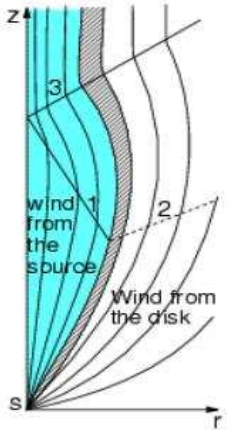

Collimation of the inner flow with the formation of a shock.

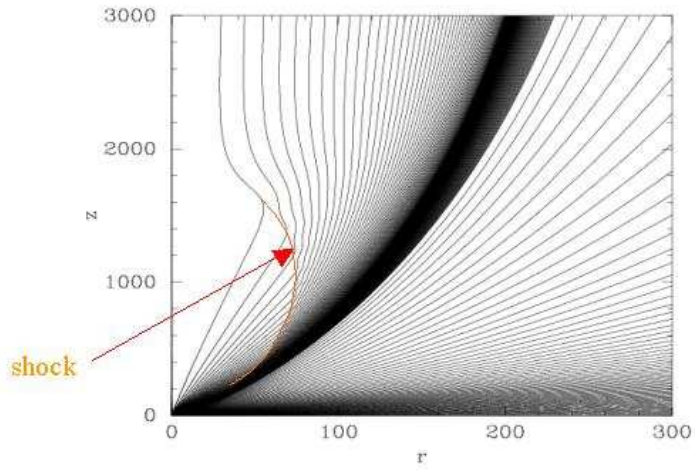

SHAPING UP
ICS in Blazars: External photon vs SSC

- Detailed model of photon densities above accretion disks + relativistic electrons in jets
  → gamma-ray emission from inverse Compton scattering
  → comparison with the gamma-ray spectra produced from SSC models
  → application to blazar observations
  (Athens/HD/?)
  Disk modelling: E. Rokaki

POSSIBILITIES

1. **Magnetic driving of relativistic outflows in AGN**

   Modelling of parsec-scale acceleration to high bulk Lorentz factors indicated in relativistic jet sources (e.g. NGC 6251, 3C 345) by magnetic driving (Vlahakis & Koenigl 2003) → spectra, polarisation,...

2. **IC Catastrophe**

   Self-consistent treatment of multiple orders of ICS in relation to the brightness temperature problem

T.o.O.
Modelling of the MW spectra of TeV Blazars

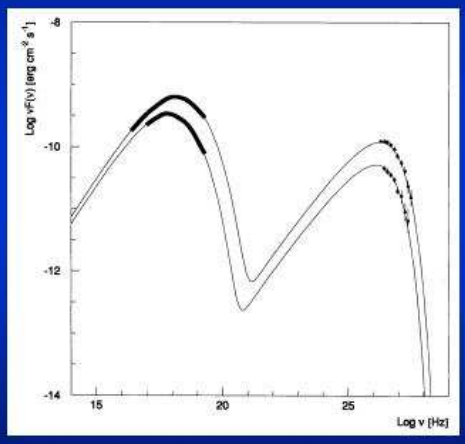

- Correction of TeV spectra due to attenuation in the Cosmic IR Background
  → application of SSC models to deabsorbed spectra
- It has already been done for the near-by objects (Mkn 421, Mkn 501)
- Higher z sources
  1416+418 (z=0.129)
  PKS 2155-304 (z=0.117)

Self consistent synchrotron self Compton emission – A. Tramacere, G. Ghisellini, A. Mastichiadis, F. Tavecchio, G. Tosti

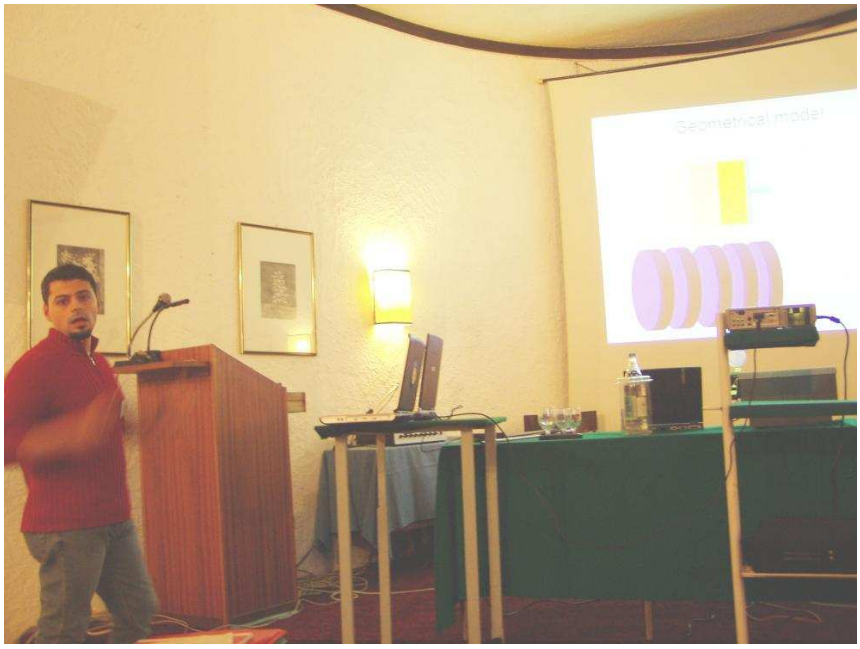

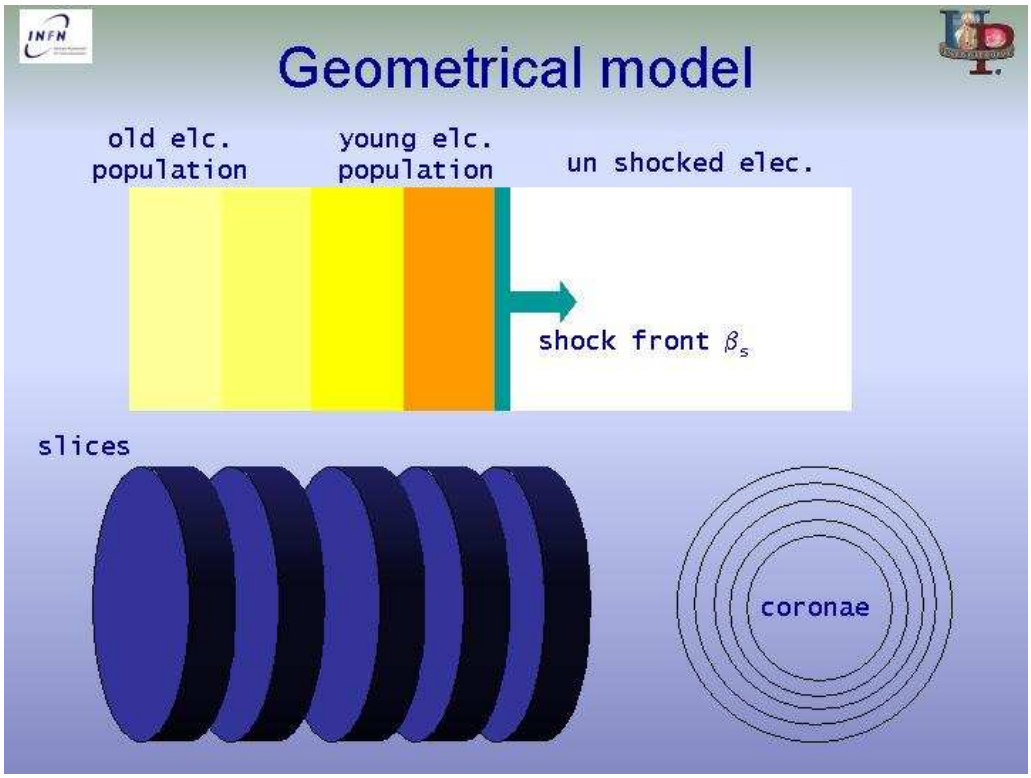
Geometrical model
old elc. population
young elc. population
un shocked elec.
shock front β_s
slices
coronae

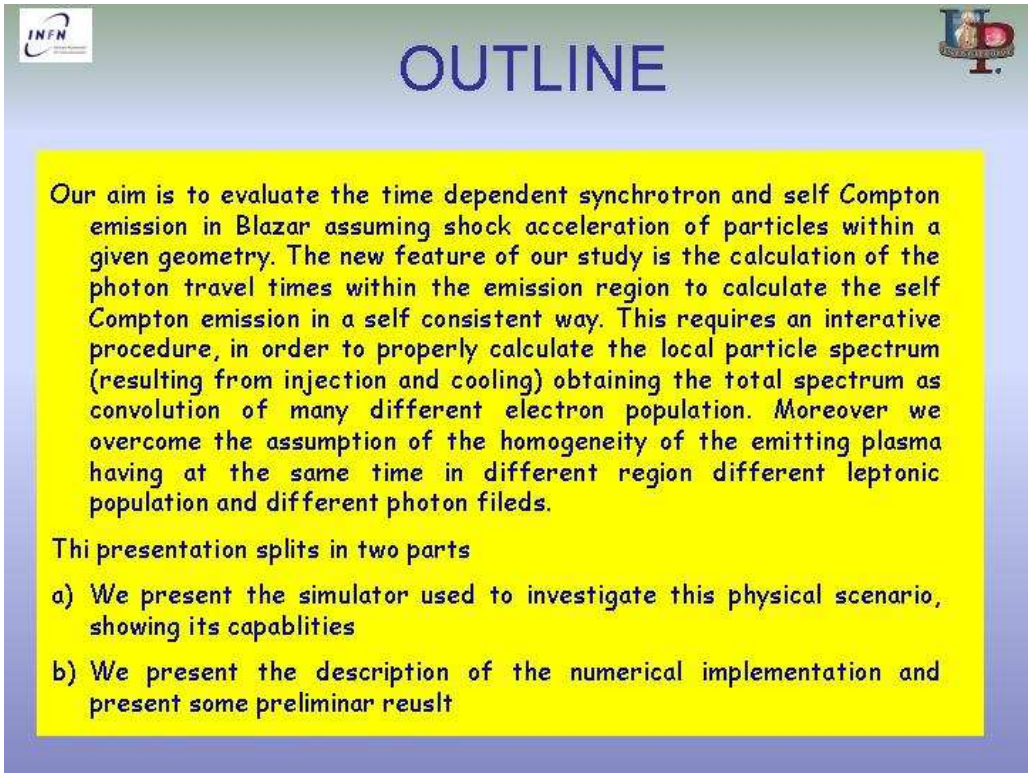
OUTLINE
Our aim is to evaluate the time dependent synchrotron and self Compton emission in Blazar assuming shock acceleration of particles within a given geometry. The new feature of our study is the calculation of the photon travel times within the emission region to calculate the self Compton emission in a self consistent way. This requires an interative procedure, in order to properly calculate the local particle spectrum (resulting from injection and cooling) obtaining the total spectrum as convolution of many different electron population. Moreover we overcome the assumption of the homogeneity of the emitting plasma having at the same time in different region different leptonic population and different photon fileds.
Thi presentation splits in two parts
a) We present the simulator used to investigate this physical scenario, showing its capablities
b) We present the description of the numerical implementation and present some preliminar reuslt

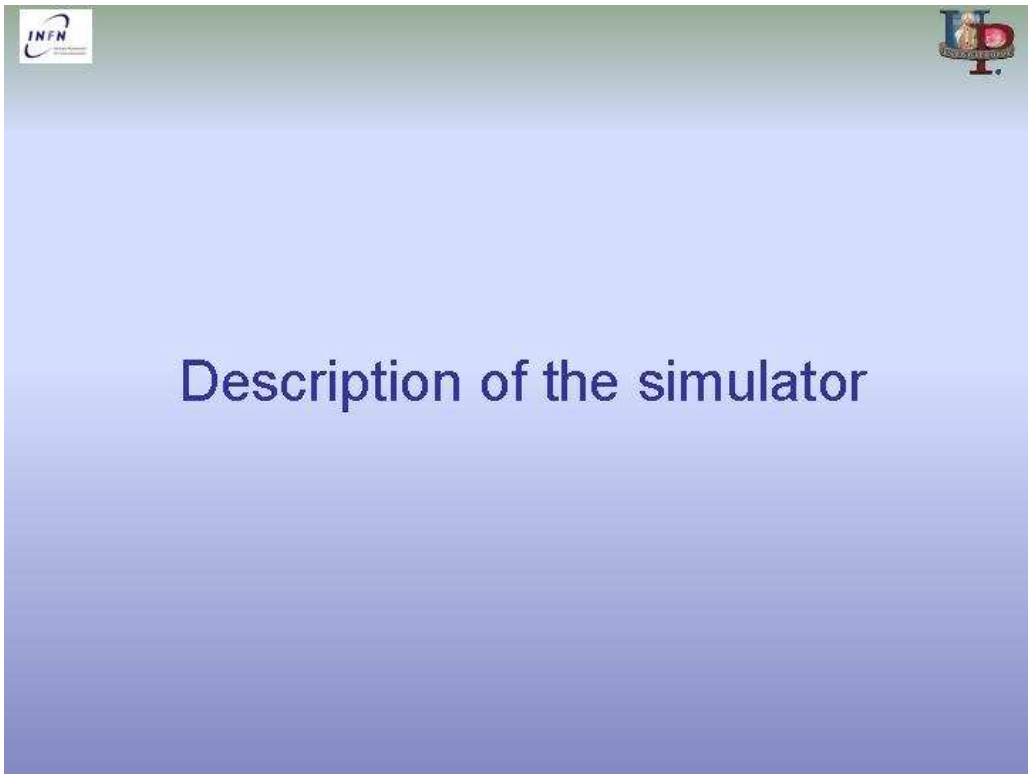
Description of the simulator

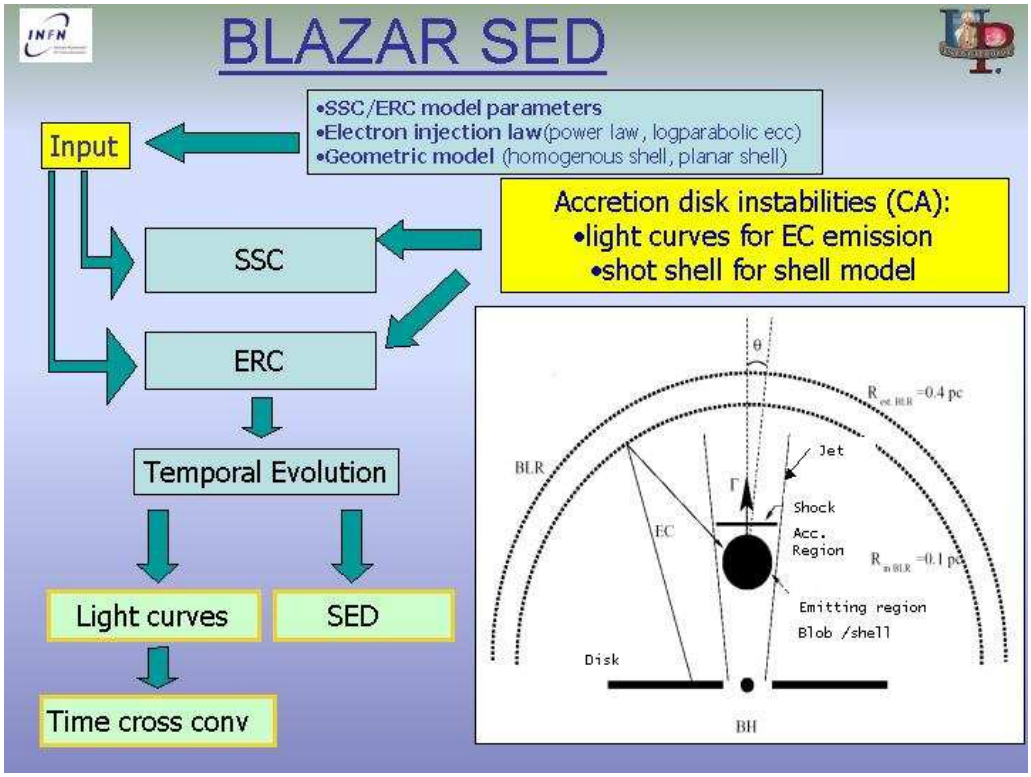
BLAZAR SED
•SSC/ERC model parameters
•Electron injection law(power law, logparabolic ecc)
•Geometric model (homogenous shell, planar shell)
Input
SSC
ERC
Temporal Evolution
Light curves
SED
Time cross conv
Accretion disk instabilities (CA):
•light curves for EC emission
•shot shell for shell model
θ
R =0.4 pc
BLR
Jet
Γ
Shock
EC
Acc.
Region
R =0.1 pc
Emitting region
Blob /shell
Disk
BH

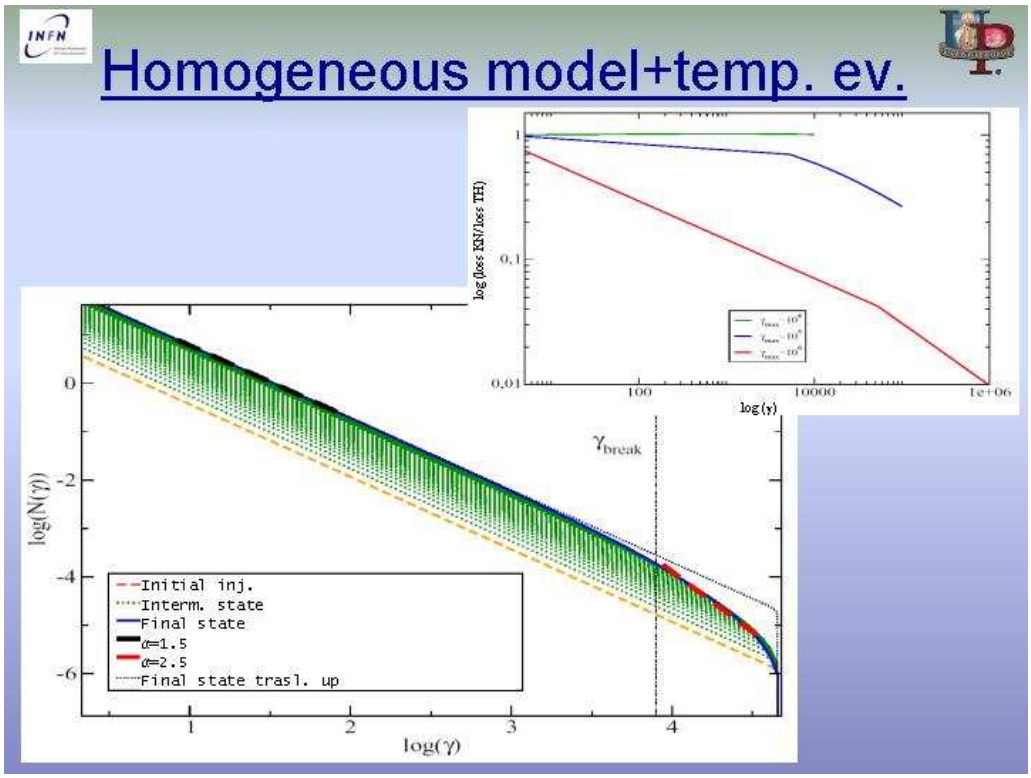
Homogeneous model+temp. ev.
log(loss KN/loss TH)
log(γ)
γbreak
log(N(γ))
log(γ)
Initial inj.
Interm. state
Final state
α=1.5
α=2.5
Final state trasl. up

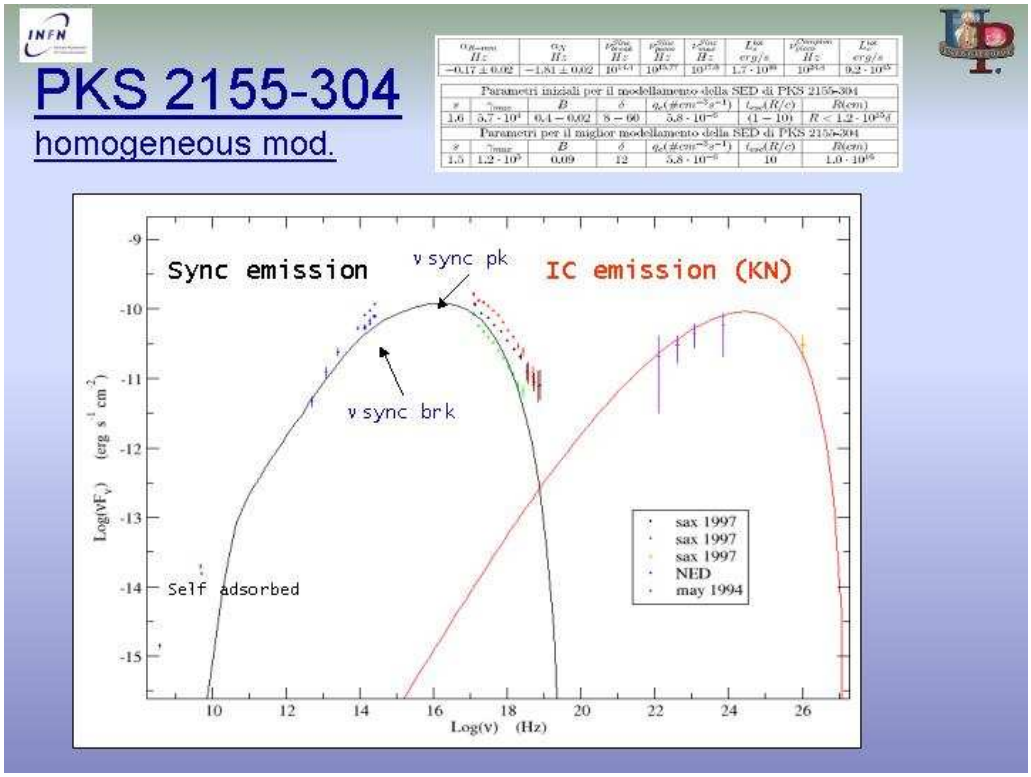
PKS 2155-304
homogeneous mod.
Parametri iniziali per il modellamento della SED di PKS 2155-304
Parametri per il miglior modellamento della SED di PKS 2155-304
Sync emission
ν sync pk
IC emission (KN)
ν sync brk
Self adsorbed
sax 1997
sax 1997
sax 1997
NED
may 1994
Log(νF_ν) (erg s^-1 cm^-2)
Log(ν) (Hz)

Simulation of EC emission homogeneous mod.

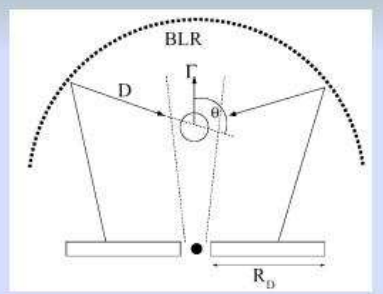

The radiation from the disk

$$I'_\nu(\epsilon',\mu') = \frac{1}{4\pi}\int_1^\infty d\Omega' I_\epsilon(\Omega,\epsilon/\Gamma)\delta^3 \qquad I_\nu = \eta\frac{L_{nuc}}{4\pi\cdot 4\pi D^2} f_\nu^{Norm}$$

$$I'_\nu(\epsilon',\mu') = \Gamma\frac{L_D}{16\pi^2 R_D^2} f_\nu^{Norm}(T_{disco}) \qquad f_\nu^{Norm} = \frac{I_\nu}{\int_{\nu_{min}}^{\nu_{max}} d\nu \int_{\frac{\nu}{2\Gamma}}^{\infty} d\epsilon \frac{I_\epsilon}{\epsilon^2}}$$

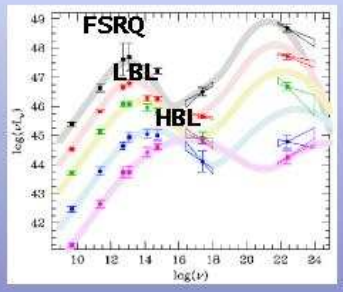

ERC simulation

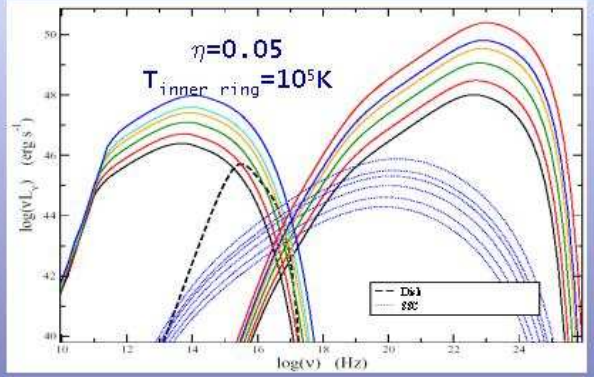

Time crossing convolution

homogeneous model.

$T_{injection.} = T_{cross}$

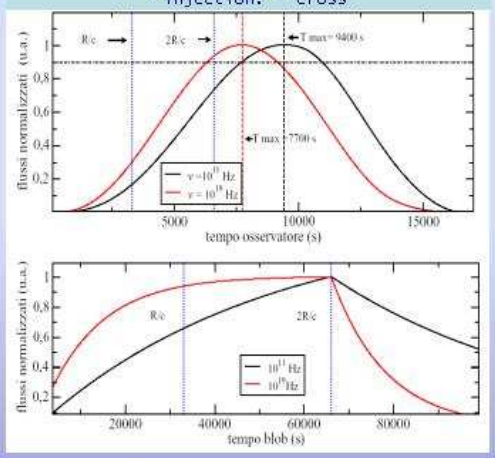

	10^{11} Hz	10^{19} Hz
limite su $T_{max}^{oss}(s)$	$6000 < t < 9900$	$8250 < t < 11550$
$T_{max}^{oss}(s)$	7700	9400

raggio blob	$R = 1.0\cdot 10^{15}$ cm
indice di iniezione	$s = 1.5$
Γ_{bulk}	10
durata dell'iniezione	$T_{inj} = 2.0R/c$
tempo di fuga	$T_{esc} = 1.5R/c$

	10^{11} Hz	10^{19} Hz
T salita (s)	27400	28000
T discesa (s)	54000	56000

	10^{11} Hz	10^{19} Hz
T salita (s)	27400	28000
T discesa (s)	54000	56000

PKS 2155-304 ASCA (Kataoka 2000)

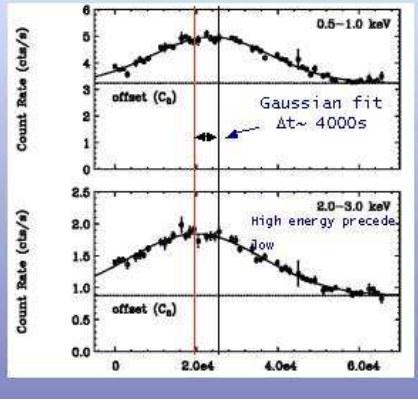

- Time lag at different energies
- Quasi-symmetric profile (oss.)

Spectral index evolution sync emission

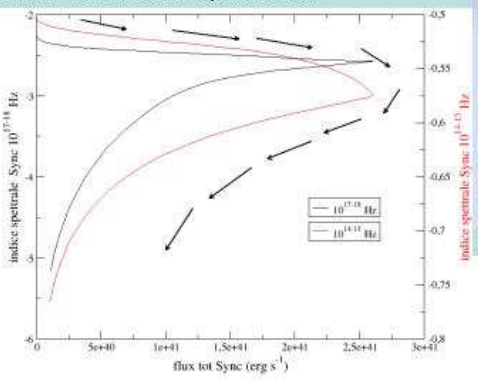

Homogeneous model is able to explain:

- SED
- Inter band correlation
- Spectral index evolution

But only at logn time scales!!!

Homogeneous model doesn't work to explain rapid time scale phenomena, which is one of the main Blazar characteristics

Spectral index evolution IC emission

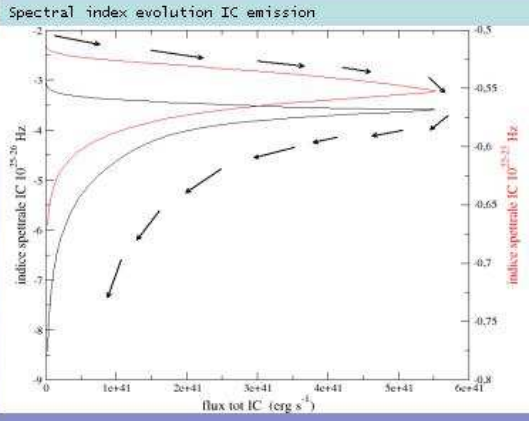

Shell model requirement

- An engine which shots shells(accr. Disk)
- The shells have the right frequency of ejection (~Rs/c)
- The shells have to collide in the sub parsec scale
- The BLF has to be consistent with observations
- There has to be a sample of shell which has the right Energy and time scale to be resolved as a flare

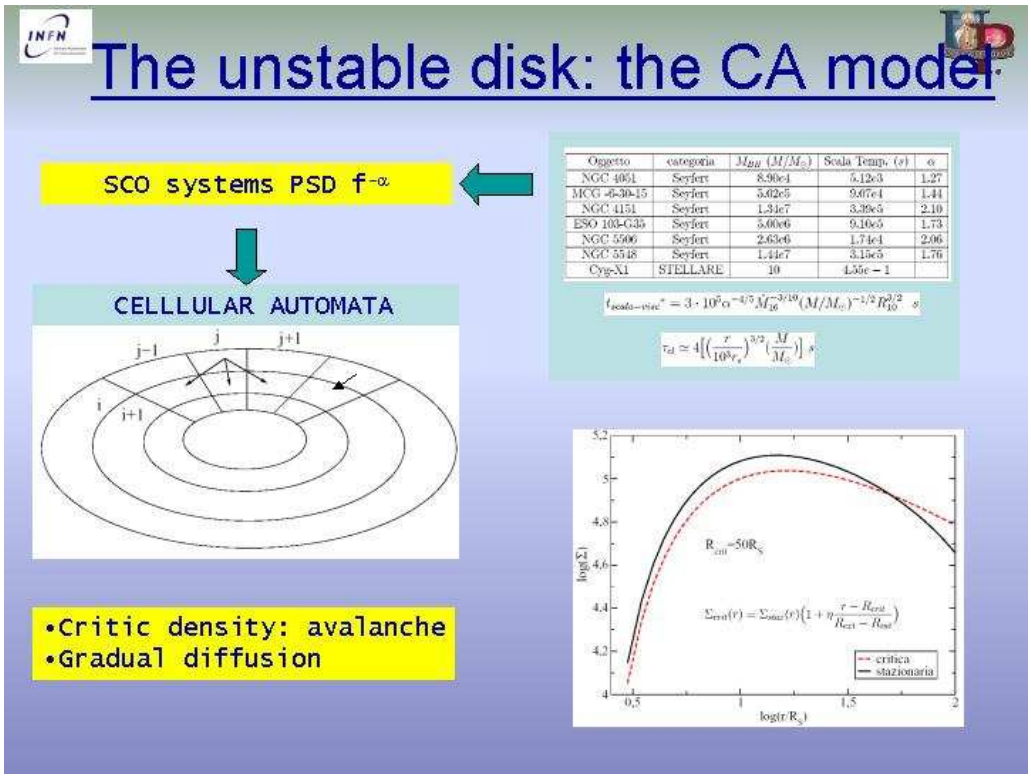
The unstable disk: the CA model
SCO systems PSD f-α
CELLLULAR AUTOMATA
j-1
j
j+1
i
i+1
•Critic density: avalanche
•Gradual diffusion
Oggetto | categoria | M_{BH} $(M/M_\odot)$ | Scala Temp. (s) | α
NGC 4051 | Seyfert | 8.90e4 | 5.12e3 | 1.27
MCG -6-30-15 | Seyfert | 5.02e5 | 9.07e4 | 1.44
NGC 4151 | Seyfert | 1.31e7 | 3.39e5 | 2.10
ESO 103-G35 | Seyfert | 5.00e6 | 9.10e5 | 1.73
NGC 5506 | Seyfert | 2.63e6 | 1.74e4 | 2.06
NGC 5548 | Seyfert | 1.44e7 | 3.15e5 | 1.76
Cyg-X1 | STELLARE | 10 | 4.55e − 1 |
$t_{scala-visc} = 3 \cdot 10^2 \alpha^{-4/5} \dot{M}_{16}^{-3/10} (M/M_\odot)^{-1/2} R_{10}^{2/2}$ s
$\tau_{el} \simeq 4\left[\left(\frac{r}{10^9 r_s}\right)^{3/2} \left(\frac{M}{M_\odot}\right)\right]$ s
R_{crit}=50R_S
$\Sigma_{crit}(r) = \Sigma_{stat}(r)\left(1 + \eta \frac{r - R_{crit}}{R_{crit} - R_{int}}\right)$
critica
stazionaria
log(Σ)
log(r/R_S)

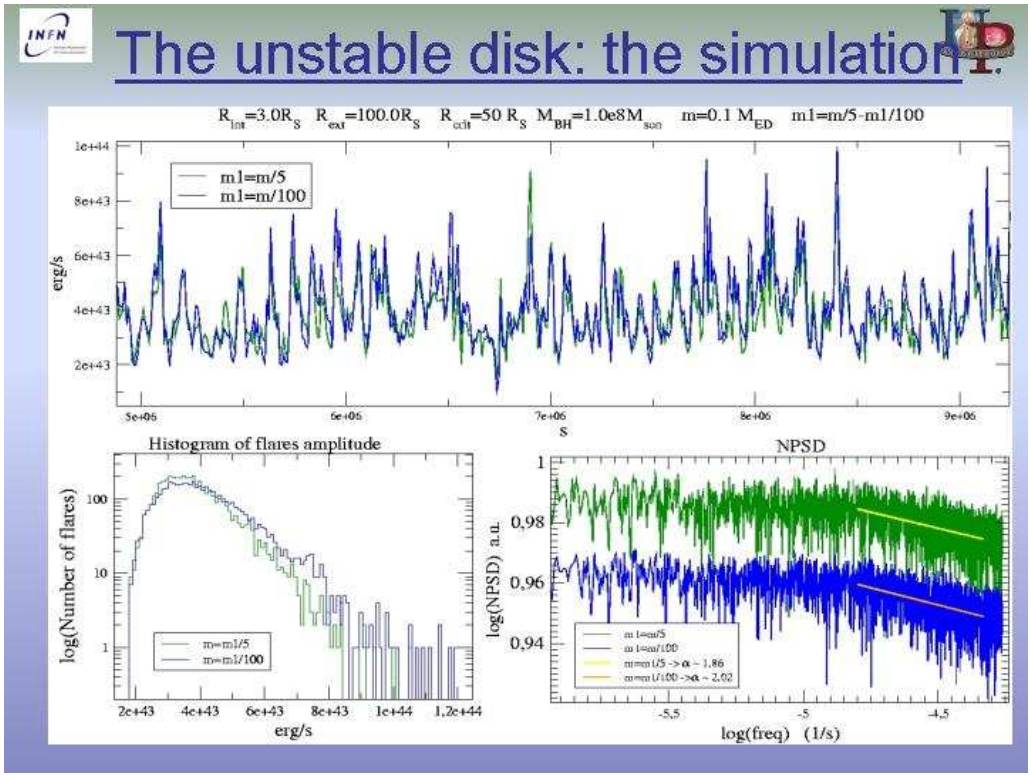
The unstable disk: the simulation
R_{int}=3.0R_S R_{ext}=100.0R_S R_{crit}=50 R_S M_{BH}=1.0e8M_{sun} m=0.1 M_{ED} m1=m/5-m1/100
m1=m/5
m1=m/100
erg/s
s
Histogram of flares amplitude
log(Number of flares)
m=m1/5
m=m1/100
erg/s
NPSD
log(NPSD) a.u.
log(freq) (1/s)

The unstable disk: observations.

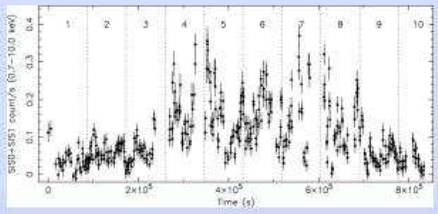

Pounds et al. 20001 RXTE observation of Arakelian 564 (Seyf. 1)

α=1.2±0.04

T_{var}~a day(10^{4-5}s)

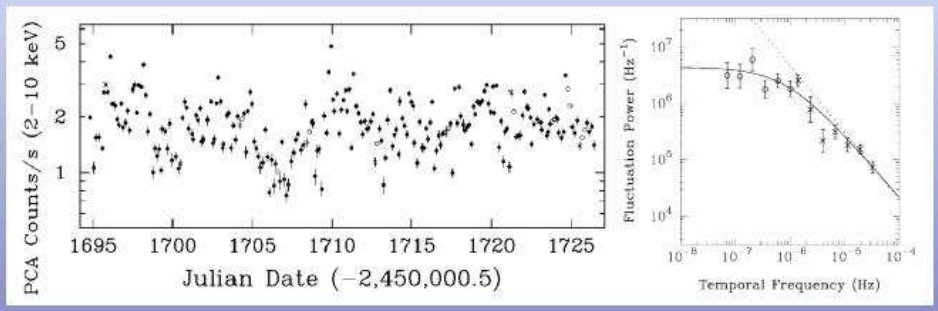

Shell model: the shell wind

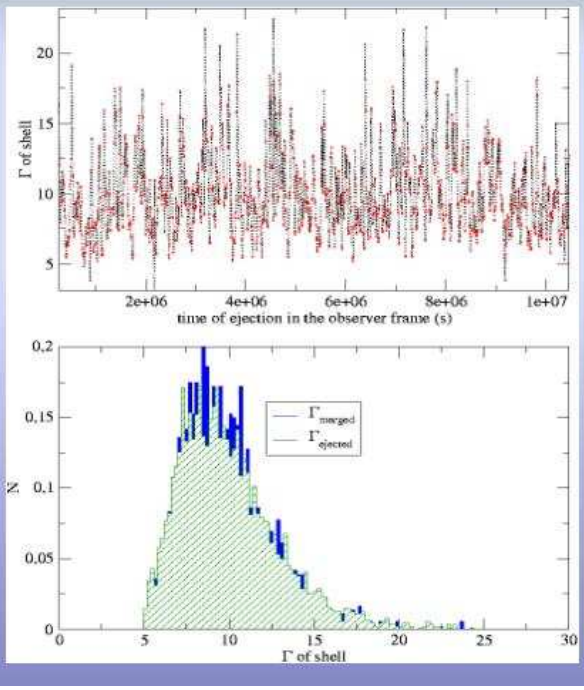

- Shot shell from accr. Disk
- Eval. shell width l=Δt_ejec*c
- Iterate to find collision
- Eval. BLF of merged shell
- Eval. Internal energy of merged shell

Eval. β_{rd} β_{fw} of shock

- Find t_crs time scale=

$$l/((c^*(\beta_r-\beta_{rs})\Gamma^2_m)$$

- Find t_ang time scale=

$$R/(c\Gamma_m)$$

- Inject $e^{-/+}$during t_crs
- Solve num. Cont. Equ.
- Obtain l.c. and spectra

Shell model: the simulation

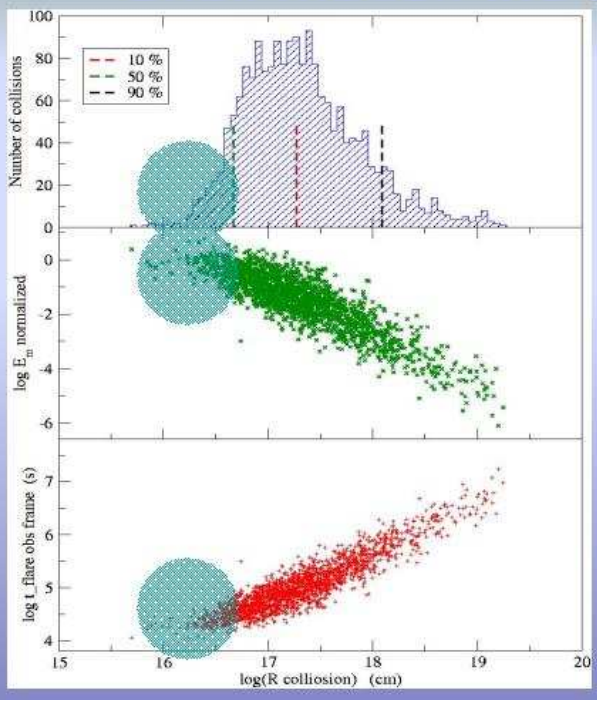

- Freq. eject. ~ 10 Ks
- Freq. Coll. ~ 40 Ks for res. flare
- Collision $R<10^{19}$cm
- Only ~10% resolved flare

Shell model: synchrotron em.

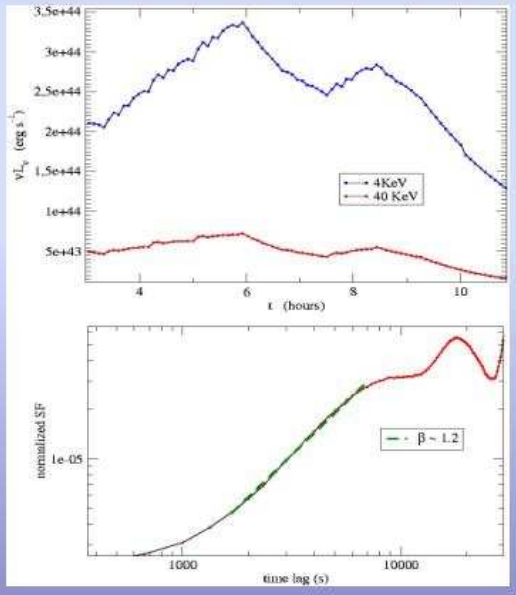

MRK 421 *XMM-NEWTON*
SEMBAY et al. 2002

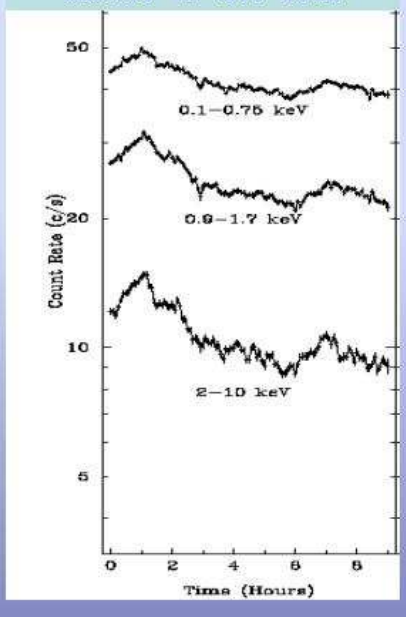

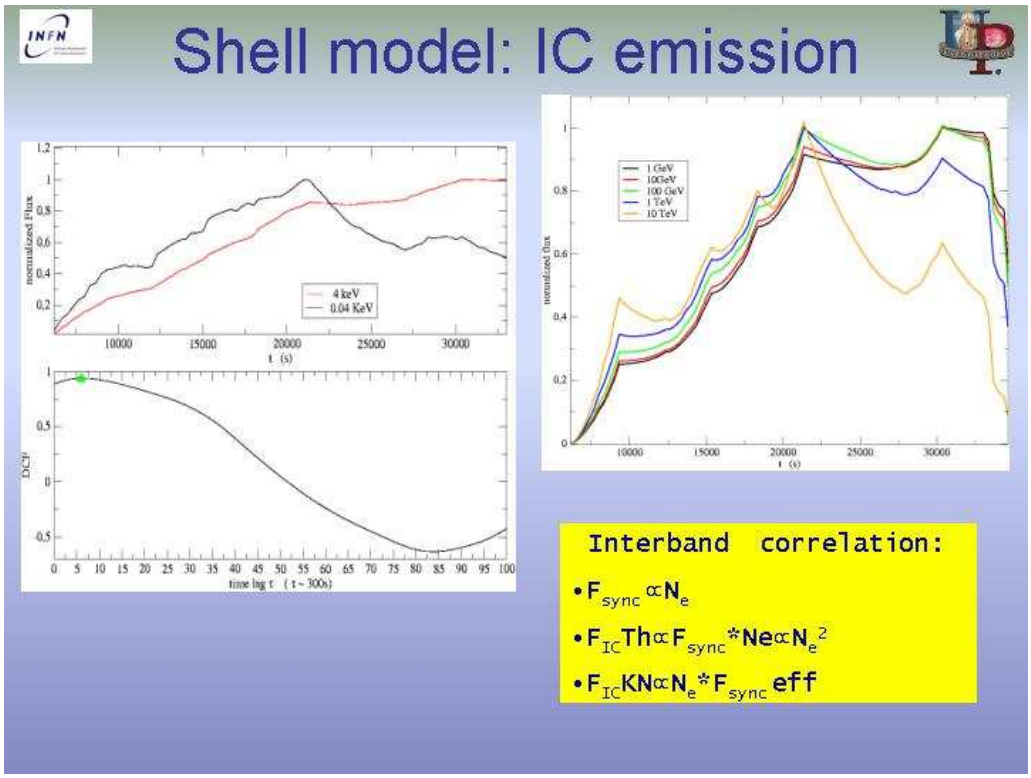
Shell model: IC emission
normalized Flux
4 keV
0.04 KeV
t (s)
DCF
time lag τ (τ ~ 300s)
1 GeV
10GeV
100 GeV
1 TeV
10 TeV
normalized flux
t (s)
Interband correlation:
• $F_{sync} \propto N_e$
• $F_{IC}Th \propto F_{sync} * Ne \propto N_e^2$
• $F_{IC}KN \propto N_e * F_{sync}$ eff

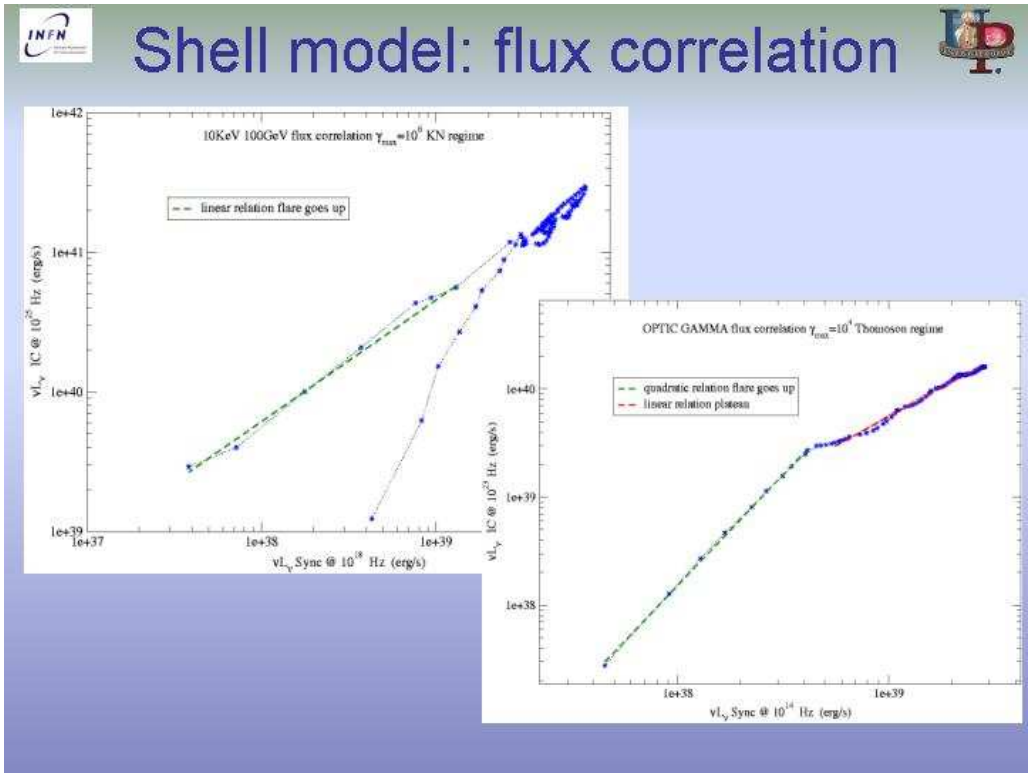
Shell model: flux correlation
10KeV 100GeV flux correlation $\gamma_{max}=10^6$ KN regime
linear relation flare goes up
νL_ν IC @ 10^{25} Hz (erg/s)
νL_ν Sync @ 10^{18} Hz (erg/s)
OPTIC GAMMA flux correlation $\gamma_{max}=10^4$ Thomoson regime
quadratic relation flare goes up
linear relation plateau
νL_ν IC @ 10^{25} Hz (erg/s)
νL_ν Sync @ 10^{14} Hz (erg/s)


Self Consistent Synchrotron Self Compton emission

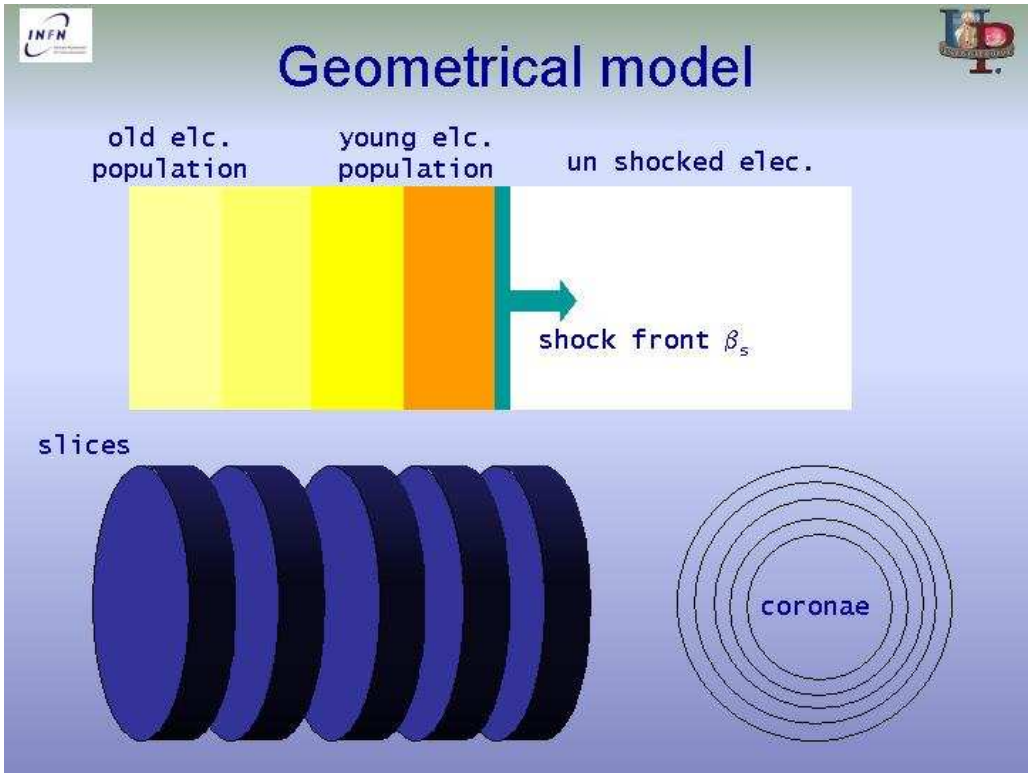
Geometrical model
old elc. population
young elc. population
un shocked elec.
shock front β_s
slices
coronae

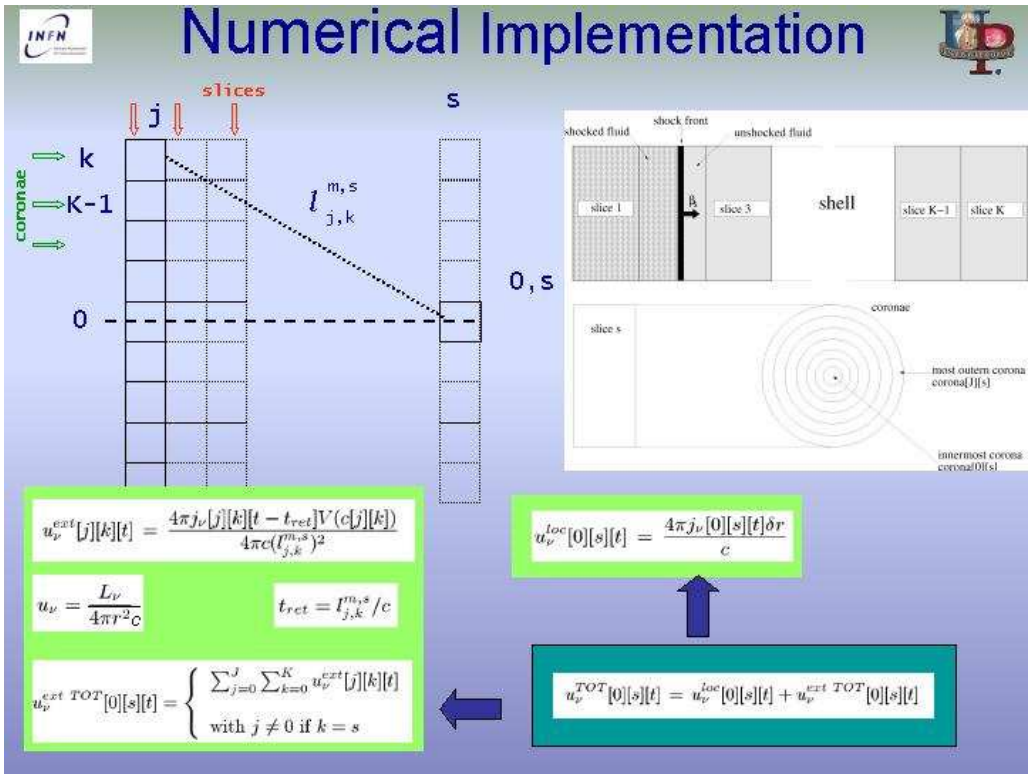
Numerical Implementation
slices
j
s
k
K-1
0
coronae
$l^{m,s}_{j,k}$
0,s
shocked fluid
shock front
unshocked fluid
slice 1
slice 3
shell
slice K-1
slice K
coronae
slice s
most outern corona
corona[J][s]
innermost corona
corona[0][s]
$u_\nu^{ext}[j][k][t] = \frac{4\pi j_\nu[j][k][t-t_{ret}]V(c[j][k])}{4\pi c(l^{m,s}_{j,k})^2}$
$u_\nu = \frac{L_\nu}{4\pi r^2 c}$
$t_{ret} = l^{m,s}_{j,k}/c$
$u_\nu^{ext\ TOT}[0][s][t] = \begin{cases} \sum_{j=0}^{J}\sum_{k=0}^{K} u_\nu^{ext}[j][k][t] \\ \text{with } j \neq 0 \text{ if } k = s \end{cases}$
$u_\nu^{loc}[0][s][t] = \frac{4\pi j_\nu[0][s][t]\delta r}{c}$
$u_\nu^{TOT}[0][s][t] = u_\nu^{loc}[0][s][t] + u_\nu^{ext\ TOT}[0][s][t]$

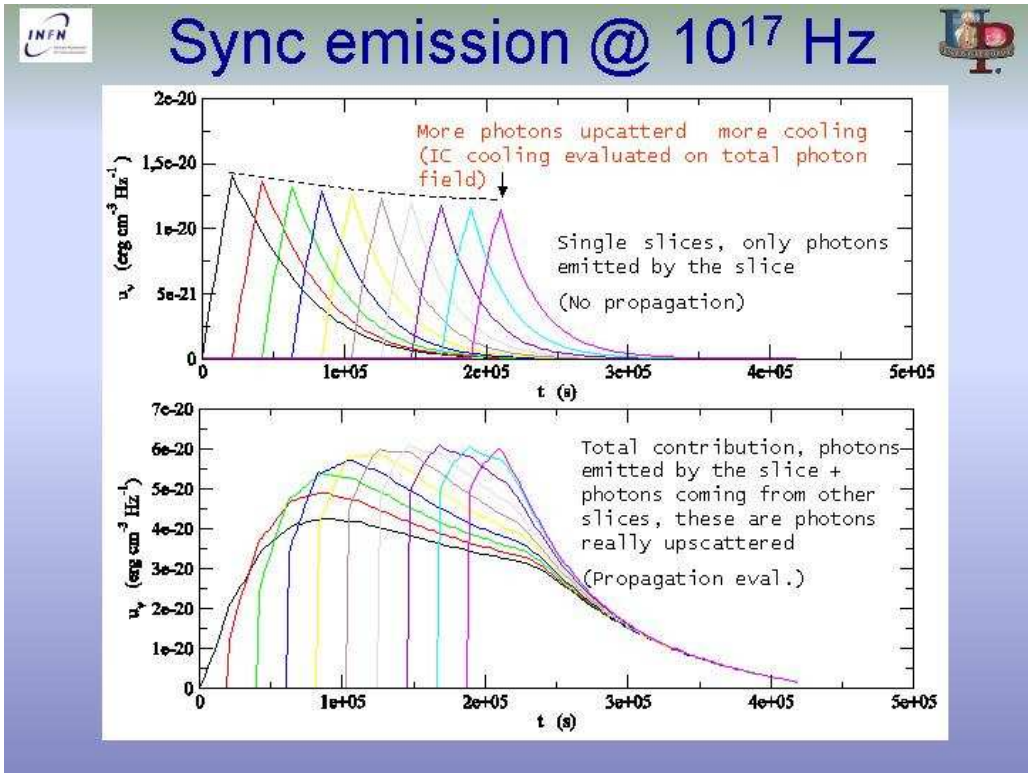
Sync emission @ 10^{17} Hz
More photons upcatterd more cooling (IC cooling evaluated on total photon field)
Single slices, only photons emitted by the slice
(No propagation)
Total contribution, photons emitted by the slice + photons coming from other slices, these are photons really upscattered
(Propagation eval.)
u_ν (erg cm^{-3} Hz^{-1})
t (s)
2e-20
1.5e-20
1e-20
5e-21
0
1e+05
2e+05
3e+05
4e+05
5e+05
7e-20
6e-20
5e-20
4e-20
3e-20
2e-20
1e-20

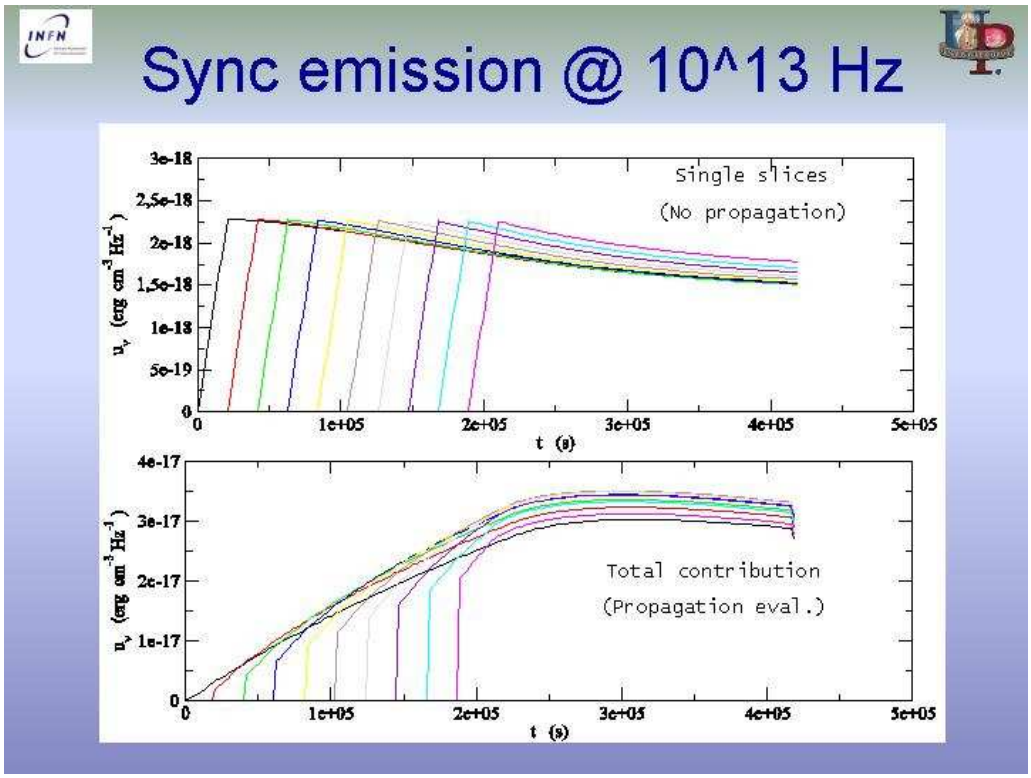
Sync emission @ 10^13 Hz
Single slices
(No propagation)
Total contribution
(Propagation eval.)
t (s)

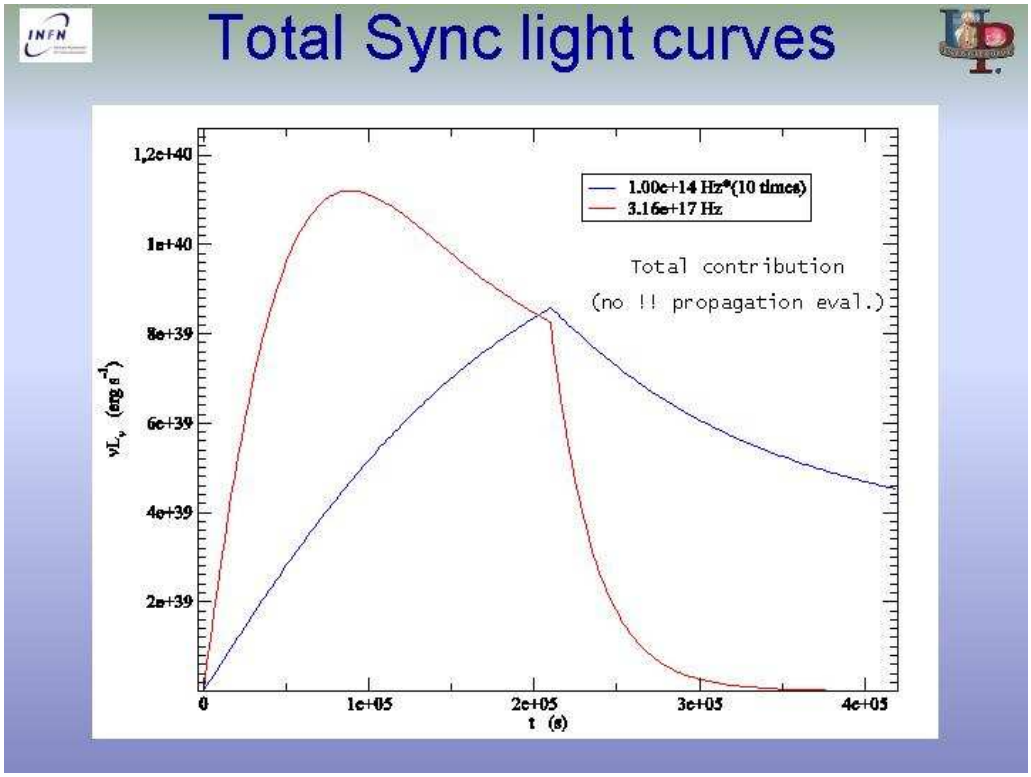
Total Sync light curves
1.00e+14 Hz*(10 times)
3.16e+17 Hz
Total contribution
(no !! propagation eval.)
t (s)

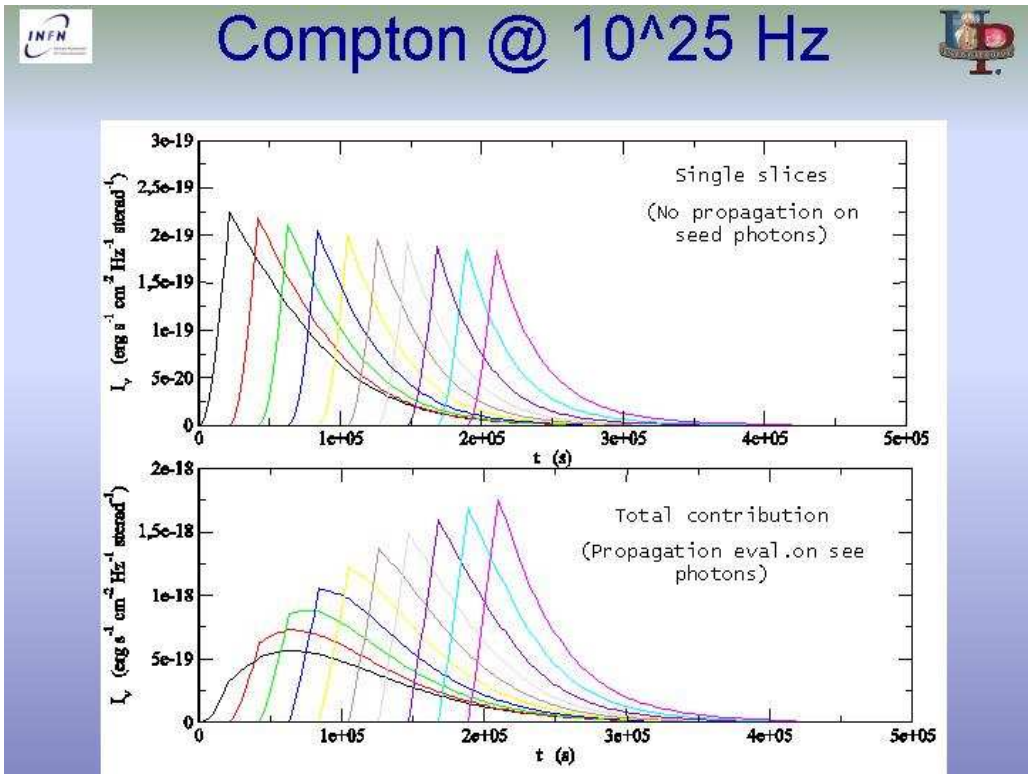
Compton @ 10^25 Hz
Single slices
(No propagation on seed photons)
Total contribution
(Propagation eval.on see photons)
t (s)

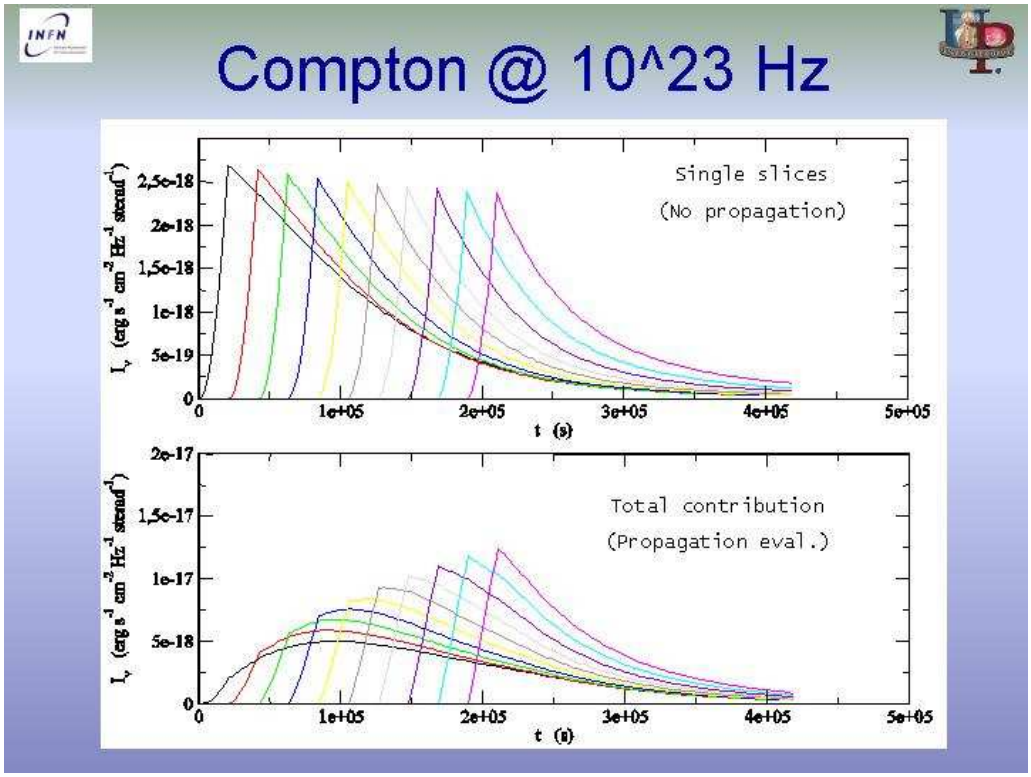
Compton @ 10^23 Hz
Single slices
(No propagation)
Total contribution
(Propagation eval.)
t (s)

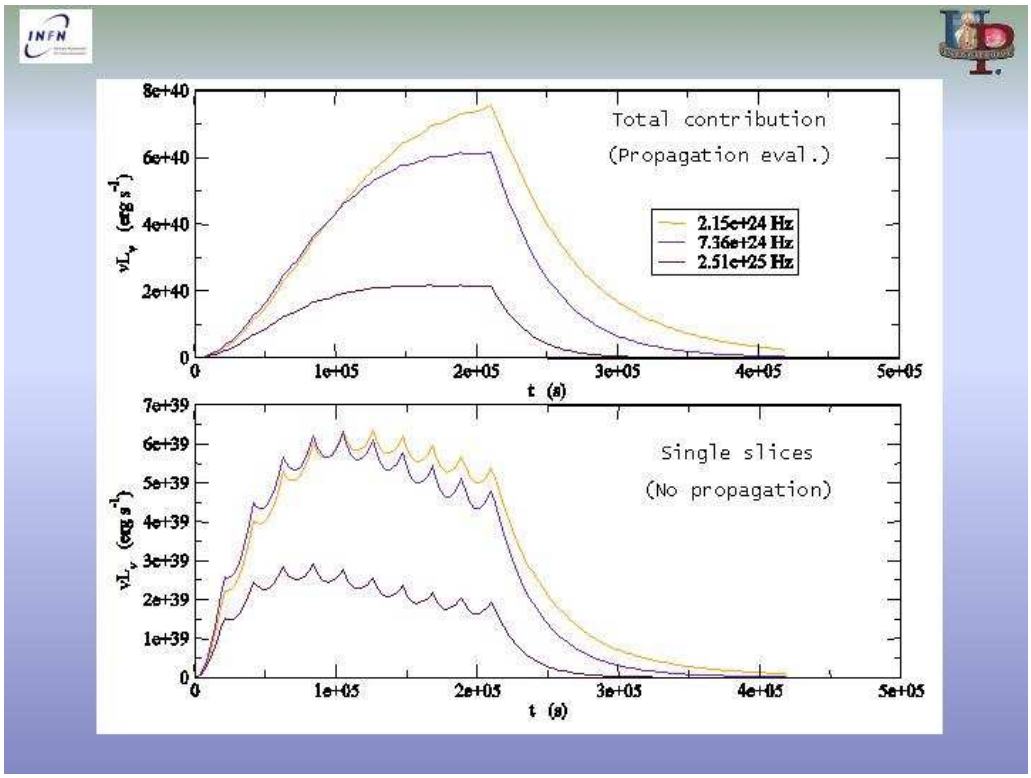
Total contribution
(Propagation eval.)
2.15e+24 Hz
7.36e+24 Hz
2.51e+25 Hz
νL_ν (erg s^-1)
t (s)
Single slices
(No propagation)
νL_ν (erg s^-1)
t (s)

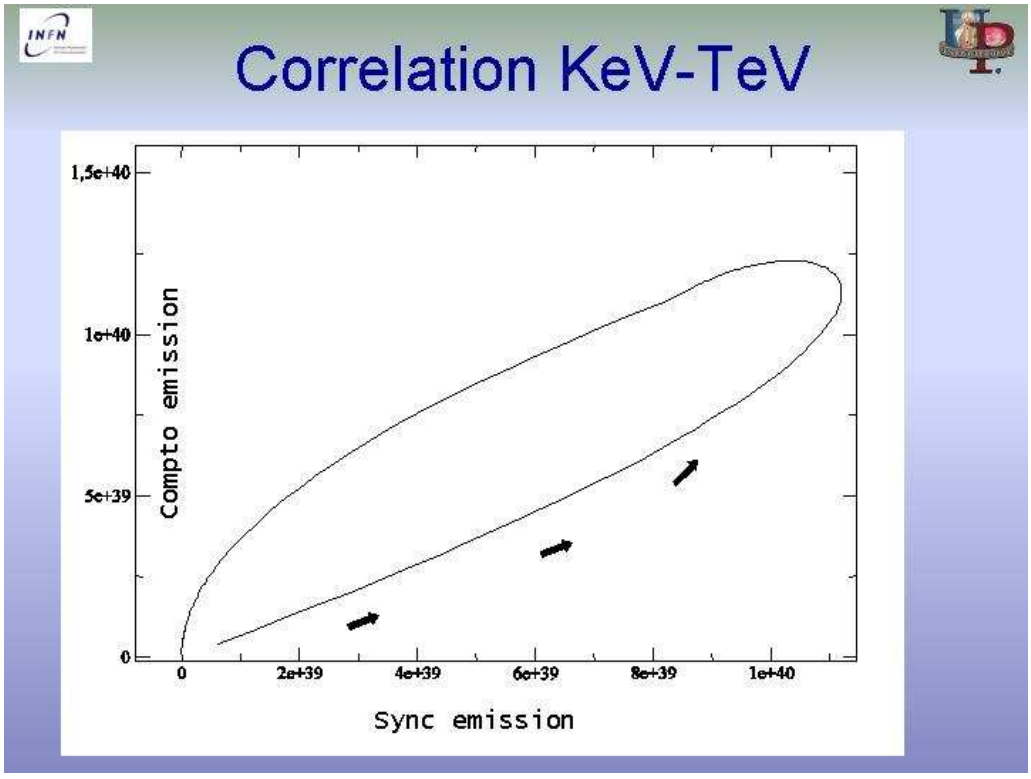
Correlation KeV-TeV
Compto emission
Sync emission

Application to Mrk 421

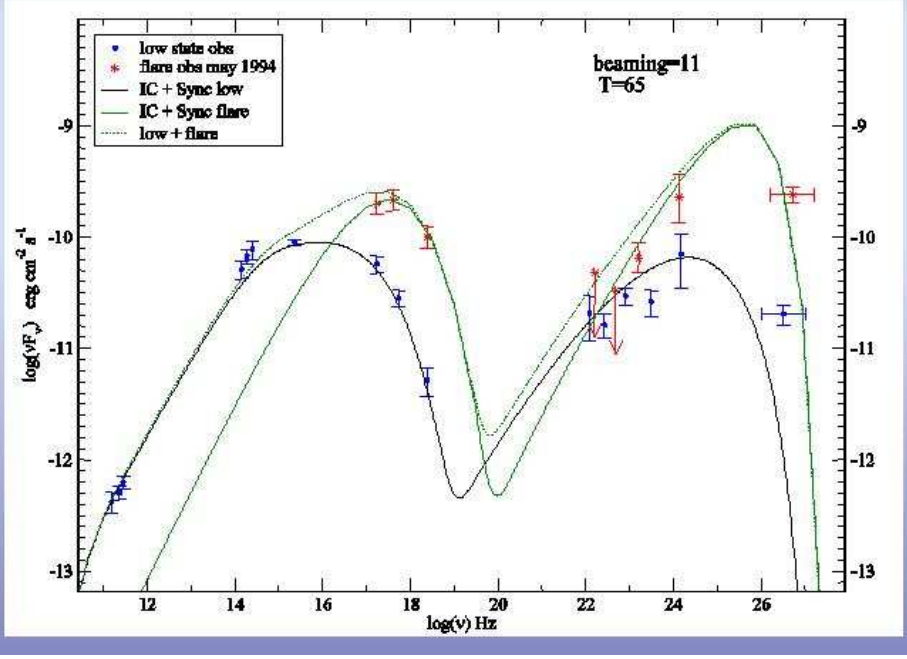

Conclusions

- Both homogenous and shell model can explain temporal and energetic behavior of Blazar.
- But observations enough accurate to validate the theoretical predictions are present only for the low energy emission (radio to X→ASCA, SAX, XMM, CHANDRA).
- To validate the high energy emission model and to discriminate between the IC and EC scenario we need gamma/TeV observations with a good temporal and energetic resolution.
- This work is useful both to compare the theoretical predictions of actual models with the observations by next generation high energy telescopes (GLAST AGILE MAGIC), and both to give realistic simulation for variable source that these telescopes will observe

Session VI: The power of jets

Task 6: The power of jets – G. Ghisellini

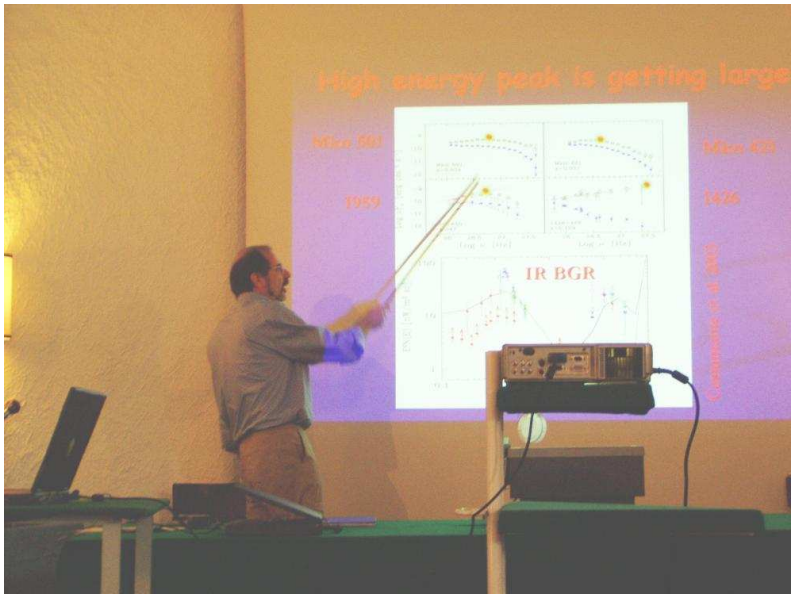

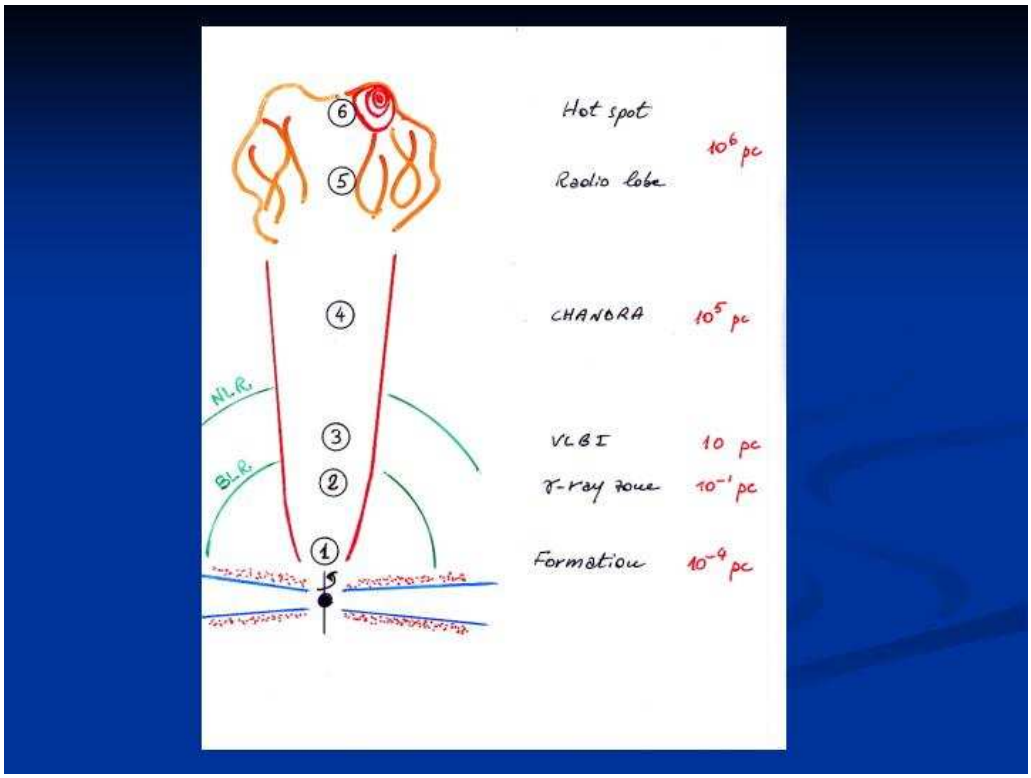
6
5
4
3
2
1
NLR
BLR
Hot spot
Radio lobe
CHANDRA
VLBI
γ-ray zone
Formation
10^6 pc
10^5 pc
10 pc
10^{-1} pc
10^{-4} pc

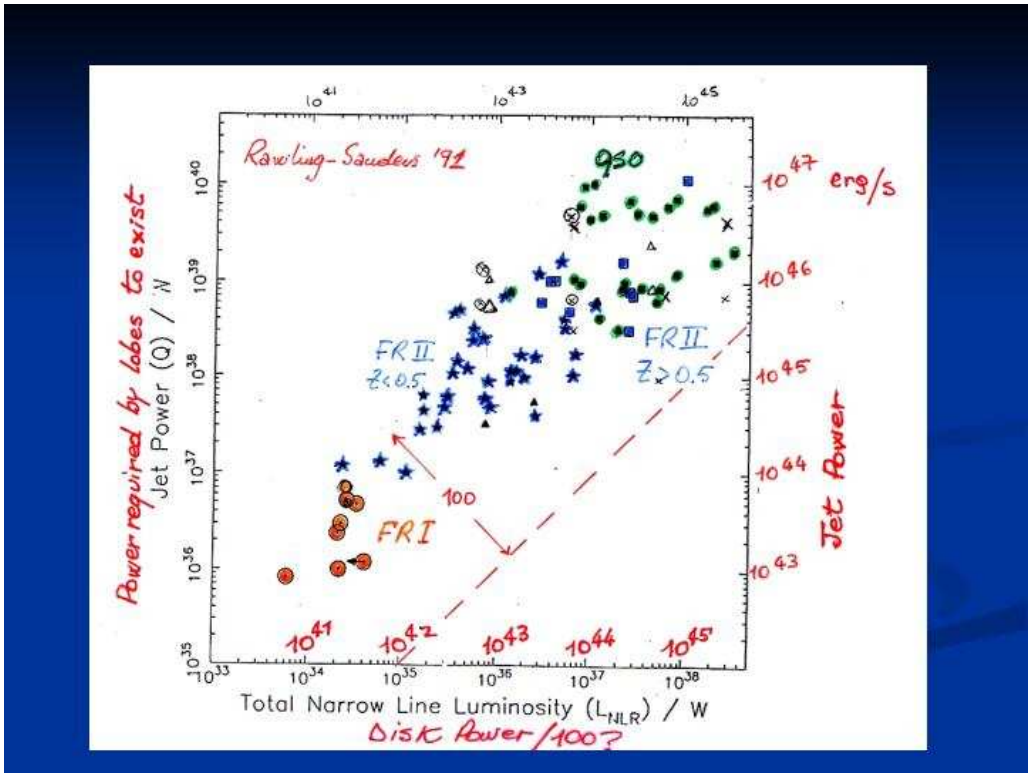
Rawling-Saunders '91
930
FR II
z<0.5
FR II
z>0.5
FR I
100
Power required by lobes to exist
Jet Power (Q) / W
Total Narrow Line Luminosity (L_{NLR}) / W
Disk Power/100?
Jet Power
10^{47} erg/s
10^{46}
10^{45}
10^{44}
10^{43}
10^{41}
10^{42}
10^{43}
10^{44}
10^{45}

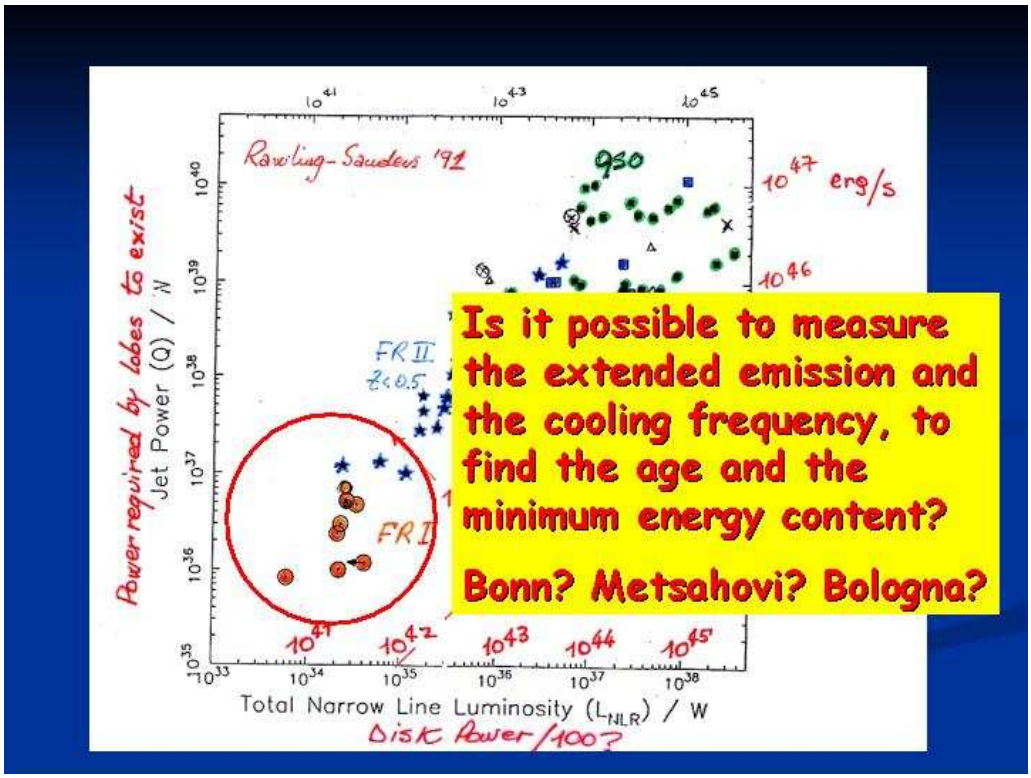
Rawlings-Saunders '91
950
10^{47} erg/s
10^{46}
FR II
z<0.5
FR I
Power required by lobes to exist
Jet Power (Q) / W
Total Narrow Line Luminosity (L_{NLR}) / W
Disk Power/100?
Is it possible to measure the extended emission and the cooling frequency, to find the age and the minimum energy content?
Bonn? Metsahovi? Bologna?

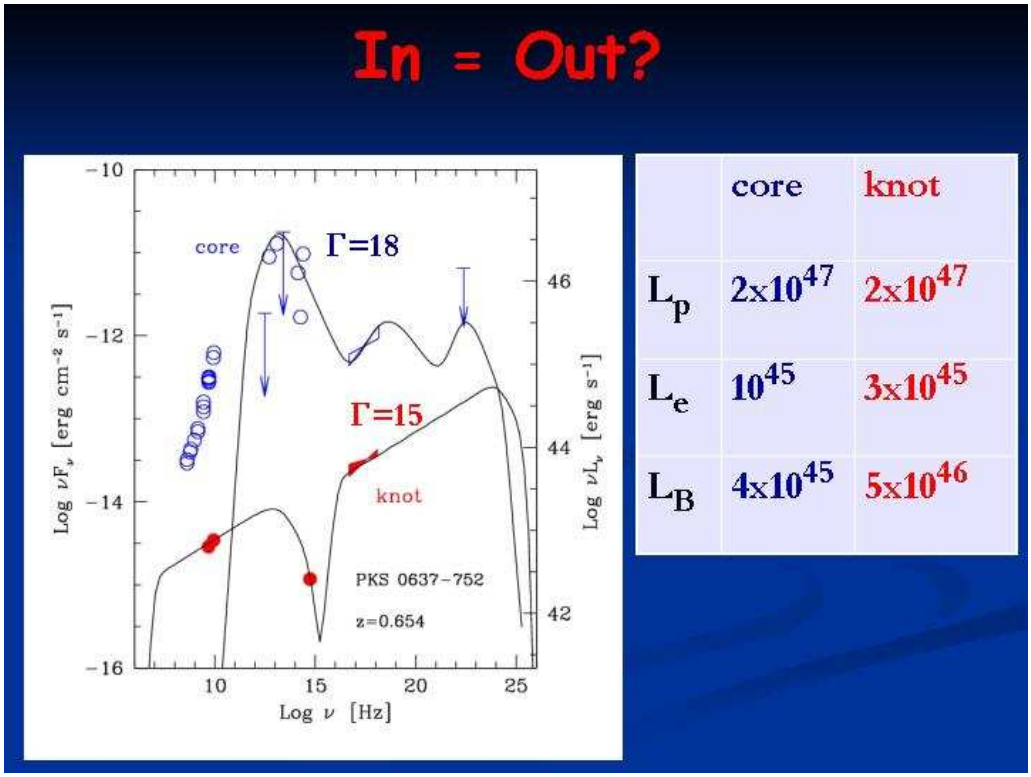
In = Out?
core
Γ=18
Γ=15
knot
PKS 0637-752
z=0.654
Log νF$_ν$ [erg cm^{-2} s^{-1}]
Log νL$_ν$ [erg s^{-1}]
Log ν [Hz]
core
knot
L_p 2x10^{47} 2x10^{47}
L_e 10^{45} 3x10^{45}
L_B 4x10^{45} 5x10^{46}

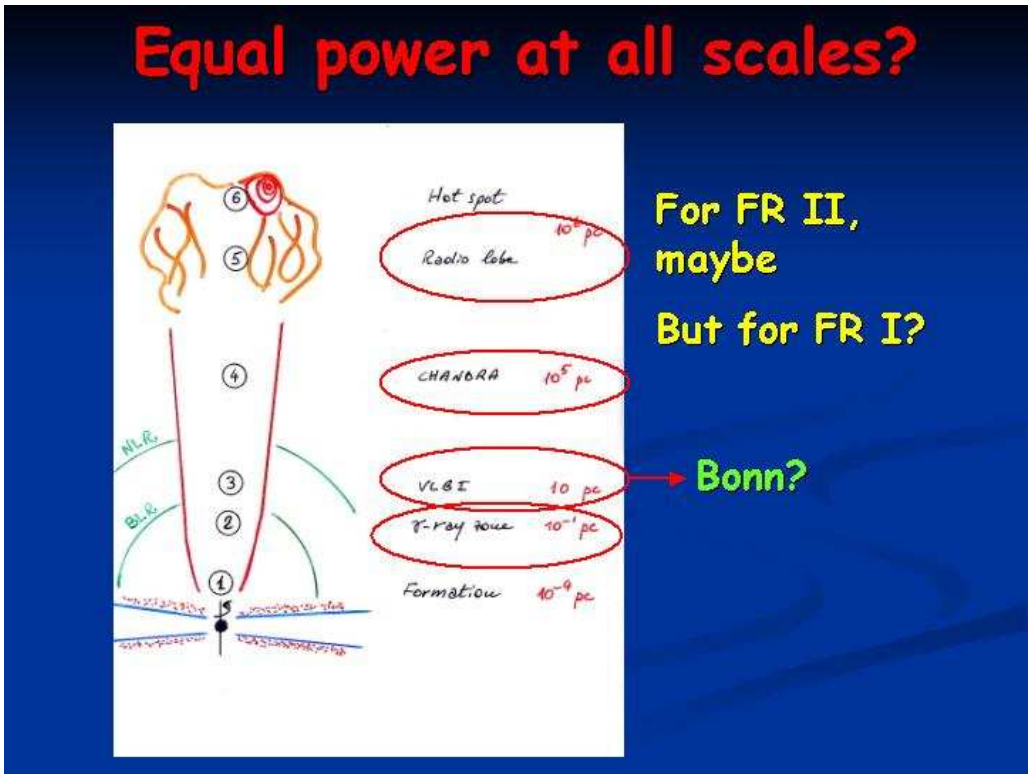
Equal power at all scales?
Hot spot
Radio lobe
CHANDRA
VLBI
Formation
For FR II, maybe
But for FR I?
Bonn?

Speculations – G. Ghisellini

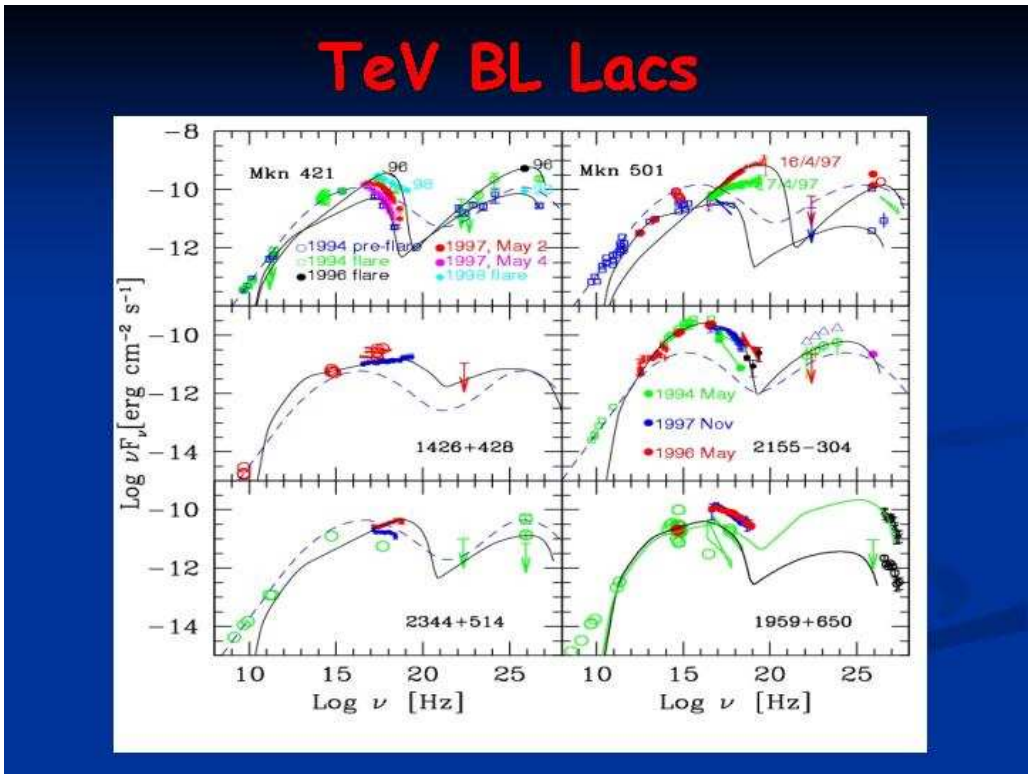
TeV BL Lacs
Mkn 421
Mkn 501
1994 pre-flare
1994 flare
1996 flare
1997, May 2
1997, May 4
1998 flare
16/4/97
7/4/97
1426+428
1994 May
1997 Nov
1996 May
2155−304
2344+514
1959+650
Log νF_ν [erg cm^-2 s^-1]
Log ν [Hz]

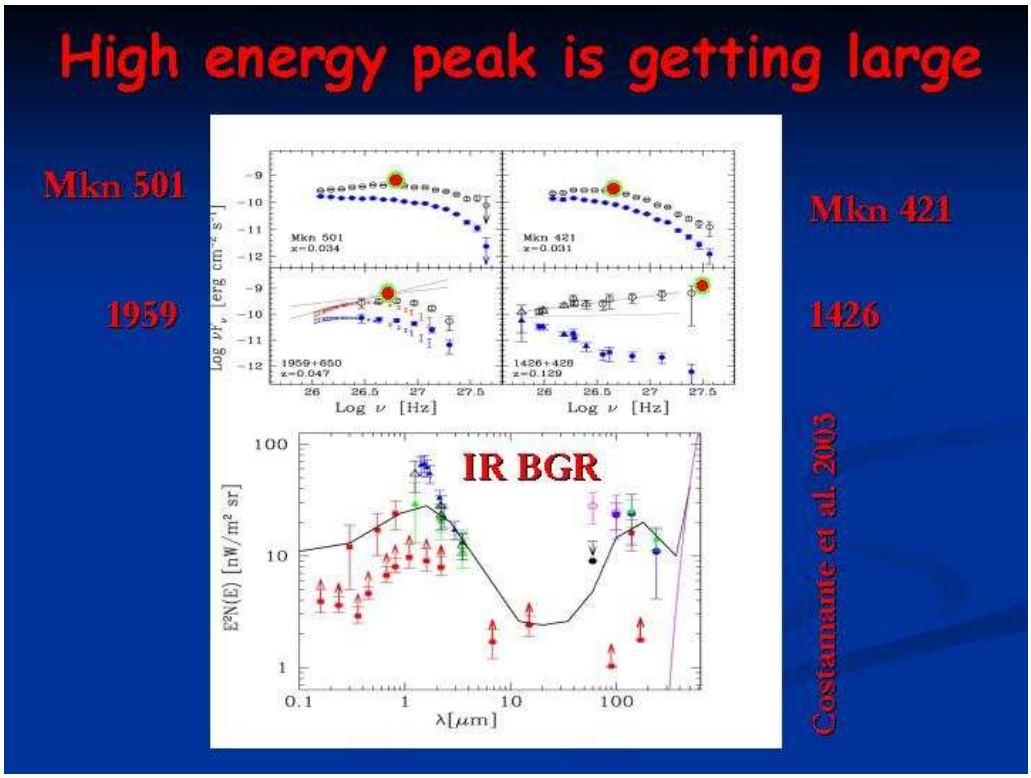
High energy peak is getting large
Mkn 501
1959
Mkn 421
1426
IR BGR
Costamante et al. 2003
E²N(E) [nW/m² sr]
λ[μm]
Log ν [Hz]

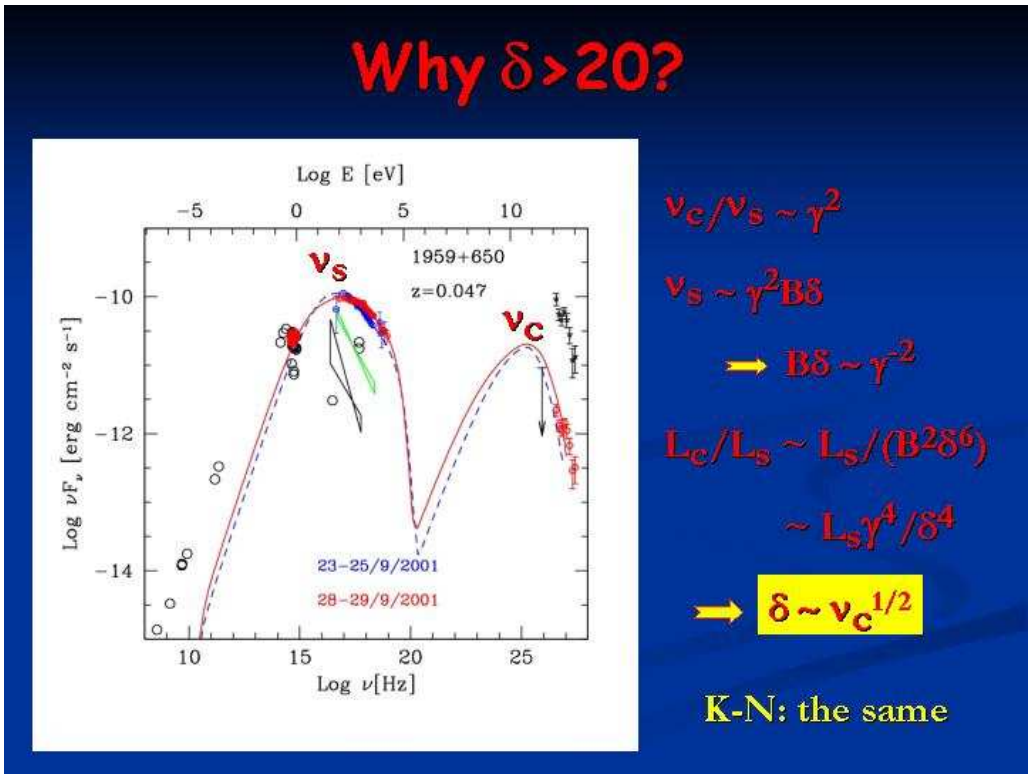
Why δ>20?
Log E [eV]
−5
0
5
10
1959+650
z=0.047
νs
νc
−10
−12
−14
Log νF_ν [erg cm⁻² s⁻¹]
23-25/9/2001
28-29/9/2001
10
15
20
25
Log ν[Hz]
νc/νs ~ γ²
νs ~ γ²Bδ
⇒ Bδ ~ γ⁻²
Lc/Ls ~ Ls/(B²δ⁶)
~ Lsγ⁴/δ⁴
⇒ δ ~ νc^1/2
K-N: the same

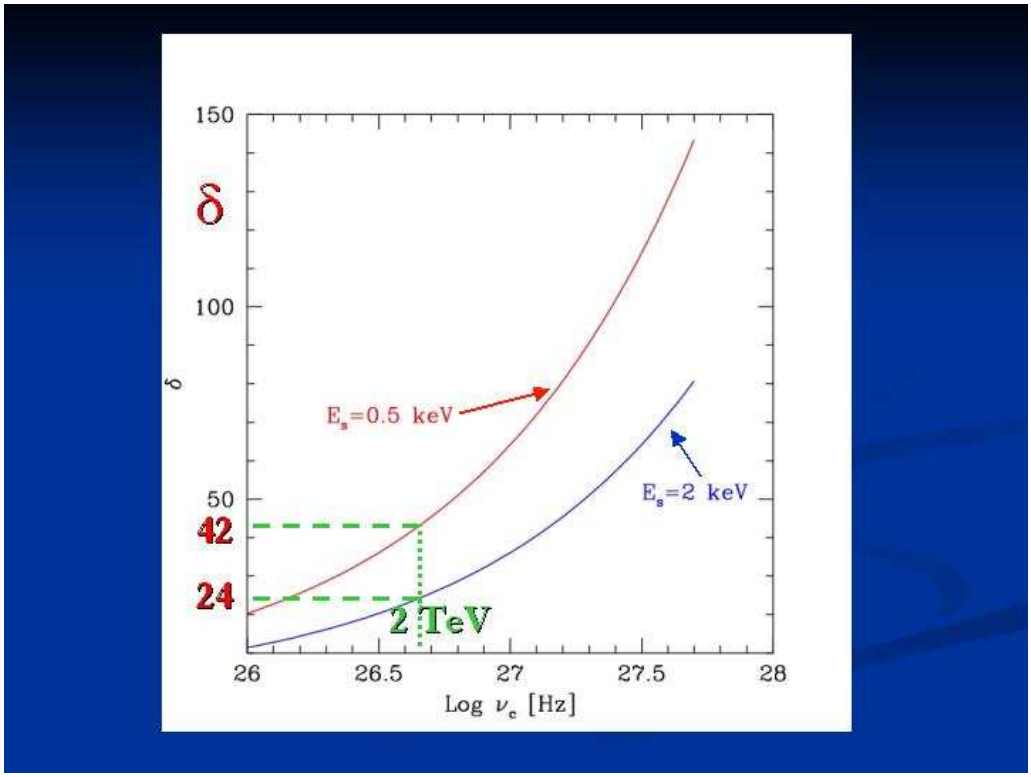
150
δ
100
δ
50
42
24
Es=0.5 keV
Es=2 keV
2 TeV
26
26.5
27
27.5
28
Log νc [Hz]

Instead, at the pc scale....

Mkn 501

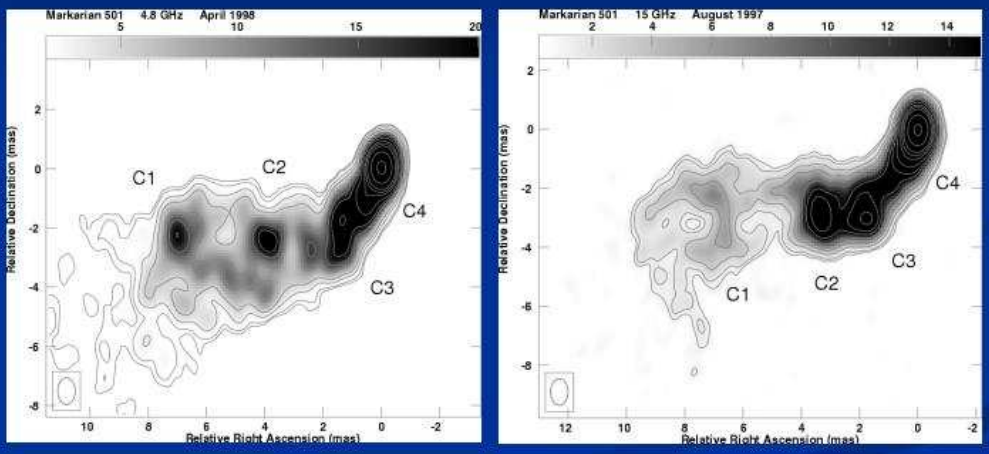

Giroletti et al. 2003, astro-ph/0309285

Subluminal motion for all TeV sources?

Piner & Edwards astro-ph/0309547

Mkn 421	$\beta_{app} \sim 0.04 - 0.18$ (+-0.06)
Mkn 501	$\beta_{app} \sim 0.05 - 0.54$ (+-0.15)
1959+650	$\beta_{app} \sim 0$
2155-304	$\beta_{app} \sim 4.4$ (+-2.9)
2344+514	$\beta_{app} \sim 0 - 0.5$ (+-0.5)

Giroletti et al: spine + layer: Mkn 501

R_{core} (pc)	θ	Γ_{spine}	δ_{spine}	Γ_{layer}	δ_{layer}
10^{-3}-0.03	4	15	15	?	?
0.03-0.15	10	15	4	10	5
0.15-7	15	15	2	3	5
7-20	15-20	15	1-2	3	3-4
20-30	25	3-10	1-2	2	2.5
50	25	1.25	1.8	1.1	1.5

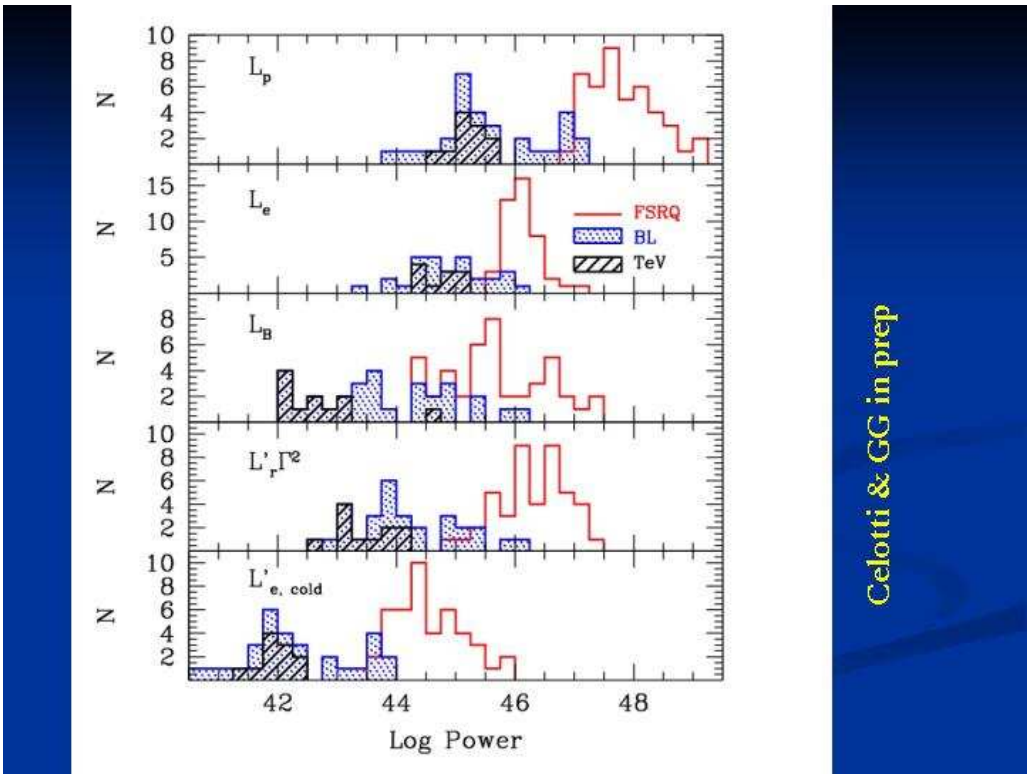

Celotti & GG in prep

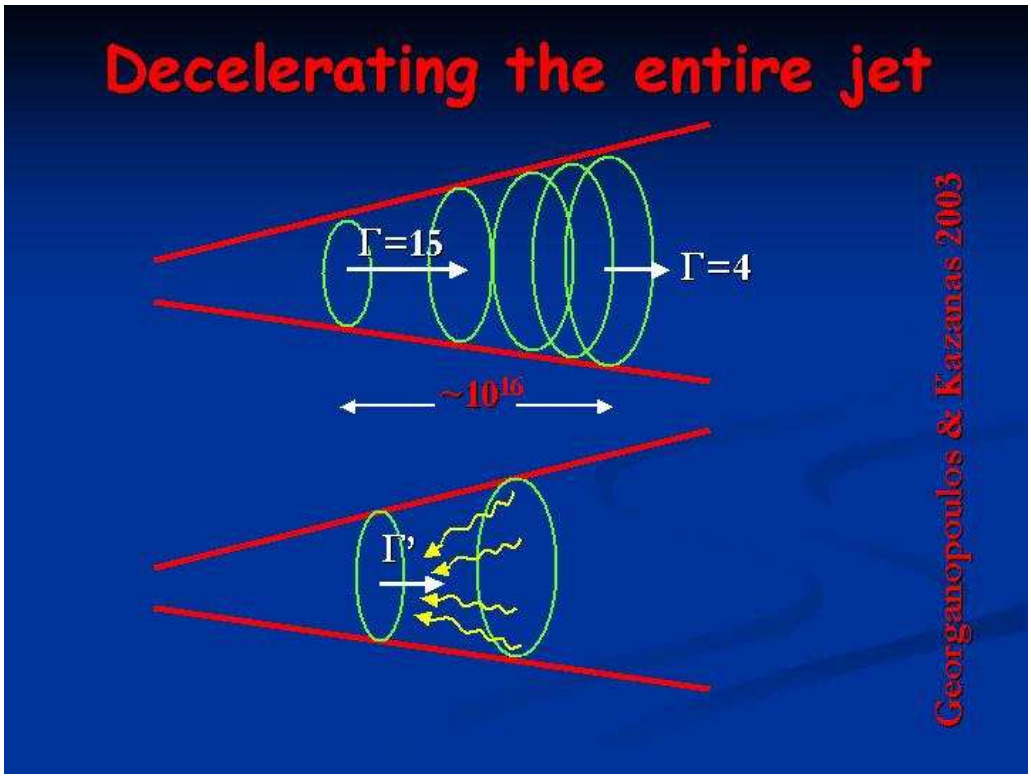
Decelerating the entire jet
Γ=15
Γ=4
~10^16
Γ'
Georganopoulos & Kazanas 2003

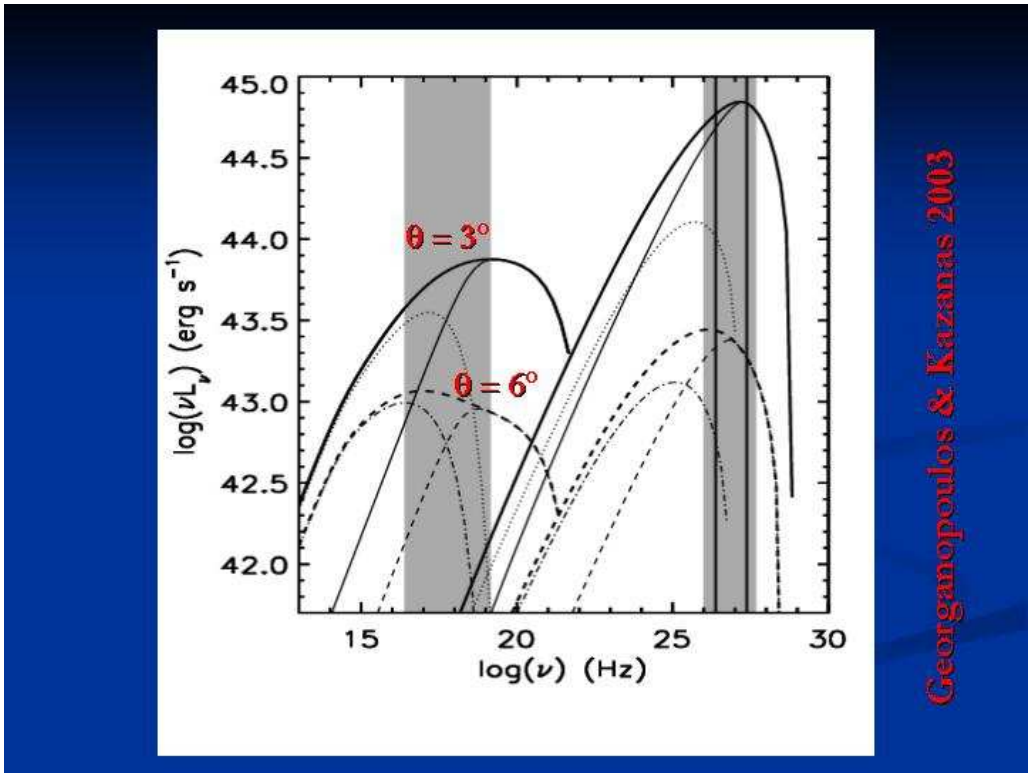
45.0
44.5
44.0
43.5
43.0
42.5
42.0
log(νL_ν) (erg s^-1)
θ = 3°
θ = 6°
15
20
25
30
log(ν) (Hz)
Georganopoulos & Kazanas 2003

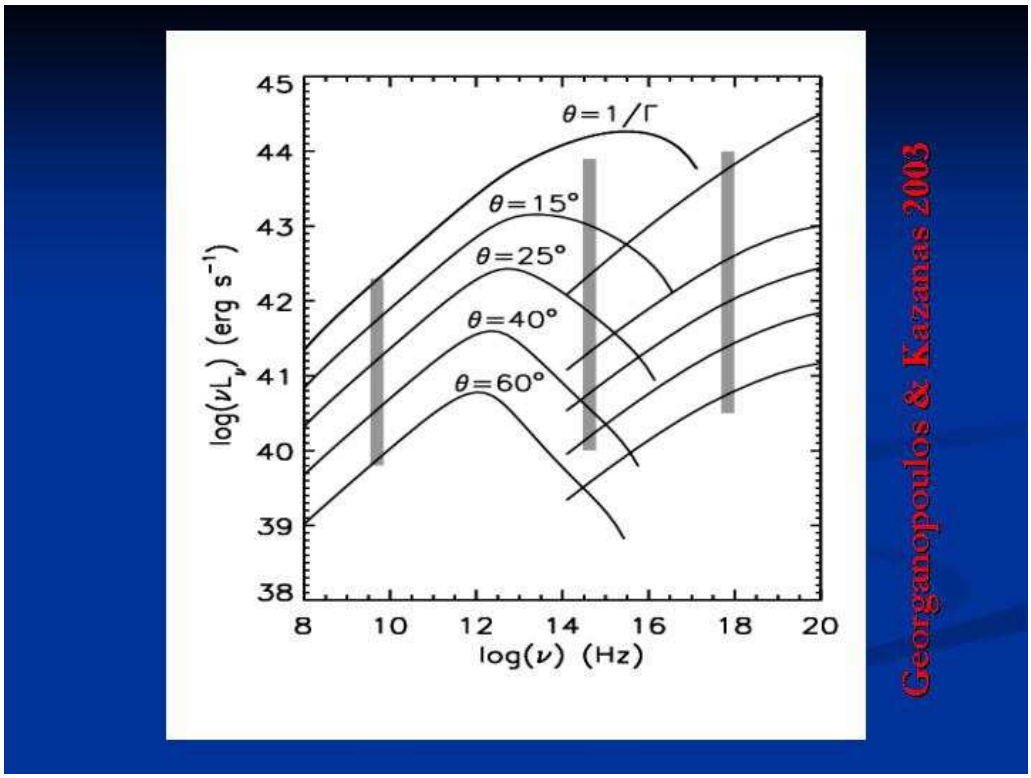
45
44
43
42
41
40
39
38
8
10
12
14
16
18
20
log(ν) (Hz)
log(νL_ν) (erg s^-1)
θ=1/Γ
θ=15°
θ=25°
θ=40°
θ=60°
Georganopoulos & Kazanas 2003

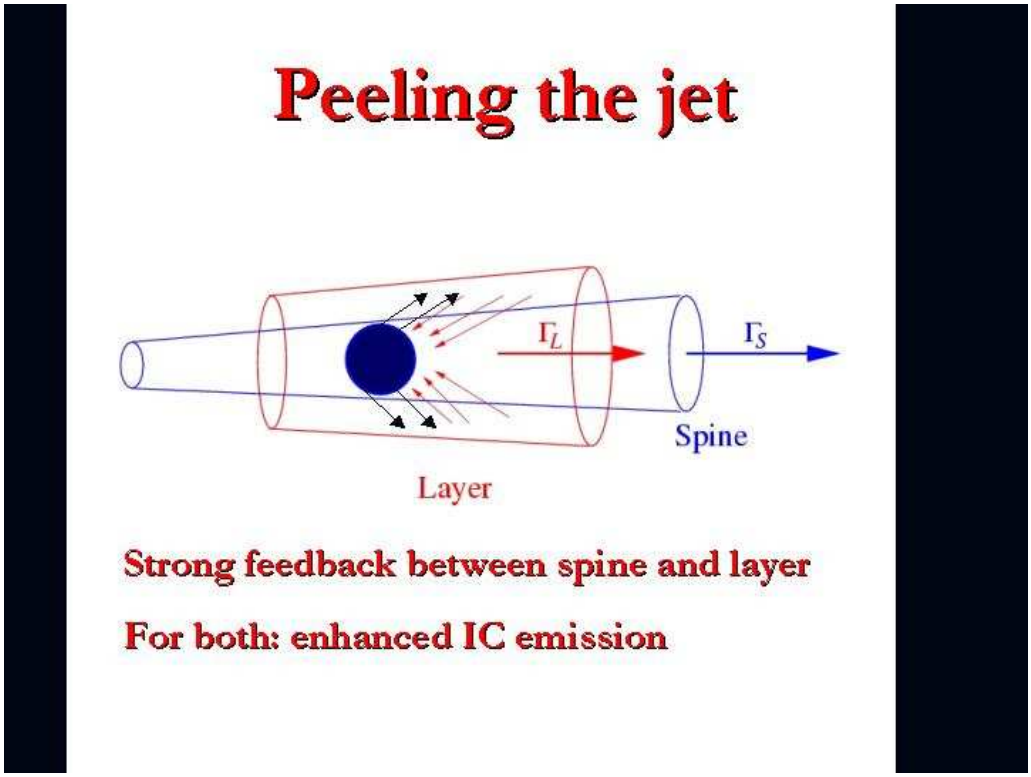
Peeling the jet
Γ_L
Γ_S
Spine
Layer
Strong feedback between spine and layer
For both: enhanced IC emission

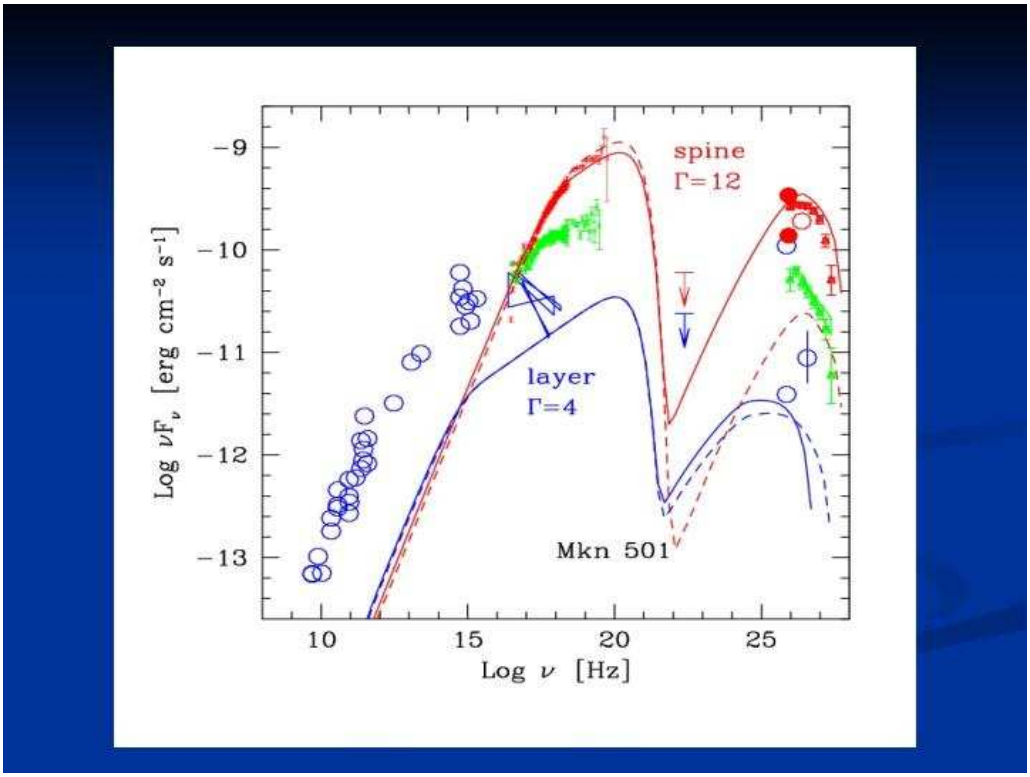

Consequences

- Jet more peeled? More dissipation. More TeV
- Low power jet are peeled more?
- Extended emission smaller for TeV?
- Large angles? Layer. Also GeV-TeV for radio-galaxies?

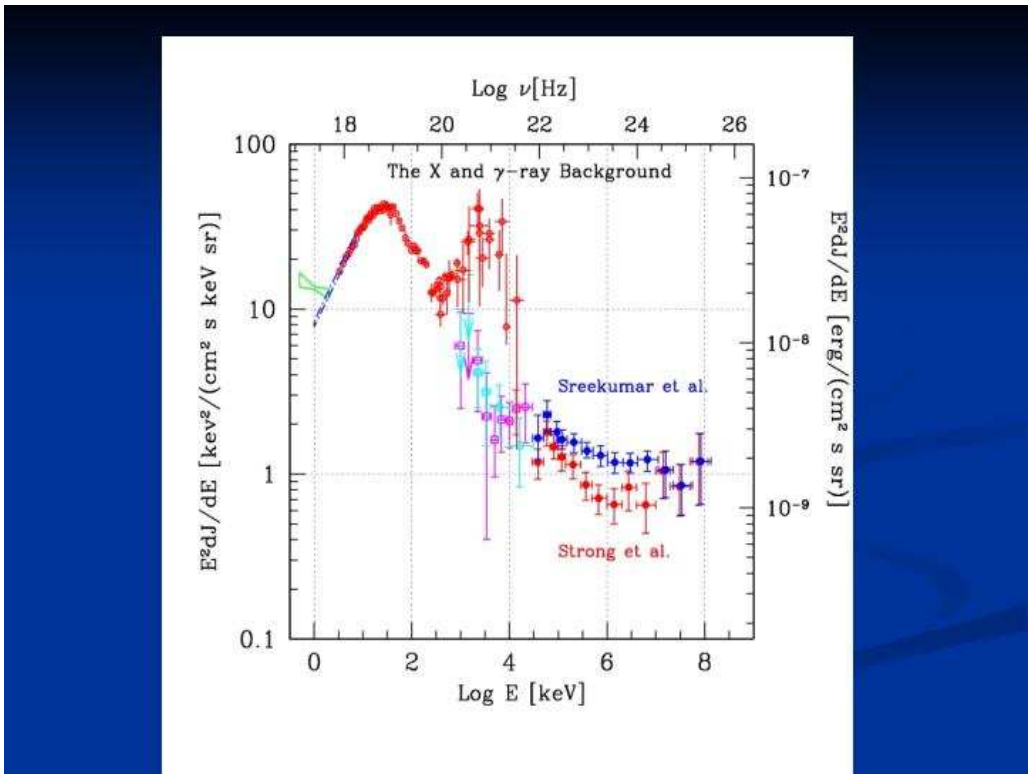
Log ν[Hz]
18
20
22
24
26
100
10
1
0.1
The X and γ-ray Background
Sreekumar et al.
Strong et al.
10^{-7}
10^{-8}
10^{-9}
E²dJ/dE [kev²/(cm² s keV sr)]
E²dJ/dE [erg/(cm² s sr)]
0
2
4
6
8
Log E [keV]

Multi-frequency & multi-epoch VLBI study of Cygnus A – U. Bach, M. Kadler, T. P. Krichbaum, E. Middelberg, W. Alef, A. Witzel, J. A. Zensus

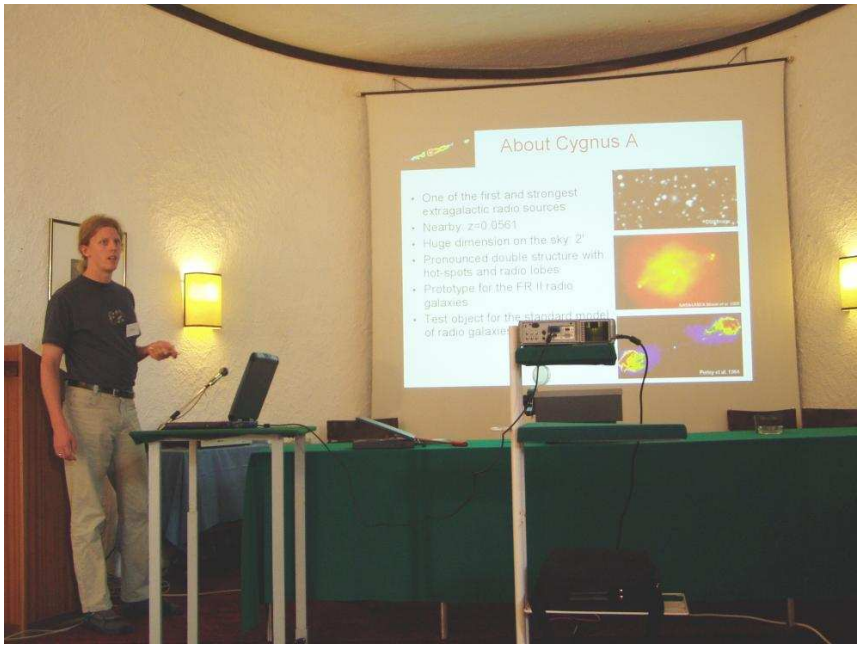

Multi-frequency & multi-epoch VLBI study of Cygnus A

Uwe Bach

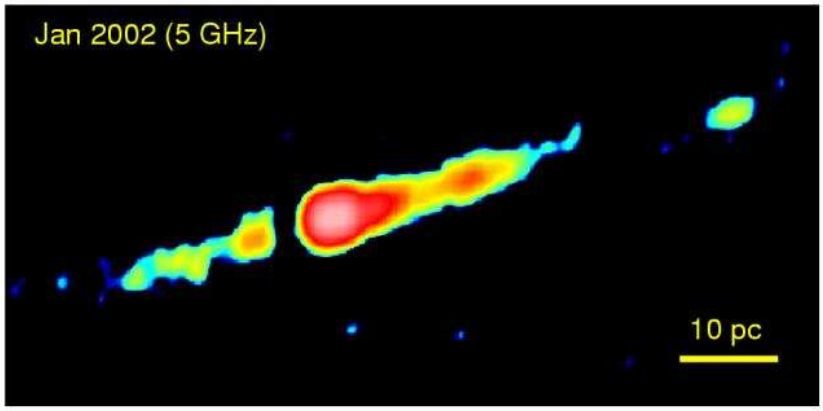

in collaboration with:

M. Kadler, T.P. Krichbaum, E. Middelberg, W. Alef, A. Witzel and J.A. Zensus

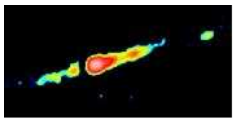

About Cygnus A

- One of the first and strongest extragalactic radio sources
- Nearby: z=0.0561
- Huge dimension on the sky: 2'
- Pronounced double structure with hot-spots and radio lobes
- Prototype for the FR II radio galaxies
- Test object for the standard model of radio galaxies and quasars

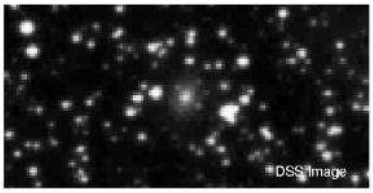

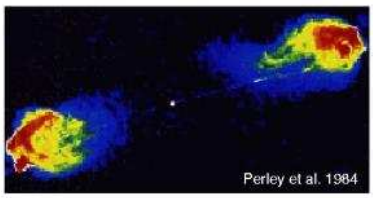

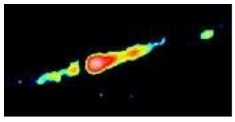

Motivation

- No phase-referencing on the core of Cygnus A was done.
- Previous proper motion studies werde done at lower frequencies (Carilli et al. 1994; Bach et al. 2002), except Krichbaum et al. 1998.
- Cygnus A is an ideal test object for jet theory and the unified scheme.

Our analysis is based on:

- Two multi-frequency epochs: 1996 at 15, 22, 43 GHz (VLBA+EB) and a phase-referencing in 2003 at 15 and 22 GHz (VLBA only)
- Two epochs at 15 GHz with VLBA+VLA1+EB in 2002

Complementary:

- 10 epochs from the VLBA 2cm Survey (Kellermann et al. 1998, AJ, 115, 1295; Zensus et al. 2002, AJ, 124, 662)

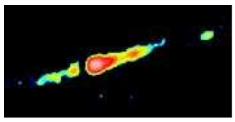

At different frequencies I

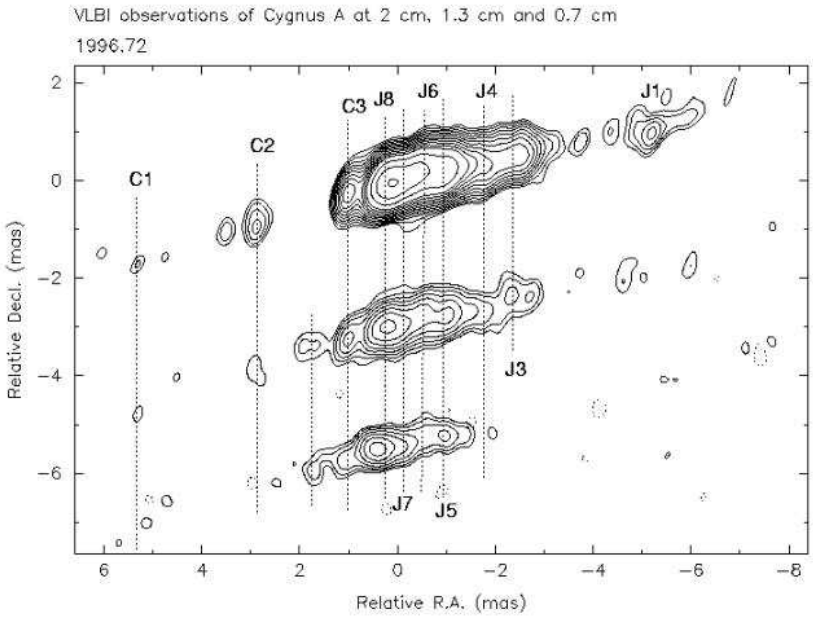

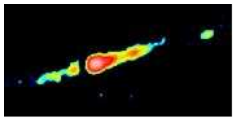

At different frequencies II

15/22 GHz

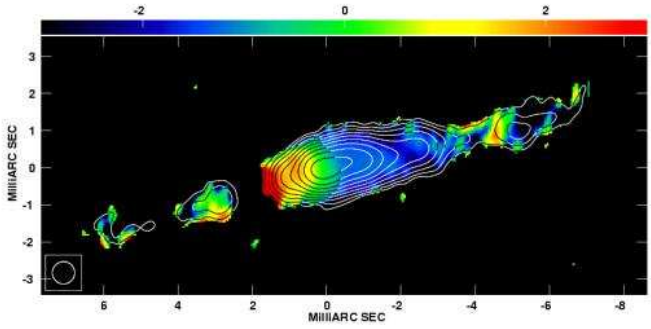

22/43 GHz

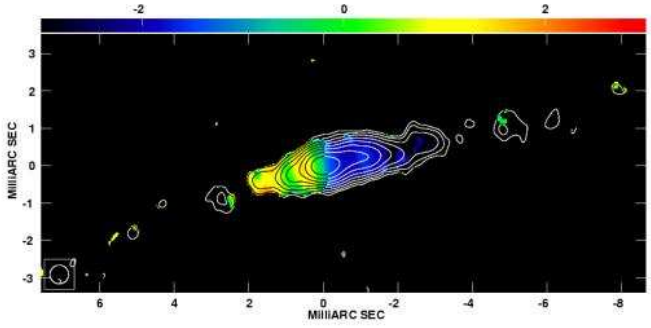

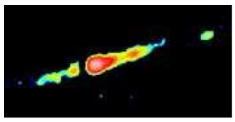

At different frequencies III

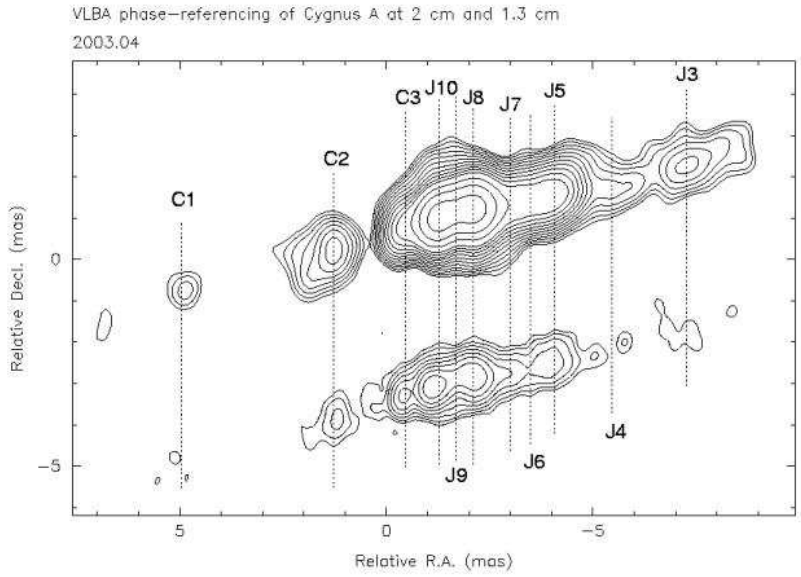

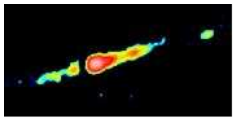

At different frequencies IV

15/22 GHz

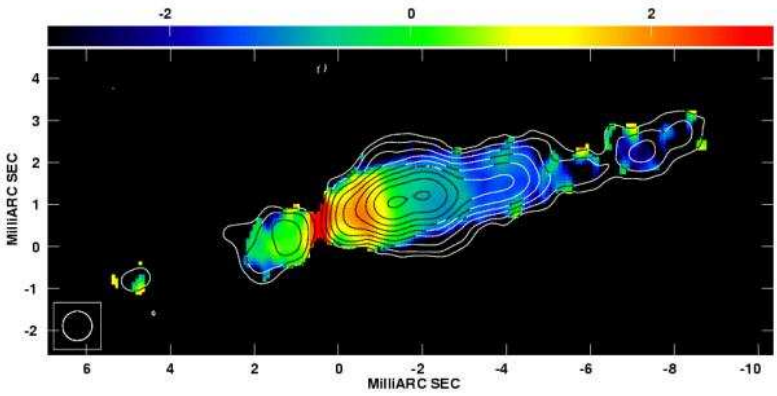

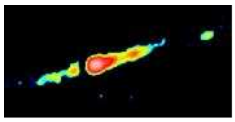

At different frequencies V

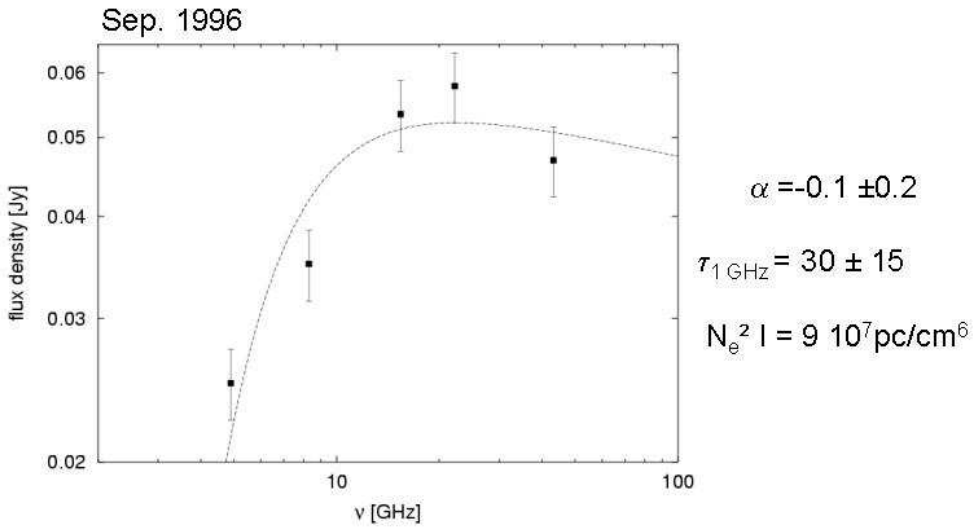

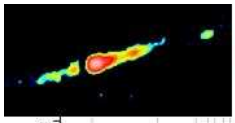

Component identification

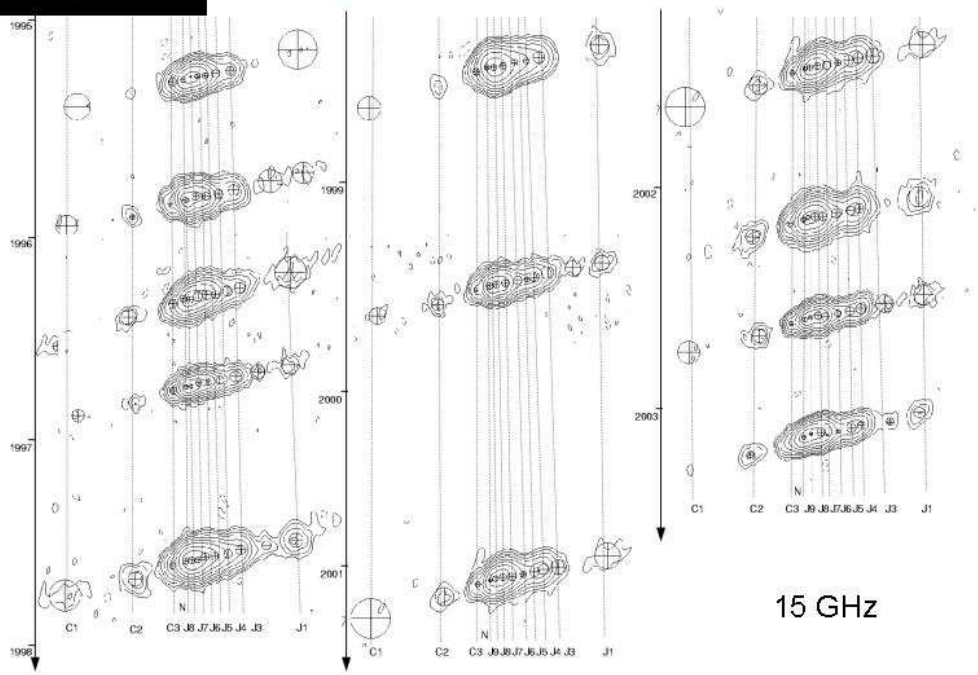

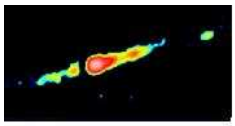

The Movie

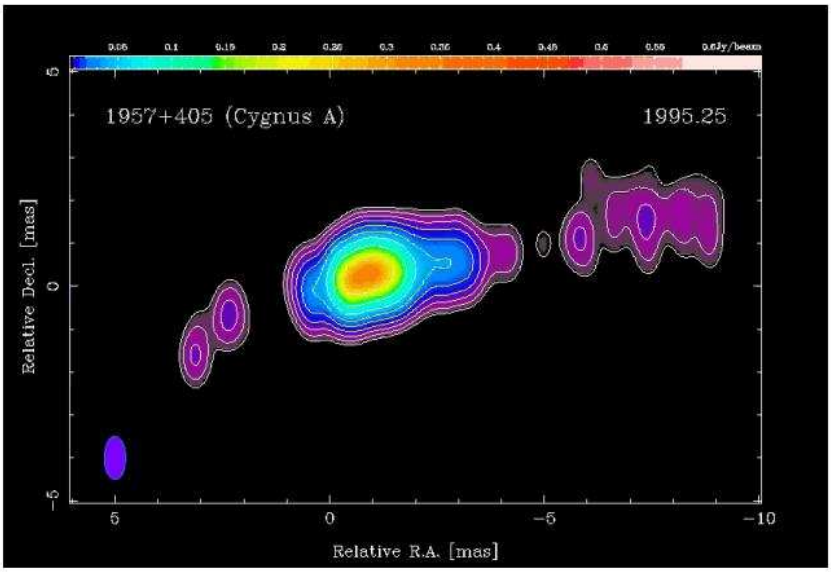

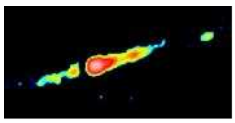

Proper motion I

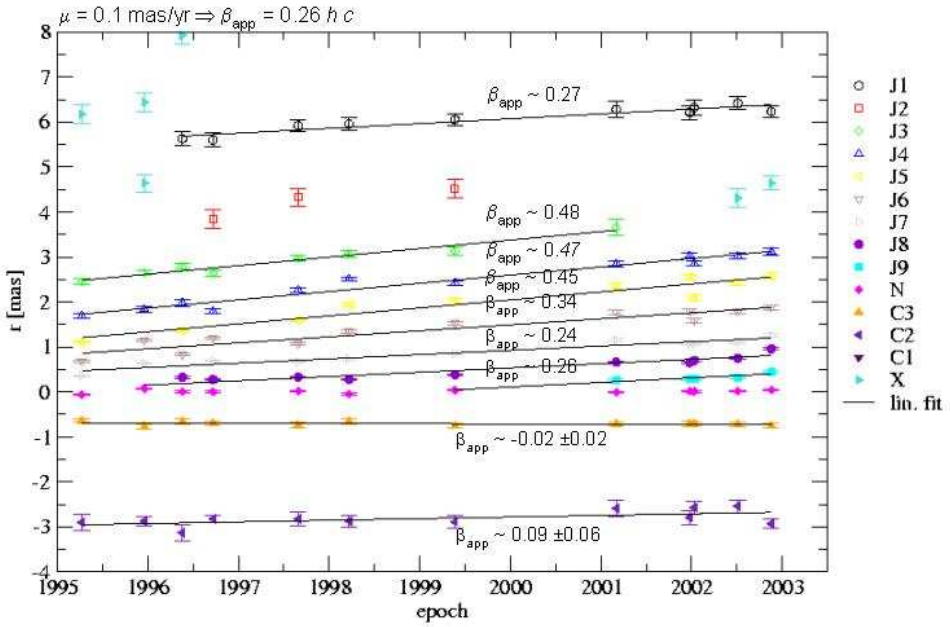

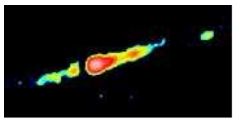

Proper motion II

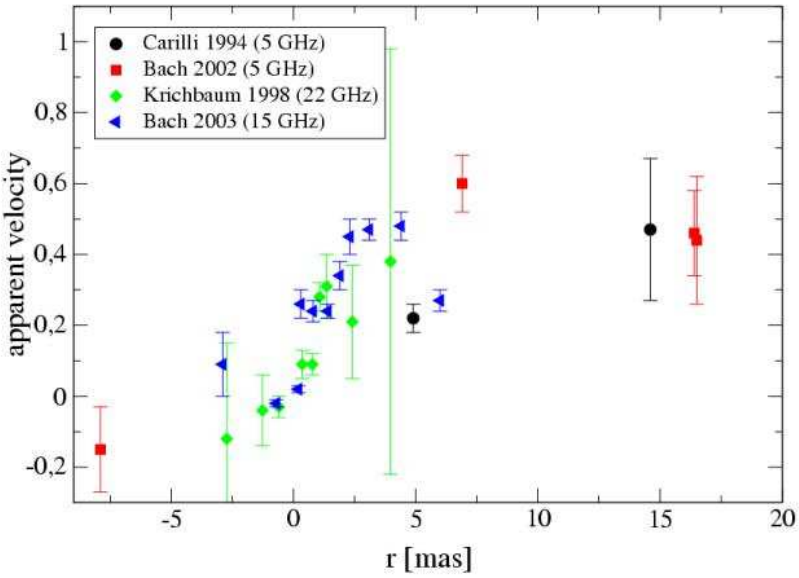

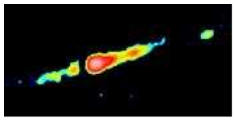

Geometry and kinematics

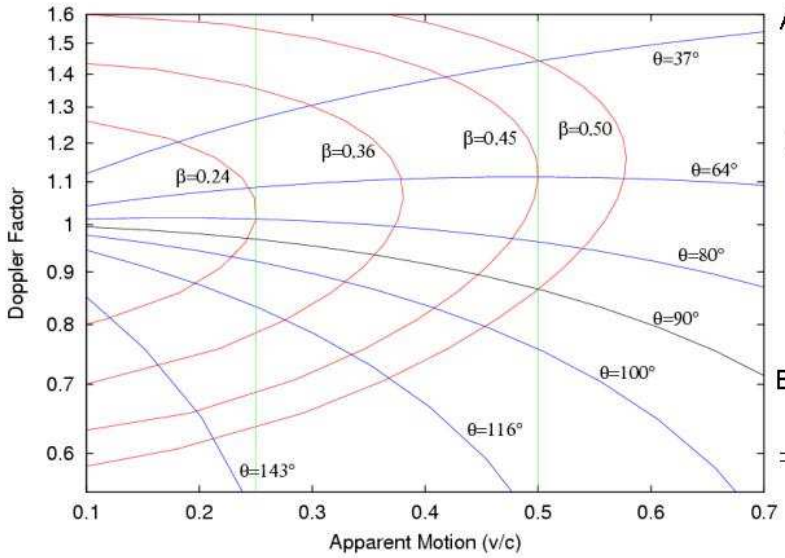

Apparent jet-speed

$\beta_{app,j} = 0.5$

Intrinsic jet-speed

$\Rightarrow \beta_{min} = 0.45$

$\Theta = 64°$

$\Rightarrow \beta_{max} = 0.50$

$\Theta = 90°$

Expected counter-jet velocity

$\Rightarrow \beta_{app,cj} = 0.32 - 0.5$

$\Theta = 90°\text{-}116°$

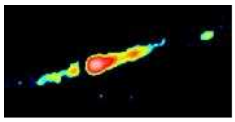

Jet to counter-jet ratio

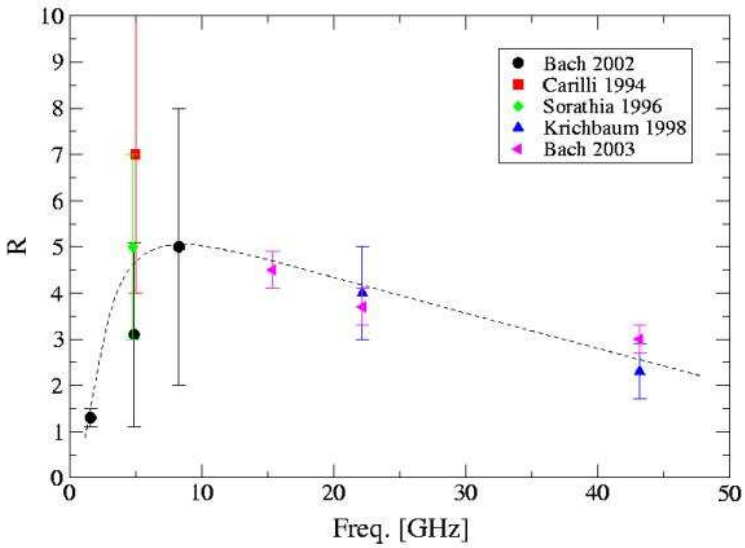

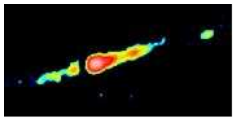

Summary

- We made the first multi-frequency phase-referencing of Cygnus A
- The spectral indices and the frequency dependent jet to counter-jet ratio can be explained by an absorber around the core
- We measured accelerated motion of up to 0.5 *c* in the jet but yet found no significant motion on the counter-jet side
- Angle to the line of sight: $\theta > 65°$
- Discrepancy between the geometry and the non-detection of apparent motion in the counter-jet questions the symmetry of jet and c-jet

→ We will continue our phase-referencing observations and will go to higher frequencies!

Jet power and spectral evolution of FRII radio galaxies – K. Manolakou, J. Kirk

Overview

- Introduction
- Why evolution?
- Previous work
- Our approach-Model description
- Results
- Conclusions
- Future trends

Introduction

- FR II sources (classical doubles): $P_{178MHz} > 10^{25}$ W Hz^{-1} sr^{-1}

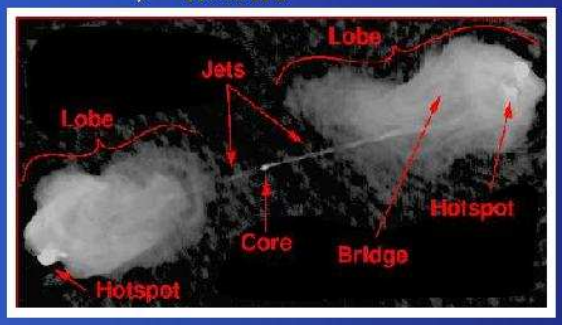

C.L. Carilli ....

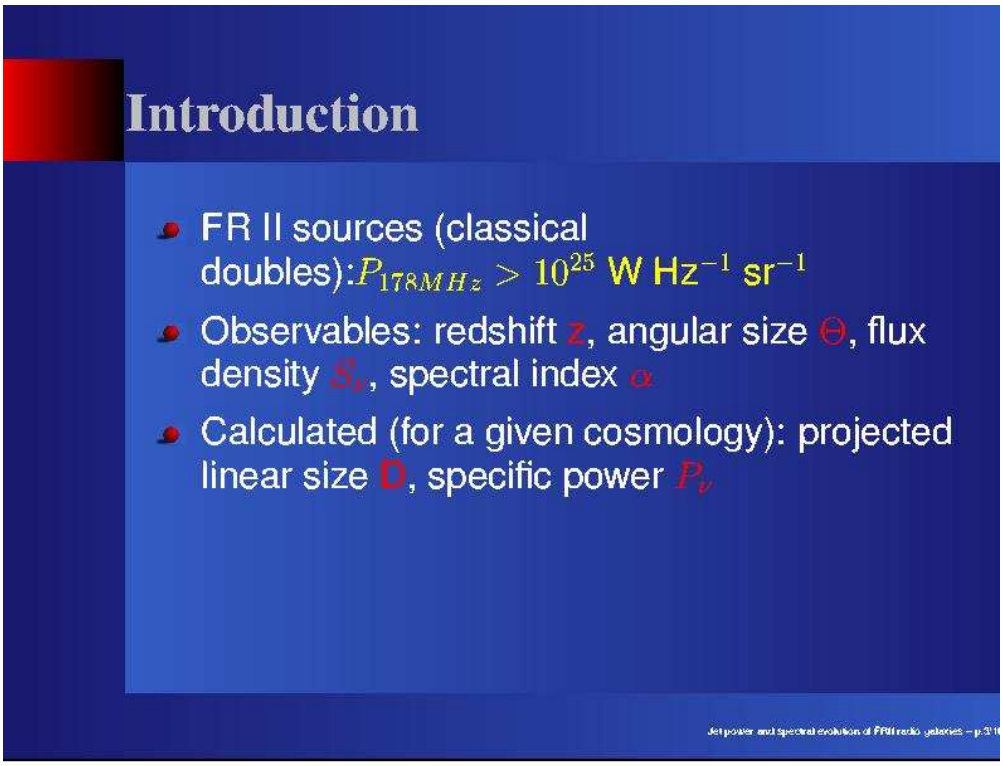
Introduction
FR II sources (classical doubles): $P_{178MHz} > 10^{25}$ W Hz^{-1} sr^{-1}
Observables: redshift z, angular size Θ, flux density S_ν, spectral index α
Calculated (for a given cosmology): projected linear size D, specific power P_ν

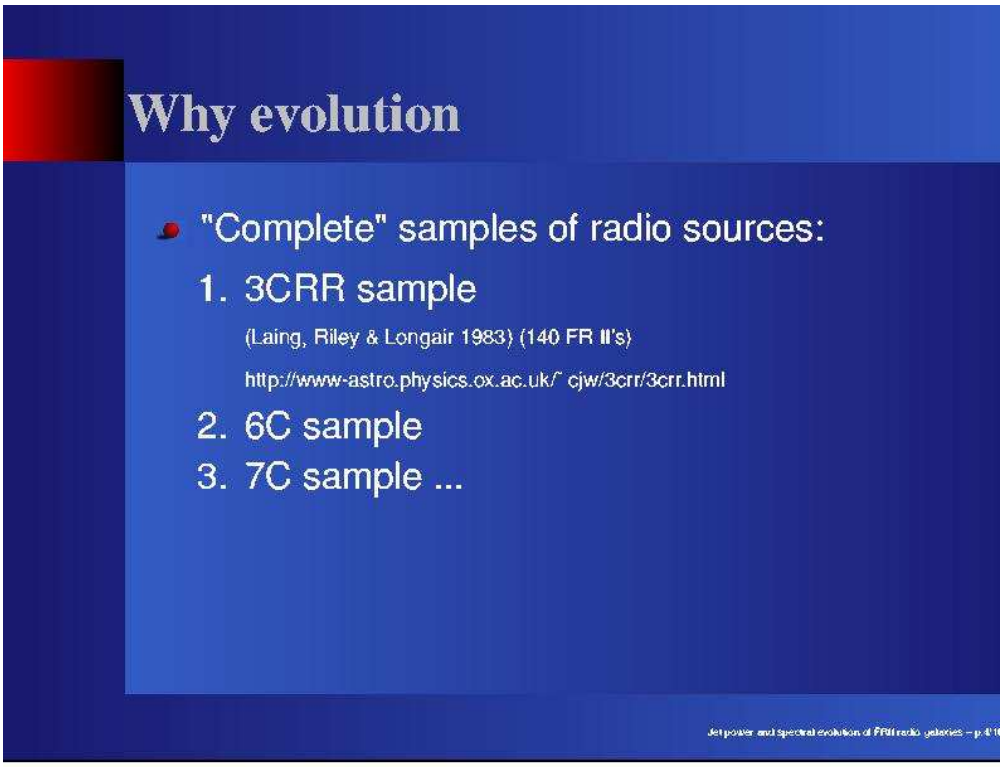
Why evolution
"Complete" samples of radio sources:
1. 3CRR sample
(Laing, Riley & Longair 1983) (140 FR II's)
http://www-astro.physics.ox.ac.uk/~ cjw/3crr/3crr.html
2. 6C sample
3. 7C sample ...

Why evolution

- Power vs linear size: P-D diagram $\Longrightarrow$ the H-R diagram of radio astronomy (Shklovsky 1963)

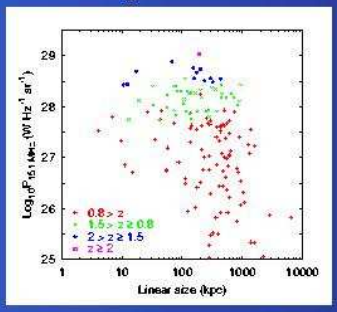

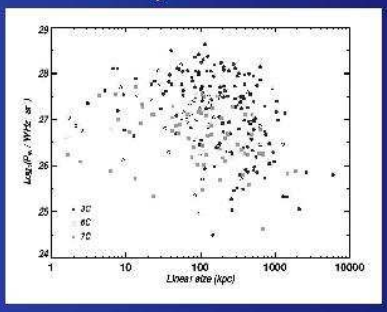

Previous work

- P_ν depends on:
  jet bulk kinetic power, Q_o,
  intergalactic(-cluster) medium $\rho(r) \propto r^{-\beta}$,
  frequency ν and
  time t.
- Falle (1991)

$$D \propto \left(\frac{t^3 Q_o}{\rho_{10\,\mathrm{kpc}}}\right)^{1/(5-\beta)} \qquad (1)$$

where $\rho_{10\,\mathrm{kpc}} = 1.27 \times 10^{-23}\mathrm{kgm}^{-3}$ and $\beta = 1.5$

- From Eq. (1) and assuming $B \equiv B_{eq}$ (at a given frequency):

$$P \propto Q_o^{(26-7\beta)/[4(5-\beta)]}\, \rho_{10\,\mathrm{kpc}}^{9/[4(5-\beta)]}\, t^{(8-7\beta)/[4(5-\beta)]} \qquad (2)$$

Previous work

- P_ν depends on:
  jet bulk kinetic power, Q_o,
  intergalactic(-cluster) medium $\rho(r) \propto r^{-\beta}$,
  frequency ν and
  time t.
- Falle (1991)

$$D \propto \left(\frac{t^3 Q_o}{\rho_{10\,\mathrm{kpc}}}\right)^{1/(5-\beta)} \qquad (1)$$

where $\rho_{10\,\mathrm{kpc}} = 1.27 \times 10^{-23}\,\mathrm{kgm}^{-3}$ and $\beta = 1.5$

- (1) and assuming $B \equiv B_{eq}$ for $\beta = 1.5$:

$$P \propto Q_o^{31/28} \rho_{10\,\mathrm{kpc}}^{9/14} t^{-5/28} \qquad (3)$$

Previous work

Blundell & Rawlings, Nature, 399, 330, 1999

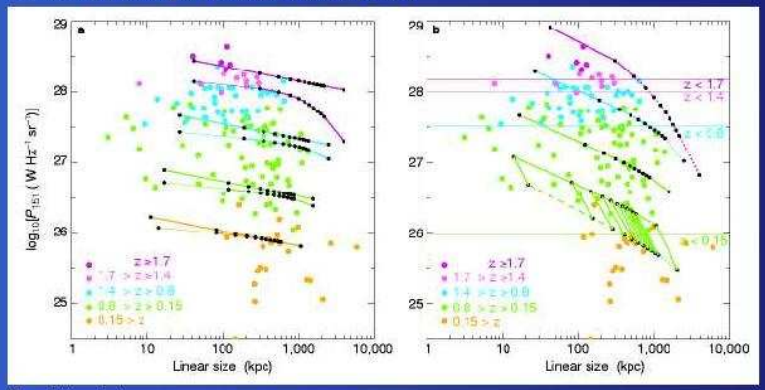

Eqs (1) & (3)

Kaiser et al., MNRAS, 292, 723, 1997
$Q_o = 5 \times 10^{39}$ W, at $z = 2$
$Q_o = 1 \times 10^{39}$ W, at $z = 0.8$

Blundell et al., AJ, 117, 677, 1999
$Q_o = 2 \times 10^{38}$ W, at $z = 0.5$
$Q_o = 5 \times 10^{37}$ W, at $z = 0.15$

Our approach: Model description I

Parameters of the model:

- Jets: constant power Q_o, constant Lorentz factor Γ; source redshift z
- External medium: $\rho = \rho_c r_c^{\beta} r^{-\beta}$, $1.5 \leq \beta \leq 1.9$
- Self-similar expansion of outer shock front (Falle 1991)
  $D(t) \propto (t^3 Q_o / \rho_c r_c)^{1/(5-\beta)}$ and of head region (Kaiser & Alexander 1997)
- but constant size of primary hot spot (Blundell at al 1999)
- Electron acceleration at the terminal jet shock: $Q_s(\gamma) = \gamma^{-p}$ for
  $\gamma_{min} \leq \gamma \leq \gamma_{max}$, $R_\gamma = \gamma_{min}/\gamma_{max}$
- Electrons are carried by turbulent fluid elements in the head region-anomalous transport: $\langle \Delta x^2 \rangle \propto t^{\alpha}$, $0 < \alpha < 2$ CTRW formalism (Ragot & Kirk 1997)
- τ = transport time/cooling time at γ_{min}

Model description II

Head:

- energy density u_h in the primary hot spot constant
- $u_{lobe} \propto t^{-(4+\beta)/(5-\beta)}$
- adiabatic losses:
  $Q_{lobe}(\gamma, t) = k Q_h(k\gamma, t)$
  where $k(t) = [u_h/u_{lobe}(t)]^{1/4}$, imposed after transport through head region

Model description II

& Lobe region:

- integrated spectrum required - no spatial transport
- adiabatic loss rate $\propto 1/t$
- synchrotron loss rate $\propto \gamma t^{-(4+\beta)/(5-\beta)}$
- inverse compton loss rate $\propto \gamma$
- We solve: $\frac{\partial N}{\partial t} + \frac{\partial}{\partial \gamma}(\dot{\gamma} N) = Q_{lobe}(\gamma, t)$

Results - I: P-D tracks

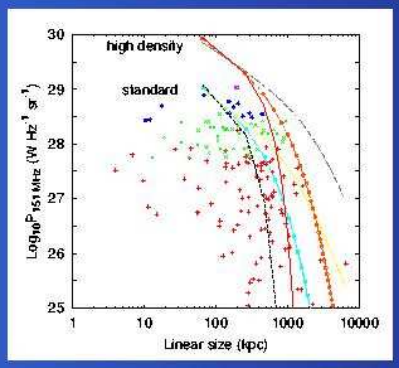

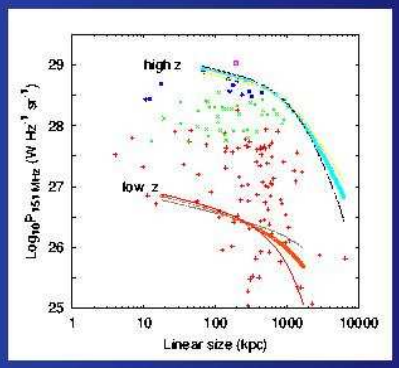

Standard model:

$Q_o = 1.3 \times 10^{40}$ W,
$\rho_c = 1.7 \times 10^{-23}$ kg m^{-3}

High density/jet power model:

$Q_o = 6.5 \times 10^{40}$ W,
$\rho_c = 1. \times 10^{-22}$ kg m^{-3}

Much more rapid decay than previous work

Low z model:

$Q_o = 1.3 \times 10^{38}$ W, $z = 0.2$

High z model:

$Q_o = 1.3 \times 10^{40}$ W, $z = 2.0$


Conclusions
New model developed with more realistic transport parameters
in contradiction with previous models and with the data
relieved by proposed additional acceleration process
hypothesis supported by studies of individual sources
model contains fewer parameters than those in literature
Suitable for extensive population simulation studies

Helical jets in blazars: Interpretation of the multifrequency variability of AO 0235+16 – L. Ostorero, M. Villata, C. M. Raiteri

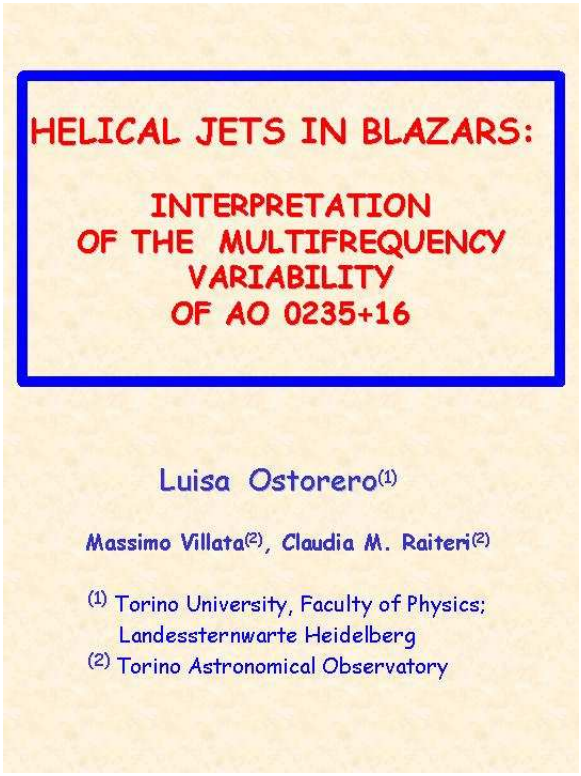

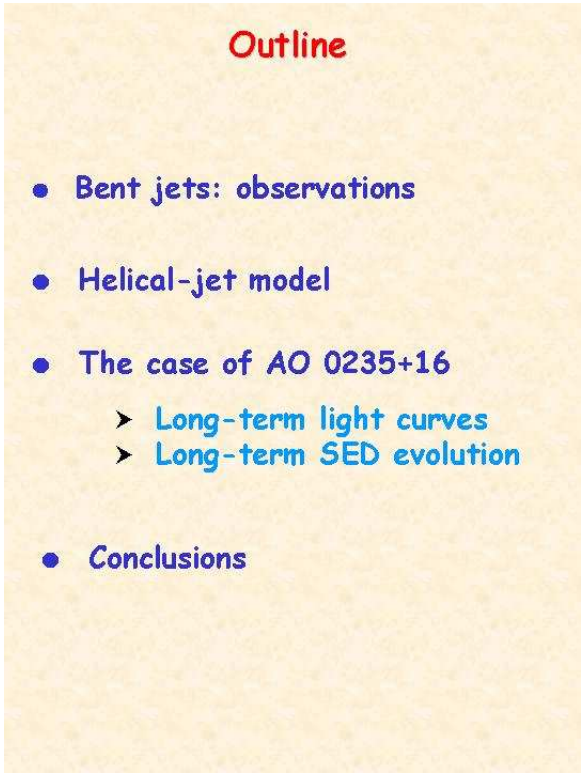

HELICAL JETS

Jet bending:

⇒ observed in radio-loud AGNs

⇒ interpretable as projection of a helical pattern possibly due to the presence of a BBHS (orbital motion, precession)

Mkn 501

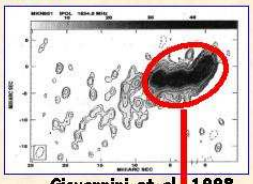

Giovannini et al. 1998

Space VLBI

~ pc scales

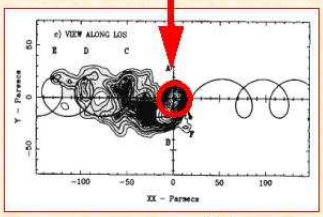

Conway & Wrobel 1995

VLBA

~ 100 pc scales

HELICAL-JET MODEL

~ pc scales distortions : ORBITAL MOTION

~100 pc scales distortions : PRECESSION

Intepretation of the blazar emission variability as:

- *Intrinsic:* originating within the source, and not between the source and the observer
- *Geometrical:* due to variation of beaming factor because of geometrical effects

PAST APPLICATIONS

THE HUGE X-RAY SPECTRAL VARIATIONS OF MKN 501 [Villata & Raiteri 1999, Raiteri et al. 2003]

THE VARIATIONS OF THE SPECTRAL ENERGY DISTRIBUTION (SED) OF S4 0954+65 (low energies) [Raiteri et al. 1999]

THE VARIABILITY OF THE SEDs OF 1219+285 (ON 231) AND S5 0716+71 (low and high energies) [Sobrito et al. 2001, Ostorero et al. 2001]

The helical jet

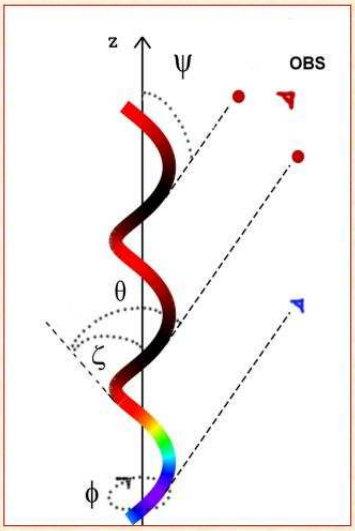

JET RADIATION

- RADIO
- IR
- OPTICAL
- X-UV

ψ : angle bw the jet axis (z) and the line of sight

θ : angle bw the local jet orientation and the l.o.s.

ζ : helix pitch angle

ϕ(t) : azimuthal orientation of the first slice of the jet, *changing with the helix rotation*

Jet emission law

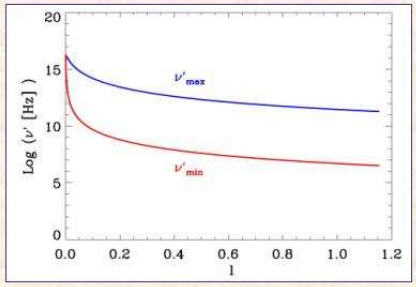

Synchrotron radiation

$$\begin{cases} \nu'^{S}_{\min}(l) = \nu'^{S}_{\min}(0)(1+l/l_1)^{-c_1} \\ \nu'^{S}_{\max}(l) = \nu'^{S}_{\max}(0)(1+l/l_2)^{-c_2} \end{cases}$$

Inverse-Compton radiation

$$\begin{cases} \nu'^{C}_{\min}(l) = \frac{4}{3}\nu'^{S}_{\min}(l) \\ \nu'^{C}_{\max}(l) = \frac{4}{3}\gamma^{2}_{\max}(l)\cdot\nu'^{S}_{\max}(l) \end{cases}$$

SSC ⇒ Only synchrotron photons are comptonized: no external contribution

Observed flux

$dF_\nu(\nu) \propto \delta^3 \cdot \nu^{-\alpha 0} \cdot dl$ where:

$$\delta = \delta(l) = \frac{1}{\Gamma[1-\beta\cdot\cos\vartheta(l)]}$$

$\vartheta = \vartheta(l; \psi, \phi, \zeta)$

$dF'_{\nu'}(\nu')$ = constant
ϑ = variable

⇨ $dF_\nu(\nu)$ = variable

SPECTRAL CHANGES WITHOUT INTRINSIC VARIATONS

THE CASE OF AO 0235+16

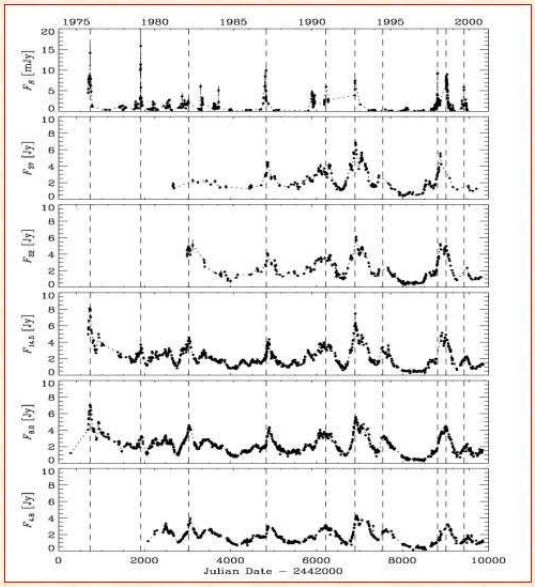

Possible periodicity : T ≅ 5 - 6 years
(Raiteri et al. 2001)

THE GOAL

(A) THE LONG-TERM MW LIGHT CURVES

(B) THE LONG-TERM SED TIME EVOLUTION

Helix rotation

$\phi = \phi(t)$ ⇨ $F_\nu = F_\nu(t)$

∃ Periodicity ⇨ calibration of $\phi = \phi(t)$

$\Delta\phi = 360°$ ⇔ $\Delta t = T$

JET PHYSICS

Emitted synchrotron frequencies

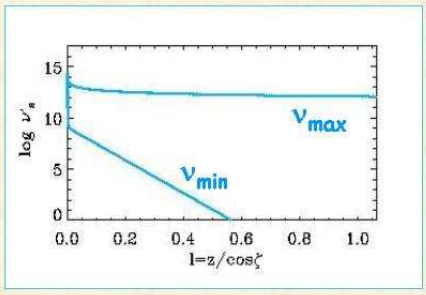

Shading factor – emissivity –

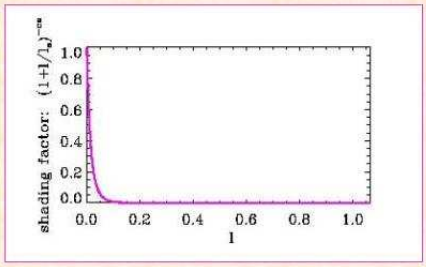

JET PHYSICS

Emitted synchrotron frequencies

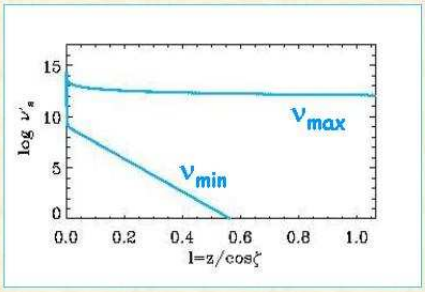

Shading factor – emissivity –

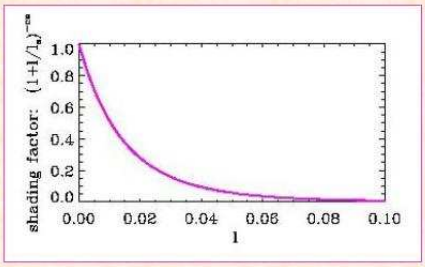

(A) THE BEHAVIOUR OF LIGHT CURVES

$\phi = \phi(t) \Rightarrow F_\nu = F_\nu(t)$

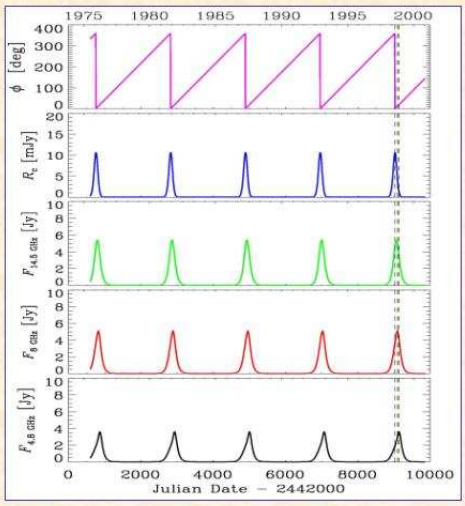

AO 0235+16: Multi-λ modelled light curves
(Ostorero et al. 2003, A&A, in prep.)

Zooming an outburst

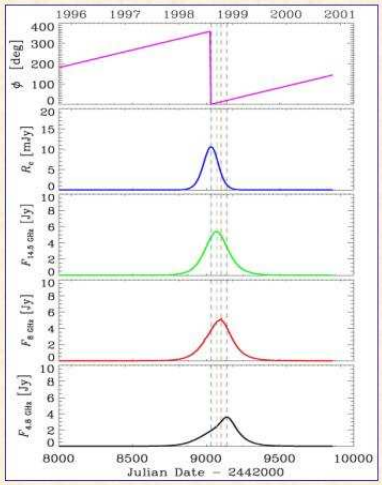

Well reproduced:

- F_{OPT} / F_{RAD}
- Deacreasing peak radio flux at low radio ν
- ~ Simultaneity of optical and radio oubursts

Model prediction and observations at ν = 8 GHz

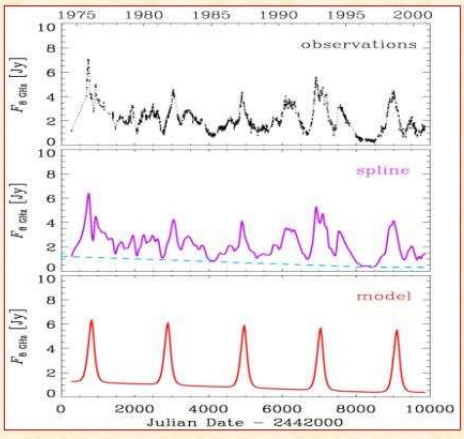

The observed light curve shows many minor outbursts interspersed among the major ones:

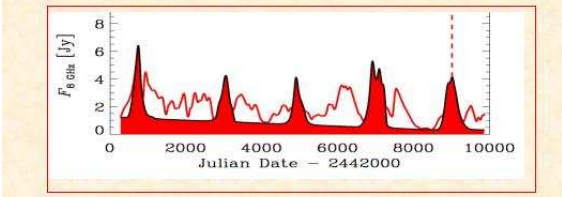

Periodical outbursts extracted from the observed LC

WHAT IS THEIR ORIGIN?

1 Distortions of the helix

2 Other phenomena

Other phenomena (energetic or geometric) originate minor outbursts

Pinching effect

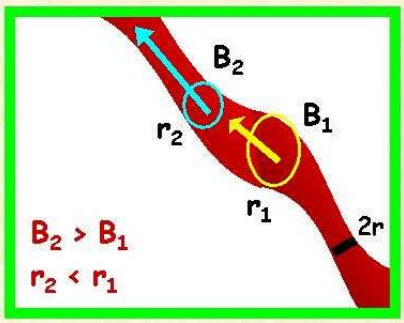

$B \propto r^{-2}$

$j_{\nu,syn} \propto B^{1+\alpha}$ ⇒ $F_{\nu,syn} \propto r^{-2\alpha}$

Pinching enhances local emissivity and flux density

Pinching effect

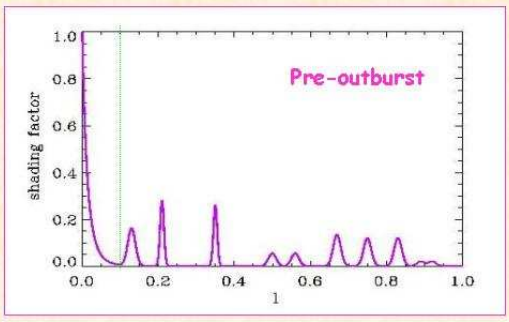

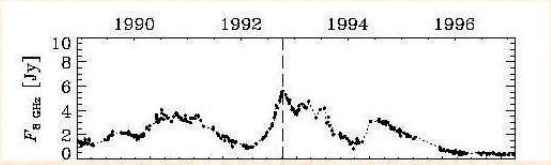

Periodic outburst 1992-93

Pinching effect

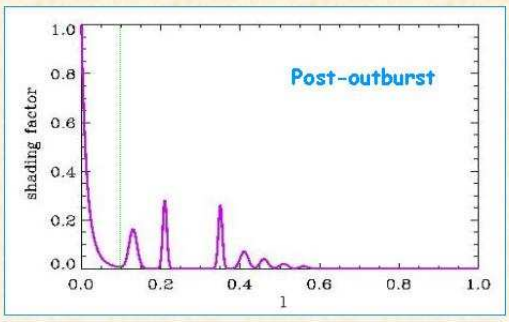

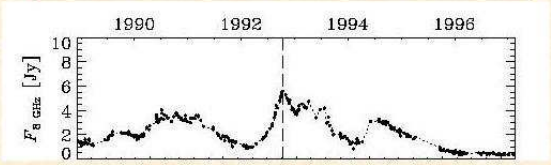

Periodic outburst 1992-93

Pinching effect

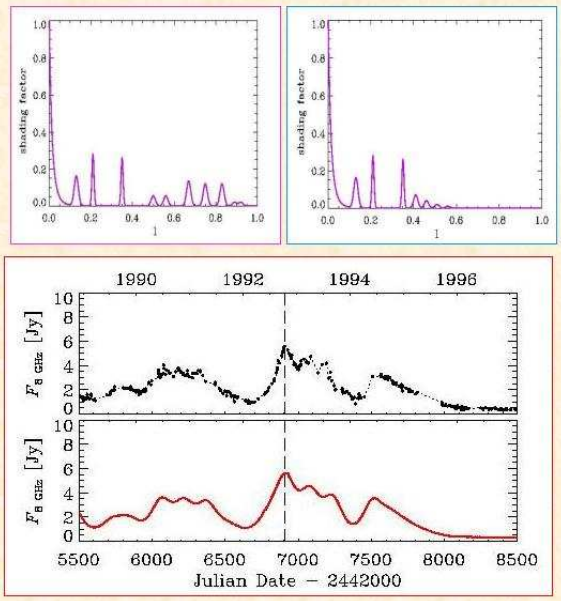

Minor outbursts are well reproduced

(B) THE SED TIME EVOLUTION

Hyp.1: X-rays from inverse-Compton process

AO 0235+16

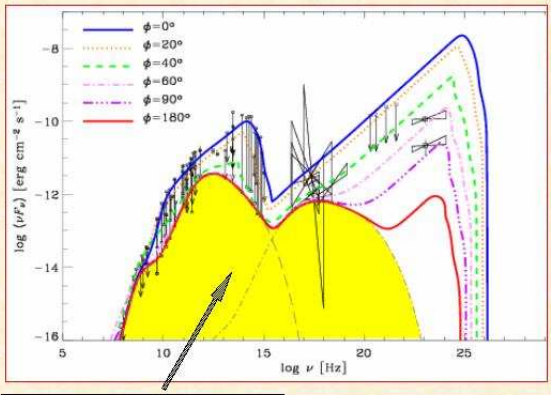

Base level (from MW light curves)

(Ostorero et al. 2003, A&A, in prep.)

Hyp.2: soft X-rays from synchrotron process

AO 0235+16

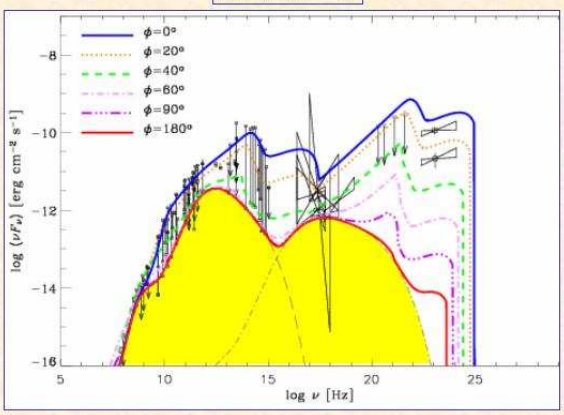

- Steep X-ray spectrum for small viewing angles ϕ
- Compton peak in the MeV region

Prediction for the next outburtsts: 2004, 2009, ...

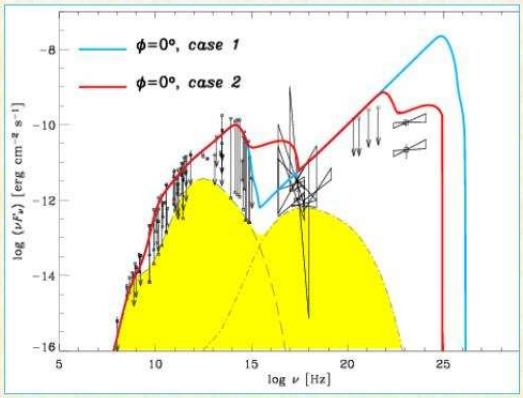

FUNDAMENTAL : Broad-band MW observing campaigns

2003-2004 ongoing campaign (see talk C.Raiteri): intensive monitoring in the radio/optical/X-ray bands

CONCLUSIONS

The helical model provides a geometrical interpretation of blazar multifrequency variability

The rotation of a steadily-emitting helical jet can describe:

- the long-term SED time evolution
- the long-term behaviour of multifrequency light curves of periodic sources

The presence of minor outbursts interspersed among the periodic ones (case of AO 0235+16) could be ascribed to:

1) geometrical distortions of the helical structure
2) contribution of some other phenomena (→ *pinching*)

Campaign session I: Past and ongoing campaigns

The ongoing WEBT/ENIGMA campaigns on AO 0235+16 and 3C 66A

– C. M. Raiteri, M. Villata, M. Böttcher, on behalf of the WEBT collaboration

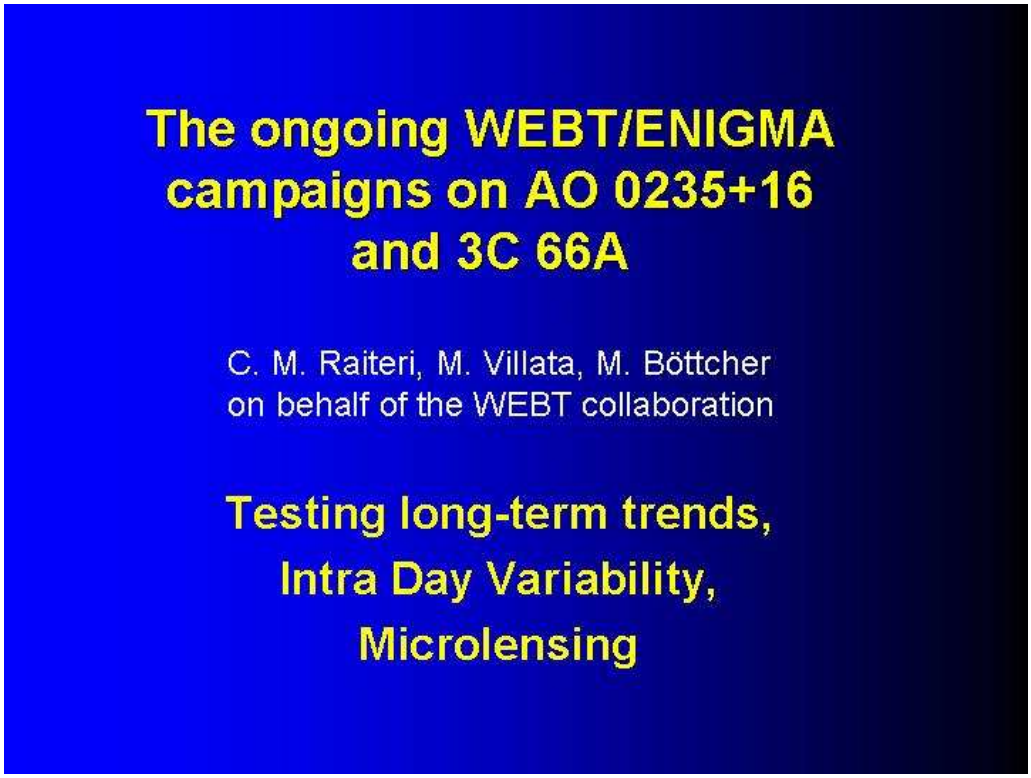

Simultaneous MW monitoring of 3C 66A

(WEBT+RXTE+STACEE+CELESTE+VERITAS+VLBA)

Campaign manager: Markus Böttcher

Period: mid Sept. – mid Dec., 2003

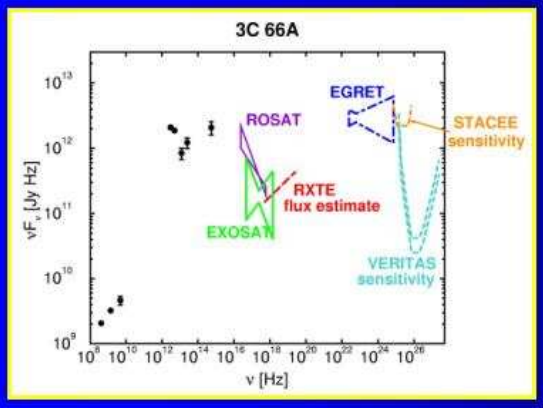

Scientific tasks:

a) *Measure simultaneous SED from radio to TeV band*

b) *Test for flux and spectral variability on long time scales (weeks)*

c) *Test for IDV, especially in X-ray and optical bands*

d) *Model the results to give predictions for intrinsic TeV fluxes*

3C 66A: recent optical behaviour

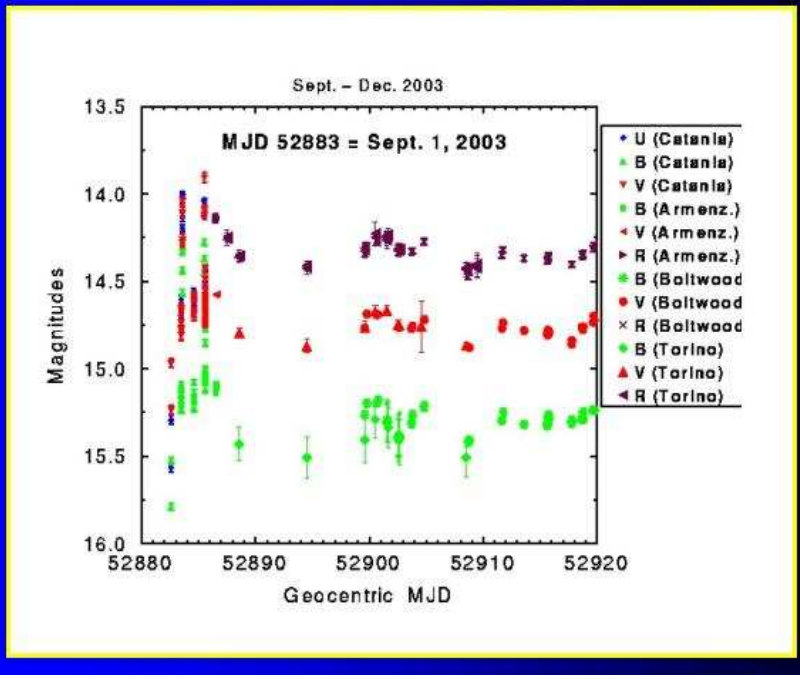

AO 0235+16: periodic behaviour?

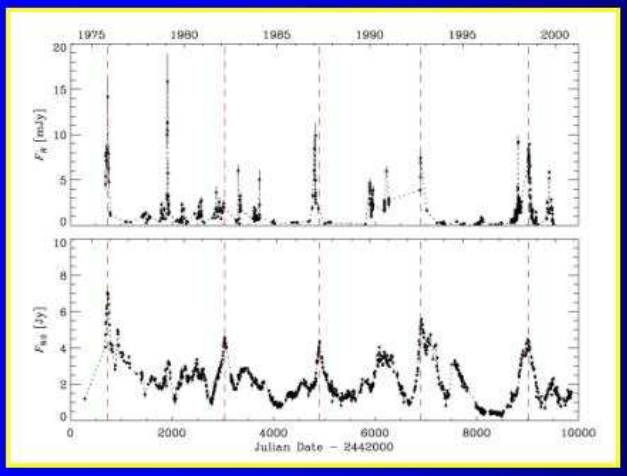

P = 5.7 ± 0.5 yr

Next outburst:

Feb-March 2004

WEBT campaign:
radio+near-IR
+optical

(Raiteri et al. 2001, A&A 377, 396)

WEBT participants

Radio observations: UMRAO + Metsähovi + RATAN

IR observations: JHK at Campo Imperatore, Italy (1.1 m)

Optical observations (preliminary):

KOREA: Sobaek Telescope (0.6 m)

INDIA: Vainu Bappu Obs. (2 m)

UZBEKISTAN: Maidanak Obs. (1.5 m)

UKRAINE: Crimean Obs. (1.25 m)

FINLAND: Tuorla Obs. (1.03 m), Nyrola Obs. (0.4 m)

GREECE: Skinakas Obs. (1.3 m)

ITALY: Catania Obs. (0.91 m), Vallinfreda Station (0.5 m),
Armenzano Obs. (0.4 m), Perugia Obs. (0.4 m), Torino Obs. (1.05 m)

SPAIN: Teide Obs. (0.82 m), NOT (2.56 m)

USA: Bell Obs. (0.6 m), SARA Obs. (1 m), Mt. Lemmon Obs. (1 m),
Coyote Hill Obs. (0.28 m)

MEXICO: San Pedro Martir (1.5 m)

AO 0235+16: XMM observations

3 XMM pointings approved with priority A:

1) 30 ksec, January 18-26, 2004

→ *Testing rapid X-ray variability and radio IDV with Effelsberg*

2) 10 ksec, August 1-15, 2004

3) 10 ksec, January 21-31, 2005

→ *Testing long-term X-ray spectral changes*

AO 0235+16: testing the microlensing scenario with TNG and NTT spectra

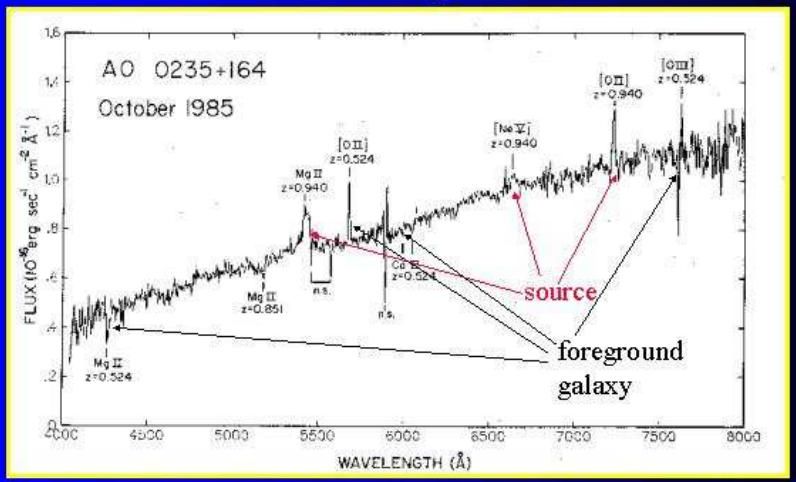

(Cohen et al. 1987, ApJ 318, 577)

AO 0235+16: frequency ranges covered

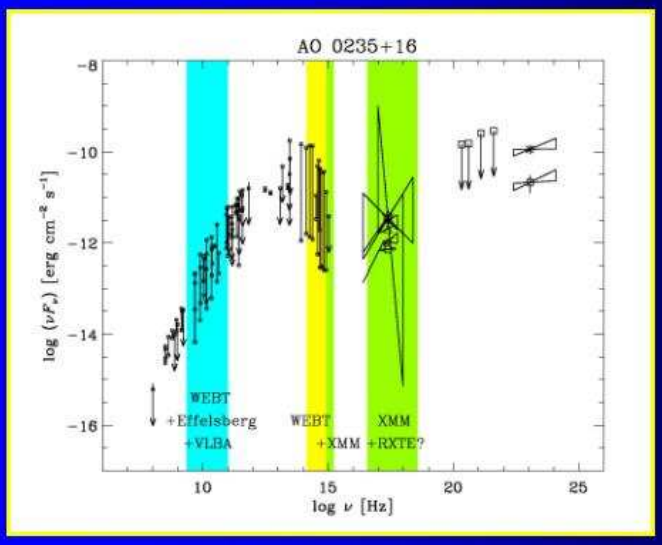

WEBT

XMM

Effelsberg

VLBA

TNG (NTT?)

RXTE?

AO 0235+16: radio behaviour
(up to mid August 2003)

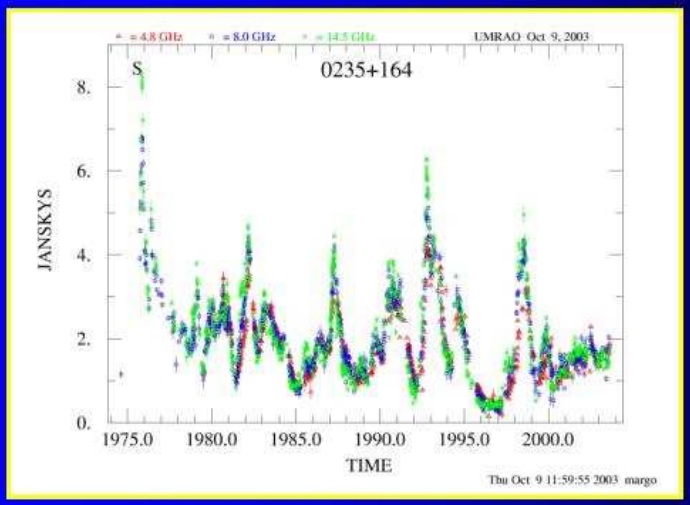

UMRAO recent data show the source in a faint state (Margo Aller, private communication)

Metsähovi data confirm these results (Harri Teräsranta, private communication)

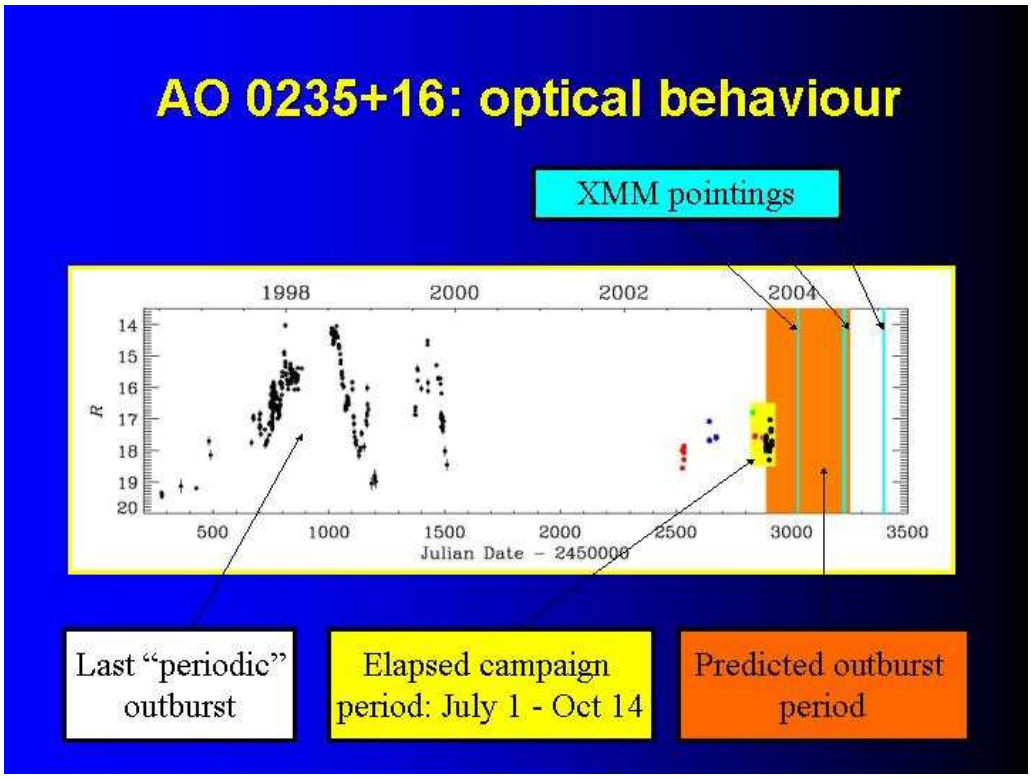
AO 0235+16: optical behaviour
XMM pointings
1998
2000
2002
2004
R
14
15
16
17
18
19
20
500
1000
1500
2000
2500
3000
3500
Julian Date – 2450000
Last "periodic" outburst
Elapsed campaign period: July 1 - Oct 14
Predicted outburst period

VLBA observation plans for AO 0235+164 and 3C 66A – L. O. Takalo, T. Savolainen, K. Wiik

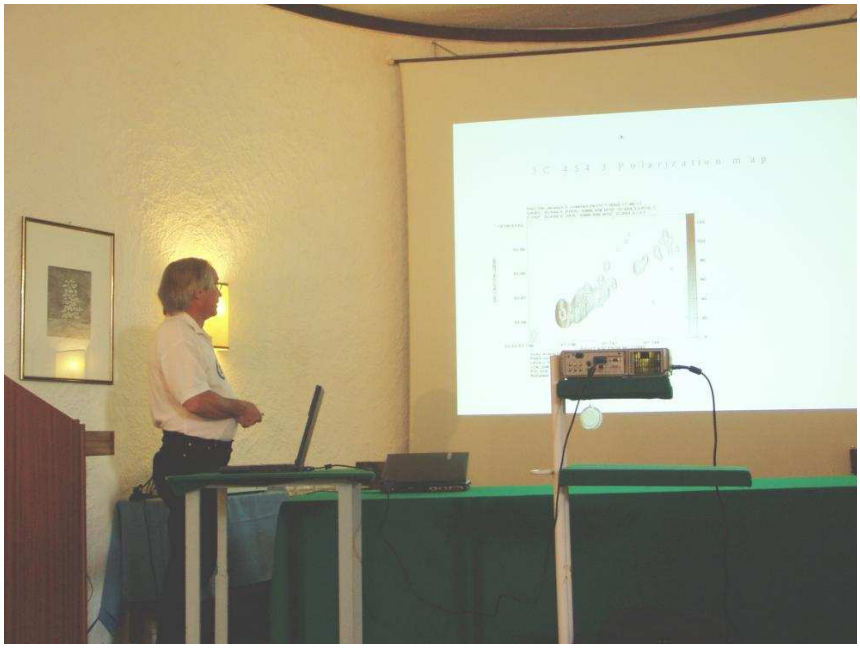

VLBA observation plans for AO 0235+164 and 3C 66A

L.O. Takalo, T. Savolainen, K. Wiik
Tuorla Observatory

Multifrequency plans

- WEBT
- KVA (Polarization)
- Radio (Metsahovi, Michigan, Bonn)
- VHE (Whipple, MAGIC, Celeste, Stacee)
- XMM (AO 0235+164)
- RXTE (3C 66A; Böttcher)

Plan

- Wavelengths: 13, 6, 3.6, 1.3, 0.7, 0.3 cm
- Frequences: 2, 5, 8, 22, 43, 86 Ghz
- Including Polarimetry
- Polarimetric calibration sources: 0420-014, 3C454.3, OJ 287

3C 454.3 Polarization map

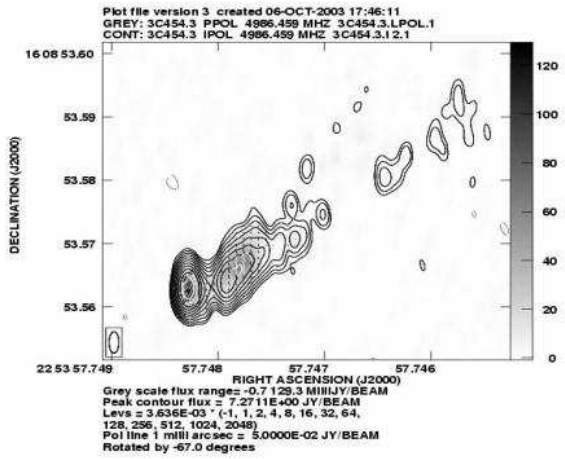

Plans for 3C 66A

- 3C 66A received 9 epochs (asked for 6)
- 3C 66A already in the "dynamical queue" with high priority. First epoch will be observed soon as weather and antennas are in optimal configuration. Then we will get observations once a month.

3C 66A (Jorstad et al. 2001)

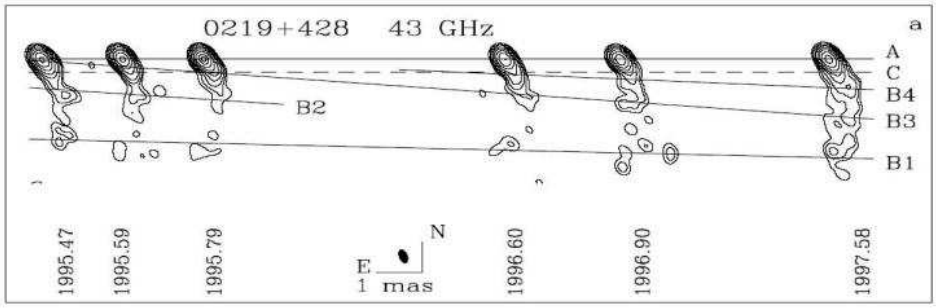

Plans for AO 0235+164

- AO 0235+164 received 15 epochs (asked for 10)
- Will be in "Dynamical queue" soon with high priority.
- Then we will get about observations once a month.

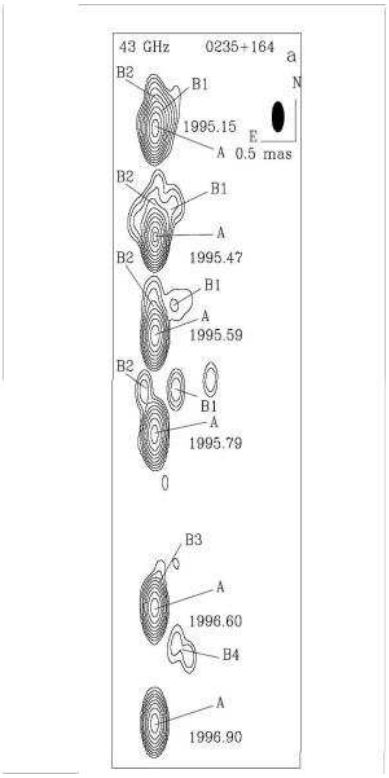

Jorstad et al. 2001

Expected Results

- Multifrequency Radio maps
- Polarization maps
- Jet changes at several epochs: Components, component movements and speeds, flux and polarization variability
- Spectra for each component and it's variability
- Frequency dependent polarization
- Multifrequency spectra

L3 CCD campaigns – update – N. Smith, A. O'Connor, A. Giltinan, S. O'Driscoll, J. Howard, S. Wagner, M. Hauser

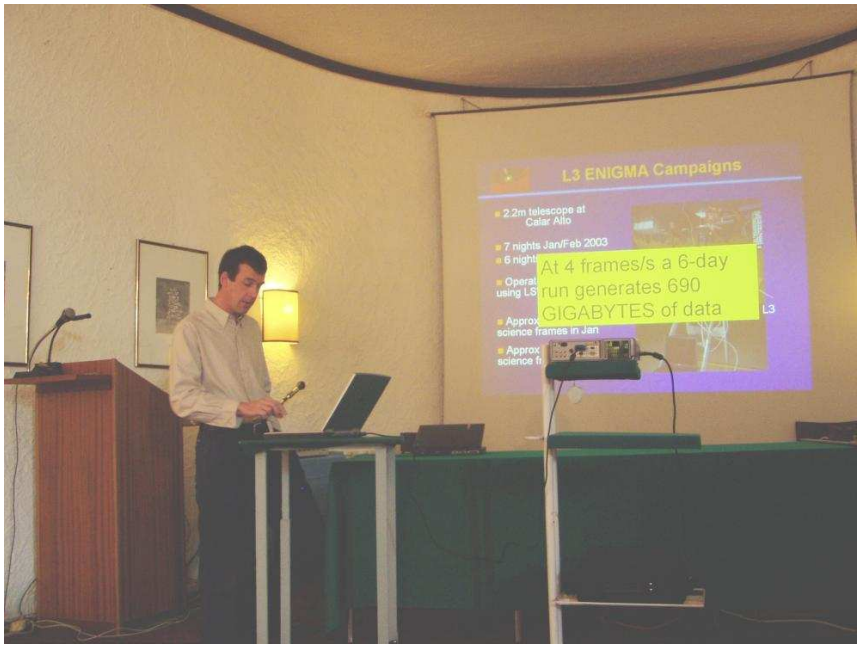

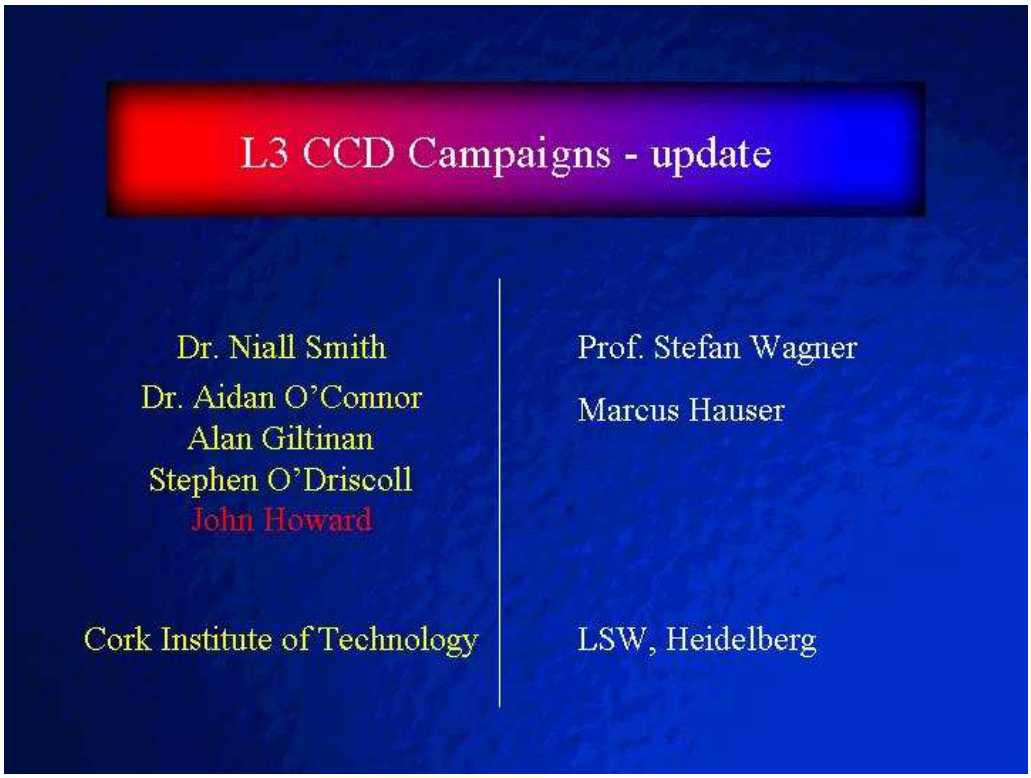

Sources Observed (Sept.)

PG 0716+714

BL Lac

PKS 2155-304

Mrk 501

PG 1718+481

L3 ENIGMA Campaigns

- 2.2m telescope at Calar Alto
- 7 nights Jan/Feb 2003
- 6 nights Sept 2003
- Operated at Cass and using LSW focal reducer
- Approx. 70,000 science frames in Jan
- Approx. 340,000 science frames in Sept.

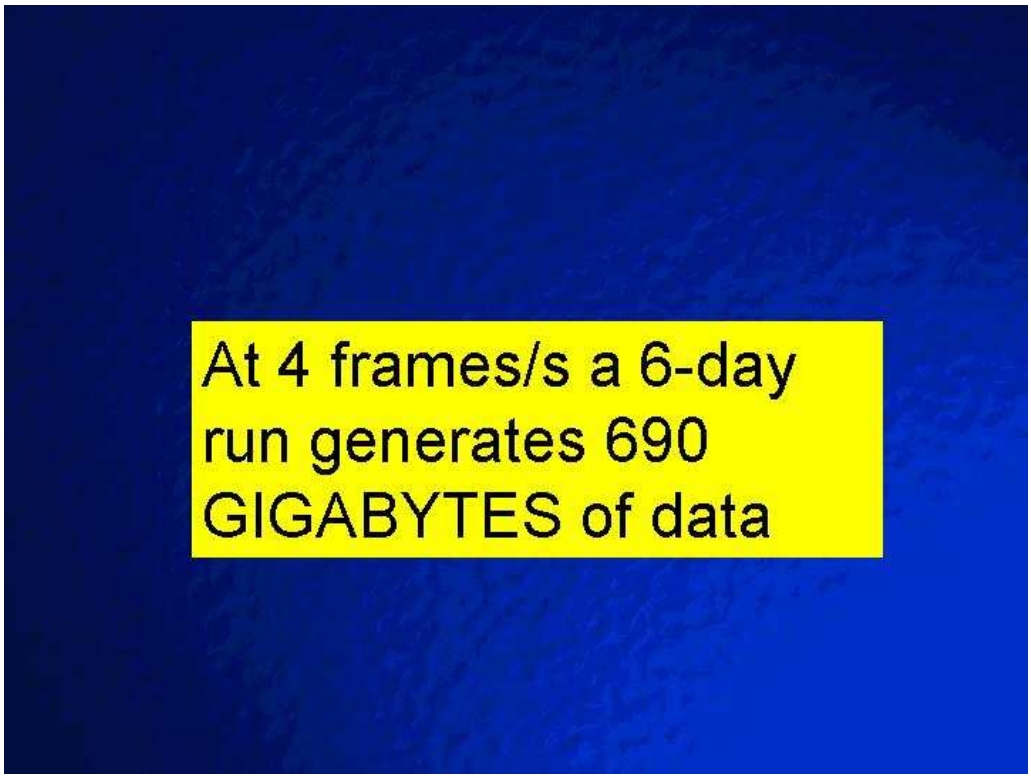
At 4 frames/s a 6-day
run generates 690
GIGABYTES of data

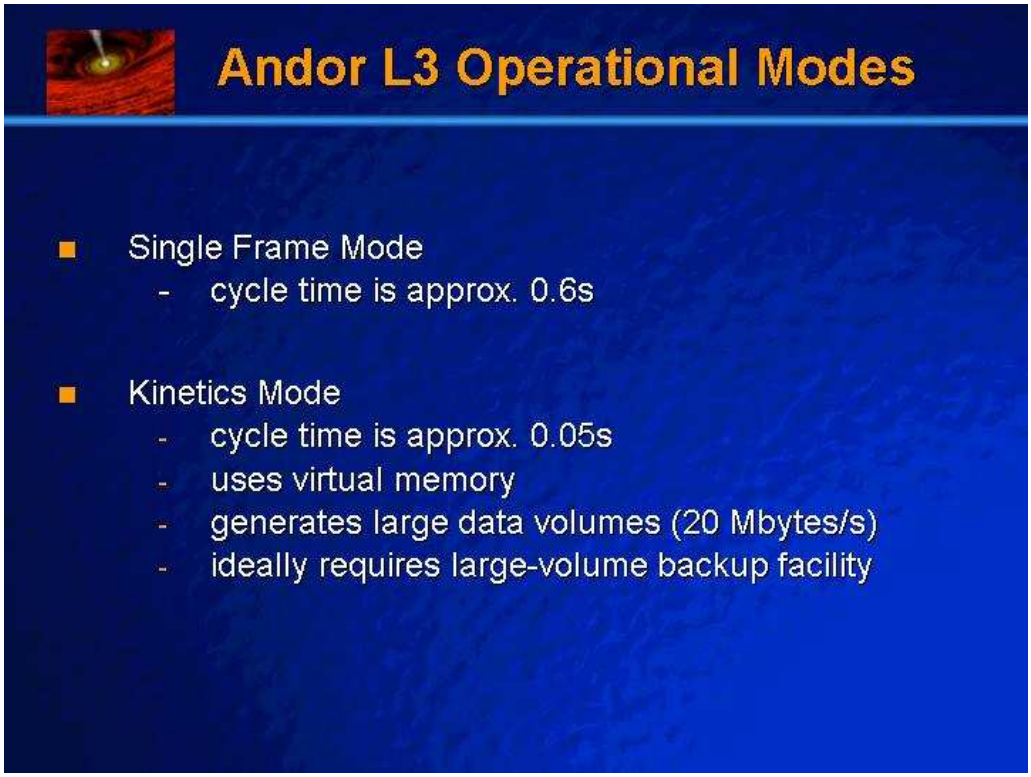
Andor L3 Operational Modes
Single Frame Mode
- cycle time is approx. 0.6s
Kinetics Mode
- cycle time is approx. 0.05s
- uses virtual memory
- generates large data volumes (20 Mbytes/s)
- ideally requires large-volume backup facility

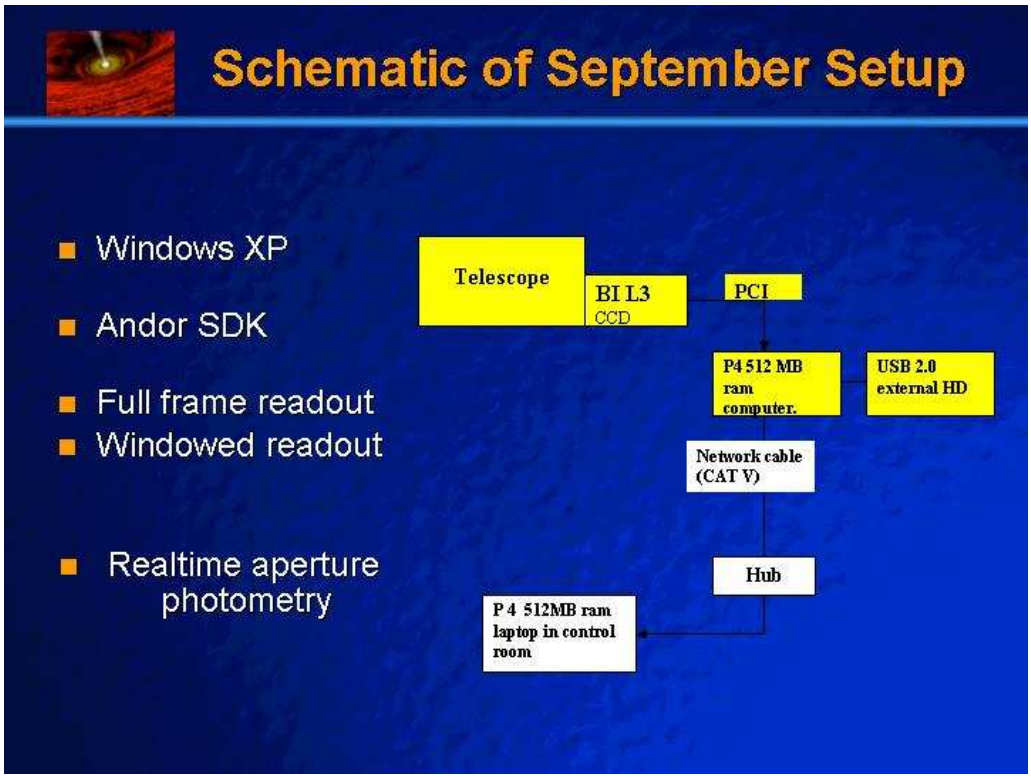
Schematic of September Setup
Windows XP
Andor SDK
Full frame readout
Windowed readout
Realtime aperture photometry
Telescope
BI L3 CCD
PCI
P4 512 MB ram computer.
USB 2.0 external HD
Network cable (CAT V)
Hub
P 4 512MB ram laptop in control room

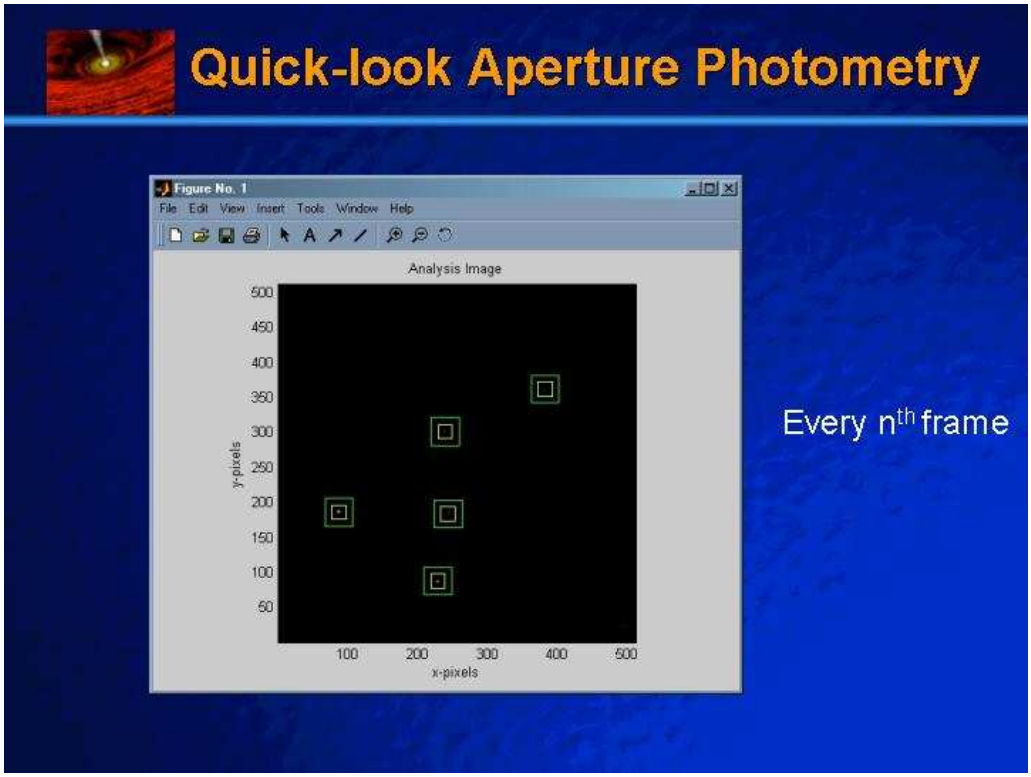
Quick-look Aperture Photometry
Figure No. 1
File Edit View Insert Tools Window Help
Analysis Image
y-pixels
x-pixels
Every nth frame

Differential Lightcurves

•Realtime photometry allows decisions to be made about the gross variability state of a quasar.

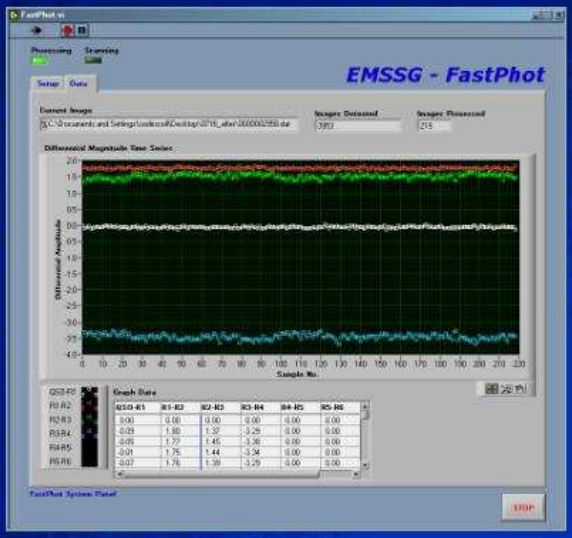

Calibration Data

- For each gain setting of L3 we took flatfield images and bias frames.
- Generated a master-flat and master-bias from these.
- Need sufficient integrated counts to define the flatfield and zerobias response.

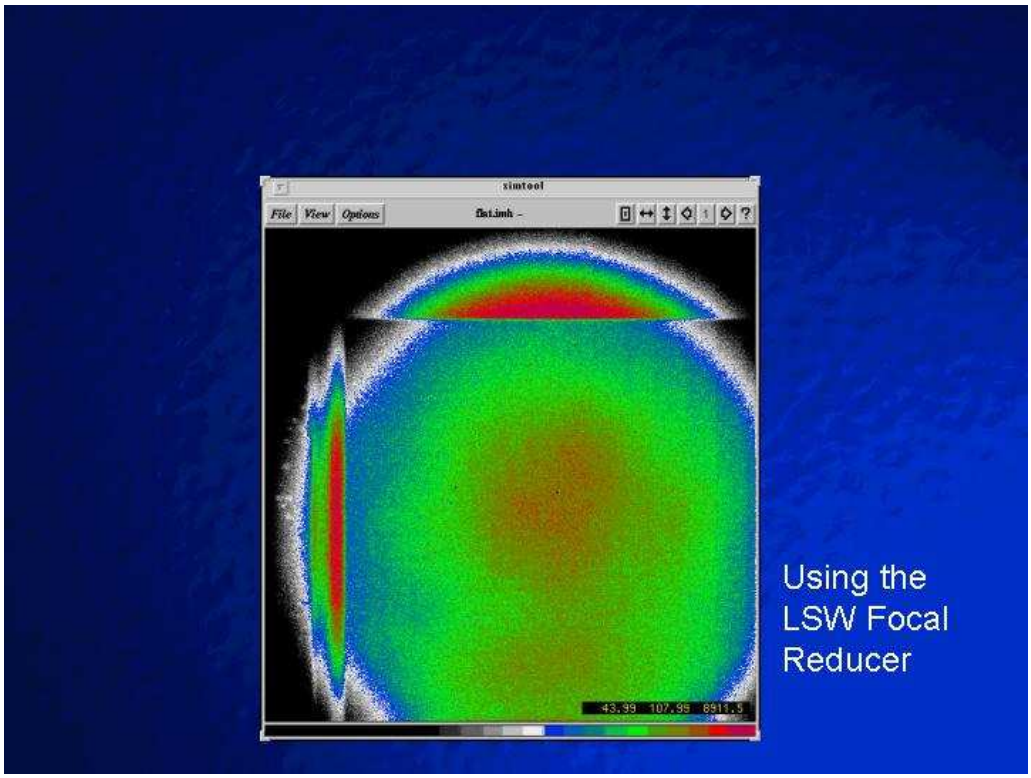
simtool
File
View
Options
flat.imh –
43.99 107.99 8811.5
Using the
LSW Focal
Reducer

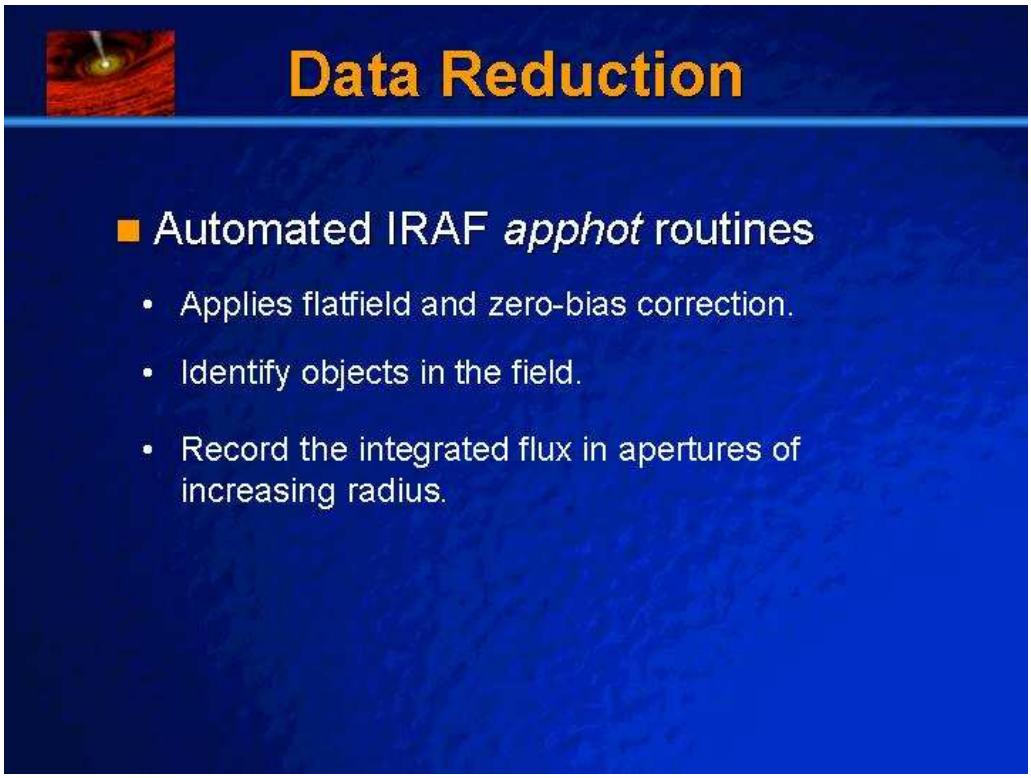
Data Reduction
Automated IRAF *apphot* routines
Applies flatfield and zero-bias correction.
Identify objects in the field.
Record the integrated flux in apertures of increasing radius.

Generation of Lightcurves

- Output is piped to IDL program "qvar"
  - performs differential photometry using a master reference star (composed of 4-8 stars typically)
  - provides statistical tests of variability
  - allows different background determination methods to be used
  - tracks variations in fwhm, position, apparent magnitude, airmass
  - allows rejection of variable stars or data points affected by cosmic rays

PG0716+714 – 0.3s (no average)

Differential Lightcurve of 0716+714 over 10 minutes

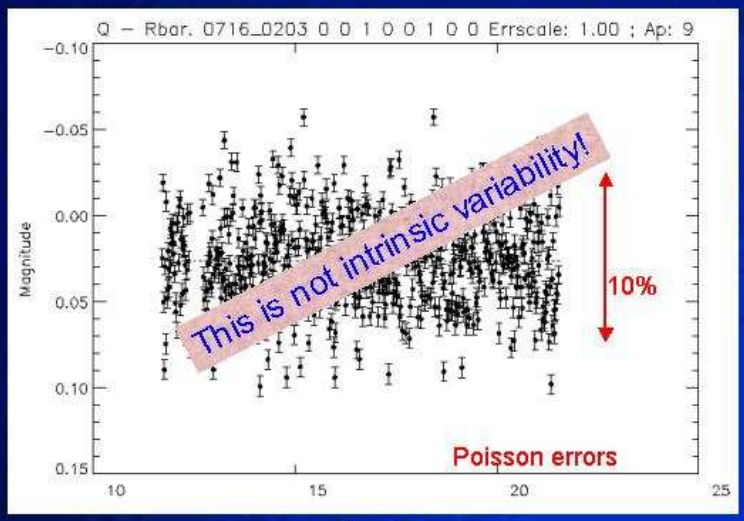

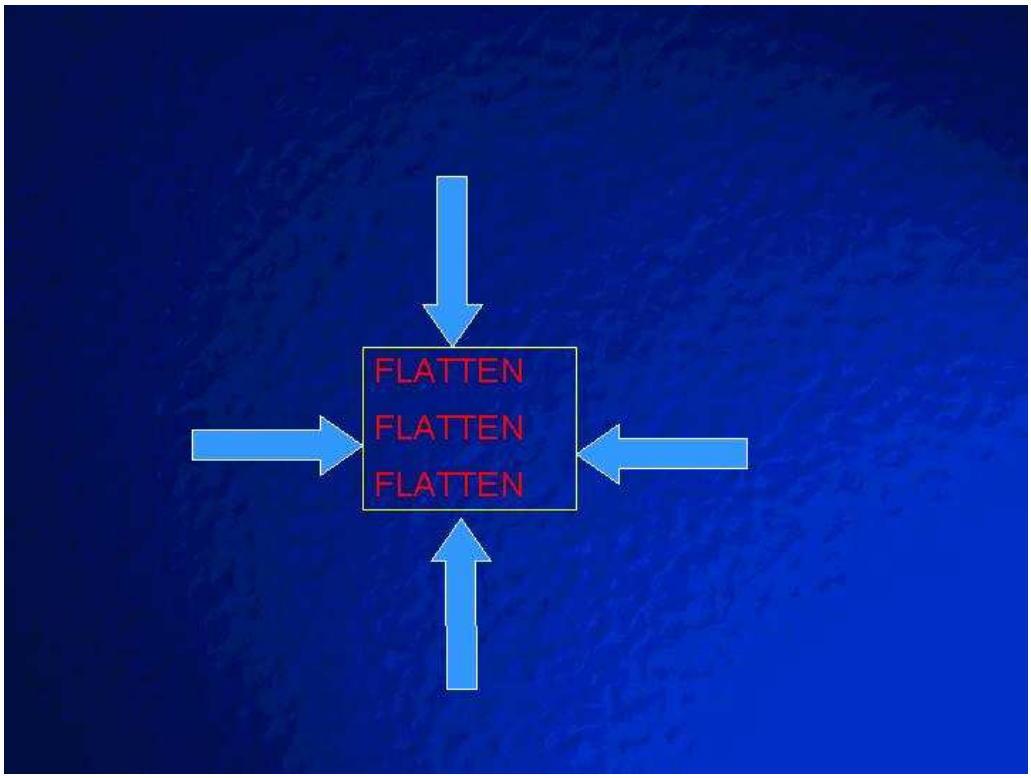
FLATTEN
FLATTEN
FLATTEN

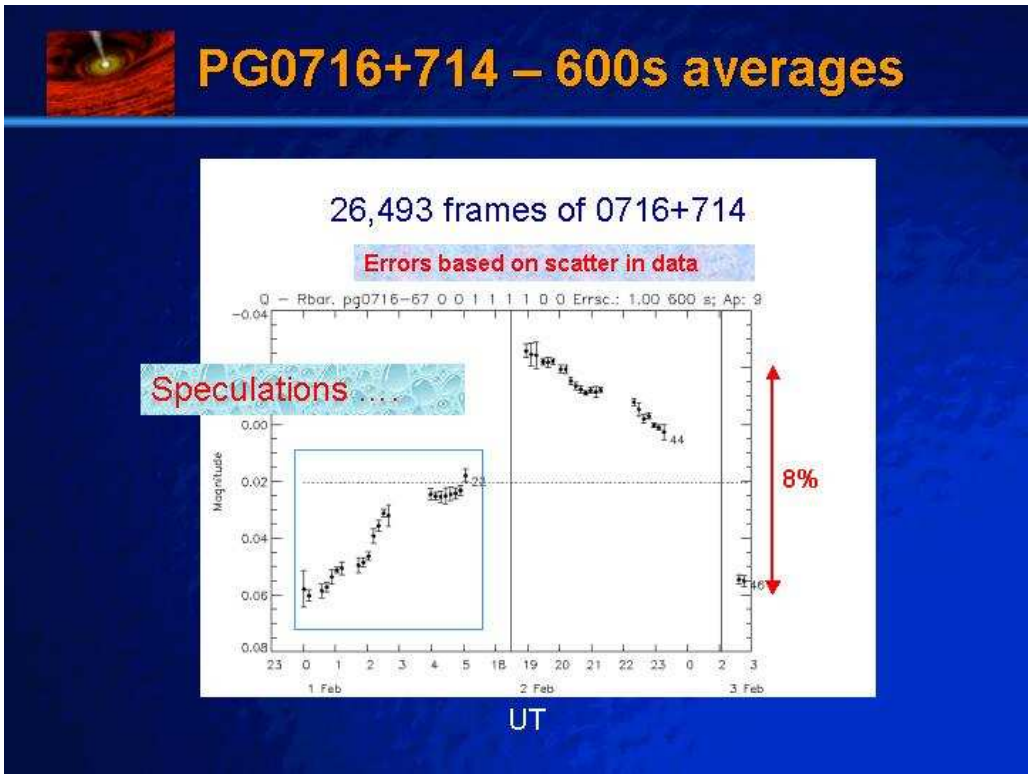
PG0716+714 – 600s averages
26,493 frames of 0716+714
Errors based on scatter in data
Speculations ....
8%
Magnitude
UT
1 Feb
2 Feb
3 Feb

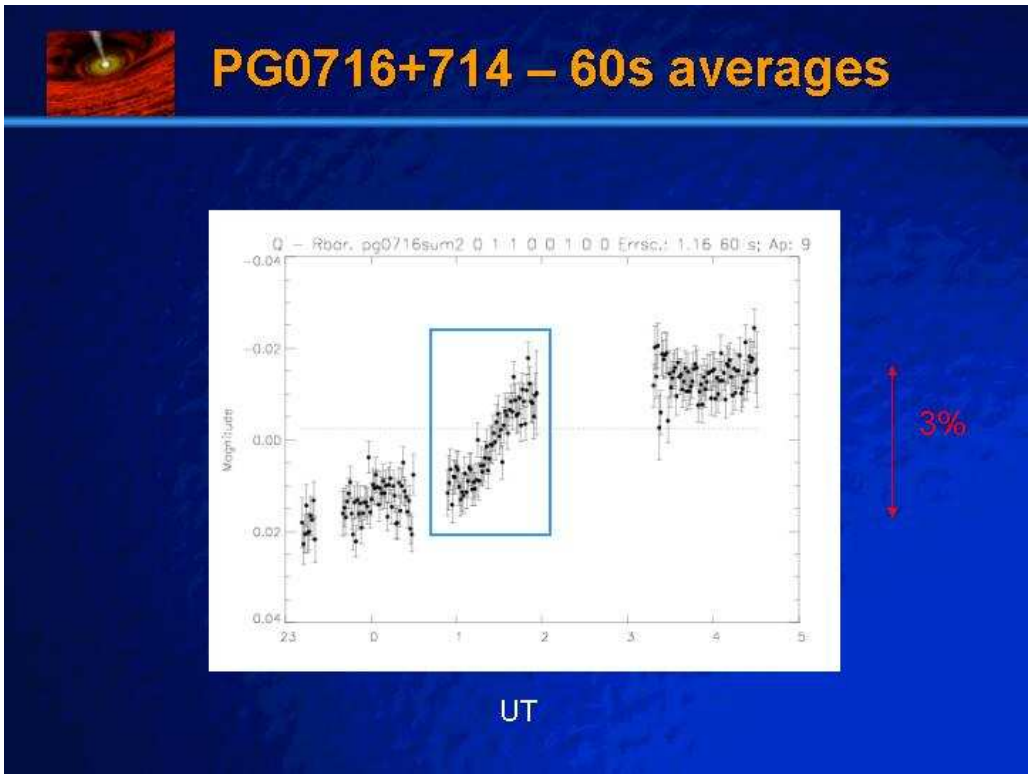
PG0716+714 – 60s averages
Q – Rbar, pg0716sum2 0 1 1 0 0 1 0 0 Errsc.: 1.16 60 s; Ap: 9
Magnitude
-0.04
-0.02
0.00
0.02
0.04
23
0
1
2
3
4
5
3%
UT

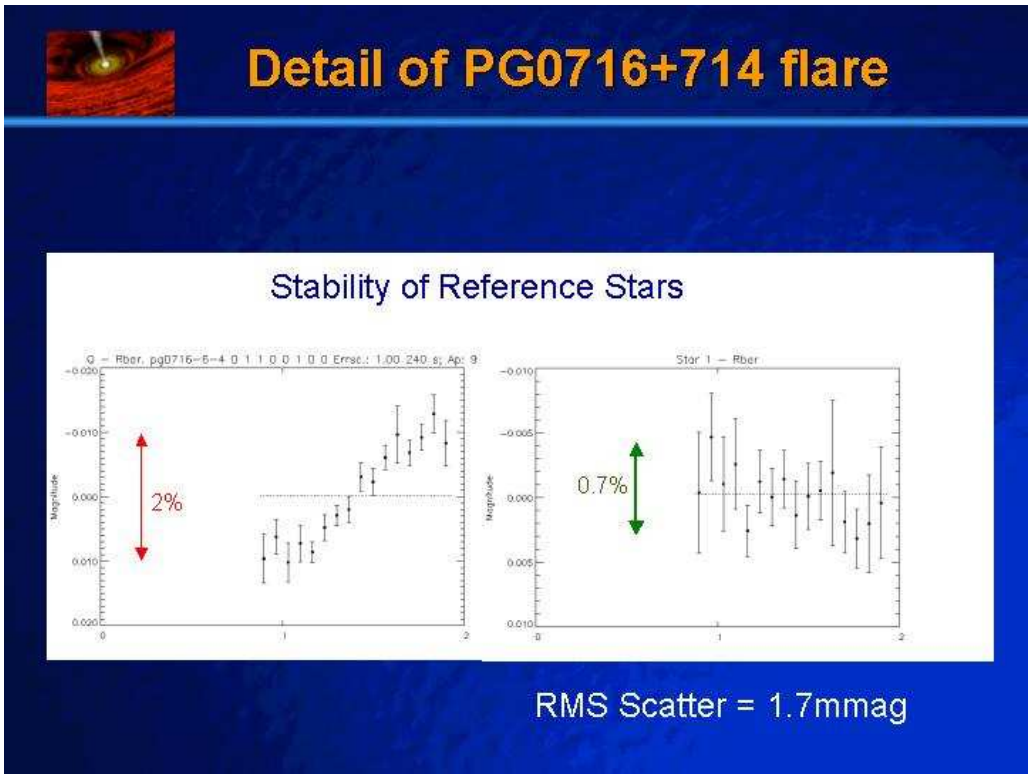
Detail of PG0716+714 flare
Stability of Reference Stars
Q – Rbar, pg0716–6–4 0 1 1 0 0 1 0 0 Errsc.: 1.00 240 s; Ap: 9
Magnitude
2%
Star 1 – Rbar
Magnitude
0.7%
RMS Scatter = 1.7mmag

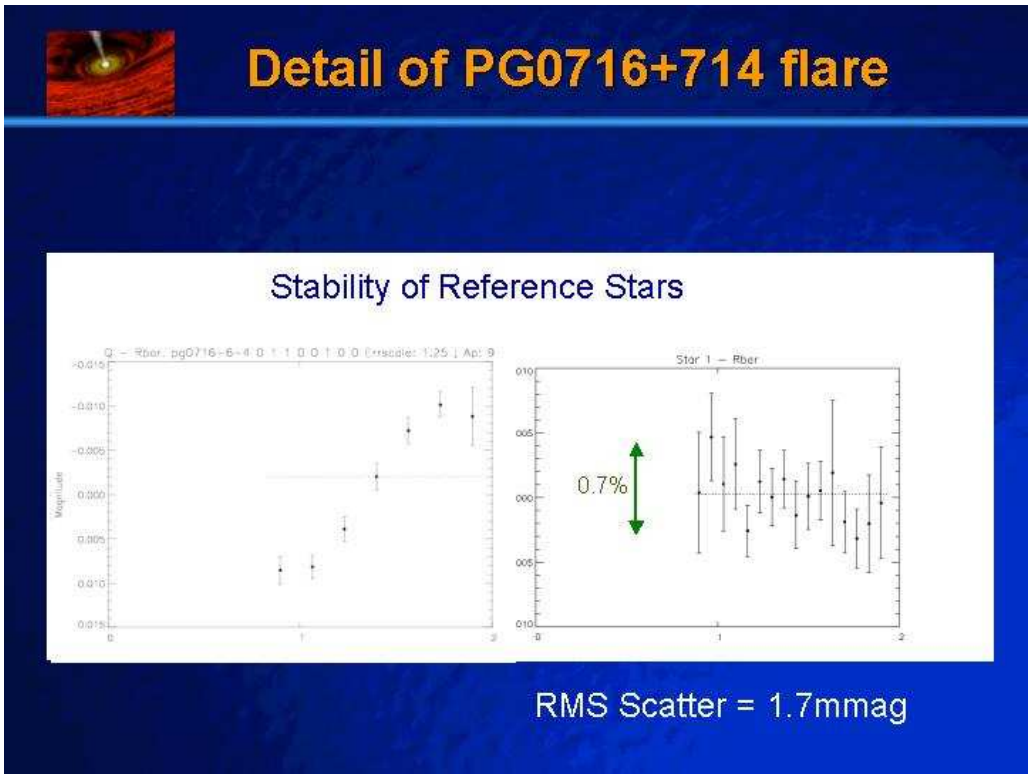
Detail of PG0716+714 flare
Stability of Reference Stars
Star 1 – Rber
0.7%
RMS Scatter = 1.7mmag

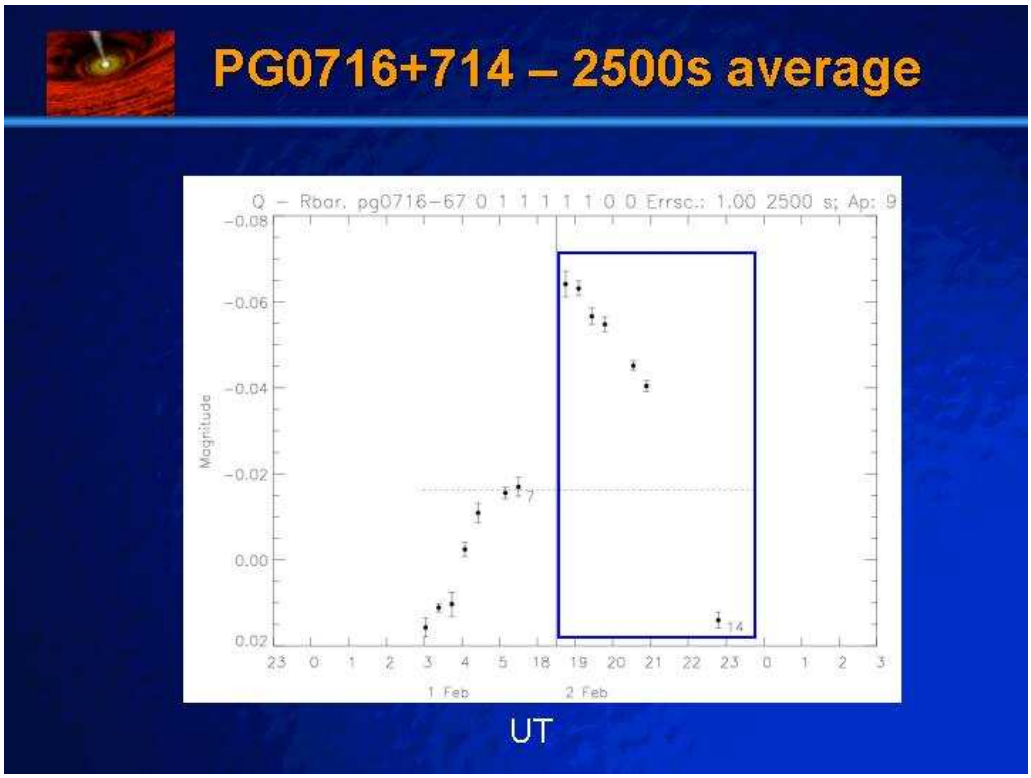
PG0716+714 – 2500s average
Q – Rbar. pg0716-67 0 1 1 1 1 1 0 0 Errsc.: 1.00 2500 s; Ap: 9
Magnitude
1 Feb
2 Feb
UT

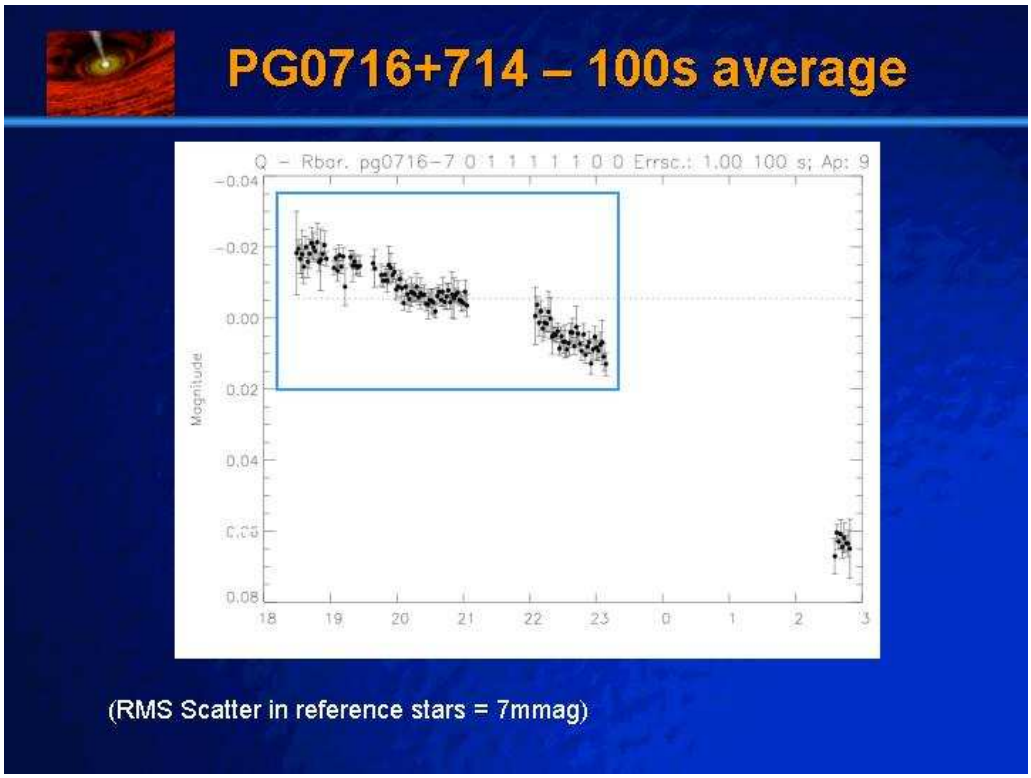
PG0716+714 – 100s average
Q – Rbar. pg0716-7 0 1 1 1 1 1 0 0 Errsc.: 1.00 100 s; Ap: 9
Magnitude
-0.04
-0.02
0.00
0.02
0.04
0.08
18
19
20
21
22
23
0
1
2
3
(RMS Scatter in reference stars = 7mmag)

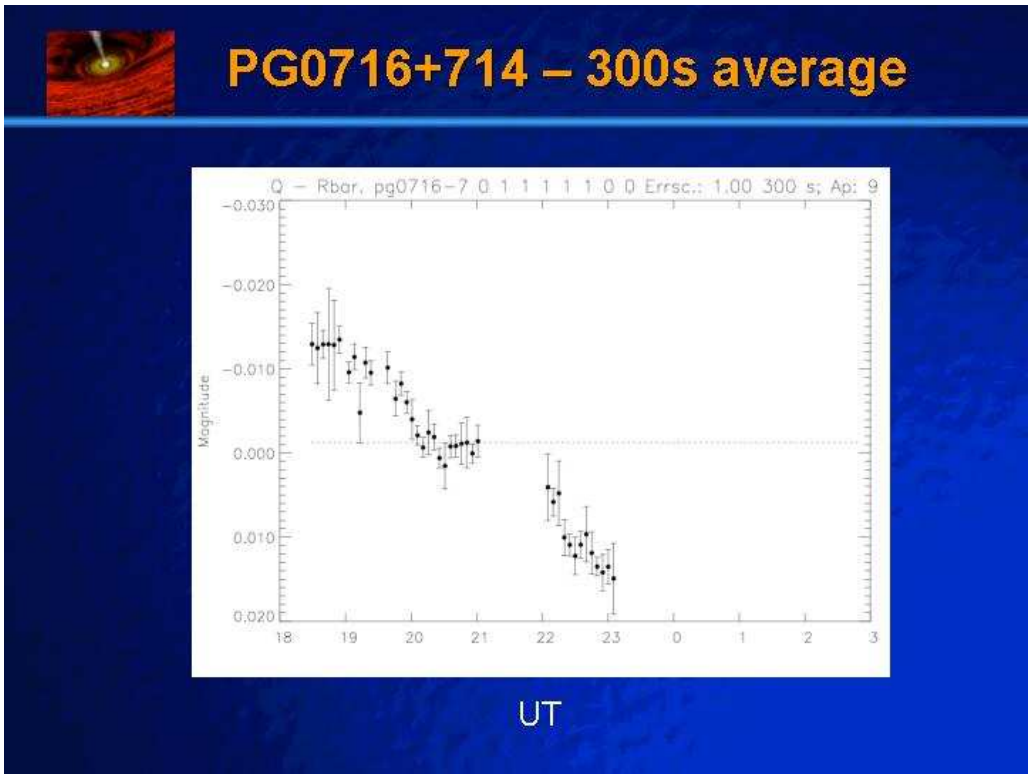
PG0716+714 – 300s average
Q – Rbar. pg0716-7 0 1 1 1 1 1 0 0 Errsc.: 1.00 300 s; Ap: 9
Magnitude
-0.030
-0.020
-0.010
0.000
0.010
0.020
18
19
20
21
22
23
0
1
2
3
UT

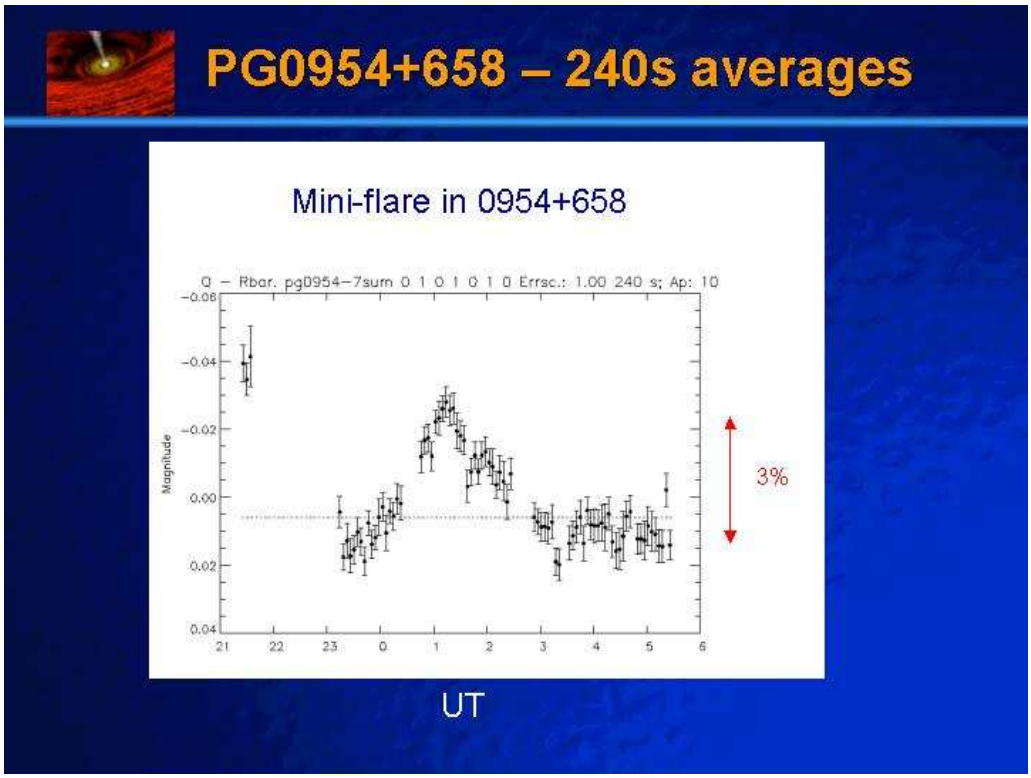
PG0954+658 – 240s averages
Mini-flare in 0954+658
Q – Rbar, pg0954–7sum 0 1 0 1 0 1 0 Errsc.: 1.00 240 s; Ap: 10
Magnitude
3%
UT

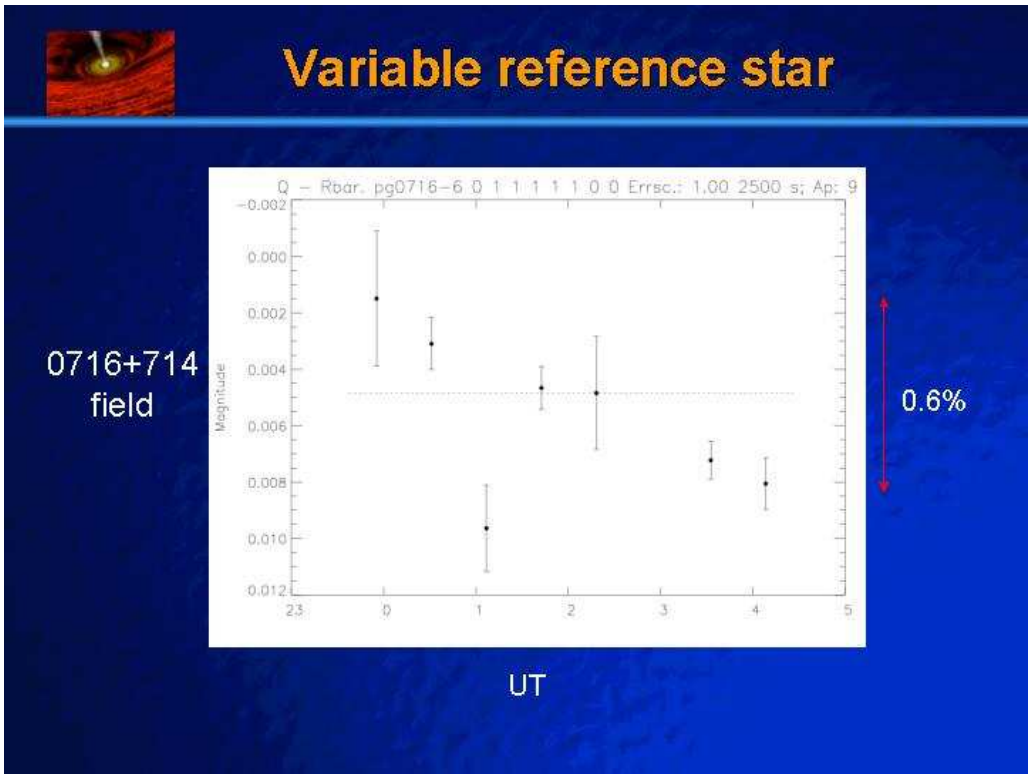
Variable reference star
0716+714
field
Q – Rbar, pg0716–6 0 1 1 1 1 1 0 0 Errsc.: 1.00 2500 s; Ap: 9
Magnitude
0.6%
UT

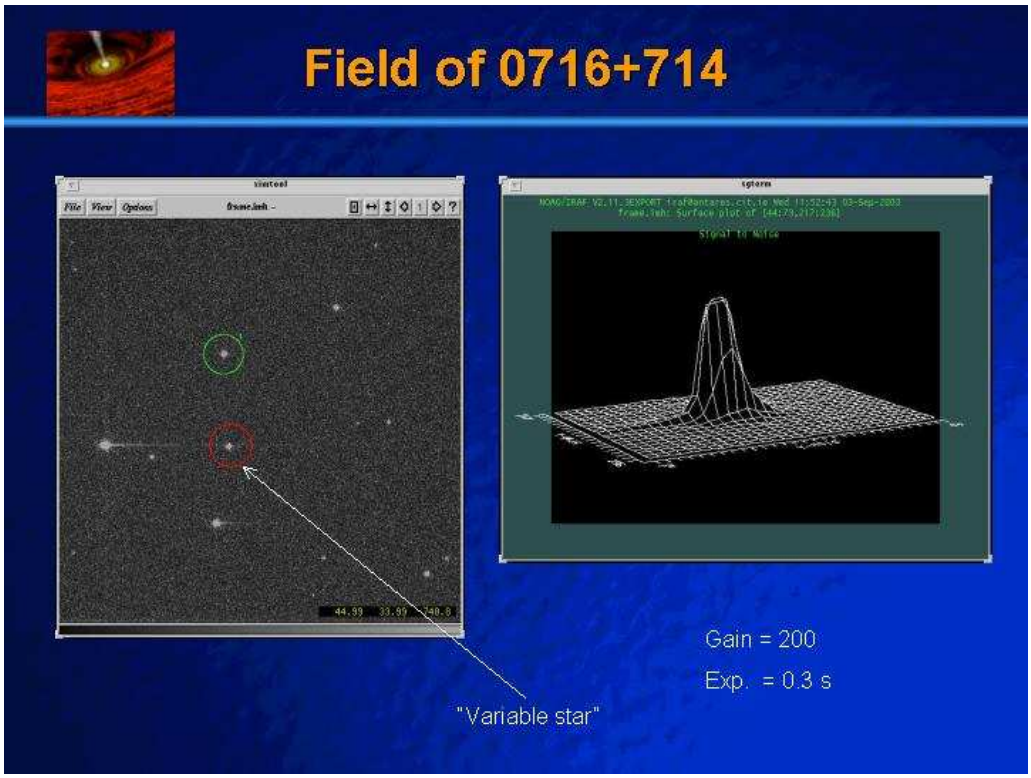
Field of 0716+714
Gain = 200
Exp. = 0.3 s
"Variable star"

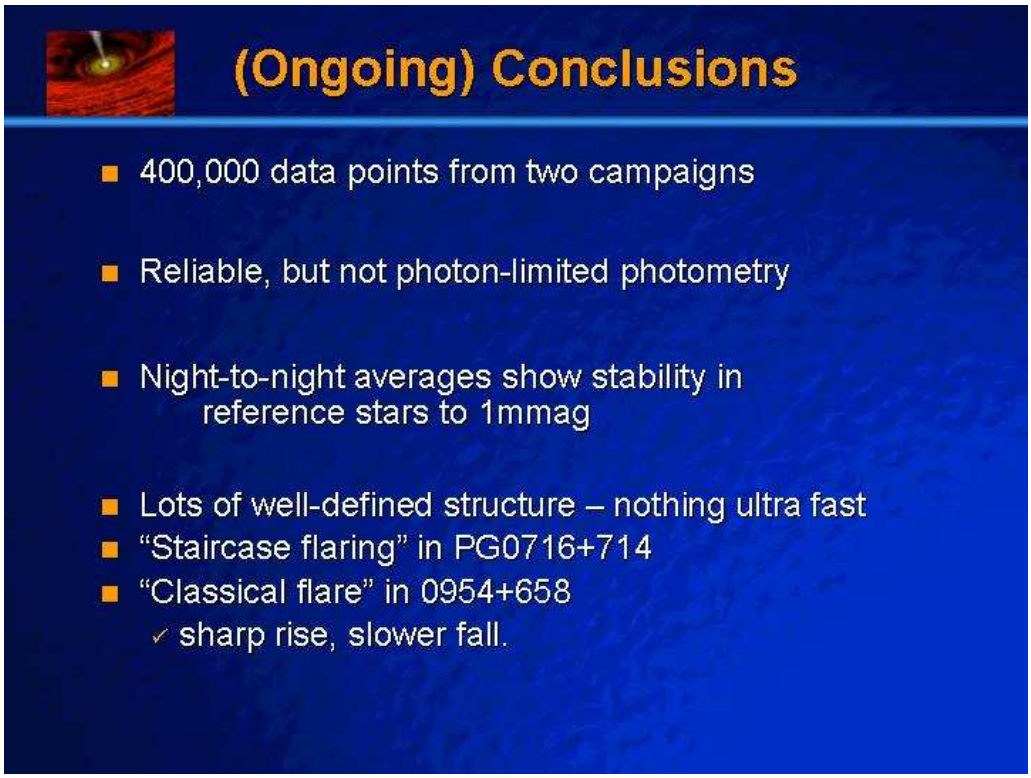
(Ongoing) Conclusions
400,000 data points from two campaigns
Reliable, but not photon-limited photometry
Night-to-night averages show stability in reference stars to 1mmag
Lots of well-defined structure – nothing ultra fast
"Staircase flaring" in PG0716+714
"Classical flare" in 0954+658
sharp rise, slower fall.


THANKS TO THE LOC!!

Campaign session II: Future campaigns

Outlook on the AGILE mission – L. Ostorero, M. Tavani, S. Vercellone, M. Villata, C. M. Raiteri

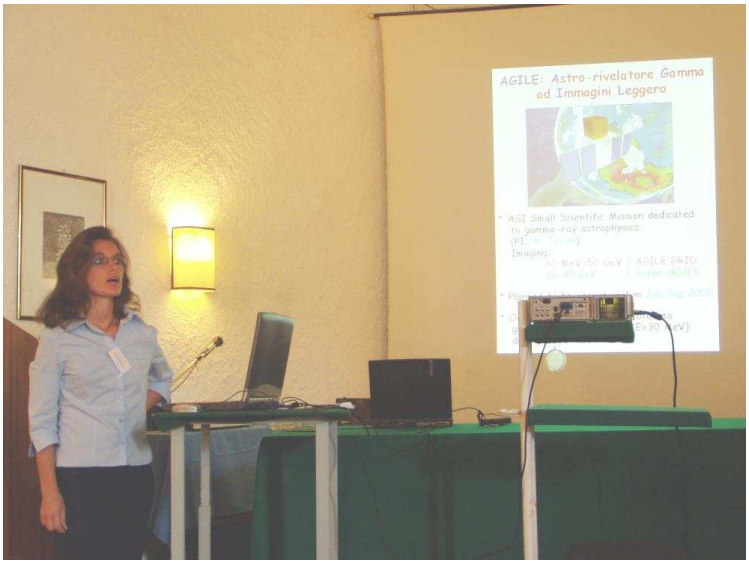

OUTLOOK
ON THE
AGILE MISSION

Luisa Ostorero (1)

M.Tavani (2), S.Vercellone (3),
M.Villata (4), C.M. Raiteri (4)

(1) Landessternwarte Heidelberg
(2) IASF, Sezione di Roma
(3) IASF, sezione di Milano
(4) Torino Astronomical Observatory

AGILE: Astro-rivelatore Gamma
ad Immagini Leggero

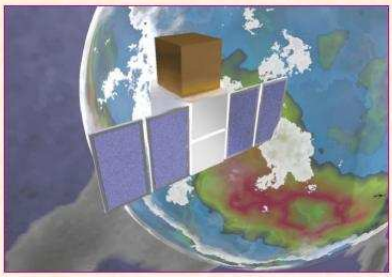

* ASI Small Scientific Mission dedicated to gamma-ray astrophysics (PI: M.Tavani)
Imaging:
30 MeV-50 GeV : AGILE GRID
10-40 keV : Super-AGILE
* Planned to be operational in Jul-Sep 2005
* Only mission entirely dedicated to gamma-ray astrophysics (E>30 MeV) during 2005-2007

AGILE INSTRUMENTS

AGILE GRID: 30 MeV - 50 GeV

FOV	~ 3 sr (1/5 sky)
Energy resolution	ΔE/E ~1 at 300 MeV
Source Loc.Accuracy	5'-20' (S/N~10)
Sensitivity at 1 GeV	4e-11 ph/cm²/sec/MeV (1000 ksec)

Super-AGILE: 10 – 40 keV

FOV	~ 0.8 sr
Energy resolution	ΔE < 4 keV
Source Loc.Accuracy	2'-3' (S/N~10)
Sensitivity @ 15 keV	5 mCrab (50 ksec)

AGILE & BLAZARS: Energy range

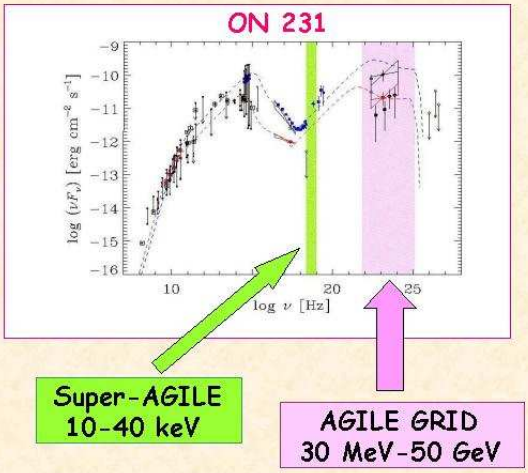

Simultaneous hard-X / γ-ray data

AGILE AND BLAZARS: Sensitivity

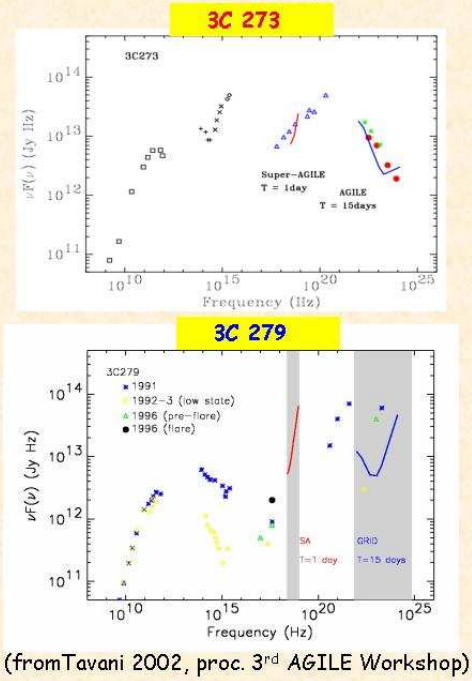

(fromTavani 2002, proc. 3rd AGILE Workshop)

AGILE EFFECTIVE AREA

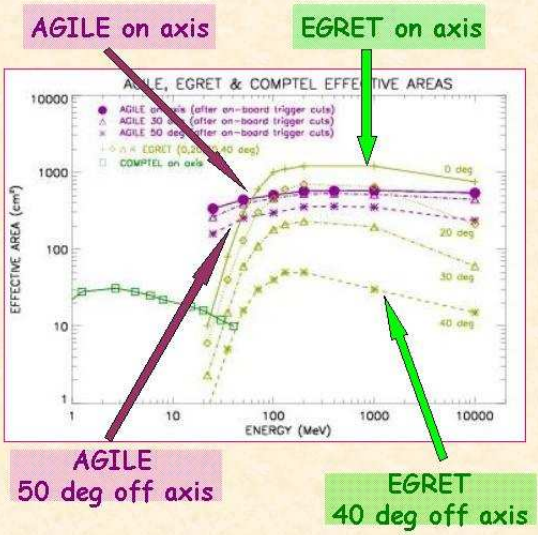

Simultaneous monitoring of many AGNs!

AGILE SOURCE LOCATION ACCURACY

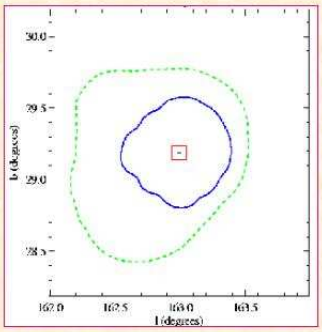

(fromTavani 2002, proc. 3rd AGILE Workshop)

F γ = 30 x 10^{-8} ph/cm^2/sec/MeV (E>100 MeV)
Teff= 1 week

θ (EGRET) = 17 ° d~1.3°
θ (AGILE) = 28 ° d~0.7°

AGILE ALLOWED POINTINGS

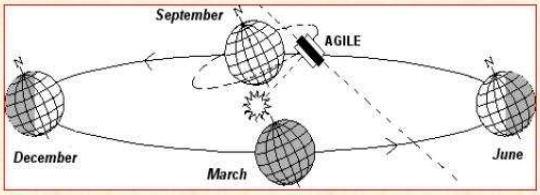

SOLAR PANELS: ⊥ SUN-EARTH LINE

TELESCOPE AXIS: // SOLAR PANELS

ALLOWED POINTINGS DIRECTED ALONG THE ECLIPTIC MERIDIAN AT ± 90° FROM THE SUN

EXAMPLE OF A POINTING

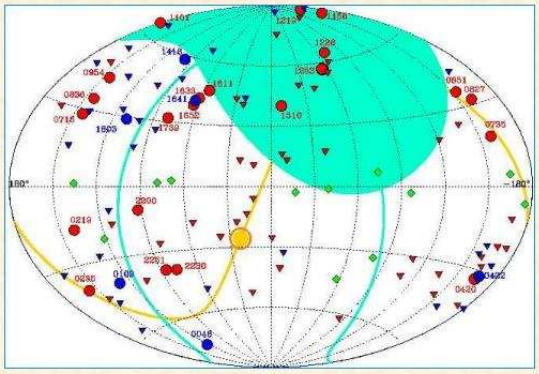

JAN 06

AGILE allowed pointing directions on January 06

ecliptic

EVOLUTION OF THE POINTING AREA

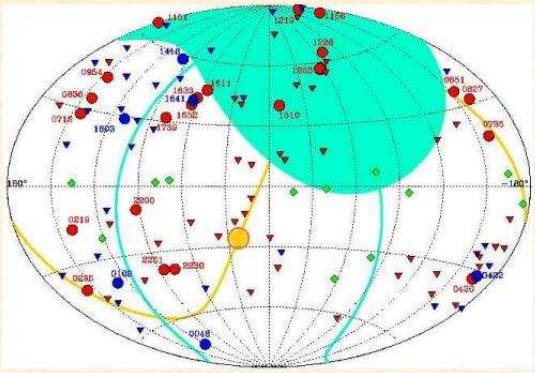

JAN 06 - FEB 05

EVOLUTION OF THE POINTING AREA

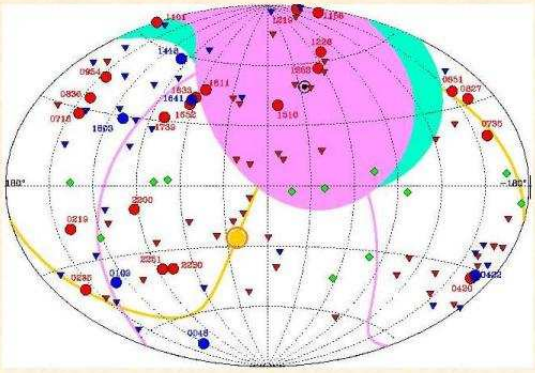

JAN 06 - FEB 05

EVOLUTION OF THE POINTING AREA

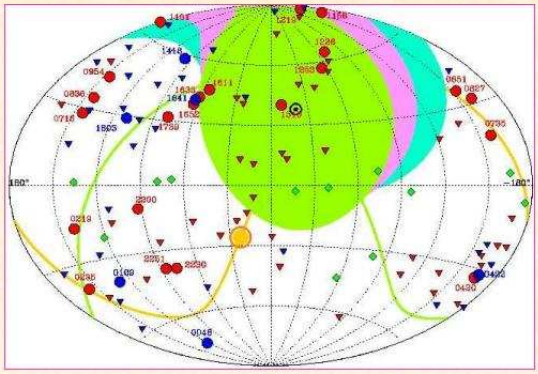

JAN 06 - FEB 05

The sources drift in the AGILE field of view

MULTIWAVELENGTH FOLLOW-UP PROGRAMS FOR BLAZARS

The AGILE mission is planned in collaboration with the MW astronomers:

The SCIENCE SUPPORT GROUP

Suggestions for an AGILE viewing-plan optimized for simultaneous MULTI-ν / γ-RAY observations of blazars

GAMMA-RAY ACCESSIBLE SKY

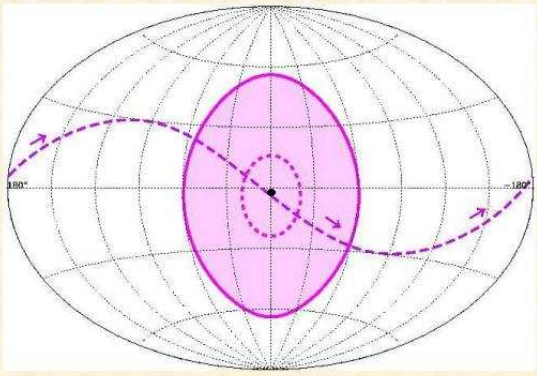

March 20

GAMMA-RAY ACCESSIBLE SKY

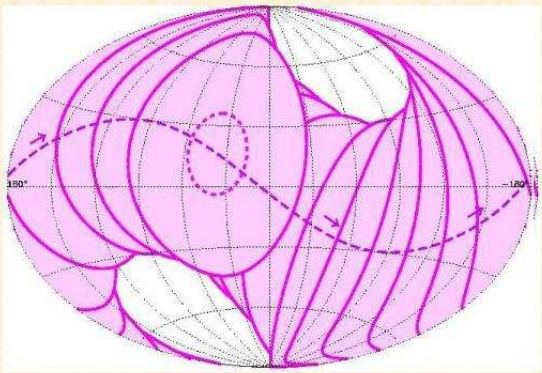

March 20

AGILE FOV radius = 60°

120°-wide sky belt
accessible to γ-ray observations

GAMMA-RAY ACCESSIBLE SKY

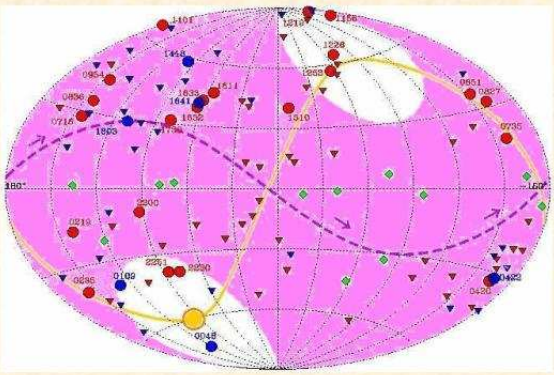

March 20

AGILE FOV radius = 60°

120°-wide sky belt
accessible to γ-ray observations

X-RAY ACCESSIBLE SKY

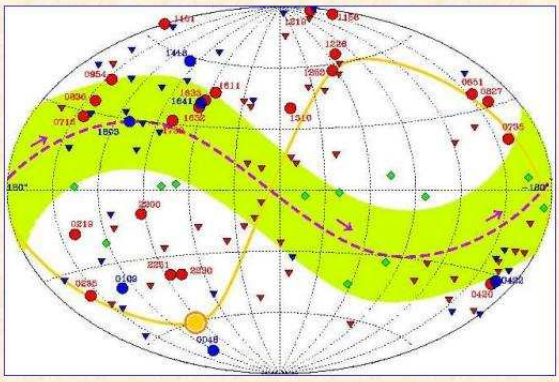

March 20

Super-AGILE FOV radius = 20°

40°-wide sky belt
accessible to X-ray observations

AGILE-OPTICAL ACCESSIBLE SKY

March 20

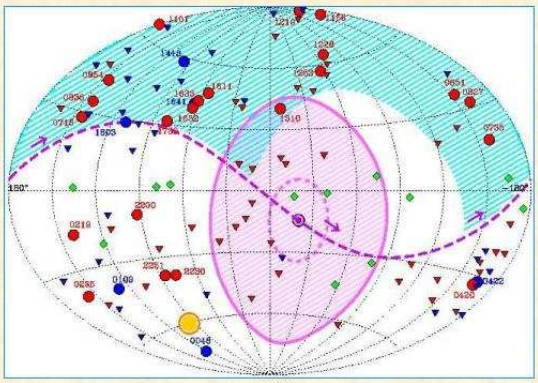

▼ 13 γ-ray blazars (3: opt. mon.)
▼ 1 blazar (γ ?)
◆ 5 Galactic sources

AGILE-OPTICAL ACCESSIBLE SKY

March 20

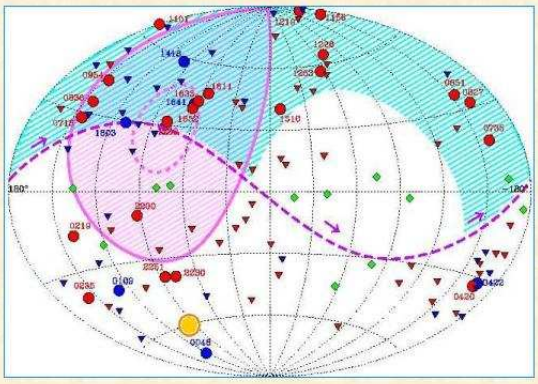

- 14 γ-ray blazars (9: opt. mon.)
- 13 blazar (γ ?)
- 2 Galactic sources

A POSSIBLE POINTING STRATEGY

To obtain the best results from coordinated AGILE & OPTICAL observations of blazars, the AGILE observing strategy should take the following criteria into account (Ostorero et al. 2003, in preparation):

- 1 YEAR CYCLE SURVEY
- 12 POINTINGS , lasting 1 MONTH, ensuring the coverage of the whole sky
- HOMOGENEITY in R.A. for sources inside each pointing area
- Choice of the POINTING PERIODS in agreement with:
  - the AGILE instrumental constraints
  - the position of the sources in the night sky
  - the position of the main X-ray sources in the Super-AGILE FOV

Sky coverage

AGILE

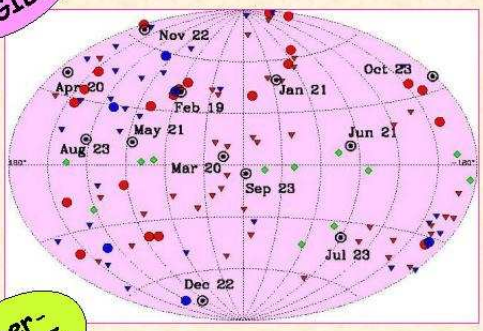

Super-AGILE

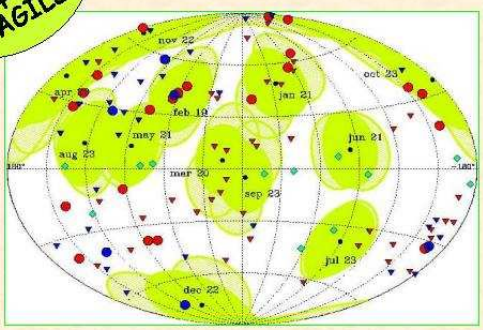

CONCLUSIONS

AGILE is the next X-ray / γ-ray mission, operating in 2005-2007

The mission will be planned in collaboration with the multiwavelength astronomers (Science Support Group) to optimize the science return.

The first result of the AGILE-OPTICAL collaboration is the viewing plan shown here.

The ENIGMA Network plans to collaborate with the AGILE Team with multiwavelength studies and coordination of telescopes operating in different energy-bands.

Souvenir photos